



City Research Online

City, University of London Institutional Repository

Citation: Skoufari-Themistou, L. (1996). Impact and yield strength behaviour of age-hardening, low-carbon copper-containing steels. (Unpublished Doctoral thesis, City, University of London)

This is the accepted version of the paper.

This version of the publication may differ from the final published version.

Permanent repository link: <https://openaccess.city.ac.uk/id/eprint/31054/>

Link to published version:

Copyright: City Research Online aims to make research outputs of City, University of London available to a wider audience. Copyright and Moral Rights remain with the author(s) and/or copyright holders. URLs from City Research Online may be freely distributed and linked to.

Reuse: Copies of full items can be used for personal research or study, educational, or not-for-profit purposes without prior permission or charge. Provided that the authors, title and full bibliographic details are credited, a hyperlink and/or URL is given for the original metadata page and the content is not changed in any way.

City Research Online:

<http://openaccess.city.ac.uk/>

publications@city.ac.uk

**IMPACT AND YIELD STRENGTH BEHAVIOUR
OF AGE-HARDENING, LOW-CARBON
COPPER-CONTAINING STEELS**

by

LEDA SKOUFARI - THEMISTOU

A dissertation submitted to
City University
in fulfilment of the requirement
for the degree of Doctor of Philosophy

Department of Mechanical Engineering and Aeronautics

CITY UNIVERSITY

London

June 1996

*To my grandparents,
Leda and Michael*

CONTENTS

	Page
LIST OF TABLES	7
LIST OF FIGURES	9
LIST OF SYMBOLS AND ABBREVIATIONS	17
ACKNOWLEDGEMENTS	20
DECLARATION	21
ABSTRACT	22
1 INTRODUCTION	23
2 LITERATURE SURVEY	25
2.1 Strengthening mechanisms in steels	25
2.1.1 Strain hardening	27
2.1.2 Solid solution strengthening	27
2.1.3 Grain size strengthening	27
2.1.4 Substructure formation	28
2.1.5 Dispersion of a second phase	29
2.1.6 Precipitation strengthening	29
2.1.6.1 Internal strain hardening	32
2.1.6.2 Chemical hardening	34
2.1.6.3 Dispersion hardening	34
2.2 The impact behaviour of steel	37
2.2.1 Brittle fracture	37
2.2.1.1 Cleavage fracture	39
2.2.1.2 Intergranular fracture	40
2.3 Structure-property relationships in steels	41
2.3.1 Polygonal ferrite microstructures	42
2.3.2 Acicular ferrite and bainitic microstructures	44
2.3.3 Martensitic structures	46
2.3.4 Tempered martensitic/bainitic microstructures	47
2.3.5 Dual phase steels	50
2.4 Age-hardening of plain low-carbon steels	51
2.5 Precipitation hardening of HSLA steels	56
2.6 Copper in steels	59
2.6.1 The solubility of copper in steels	63
2.6.2 Hardenability and transformation kinetics	65

2.6.3	Copper precipitation in steels	68
2.6.4	The influence of copper on the tensile strength of steels	73
2.6.5	Commercial copper-containing steel alloys.....	75
3	EXPERIMENTAL PROCEDURES	84
3.1	Heat treatments.....	84
3.2	Mechanical tests.....	86
3.2.1	Impact tests.....	86
3.2.2	Tensile tests	88
3.2.3	Hardness tests	89
3.3	Metallography.....	89
3.3.1	Sample preparation	90
3.3.2	Microscopy	92
3.3.2.1	Optical microscopy	93
3.3.2.2	Scanning electron microscopy.....	93
3.3.2.3	Transmission electron microscopy.....	95
4	THE STRENGTH AND IMPACT PROPERTIES OF LOW-CARBON QUENCHED-AGED STEELS	99
4.1	Introduction.....	99
4.2	Experimental	100
4.3	Test results.....	102
4.3.1	Hardness and tensile test results.....	102
4.3.2	Impact test results	103
4.4	Metallography.....	103
4.4.1	Optical microscopy	103
4.4.2	Scanning electron microscopy.....	104
4.5	Discussion of results.....	105
4.5.1	The influence of ageing on hardness and tensile properties	105
4.5.2	The effect of ageing on the impact properties of low carbon steels	107
4.5.2.1	The impact behaviour of steels No1 and 2P1H.....	107
4.5.2.2	The impact behaviour of steel 4P28H.....	108
5	THE STRENGTH AND IMPACT PROPERTIES OF LOW-CARBON, COPPER-CONTAINING, FERRITE-PEARLITE STEELS	129
5.1	Introduction.....	129
5.2	Experimental	130
5.3	Test results.....	131
5.3.1	Hardness test results.....	131

5.3.2	Tensile test results.....	132
5.3.3	Impact test results	133
5.4	Metallography	134
5.4.1	Optical microscopy	134
5.4.2	Scanning electron microscopy.....	135
5.4.2.1	Copper-free steel.....	135
5.4.2.2	1.22% Cu-steel.....	136
5.4.2.3	2.02% Cu-steel.....	137
5.4.3	Transmission electron microscopy.....	138
5.4.3.1	1.22% Cu-steel.....	138
5.4.3.2	2.02% Cu-steel.....	139
5.4.3.3	A TEM study on the effect of straining on the 2.02% Cu-steel.....	140
5.4.3.4	A TEM study on the effect of cooling rate on the 2.02% Cu-steel.....	141
5.5	Discussion of results.....	142
5.5.1	The microstructures.....	142
5.5.2	The influence of tempering on hardness and tensile properties.....	142
5.5.3	The effect of precipitation hardening on the impact properties	149
6	THE STRENGTH AND IMPACT PROPERTIES OF LOW-CARBON, COPPER-CONTAINING STEELS OF A COMMERCIAL COMPOSITION	191
6.1	Introduction.....	191
6.2	Experimental	192
6.3	Test results.....	193
6.3.1	Hardness test results.....	193
6.3.2	Tensile test results.....	194
6.3.3	Impact test results	194
6.4	Metallography	195
6.4.1	Optical microscopy	195
6.4.2	Scanning electron microscopy.....	196
6.4.2.1	Normalised microstructures	196
6.4.2.2	Quenched microstructures.....	198
6.4.3	Transmission electron microscopy.....	200
6.4.3.1	Normalised microstructures	200
6.4.3.2	Quenched microstructures.....	202
6.5	Discussion of results.....	203
6.5.1	The influence of tempering on hardness and tensile properties.....	203
6.5.1.1	Normalised and over-aged condition (NT650)	204

6.5.1.2	Quenched and over-aged condition (QT650).....	205
6.5.1.3	The influence of martensite and copper precipitation on the yield properties, other than the over-aged conditions.....	205
6.5.1.4	Normalised and fully-aged condition (NT550).....	206
6.5.1.5	As-normalised condition (N)	207
6.5.1.6	As-quenched condition (Q).....	208
6.5.1.7	Quenched and fully-aged condition (QT500).....	209
6.5.2	The effect of precipitation of hardening on the impact properties	209
6.5.2.1	Normalised and over-aged condition (NT650)	210
6.5.2.2	Quenched and over-aged condition (QT650).....	211
6.5.2.3	As-normalised and normalised and fully-aged conditions (N) & (NT550).....	211
6.5.2.4	As-quenched and quenched and fully-aged conditions (Q) & (QT500).....	212
6.5.2.5	The influence of copper precipitate size and volume fraction on the impact transition temperatures	213
6.5.2.6	The impact behaviour of the normalised commercial 1.26% Cu and the simpler 2.02% Cu containing steels.....	217
7	CONCLUSIONS	252
8	FUTURE WORK	257
	APPENDIX EDAX analysis (TEM) of copper containing steels	259
	REFERENCES AND BIBLIOGRAPHY	265

LIST OF TABLES

2.1	Typical composition of IN-787 steel	60
2.2	ASTM A710, Grades A and B, chemistry specification [93]	61
2.3	Minimum tensile and charpy V-notch impact property requirements for ASTM A710 Grade A steels [3].....	62
2.4	Mechanical properties of an ASTM A710 steel [2]	78
2.5	Heat treatments of an ASTM A710 steel [2]	78
3.1	Chemical composition of steel plates.....	96
4.1	Chemical composition of steels No1, 2P1H and 4P28H (% by weight)	112
4.2	Heat treatment of steels No1, 2P1H and 4P28H	112
4.3	Hardness and tensile properties of steels No1 and 2P1H.....	113
4.4	Hardness and tensile properties of steel 4P28H.....	113
4.5	Impact properties of steels No1 and 4P28H	113
4.6	Scanning electron microscopy of steel 4P28H.....	113
4.7	Mechanical properties of steel 4P28H, as they have been recorded at British Steel by Crowther and Thulaseetharan [96].....	114
4.8	Comparison between observed and calculated (Equation 2.10) lower yield strength values, of steels No1, 2P1H and 4P28H	114
4.9	Comparison between observed and calculated impact transition temperatures, of steel 4P28H.....	114
5.1	Chemical composition of steels 2P148H, 2P149H and 2P150H (% by weight).....	152
5.2	Heat treatments of steels 2P148H, 2P149H and 2P150H.....	152
5.3	Diamond pyramid hardness of steels 2P148H, 2P149H and 2P150H.....	153
5.4	Tensile properties of steels 2P148H, 2P149H and 2P150H.....	153
5.5	Impact properties of steels 2P148H, 2P149H and 2P150H	154
5.6	Optical and scanning electron microscopy of steels 2P148H, 2P149H and 2P150H	154
5.7	(a) TEM (thin foil) and SEM copper precipitate size measurements	155
5.7	(b)The effect of cooling rate and straining on the size of copper precipitates, on the 2.02% Cu steel (TEM thin foils)	155
5.8	Comparison between observed and calculated lower yield strength values, of steels 2P148H, 2P149H and 2P150H.....	156

5.9	Estimated dispersion strengthening effect (Ashby-Orowan), based on copper precipitate size as measured from SEM photographs.....	156
5.10	(a) Comparison between observed and calculated impact transition temperatures, of steels 2P148H, 2P149H and 2P150H.....	157
5.10	(b) Comparison between observed and calculated impact transition temperatures, of steels 2P148H, 2P149H and 2P150H.....	157
6.1	Chemical composition of copper containing steels (% by weight).....	219
6.2	Designated tensile and impact properties of ASTM A710.....	219
6.3	Heat treatments of steel 1P140M.....	220
6.4	Tensile properties of steels 1P140M.....	220
6.5	Impact properties of steel 1P140M.....	220
6.6	Optical microscopy of steel 1P140M.....	221
6.7	Scanning electron microscopy of steel 1P140M.....	221
6.8	TEM (replica) copper precipitate size measurements on steel 1P140M.....	221
6.9	Estimated dispersion strengthening effect (Ashby model), based on copper and niobium precipitate size as measured from TEM micrographs..	222
6.10	Comparison between observed and calculated lower yield strength values, of steel 1P140M.....	222
6.11	Crowther's results for a modified IN-787 steel [52].....	222
6.12	Comparison between observed and calculated impact transition temperatures, of steel 1P140M.....	223

LIST OF FIGURES

	Page
2.1	(a) Edge dislocation (b) Screw dislocation.....26
2.2	Stages of age-hardening and the produced microstructures, in a Al-4%Cu alloy[11]30
2.3	The effect of ageing temperature and time on the yield strength of an Al-4%Cu alloy [11]31
2.4	(a) a precipitate which is coherent with the matrix (b) a precipitate which is incoherent with the crystal structure of the matrix [11]32
2.5	Schematic representation of a dislocation (a) curling around the precipitate stress fields from precipitates (b) passing (bowing) between widely spaced precipitates (c) cutting through a fine particle (or a GP zone) and (d) piling up at grain boundaries [13,15]33
2.6	Representation of the variation of yield stress with ageing time, for a typical age-hardening alloy. τ is the shear stress needed to force dislocations between precipitate particles [13]33
2.7	Dislocation held up at dispersed particles or precipitates, showing definition of the bowing angle ϕ [12].....36
2.8	The dependence of the ductile-brittle transition temperature on the prior austenite grain size or the fracture facet size in: (a) bainitic microstructures (b) martensitic-bainitic microstructures [28].....46
2.9	Hardness of iron-carbon martensites tempered for 1 h at 100-700°C [91]
2.10	The relation between tensile strength and impact value of plain carbon and alloy steels tempered at 200°C [92]49
2.11	The effect of tempering on the relationship between the 0.2% proof stress and the ductile-brittle transition temperature for low-carbon bainitic microstructures, showing the effect of different strengthening mechanisms [28]50
2.12	Variation in yield strength with increasing martensite volume fraction [41].....51
2.13	Fe-rich side of Fe-C diagram, showing the extent of ferrite phase field and the decrease of carbon solubility with decreasing temperature [42]52
2.14	The influence of soaking time at 900°C and 1150°C on the precipitation hardening effect (Δy) of 0.02% Nb in a commercial C-Mn steel [47]57
2.15	Solubility relationships of various carbides and nitrides in austenite [48]58

2.16	The Fe-Cu diagram (based on data from ref.[12])	64
2.17	Fe-rich side of the Fe-Cu diagram (based on data from ref.[82])	64
2.18	The effect of copper on (a) equilibrium transformation temperatures and (b) M_s temperature [7]	65
2.19	The effect of copper on the time for 50% isothermal transformation in a medium carbon steel [83]	66
2.20	CCT diagram of COR-TEN steel [7]	66
2.21	CCT diagram for a low-carbon copper-containing steel [34]	68
2.22	The precipitation kinetics (tempering at 500°C) of copper in a Fe-1.4%Cu alloy [74]	72
2.23	(a) Variation in hardness as a function of ageing time and temperature in a low-carbon Nb-Cu steel (b) Ageing characteristics of a plain copper bearing steel and a Cu-Nb steel [89]	76
2.24	The effect of 0.3% Mo addition on the ageing characteristics of a Cu-Ni-Nb steel (a) water-quenched (from 1250°C) and tempered (at 500°C) condition [12] (b) normalised (at 950°C for 30 min) and tempered at 500°C [60]	77
2.25	The effects of varying austenitising temperature on the ultimate tensile and 0.2% offset yield strength for precipitation hardened specimens at either 482 or 538 °C [6]	79
2.26	The effect of tempering on the 0.2% offset yield strength and tensile strength of a water-quenched HSLA-100 steel [36]	81
2.27	Charpy impact transition temperature curves for as-quenched and quenched and aged (a) HSLA-100 steel (b) HSLA-100 steel with increased copper content [36]	81
2.28	The effect of tempering on the 0.2% offset yield strength of a water-quenched (60 min at 950°C) HSLA-100 steel plate (19 mm in thickness) [73]	82
2.29	The relationship between the -84°C impact strength and the yield strength of a water-quenched and tempered HSLA-100 steel plate [73]	82
2.30	The effect of tempering (1 h) of (a) the yield strength and (b) -84°C impact strength, of a water-quenched (60 min at 900°C) HSLA-100 steel plate (25 mm in thickness) [39]	83
3.1	Standard outlook of steel plates used for heat treatments	97
3.2	V-notch impact test specimens (a) Izod (round) (b) Charpy (as used in	

	the present exercise	97
3.3	(a,b) Tensile test specimens.....	98
4.1	(a) Impact transition temperature curves, for quenched and aged steel No1 (b) Impact transition temperature curves for quenched and aged steel 2P1H	115
4.2	Age-hardening behaviour of steel 4P28H, quenched from 720°C and then aged at 60 and 100 °C for various periods of time	117
4.3	Impact transition temperature curves, for quenched and aged 4P28H steel.....	118
4.4	Optical micrograph of steel No1, solution treated at 700°C for 1 h and ice-quenched and then aged at 60°C for 16h	119
4.5	(a) Optical micrograph of steel 4P28H, as-quenched from 720°C	119
4.5	(b) Optical micrograph of steel 4P28H, as-quenched from 720°C, showing carbide precipitation in ferrite.....	120
4.6	Optical micrograph of steel 4P28H, quenched from 720°C and aged at 60°C for 10 h, showing carbide precipitation in ferrite.....	120
4.7	(a,b) Optical micrographs of steel 4P28H, quenched from 720°C and aged at 100°C for 3 h, showing carbide precipitation in ferrite	121
4.8	(a,b) Scanning electron micrographs of steel 4P28H, as-quenched from 720°C	122
4.9	Scanning electron micrographs of steel 4P28H, quenched from 720°C and aged at 60°C for 10 h, showing (a) coarse carbides at grain boundaries and (b) carbide precipitation in the ferrite matrix	123
4.10	Scanning electron micrographs of steel 4P28H, quenched from 720°C and aged at 100°C for 3 h, showing (a) carbides at grain boundaries and in ferrite matrix and (b) coarse carbide precipitation in ferrite matrix	124
4.11	Transmission electron micrographs of steel 4P28H, quenched from 720°C and aged at 60°C for 10 h, showing (a,b) fine precipitation of iron carbides in ferrite matrix and coarse particles at grain boundaries.....	125
	(c,d) grain boundary carbides and fine iron-carbide precipitates, probably coherent	126
	(e,f) fine iron-carbide precipitates and dislocations, in the ferrite matrix	127

4.12	Impact transition temperature curves for quenched and aged steel 4P28H (the tests have been carried out at British Steel [96]).....	128
5.1	Age-hardening effect of tempering, on “normalised” 2P148H, 2P149H and 2P150H steels	158
5.2	Impact transition temperature curves for “normalised” and aged 2P148H steel.....	159
5.3	Impact transition temperature curves for “normalised” and aged 2P149H steel.....	160
5.4	Impact transition temperature curves for “normalised” and aged 2P150H steel.....	161
5.5	(a) Optical micrograph of “normalised” copper-free steel.....	162
5.5	(b) Optical micrograph of the NT525 copper-free steel, showing banding ...	162
5.6	(a,b) Optical micrographs of the NT525 1.22% Cu-steel	163
5.7	(a) Optical micrograph of the NT650, 2.02% Cu-steel	164
	(b) Optical micrograph of the NT650, 2.02% Cu-steel, showing the banding effect and the variation in ferrite shade	164
5.8	(a,b) Scanning electron micrographs showing pearlite colonies of the “normalised”, copper-free steel.....	165
5.9	Scanning electron micrograph of the NT525, copper-free steel, showing a pearlite colony	166
5.10	(a,b) Scanning electron micrographs of NT650, copper-free steel, showing spheroidised pearlite and carbides	166
5.11	Scanning electron micrograph, showing carbides at the grain boundaries of a “normalised” (N), copper-free steel.....	167
5.12	(a,b) Scanning electron micrograph, showing a fine and long grain boundary carbide of the copper-free steel, in the “normalised” condition.....	168
5.13	Scanning electron micrograph of NT525, copper-free steel; showing fine grain boundary carbides	169
5.14	Scanning electron micrograph, showing grain boundary carbides of “normalised” 1.22% Cu-steel	169
5.15	Scanning electron micrograph, showing pearlite colonies of the “normalised”, 1.22% Cu-steel	170
5.16	(a,b) Scanning electron micrograph, showing ghost boundaries formed by fine particles, on the ferrite matrix of “normalised”, 1.22% Cu-steel	170

5.17	Scanning electron micrograph, showing the shade difference between adjacent ferrite grains, of “normalised” and fully-aged (NT525) 1.22% Cu-steel.....	171
5.18	Scanning electron micrographs of “normalised” and over-aged (NT650), 1.22% Cu-steel, showing (a) spheroidised pearlite (b) unaffected pearlite	172
5.19	Scanning electron micrograph, showing grain boundary carbides of the 1.22% Cu-steel, in the over-aged condition (NT650)	173
5.20	Scanning electron micrograph, showing a network of fine particles and very fine grain boundary particles, of the “normalised” and over-aged 1.22% Cu-steel.....	173
5.21	Scanning electron micrographs, showing very fine grain boundary particles and ferrite grains of the 2.02% Cu-steel, saturated with precipitation particles: (a) N condition (b) NT550 condition.....	174
5.22	Scanning electron micrographs showing carbides at the grain boundaries of 2.02% Cu-steel. (a) N condition (b) NT650 condition.....	175
5.23	(a,b) Scanning electron micrographs showing ferrite grains of different shade, 2.02% Cu-steel, in the “normalised” and fully-aged (NT550) condition	176
5.24	Scanning electron micrographs, showing the effect of tempering on the pearlite phase of 2.02% Cu-steel (a) as “normalised” (N) condition (b) over-aged (NT650) condition	177
5.25	TEM of thin foil, showing copper precipitation, in the as “normalised” 1.22% Cu-steel.....	178
5.26	TEM of thin foil, showing copper precipitation, in the fully-aged 1.22% Cu-steel.....	178
5.27	(a,b) Transmission electron micrographs, showing copper precipitation in the as “normalised” 2.02% Cu steel (thin foils).....	178
5.28	(a,b) TEM of thin foils, showing the intensity of copper precipitation, in the NT550 condition of 2.02% Cu-steel	179
5.29	(a,b) TEM of thin foils, showing copper precipitates of the 2.02% Cu-steel, in the fully-aged condition (NT550).....	180
5.30	(a,b,c,d) Transmission electron micrographs of thin foils, showing copper precipitation, in the “normalised” and over-aged 2.02% Cu-steel.....	181

5.31	TEM (thin foil) of vermiculite-cooled and tempered, (NT700), 2.02% Cu-steel, showing (a) the intensity of precipitation (thin foil) (b,c) the morphology of copper precipitates (thin foil).....	182
5.32	(a,b) TEM of NT700, 2.02% Cu-steel, that has been strained by 15%, showing precipitates surrounded by dislocations (thin foil)	183
5.33	TEM of NT700, 2.02% Cu-steel that has been strained by 15% (thin foil) ...	184
5.34	TEM of NT700, 2.02% Cu-steel that has been strained by 15%, showing elongated copper particles (thin foil)	185
5.35	TEM of NT700, 2.02% Cu-steel that has been strained by 15%, showing deformed particles (thin foil)	186
5.36	(a,b,c) TEM of air-cooled (after austenitising at 910°C for 30 min), 2.02% Cu-steel, showing copper precipitation (thin foil)	187
5.37	Comparison between calculated and observed LYS.....	188
5.38	Comparison between observed and calculated 50% FATT values	188
5.39	Comparison between observed and calculated 54J ITT values	189
5.40	Comparison between observed and calculated 27J ITT values	189
5.41	The variation of the observed impact transition temperatures as a function of the observed lower yield strength, of steels 2P148H, 2P149H and 2P150H	190
6.1	Age-hardening effect of tempering on normalised and quenched 1P140M steel.....	224
6.2	Impact transition temperature curves for normalised and tempered 1P140M steel.....	225
6.3	Impact transition temperature curves for quenched and tempered 1P140M steel.....	226
6.4	Fibrous appearance transition temperature curves for normalised and tempered 1P140M steel.....	227
6.5	Optical micrograph of the as-normalised 1.26% Cu-steel.....	228
6.6	Optical micrograph of the as-normalised 1.26% Cu-steel.....	228
6.7	The distinction between the ferrite and the second phase in the normalised and aged (at 200°C for 1h)1.26% Cu steel (light etching, optical micrograph).....	229
6.8	The darkening of the second phase after tempering the normalised 1.26% Cu-steel at 550°C for 1h. (Optical micrograph).....	229
6.9	Optical micrograph of sample (NT550), 1.26% Cu-steel.....	230

6.10	Optical micrograph of the normalised and over-aged 1.26%-Cu steel plate, (NT650)	230
6.11	Optical micrograph of the oil-quenched 1.26% Cu-steel	231
6.12	Quenched and fully-aged (QT500) microstructure of 1.26% Cu-steel.....	231
6.13	Optical micrograph showing the darkening of the martensite after tempering the quenched 1.26% Cu-steel at 650°C for 1 h, (optical micrograph).....	232
6.14	Scanning electron micrograph showing the microstructure of the as-normalised 1.26% Cu-steel.....	232
6.15	Scanning electron micrographs of the as-normalised (N) 1.26% Cu steel, showing: (a) a group of martensite-austenite islands (b) coarse precipitation -possibly copper- in the ferrite matrix and in the (MA) constituent	233
6.16	Scanning electron micrograph of the as-normalised 1.26% steel, showing a coarse martensite colony.....	234
6.17	Scanning electron micrograph, showing coarse grain boundary particles, in the as-normalised 1.26% Cu-steel	234
6.18	Scanning electron micrograph of the normalised and fully-aged 1.26% Cu-steel (NT550), showing tempered (MA) particles	235
6.19	Scanning electron micrographs of (NT550) 1.26% Cu-steel, showing groups of (MA) islands: (a) fully tempered	235
	(b) unaffected by the tempering treatment.....	236
6.20	Scanning electron micrograph of the (NT550) 1.26% Cu-steel, showing two (MA) particles, one showing carbide precipitation, the other being unaffected by tempering	236
6.21	Scanning electron micrograph of normalised and over-aged 1.26% Cu-steel (NT650), showing carbide precipitation from a tempered martensitic particle.....	237
6.22	Scanning electron micrograph, of the 1.26% Cu-steel in the normalised and over-aged condition (NT650)	237
6.23	Scanning electron micrograph of sample (NT650), 1.26% Cu-steel, showing the increased number of grain boundary carbides	238
6.24	Scanning electron micrograph, of the as-quenched (Q), 1.26% Cu-steel	238
6.25	Scanning electron micrographs, showing (MA) particles, in the as-quenched 1.26% Cu-steel	239

6.26	Scanning electron micrograph of the as-quenched (Q) 1.26% Cu-steel, showing the arrangement of ferrite laths and (MA) particles.....	240
6.27	Scanning electron micrograph of the quenched and fully-aged (tempered at 500°C for 1 h) 1.26% Cu-steel, showing carbide precipitation from a martensitic particle.....	240
6.28	Scanning electron micrograph of the quenched and fully-aged 1.26% Cu-steel (QT500), showing evidence of copper precipitation.....	241
6.29	Scanning electron micrograph of the (QT500) condition, 1.26% Cu-steel, showing a martensitic particle unaffected by tempering.....	241
6.30	Scanning electron micrographs of the 1.26% Cu-steel plate, showing complete carbide precipitation of the (MA) particles after tempering the quenched sample at 650°C for 1h	242
6.31	Transmission electron micrographs (replica) of the as-normalised 1.26% Cu-steel. The coarse precipitates are Cu, the fine are Nb(CN).....	243
6.32	Transmission electron micrograph (replica), showing copper precipitation in the normalised and fully-aged (NT550) 1.26% Cu-steel.....	244
6.33	Transmission electron micrographs (replica) of the normalised and over-aged (NT650) 1.26% Cu-steel, showing : (a) Cu and Nb(CN) precipitation 244 (b) Cu and Nb(CN) precipitation and grain boundary carbides	245
	(c) grain boundary particles and Nb(CN) precipitates	245
6.34	Transmission electron micrograph (replica) showing copper precipitation in the as-quenched (Q) condition of 1.26% Cu-steel	246
6.35	Transmission electron micrograph (replica), showing coarse Cu and fine Nb(CN) precipitates in the quenched and fully-aged condition, (QT500), of 1.26% Cu-steel plate	247
6.36	Transmission electron micrographs (replica) of the quenched and over-aged (QT650) 1.26% Cu-steel plate showing Cu and Nb(CN) precipitation. 247	
6.37	The variation of the observed impact transition temperatures as a function of the observed lower yield strength, of steel 1P140M. (a) Recorded values	249
	(b) Corrected values to account for the presence of martensite in the non-aged and fully-tempered conditions.....	249
6.38	The relationship between impact transition temperature improvement and copper precipitate size (a) 54J ITT criterion (b) 27J ITT criterion.....	250

LIST OF SYMBOLS AND ABBREVIATIONS

ASTM	American Standard of Materials
HSLA	High Strength Low Alloy
b	Burger's vector
σ_y	yield stress
d	mean linear intercept of the ferrite grain size
k_y	dislocation locking term
σ_o	strengthening parameter
σ_s	solid solution strengthening term
σ_d	dislocation strengthening term
σ_{ss}	sub-structure strengthening term
σ_t	texture strengthening term
σ_p	precipitation strengthening term
σ_f	friction stress opposing dislocation motion
σ_b	low angle lath boundaries strengthening term
σ	applied stress
GP	Guinier-Preston
θ'	coherent precipitate in the Al-4%Cu alloy system
θ	stable incoherent AlCu ₂ precipitate
f	volume fraction of precipitate
ϕ	angle between bowing dislocations
μ	shear modulus of matrix
μ'	shear modulus of precipitate
F	shearing force
λ	precipitate interparticle spacing
T_d	dislocation line tension
n_A	number of precipitates per unit area
L	square array precipitate spacing
c	crack length
E	Young's modulus
G	strain energy release rate
γ	surface energy
γ_p	plastic work
T_c or ITT	Impact Transition Temperature

K	stress intensity factor
K_c	critical stress intensity factor
BCC	body centre cubic
FCC	face centre cubic
τ	shear stress
n	number of dislocations
FATT	Fibrous appearance Transition Temperature
t_c	grain boundary carbide thickness
Δy	precipitation hardening component
N_f	free nitrogen content
x	mean planar intercept diameter of precipitates
%p	pearlite volume fraction
CR	Cooling Rate
(MA)	Martensite-Austenite constituent
d_L	mean linear intercept of the bainitic ferrite grain size
ρ	dislocation density
λ_c	carbide spacing
D	carbide particle diameter
ϵ -Cu	face centre cubic incoherent copper precipitate
HP	Holloman-Jaffe Parameter
k_h	Holloman-Jaffe Parameter constant
A_{e3}	Austenite \rightarrow ferrite transformation temperature (austenite ends)
M_s	Martensite start temperature
INCO	International Nickel Company
α -Fe	body centre cubic ferrite
γ -Fe	face centre cubic ferrite
CCT	continuous cooling transformation diagram
D_f	volume diffusion coefficient
G_c	chemical strain energy
G_E	strain energy of nucleation
ι	number of atoms in a nucleus
OM	Optical Microscope
SEM	Scanning Electron Microscope
TEM	Transmission Electron Microscope
LYS	Lower Yield Stress

UTS	Ultimate Tensile Stress
% ϵ	percentage elongation
%RA	percentage Reduction in Area
Hr	Hardness
HV10	Vickers Hardness (10kg weight)
PS	Proof Stress
δ LYS	difference between observed and predicted lower yield strength
δ ITT	difference between observed and predicted impact transition temperature
obs	observed
calc	calculated
t_m	thickness of martensitic particles situated at ferrite grain boundaries
t_{cm}	grain boundary particle thickness
l_p	precipitate length
d_p	precipitate diameter
t_p	precipitate thickness
Q	As-quenched
QA60	Quenched and Aged at 60°C
QA100	Quenched and Aged at 100°C (3h)
N	As normalised
NT525	Normalised and Tempered at 525°C (1h)
NT550	Normalised and Tempered at 550°C (1h)
NT650	Normalised and Tempered at 650°C (1h)
NT700	Normalised and Tempered at 700°C (1h)
QT500	Quenched and Tempered at 500°C (1h)
QT650	Quenched and Tempered at 650°C (1h)

ACKNOWLEDGEMENTS

My special thanks are due to my supervisor, Prof. B. Mintz, for his guidance and support throughout the project and the writing-up of this thesis.

I am grateful to British Steel Corporation for the financial support of the project, the supply and machining of steels and the permission to use their laboratory and library facilities. Thanks are also due to the technical staff of B.S.C. Swindon Laboratories, especially to Dr. D. Crowther for assisting me in TEM work.

I acknowledge with thanks the financial support of my studies given by the Worshipful Company of Saddlers (Robert Kitchin award) and the A.G. Leventis Foundation.

I would also like to express my sincere thanks to Prof. A.R.D. Thorley for the provision of laboratory facilities and to the staff of the Department of Mechanical Engineering, in particular to Mr. R. Vipond who has never denied to offer his advice when needed and to Mr. T. Rose for all his help with the laboratory work.

Last but not least, my thanks are due to my family and my husband for their support and to friends and colleagues who have helped me to complete this work: Dr. R. Abu-Shosha for her valuable help with the preparation and examination of TEM replicas, Dr. H. Mehrabi for his help during my first steps in metallography and Dr. A. Nassar for his help during the high temperature impact tests in chapter 4. I would also like to express my appreciation to Mr. S. Khan, Mr. A.K. Razavi and Mr. H. Rajabali for checking the grammar of the thesis text.

DECLARATION

I grant powers of discretion to the University Librarian to allow this thesis to be copied in whole or in part without further reference to me. This permission covers only single copies made for study purposes, subject to normal conditions of acknowledgement.

ABSTRACT

The influence of copper on the structure and the mechanical properties of low carbon steels has been examined. The investigation included three sets of heat treated steels as follows.

- Three very low-C, Mn-Al steel plates have been quenched in ice-brine and aged at 60 and 100°C for various periods of time in order to obtain the age-hardening behaviour. The purpose of this exercise has been the examination of a simple age-hardening system before proceeding to the more complex Cu-containing steels. The mechanical properties and structure of the steels have been examined for the as-quenched, the quenched and fully-aged and the quenched and over-aged conditions. In all conditions the steel microstructure consisted of polygonal ferrite the size of which did not vary with ageing. The yield strength of the steels has been found to increase after ageing at peak hardness and then reach a minimum value after over-ageing. There have not been any significant changes on the impact transition temperatures after ageing the steel. The relative insensitivity of impact transition temperatures to ageing has been attributed to the presence of coherent iron-carbide precipitates.
- The age-hardening behaviour and structure-property relationships of three simple low-C, Mn-Al steel plates with 0%, 1.22% and 2.02% Cu content have been examined. The steels were austenitised at 910°C for 1/2 h and slowly cooled (5°C/min) to produce a ferrite-pearlite microstructure and then tempered at various temperatures for 1 h. The copper-free steel did not show any structural or property changes on tempering whereas the two copper steels showed peak strength and hardness after tempering at 525-500°C. The impact transition temperatures were observed to rise, but analysis of the results has indicated that the increase was much lower than expected. The best combination of yield strength and impact properties was given by the 2.02% Cu steel in the over-aged condition (ageing at 650°C for 1 h). SEM and TEM examination has confirmed the presence of a coarse copper precipitate which is incoherent with the matrix in all the steel conditions. Numerical analysis of the yield strength results has shown that there is a constant vector of precipitation strengthening due to the presence of incoherent precipitation and this is in accord with the Ashby-Orowan strengthening model.
- A 1.26% Cu-containing steel plate of commercial composition has been examined. The steel was austenitised at 920°C for 1/2 h, cooled either in air or in oil and tempered as in the case of the simple copper containing steels. The prime phase of the microstructure was ferritic with 10-20% martensite and retained austenite. TEM examination has confirmed the presence of coarse incoherent copper precipitates and finer niobium-carbide precipitates in all the steel conditions. The mechanical properties of this steel were largely influenced by the presence of martensite, however when this was accounted for, the analysis of the results showed that as in the case of the simpler copper containing steels, the presence of copper precipitates leads to good impact performance.

The relative improvement of the impact transition temperatures of the copper containing steels has been attributed to the ability of the copper precipitates to deform. This has been verified by straining an over-aged 2.02% Cu sample at 15% plastic deformation. Finally, it has been observed that for a given copper content, a fine dispersion of the incoherent copper precipitate is more preferable than a coarse one. The presence of the coherent copper precipitation has also been found to enhance the favourable effect of the incoherent precipitate on the impact transition temperatures.

1

INTRODUCTION

The decline of petroleum resources from conventional sources has led to an ever-increasing demand for the development of frontier oil and gas. This imposes tremendous challenges to the pipeline industry for safe and economical transportation of hydrocarbons from distant and environmentally sensitive Arctic regions [1]. The steel needed, is required to be strong and tough yet weldable, imposing restrictions on carbon levels. The recent development of High-Strength Low-Alloy (HSLA) steels seems to be a good answer to the above demand. Specifically, a family of HSLA steels have been developed which contain low carbon and high copper levels. These steels are age-hardenable and can combine good impact properties with high strength. The first such commercial steel was developed by INCO, IN-787, and contains nickel and copper as its major microalloying additions. A more recently developed copper-steel is the NI-COP alloy steel which was developed by ARMCO and conforms to ASTM standards, specification A710.

Typical yield strengths of ASTM A710 (Grade A) steel, range from 415 to 585 MPa for the precipitation treated alloy which had been previously hot rolled, normalised or quenched for a thickness of up to 50.8 mm. Notch toughness requirements specify a

minimum of 20 to 27J at -51°C for the rolled and heat treated condition, -73°C for the normalised and precipitation treated condition and -101°C for the quenched and precipitation treated condition. However, some authors [2,3] have reported improved tensile/impact combinations for the normalised and aged NI-COP steel, giving transition temperatures as low as -105°C at 47J for a 0.2% offset yield strength of 501 MPa.

Whereas most strengthening methods have an adverse effect on the impact behaviour of a steel by increasing the impact transition temperature (ITT) [4], the copper containing steels seem to retain their impact properties after strengthening [2,5]. This raises justified questions as to how the copper has a favourable effect upon strengthening and yet does not influence impact behaviour. One explanation for this exceptional combination of strength and impact behaviour is that the size and coherency of the copper precipitates may be such that a dislocation can easily move past the precipitates, rather than shear it, and so encourages cross-slip [6]. This results in a more uniform slip distribution throughout each grain, resulting in good toughness.

The unquestionable qualities of the steels mentioned above, in addition to the positive effect of copper on corrosion resistance [5,7], have resulted in the replacement of HY-80 and HY-100 steels [6] which used to dominate the Arctic, for line-pipes and many structural and naval applications.

However, despite the fact that low-carbon, copper HSLA steels have been successfully used over a wide range of applications, the exact reasons for their exceptional tensile/impact properties have not yet been established. Although extensive research has been carried out during the last thirty years, this has not resulted in a unique theoretical explanation. On one hand, industry seems to exploit the benefits of copper containing steels by exploring manufacturing processes that will improve existing ones, whereas scientific research tends to concentrate either on copper precipitation or on mechanical properties. There is very little work attempting to interrelate both aspects. There is a need, therefore, to establish structure-property relationships in copper HSLA steels.

2

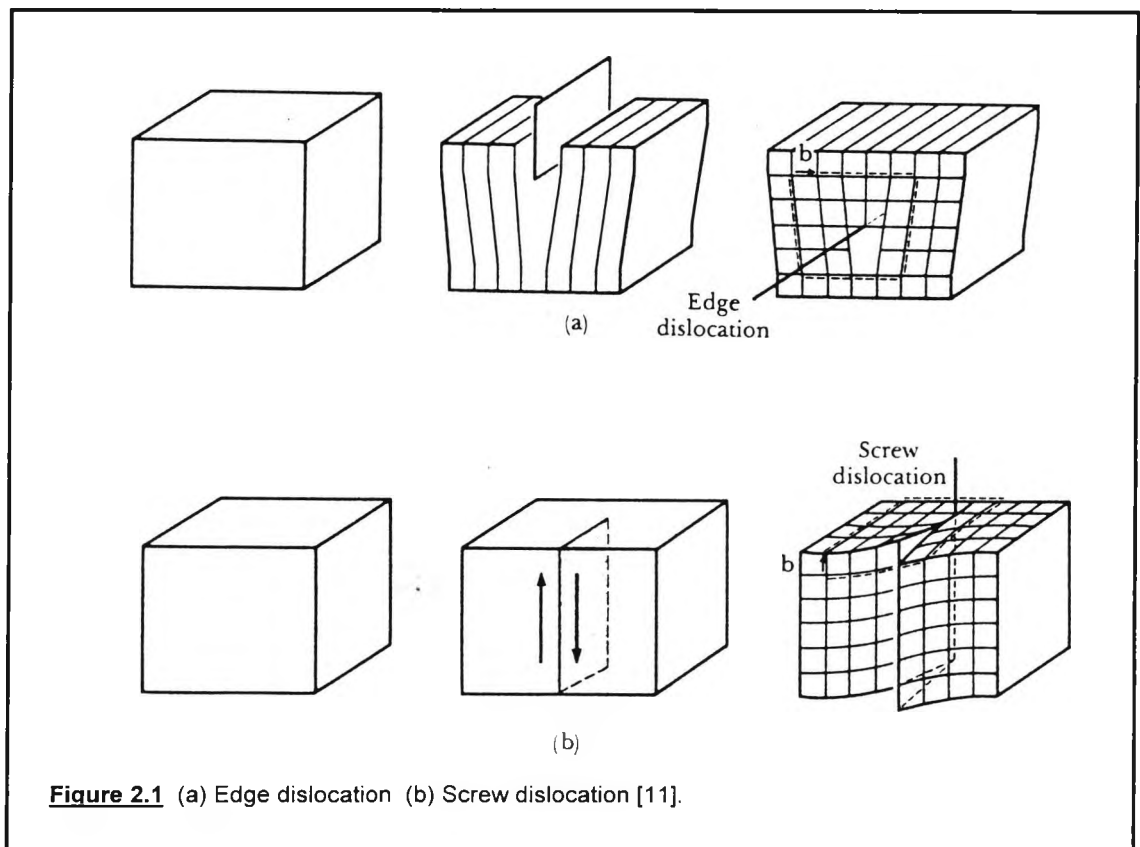
LITERATURE SURVEY

Having underlined the importance of structure-property relationships, it is wise to control the metal structure in order to achieve desirable mechanical properties. This literature survey, therefore, refers to the basic aspects of metal structure, key mechanisms of strengthening such as dislocations and of course impact behaviour. There is also a considerable review of past work on the age-hardening (precipitation hardening) behaviour of low carbon steels. The review concludes with a detailed reference to the effect of copper on the structure and the mechanical properties of steels, which again is based on previous laboratory and commercial research.

2.1 Strengthening mechanisms in steels

The best known mechanism of controlling metal and alloy strength is by taking advantage of their lattice imperfections. All materials contain faults in their atomic arrangement such as point defects (interstitial atoms), surface defects (grain boundaries) and line defects (dislocations). These defects can be controlled in such a way as to increase strength, the dislocations being one of the most important methods.

Dislocations are line imperfections in an otherwise perfect lattice. There are two types of dislocations. One is the edge dislocation which is introduced into the lattice by adding an extra half plane of atoms, Figure 2.1 (a), and the other is the screw dislocation which is produced by skewing a crystal so that one atomic plane produces a spiral ramp about the dislocations, Figure 2.1 (b). The direction and distance that a dislocation moves in each step is called Burgers vector, b . In edge dislocations, the Burger vector is perpendicular to the dislocation whereas in a screw dislocation it is parallel to the dislocation. The reason that dislocations are very important, is that their movement, *slip*, affects the deformation of metals and therefore their mechanical properties. Extensive work has been carried out in the last three decades about the importance of dislocations and authors such as Cottrell, Friedel, Hirsch, Hirth and Nabarro [8,910] have written excellent literature surveys on this subject.



Successful control of the slip process can provide stronger materials. When a crystal has imperfections, the local energy is increased because near the imperfection, the atoms are either squeezed too closely together or are forced apart. Thus, a higher stress is required to force a dislocation past the region of high local energy, i.e. the material is stronger. Strengthening mechanisms that take advantage of lattice

imperfections are strain hardening, solid solution strengthening and grain size strengthening. Of course there are other strengthening methods such as precipitation or dispersion strengthening, substructure formation and dispersion of a second phase. The most important mechanisms are briefly described below concentrating particularly on precipitation hardening.

2.1.1 Strain hardening

Strain hardening or work hardening is the strengthening of a material by increasing the number of dislocations by deformation (cold work). When a stress higher than the yield strength is applied, the dislocations begin to slip. Eventually a dislocation moving on its slip plane encounters obstacles that pin the ends of the dislocation line. As the stress continues to be applied, the dislocation attempts to move by bowing in the centre. The dislocation may move so far that a loop is produced. When the loop finally touches itself, a new dislocation is created. The original dislocation is still pinned and can create additional dislocation loops. This multiplication mechanism is called a *Frank-Read* source. The more dislocations present in the structure, the more likely they are to interact with one another, and the stronger the metal becomes [11].

2.1.2 Solid solution strengthening

Solid solution strengthening increases the strength of a material by introducing point defects into the structure in a deliberate and controlled manner. This method is sometimes termed matrix strengthening and is an effective way to increase the resistance of a metal to the motion of a dislocation. Pure metals have low yield stresses and substitutional atoms cause a stress field to be set up around each impurity atom. These stress fields (negative in some places and positive in others) interact with dislocations and impede their motion. The final result is dislocation bending and extension since the stress fields mentioned above never balance. The magnitude of the strengthening effect is a function of the binding energy between the solute atom and the dislocation, and of the solute concentration. Thus, the strengthening increment depends on the amount of solute in the matrix and is limited by the maximum amount which can be maintained in solution [12].

2.1.3 Grain size strengthening

One method of controlling the properties of a material through its structure is through controlling the grain size. By reducing the grain size, we increase the number of grains

and hence increase the amount of grain boundary. A dislocation may then move only a short distance before encountering a grain boundary hence increasing the metal strength. The Hall-Petch equation relates the grain size to the yield strength of the metal.

$$\sigma_y = \sigma_o + k_y * d^{-1/2} \quad \dots(2.1)$$

where σ_y is the stress at which the material permanently deforms, d is the average diameter of the grains, and σ_o and k_y are constants for the metal. The term σ_o often contains other strengthening parameters such as: σ_i the friction stress opposing dislocation motion, σ_s the solid solution strengthening, σ_p the precipitation strengthening, σ_d the dislocation strengthening, σ_{ss} the sub-structure strengthening and σ_t the crystallographic texture strengthening parameter. The other constant, k_y , is related to the difficulty of unlocking dislocations, or of activating dislocation sources at grain boundaries, sometimes called the dislocation locking term.

The Hall-Petch equation is of great importance since it gives an accurate, direct and quantitative relationship between yield strength and structure.

The main ways by which the microstructure can be refined are: **1)** thermomechanical working, **2)** controlled cooling and **3)** alloying. The first and last methods refine austenite which leads to a subsequent ferrite refinement, whilst the second refines ferrite by restricting the diffusion process during the transformation of austenite to ferrite.

2.1.4 Substructure formation

Substructure formation can occur when a metal is heat treated after cold work. Referred to as annealing, this treatment is given to metals after cold work to recover their original properties. The first stage of annealing is the recovery stage and is chiefly concerned with the rearrangement of the dense dislocation networks to reduce the lattice energy and does not involve the migration of large angle boundaries. One of the most important recovery processes which leads to a resultant lowering of the lattice strain energy, is the rearrangement of the dislocations into cell walls. This is termed *polygonization*, during which dislocations all of one sign align themselves into walls to form small-angle or sub-grain boundaries. The basic movement is climb whereby the

edge dislocations change their arrangement from a horizontal to a vertical grouping. This process involves the migration of vacancies to or from the edge of the half-planes of the dislocations.

The above description may seem simple but is in fact very complex and a variety of models have been developed which relate the strength of the material to the scale of the sub-structure developed during plastic flow in a manner analogous to the description of the influence of the grain size on the flow properties of polycrystals developed by Petch [13,14].

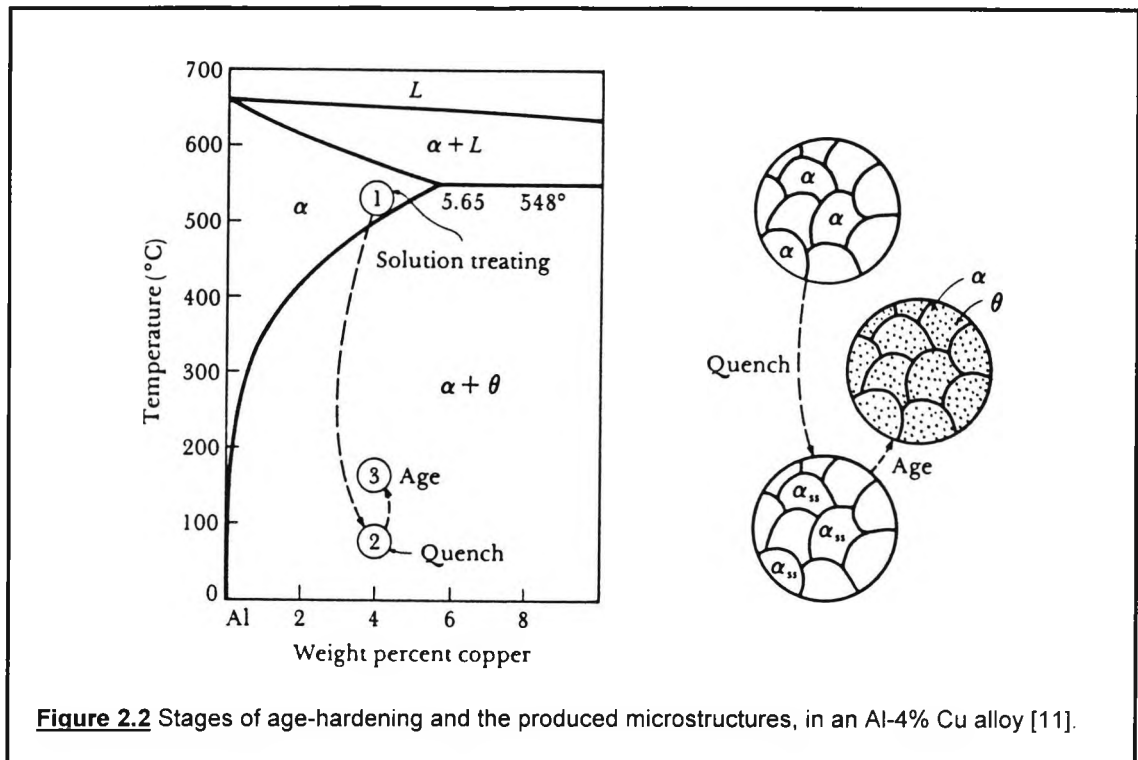
2.1.5 Dispersion of a second phase

Many two-phase steel alloys of technical interest consist of a coarse, hard constituent embedded in a relatively soft, ductile matrix phase. In general, the hard constituent contributes strength and hardness, and the ductile matrix supplies ductility and toughness. The limits of the composition of this class of alloys range from approximately 5 to 95 %vol. of the hard phase, encompassing, for example, pearlitic or spheroidized steels (ferrite-pearlite, ferrite-cementite) and dual-phase steels (ferrite-martensite). At the low end of the composition range, the hard phase serves to increase the flow strength of basically tough metals; this is, for instance, the role of cementite in mild steels. At the other end of the composition range, the function of the ductile matrix is to incorporate a minimum of toughness into hard, but inherently brittle, materials. Some of the alloys of intermediate composition, such as the dual-phase steels, offer an interesting combination of high strength with good ductility.

2.1.6 Precipitation strengthening

Precipitation strengthening or age hardening is a special dispersion strengthening heat treatment. Niobium, titanium, vanadium and copper are common alloying elements that are added to the steel composition in order to promote precipitation hardening.

Although the principal subject of this research is steel and its alloys, it would be more appropriate to use an aluminium alloy system in order to explain the whole process since this strengthening method was first developed in that system. A typical example of an age-hardenable alloy is the Al-4%Cu alloy. Extensive reference to this strengthening method will be made in this chapter since its influence on microstructure and mechanical properties are the major subjects of this research.



Solution treatment is the first step of the process and it involves heating the alloy to a temperature above the solvus and soaking it there until a homogeneous solid solution α is produced, Figure 2.2. Copper is dissolved during this stage. The second step is the rapid cooling, or quenching of the alloy which prevents copper atoms from diffusing to nucleation sites and therefore prohibits precipitation. This results in α being a supersaturated solid solution that contains excess copper. This is a non-equilibrium structure. Finally, the alloy is heated at a temperature below the solvus line and this gives the opportunity to copper atoms to diffuse at short distances. This stage, is a controlled decomposition of the supersaturated solid solution, to form a finely dispersed precipitate, and is termed as ageing. The temperatures and times used, affect the final properties of the alloy, Figure 2.3, [11].

Ageing is a complex process during which several stages take place [13]. A continuous series of precipitates form before the equilibrium θ is produced. At the start of ageing, the copper atoms cluster on $\{100\}$ planes in the α -matrix producing very thin precipitates called *Guinier-Preston*, or **GP-I** zones. These may be only one or two atom planes in thickness, they retain the structure of the matrix and are coherent with it, although they usually produce appreciable elastic strains, Figure 2.4(a). They are

also very finely dispersed in the matrix in high densities since the Cu atoms move only very short distances. As ageing continues, more copper atoms diffuse to the precipitates and the **GP-I** zones thicken into thin disks, the **GP-II** zones. With continued diffusion, the precipitates develop a greater degree of order and are called θ' . During the stages mentioned above, the strength and hardness of the alloy increase, Figure 2.3, until they reach a peak, this condition is termed as the *fully-aged* condition. Finally, if ageing is continued, the stable θ precipitate is produced. The intermediate precipitate is normally much larger in size than the **GP** zones and is only partly coherent with the lattice planes of the matrix. It has a definite composition and crystal structure which may differ only slightly from those of the equilibrium precipitate. In some alloys, the intermediate precipitate may be nucleated from, or at, the sites of stable **GP** zones. In others, this phase nucleates heterogeneously at lattice defects such as dislocations. Formation of the final equilibrium precipitate results in complete loss of coherency with the matrix, Figure 2.4(b). Now the alloy is in the *over-aged* condition and its strength and hardness decrease.

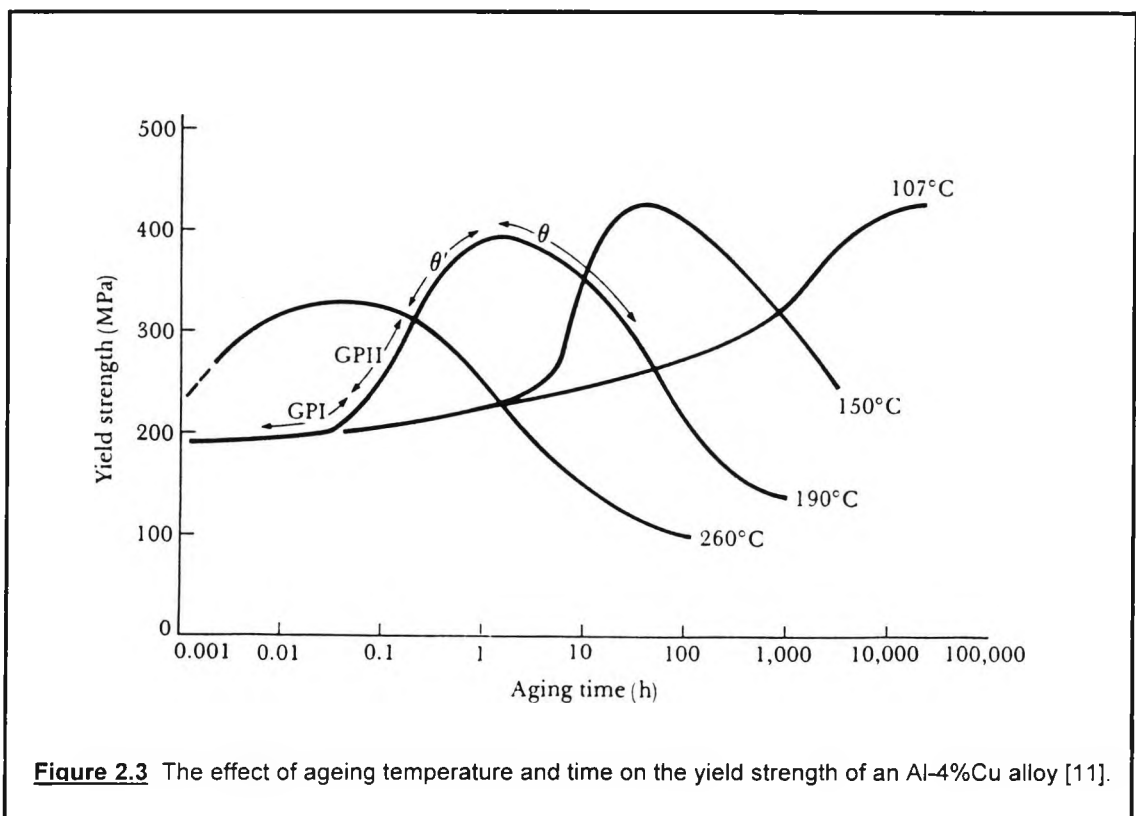
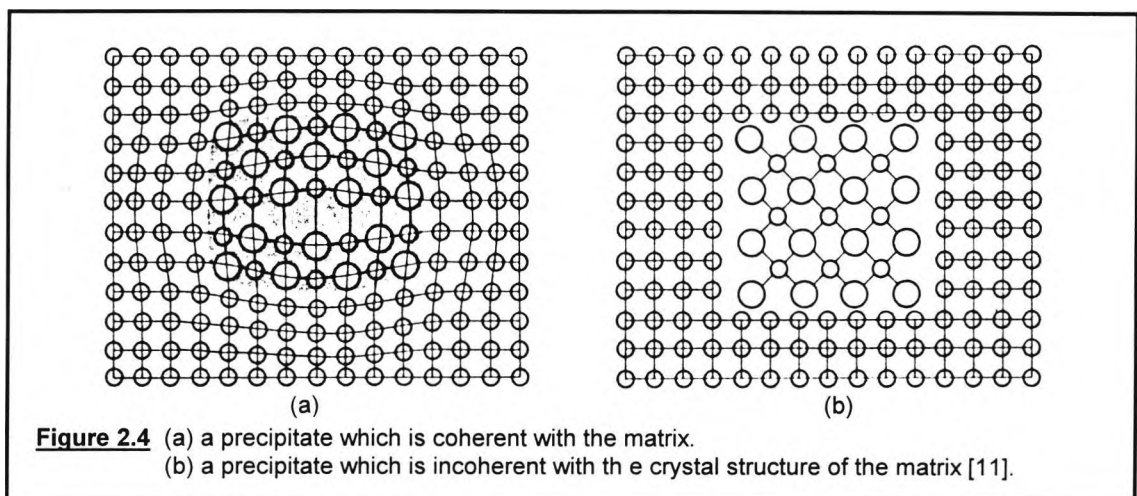


Figure 2.3 The effect of ageing temperature and time on the yield strength of an Al-4%Cu alloy [11].

Although early attempts to explain the mechanisms that govern age-hardening were limited by a lack of experimental data, two important concepts were postulated [13]: one was that hardening is the result of interference to slip by particles precipitating on

crystallographic planes and the other was that maximum hardening is associated with a critical particle size. Modern concepts of precipitation hardening are essentially the consideration of these two ideas in relation to dislocation theory, since the strength of an age-hardenable alloy is controlled by the interaction of moving dislocations with precipitates [13].



The obstacles in precipitation hardening alloys which hinder the motion of dislocations may be either: 1) the internal strains around GP zones, 2) the zones or precipitates themselves, or both [15]. Clearly, if it is the zones themselves which are important, it will be necessary for the moving dislocations to either cut through them or go round them. Hence, it would appear that there are at least three causes of hardening [15]:

- internal strain hardening,
- chemical hardening, i.e. when the dislocation cuts through the precipitate, or
- dispersion hardening, i.e. when the dislocation goes round or over the precipitate.

2.1.6.1 Internal strain hardening

The internal strain hardening mechanism, originally suggested by Mott and Nabarro, is based on the knowledge that the precipitation of particles having a slight misfit in the matrix gives rise to internal stress fields which hinder the movement of moving dislocations [15]. For the dislocations to pass through the regions of internal stress, the applied stress must be at least equal to the average internal stress. It has been shown [15] that maximum impedance to the dislocation motion, i.e. maximum hardening is to be expected when the spacing between particles is equal to the limiting radius of curvature of moving dislocation lines, about 50 atomic spacings. When such conditions exist, the dislocations can avoid the obstacles by taking a form like that

shown in Figure 2.5(a). With a dislocation line taking such a configuration, each section of the dislocation line has to be taken over the adverse region of internal stress without any help from other sections of the line; the alloy is then hard. If the precipitate is dispersed on too fine a scale (under-aged) the dislocation is unable to bend sufficiently to lie entirely in the regions of low internal stress. Instead it has to ride over the stress field in such a manner that the dislocations sometimes lies on top of the potential hills and sometimes in the valleys. As a result, the internal stresses acting on the dislocation line largely cancel and the force resisting its movement is small; the alloy then appears soft [15]. When the dispersion is on a coarse scale, the dislocation line is thought to move or bow between the particles by a mechanism first proposed by Orowan [16], shown in Figure 2.5(b), and the hardening is again small.

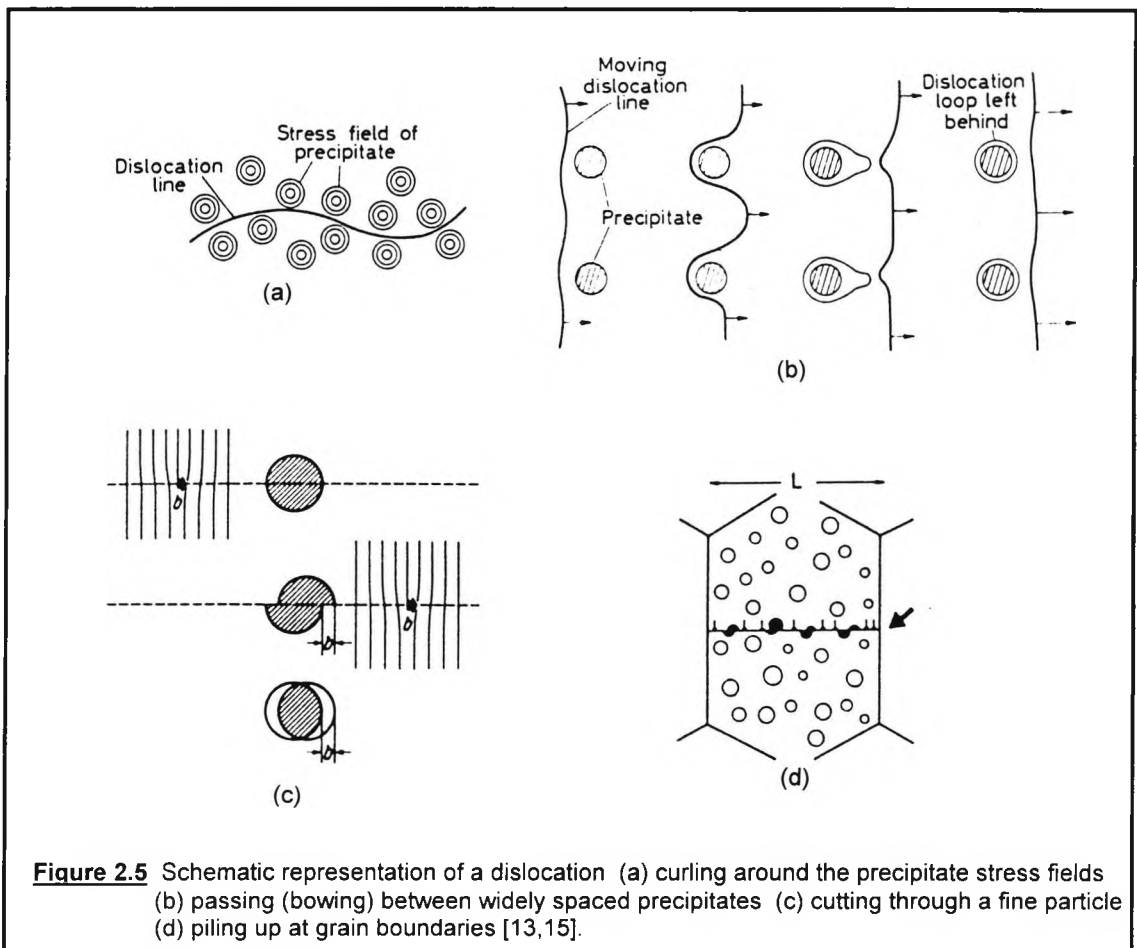


Figure 2.5 Schematic representation of a dislocation (a) curling around the precipitate stress fields (b) passing (bowing) between widely spaced precipitates (c) cutting through a fine particle (d) piling up at grain boundaries [13,15].

2.1.6.2 Chemical hardening

When a dislocation actually passes through a zone, the number of solvent-solute bonds increases across the slip planes in the manner depicted in Figure 2.5(c). This tends to reverse the process of clustering and, hence, additional work must be done by the applied stress to bring this about. The magnitude of the applied stress is controlled by factors such as the relative atomic sizes of the atoms concerned and the difference in stacking fault energy between matrix and precipitate [13]. This process, known as chemical hardening, then provides a short-range interaction between dislocations and precipitates and involves disruption of the atomic bonds at the surface and inside the precipitate [15].

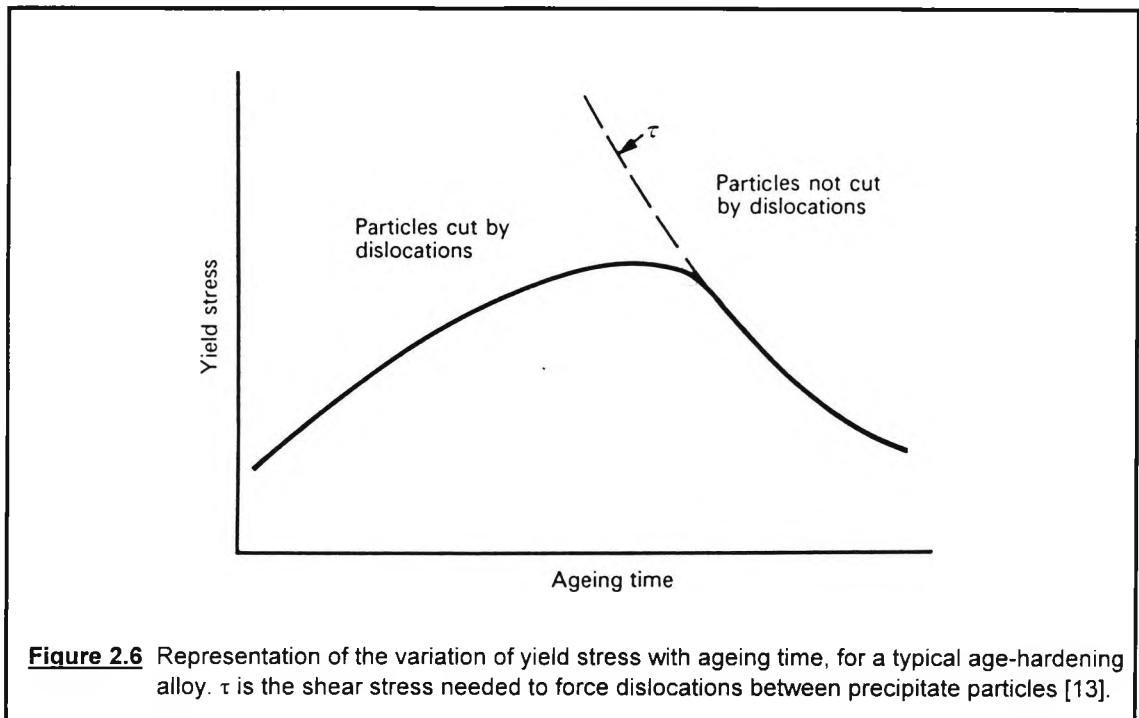
Once the GP zones are cut, the dislocations continue to pass through the particles on the active slip planes and work hardening is comparatively small [13]. Deformation tends to become localised on only a few active slip planes so that some intense bands develop which allow dislocations to pile up at grain boundaries, Figure 2.5(d). The development of this type of microstructure may have an adverse effect on ductility and toughness.

2.1.6.3 Dispersion hardening

If precipitates are large, undeformable and widely spaced, as they are when over-aged, they can be readily by-passed by moving dislocations which bow out between them and rejoin by a mechanism first proposed by Orowan Figure 2.5(b), [16,13]. As loops are formed around the precipitates, the yield strength decreases, but as the work hardening rate is high, plastic deformation tends to be spread more uniformly around the grains. This is the situation with over-aged alloys and the typical age-hardening curve in which strength increases, then decreases with ageing time has been associated with a transition from shearing to by-passing precipitates, as shown schematically in Figure 2.6.

Dispersed particles or precipitates cause strengthening because a mobile dislocation, moving under the influence of applied strength, is bent to some angle, $0 \leq \phi \leq \pi$, before it can move through the crystal, Figure 2.7, [12]. In the case of strong impenetrable particles, the dislocation will bow out until it passes them by looping as in the Orowan mechanism [16]: in this case dislocation loops are left behind around each particle.

Alternatively, for weaker particles, the dislocation may cut through them at some value of $\phi > 0$, with the value depending on the obstacle strength.



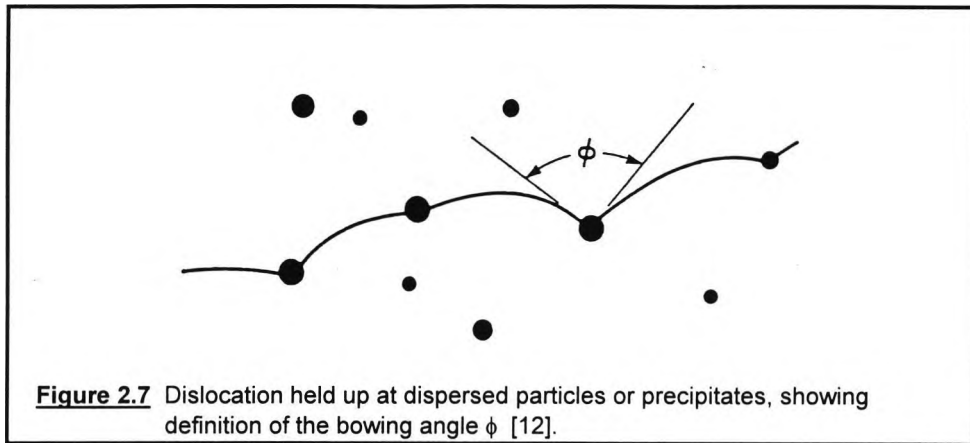
In the over-aged condition, particles are generally large, relatively strong and noncoherent with the matrix. The mechanism providing the strength increment is the Orowan one for impenetrable particles [12], but, more generally, when the particles are in fact cut, the strength increment, $\Delta\tau$, may be given as [12]:

$$\Delta\tau = (1.6 * \mu * b / l) * (f / \pi)^{1/2} * [\cos(\phi / 2)] \quad \phi \leq 100^\circ \quad \dots(2.2a)$$

or

$$\Delta\tau = (2 * \mu * b / l) * (f / \pi)^{1/2} * [\cos(\phi / 2)]^{3/2} \quad \phi \geq 100^\circ \quad \dots(2.2b)$$

where μ is the shear modulus and b the Burgers vector of the matrix, l is the particle diameter and f the volume fraction of particles. The value of ϕ when cutting takes place, is generally assumed to be constant in a particular alloy in the over-aged condition, and it has been demonstrated that it depends on the ratio of the shear moduli of precipitate and matrix (μ'/μ), with full Orowan strengthening occurring only when $\mu'/\mu > \sim 0.95$ and providing the particles are noncoherent with the matrix.



An alternative strengthening mechanism that was developed for alloys containing fine, weak precipitates, is presented by Brown and Ham [17] and is based on the work of Friedel, who has proposed that dislocations move by a "sidewise unzipping process". At breakaway,

$$\Delta\tau = F / b*\lambda = [2T*\cos (\phi/2)] * b*\lambda \quad \dots(2.3)$$

where F is the strength of the obstacle, λ the effective interparticle spacing, T the dislocation line tension, and b the Burgers vector as before. Alternatively, from Brown and Ham [17], the strength increment can be written as:

$$\Delta\tau = (0.8 \mu*b / L) * \cos (\phi/2) \quad \phi \leq 100^\circ \quad \dots(2.4a)$$

or

$$\Delta\tau = (\mu*b / L) * [\cos (\phi/2)]^{3/2} \quad \phi \geq 100^\circ \quad \dots(2.4b)$$

where L is the square array obstacle spacing = $(1/n_A)^{1/2}$, where n_A is the number of particles per unit area intersecting the slip plane, and the other symbols are as already defined. In such underaged alloys, the yield strength increment varies linearly with $1/L$ over a considerable range of particle sizes or spacings, the slope being of opposite sign to that for over-aged material. This implies a systematic variation in the critical value of ϕ at breakaway, it depending on particle size except perhaps where strengthening is based on mechanisms arising from disorder at the precipitate surface when it may be independent of size. To apply Equations (2.3) or (2.4), either the force F or the critical value of ϕ must be evaluated and substituted appropriately.

Le May and Krishnadev [12] have listed the sources from which the shearing force, F , may arise, as follows:

- Coherency hardening, involving coherency strains between particle and matrix.
- Surface hardening, or chemical hardening, involving the energy requirement to produce additional particle/matrix interface.
- Stacking fault hardening, involving differences in the stacking fault energies of precipitate and matrix.
- Modulus hardening, involving differences in the elastic moduli of particle and matrix.
- Order hardening, involving the work required to create internal or antiphase boundary in case of internally ordered particles.

Although many theories have been developed for these various strengthening mechanisms, it is difficult to state which one specifically applies to an alloy system. Usually more than one mechanism are present, both contributing to the final strengthening.

2.2 The impact behaviour of steel

A material may have a high tensile strength but yet be unsuitable for shock loading conditions. This means that the microstructure has other important effects on steel apart from controlling its strength and one of these is controlling its toughness. Strength is generally associated with hardness, thus brittleness, and toughness with ductility. It is therefore desirable, that a steel should possess both combinations. This was made inevitable after the second world war when there were numerous naval catastrophies due to brittle fracture.

2.2.1 Brittle fracture

Because metals contain microcracks in their structure which propagate through the crystal under stress, they always break at a stress below the theoretical fracture stress. According to the Griffith criterion [15], the smallest tensile stress σ that is needed to propagate a pre-existing crack of length $2c$, is given by the following equation:

$$\sigma = \sqrt{(EG / \pi c)} \quad \dots(2.5)$$

where **E** is the Young's modulus and **G** is the strain energy release rate (which consists of the surface energy, γ and the plastic work γ_p). The Griffith theory is the starting point of all theories that were developed later for individual materials.

Brittle fracture is a crack propagation connected with very little plastic deformation. This propagation requires much less energy than that associated with the growth of a ductile crack. This can easily be shown by carrying out impact tests on a pendulum apparatus. The energy absorbed by the specimen from the pendulum when plotted as a function of temperature usually exhibits a sharp change in slope (an S shape) as the mode of fracture changes from ductile to brittle. These impact transition curves are a simple way to determine the effect of metallurgical variables on fracture behaviour of a steel from which a transition temperature, T_c (or ITT) can be obtained. This is not an absolute value as it varies with the mode of testing, but is a simple way for comparison purposes between different metallurgical variables such as the various heat treatments.

More advanced fracture toughness tests, recently developed, involve the use of notched and pre-cracked specimens in which the cracks have been previously initiated by fatigue. These were developed when it was recognised that the propagation of the fracture is the important stage. The stress intensity factor, **K**, at the root of the crack is defined in terms of the applied stress σ and the crack size **c**:

$$K = \sigma * (\pi c)^{1/2} \quad \dots(2.6)$$

When a critical stress intensity factor K_c is reached, the transition to rapid fracture takes place[18].

The most commonly identified brittle fractures in metals are cleavage and intergranular fracture. Both are of significance in the world of technology, the dire practical consequences of the occurrence of cleavage fracture in engineering structures made in mild steel are well recognised and documented, while temper embrittlement and other manifestations of intergranular fracture are also well known. In recent years, much emphasis has been placed on the engineering aspects of brittle fracture in metals, and the techniques of fracture mechanics have been developed to relate applied fracture stresses to the size of any defect present in the structure [19].

2.2.1.1 Cleavage fracture

We define cleavage as brittle fracture occurring on a low-index crystallographic plane, which means that intergranular fracture cannot, in general, be termed cleavage. The cleaved surface is composed of {100} cleavage facets.

The main factors that influence the onset of cleavage fracture are the following [18]:

- **The temperature dependence of the yield stress.** This is a common characteristic among BCC metals, even when the interstitial impurity content is very low. As the temperature is lowered, the first dislocations to move will do so more rapidly as the velocity is proportional to the stress, and so the chances of forming a crack nucleus will increase. Thus, in a given material brittleness should be favoured by low temperatures.
- **The development of a sharp yield point.** This is caused by the interstitial atoms, carbon and nitrogen. The metal condition enables localised rapid movement of dislocations as a result of high stresses, which provides a favourable situation for the nucleation of cracks by nucleation coalescence.
- **Nucleation of cracks at twins.** The flow stress of iron increases rapidly with decreasing temperature to a point where the critical stress for deformation twinning is reached, so that this becomes a significant deformation mechanism. It has been shown [18] that cracks prefer to nucleate at twin intersections and at points where twins intersect grain boundaries, hence under the same conditions crack propagation is more likely in a twinned iron. This factor interacts with the temperature dependence factor since lower temperatures will raise the flow stress, thus making plastic deformation more difficult at the end of the crack, so less plastic blunting of the crack tip will take place and propagation will be aided.
- **Nucleation of cracks at carbide particles.** In the presence of a hard second phase such as cementite, cracks are more easily formed than in single phase materials. Plastic deformation can crack the hard grain boundary carbides or cementite lamellae in pearlite so as to produce microcracks which in conjunction with other factors can propagate and cause catastrophic brittle fracture. Recent work by Mintz *et al.* [4] has shown that carbide particles play a determining role in the fracture characteristics of steel and this is also confirmed by other investigators [20-24].

- **Grain size.** As mentioned earlier, control of the grain size is a very interesting aspect in terms of strengthening methods. Although T_c increases along with any increase in strength since the reasons that contribute to strength are also a cause for cleavage fracture, any strengthening by grain refinement actually lowers T_c . It has been shown by Petch [25,26], that T_c is linearly related to $\ln(d^{-1/2})$, and an appropriate relationship of this type can be derived from a dislocation model involving the formation of crack nuclei at dislocation pile-ups at grain boundaries. The smaller the grain size, the smaller the number of dislocations piling-up where a slip band arrives at a boundary. Bearing in mind that the shear stress at the head of such a pile-up is $n\tau$ where n is the number of dislocations and τ is the shear stress in the slip direction, it follows that as the grain size is reduced, n will be smaller and the local stress concentrations at grain boundaries will be correspondingly less. The situation will lead to less likelihood of cracks propagating, regardless of whether they are formed by dislocation coalescence or by dislocation pile-ups causing the carbides to crack or by twinning interactions.

2.2.1.2 Intergranular fracture

In intergranular fracture, the fracture is characterised primarily by its path, namely along the grain boundaries. Since at relatively low temperatures, metals normally exhibit greater grain boundary strength than grain interior strength, that is, fracture is transgranular, the evident grain boundary weakness requires explanation. It is often found that brittle intergranular fracture at ambient temperatures is associated with the segregation of solute or impurity elements to grain boundaries, altering their cohesion, although there are counter examples in which the intergranular weakness appears to be intrinsic and not a function of segregated elements [19].

The elements that segregate at grain boundaries are phosphorus, tin, sulphur, antimony and hydrogen. Effects of grain size may be exhibited due to the degree of coverage of grain boundaries by impurity elements. Knott [27] denotes that a coarse austenite grain size gives rise to a smaller ratio of grain boundary area to total volume, than does a fine grain size and so the degree of coverage by a given impurity content in the material will be greater. He continues, that it should be noted that not all boundaries are identical; the amount of impurity that each can take up is a function of its misorientation.

2.3 Structure-property relationships in steels

Having referred to strength and toughness as individual mechanical properties, it is evident that any change of the tensile strength (e.g. precipitation hardening) is linked to subsequent impact property changes of a material and both of these are directly related to the structure of the material in question.

Although there are not sufficient structure-property relationships for the steels that are examined in the present exercise, i.e the copper containing low carbon steels, it would be of advantage to review previous work on structure-property relationships in steels in general.

A recent review of the literature by Pickering [28] summarises the investigations of structure-property relationships that were carried out during the past 30-40 years. That review provides the reader with specific information on mechanical properties such as:

1. The yield stress
2. The flow stress and work hardening rate
3. Ductility
4. Toughness
5. The ductile-brittle transition temperature and
6. The shelf energy value

for structures of the following types:

1. Polygonal ferrite microstructures
2. Higher carbon ferrite-pearlite and fully pearlitic microstructures
3. Acicular ferrite and bainitic microstructures
4. Martensitic microstructures
5. Tempered bainite or tempered martensite microstructures
6. Structures observed in dual phase steels and
7. Structures observed in stainless steels

For the interest of the present exercise, only the yield stress and the impact transition temperatures of the structures described in 1, 3, 4, 5 and 6 will be reviewed in the following sections.

2.3.1 Polygonal ferrite microstructures

Polygonal ferrite microstructures are perhaps the commonest of the structures mentioned above and structure-property relationships are the most reliable since extensive investigations and reviews have been published considering these structures.

As Pickering quotes [28], many relationships show that pearlite in volume fractions less than 0.2 does not affect σ_y , but some equations show an effect of pearlite. The inclusion of a pearlite vector may indicate that carbon has the effect of lowering the transformation temperature and decreasing the grain size, but there is also a suggestion that pearlite may affect k_y , by as much as 11% at constant grain size.

Mintz *et al.* [4,29-31] have researched ferritic and pearlitic structures in the past, in order to establish structure-property relationships on these steels and the results of their research will be used as an aid to the current work.

A large number of ferrite-pearlite steels containing variable amounts of alloying elements such as Nb, V, Ti, Al and of course Mn, Si and N were examined by Mintz *et al.* [4]. Measurements of grain size, grain boundary carbide thickness, pearlite volume fraction and precipitation hardening were made in order to obtain the best structure-property relationship for 50% FATT and the 54J and 27J charpy impact transition temperatures by using multilinear regression analyses. The result of this analysis were the following equations:

$$54J \text{ ITT, } (^{\circ}\text{C}) = 192*t_c^{1/2} - 10.1*d^{-1/2} + 0.5*\Delta y - 23 \quad \dots(2.7)$$

$$27J \text{ ITT, } (^{\circ}\text{C}) = 173*t_c^{1/2} - 8.3*d^{-1/2} + 0.37*\Delta y - 42 \quad \dots(2.8)$$

$$50\% \text{ FATT, } (^{\circ}\text{C}) = 131*t_c^{1/2} - 12.7*d^{-1/2} + 0.45*\Delta y + 46 \quad \dots(2.9)$$

where t_c is the grain boundary carbide thickness (μm), d is the grain size (mm) and Δy is the precipitation hardening component (N/mm^2) which is calculated by subtracting the calculated yield strength from the observed one. The calculated yield strength is given by the following formula which is also the result of a regression analysis on non-precipitation hardened laboratory pearlite containing steels:

$$\sigma_y, (\text{N/mm}^2) = 43.1*\%Mn + 83*\%Si + 15.4*d^{-1/2} + 1540*\%N_f + 105 \quad \dots(2.10)$$

where σ_y is the lower yield stress, N_f is the free nitrogen content and the final term is referred to as σ_i and is a combination of the Petch friction-stress and residual substitutional hardening. It was noted by Mintz *et al.* [4] that in the case of pearlite-free steels, the significantly lower residual level results in a lower σ_i which, using Equation 2.10, gives an apparent value of Δy that is lower than the true value. Thus, the Δy component as defined above contains both precipitation hardening and solid solution strengthening contributions. It is also added that the influence of solid solution hardening and precipitation hardening on impact behaviour in general had been found to be similar. It is also important to mention that the regression equations can only be used for the range of compositions considered. More information on that can be obtained from reference [4].

An alternative equation for the calculation of the expected lower yield stress for ferrite/pearlite structures was developed by Morrison, Mintz and Cochrane [31,32] for HSLA steels and this is the following:

$$\begin{aligned} \sigma_y, (\text{N/mm}^2) = & 70 + 32*\%Mn + 84*\%Si + 680*\%P - 30*\%Cr + 38*\%Cu + 33*\%Ni \\ & + 11*\%Mo + 5000*\%(C + N) + 18.1*d^{-1/2} + \sigma_p + \sigma_d + \sigma_t \quad \dots(2.11) \end{aligned}$$

where d is the ferrite grain size (mm), σ_p , σ_d , and σ_t are the respective contributions to yield strength from precipitation hardening, dislocation hardening and texture development.

Instead of using Δy for estimating the precipitation hardening effect a different approach can be used. Morrison *et al.* [33] refer to the following Ashby-Orowan equation that describes precipitation effects:

$$\sigma_p = \frac{5.9f}{x} * \ln \left(\frac{x}{2.5*10^{-4}} \right) \quad \dots(2.12)$$

where f is the precipitate volume fraction and x is the mean planar intercept diameter of precipitates. The above equation gives good predictability for the precipitation

strengthening for quenched aged carbides and for precipitated carbonitrides in Nb, V and Ti microalloyed steels but is however, difficult to use because of the complex measurements required. Morrison *et al.* [33] have adopted a simpler approach which estimates precipitation hardening from an equation $\sigma_p = B * (\% \text{ alloy, ppt})$ for controlled processed steels that contain V, Nb and Ti where the B value is a constant that depends on a number of factors.

Recent work by Mintz, Peterson and Nassar [30], has simplified the ITT equations by deriving new regression equations that eliminate carbide thickness and Δy vectors from the impact transition temperature equations. These latest ITT equations cover a wide range of normalised plain C-Mn, C-Mn-Al and C-Mn-Al-Nb steels and are the following:

$$27J, \text{ ITT } (^{\circ}\text{C}) = 80.1 - 7.41 * d^{-1/2} + 1.4 * \%p - 57.2 * \%Si + 1224 * \%S - 1360 * \%P \\ - 3.7 * CR^{-1/2} - 57.8 * \%Mn \quad \dots(2.13)$$

$$54J, \text{ ITT } (^{\circ}\text{C}) = 84.8 - 5.65 * d^{-1/2} + 1.67 * \%p - 53.1 * \%Si + 1490 * \%S - 1379 * \%P \\ - 4.97 * CR^{-1/2} - 70.1 * \%Mn \quad \dots(2.14)$$

where **d** is the grain size (mm), **%p** is the pearlite volume fraction and **CR** is the cooling rate from the austenitising temperature ($^{\circ}\text{K}/\text{min}$).

2.3.2 Acicular ferrite and bainitic microstructures

These microstructures have many similarities and often co-exist in HSLA steels [28], but there is only limited information regarding the quantitative relationship between the microstructure and the mechanical properties. The reason is the complexity of the microstructures, due to high dislocation densities, solid solutions of substitutional solutes and alloy enriched ferrite islands, or retained austenite between the ferrite laths termed as the martensite-austenite (MA) constituent. Considerable confusion also exists regarding the terminology for the microstructures, which look like “packets” of lath-like ferrite grains of low misorientation between the grains within a “packet”, and have large carbides situated at the ferrite laths. Some authors refer to such microstructures either with the term acicular or “granular” ferrite [34] and others with the term “granular” bainite [35,36].

Pickering [28], in reviewing the factors that affect impact transition temperatures for bainitic structures has pointed out the importance of the spacing of the high angle packet or prior austenite grain boundaries, which act as effective barriers to cleavage crack propagation. On the contrary, low angle ferrite lath boundaries do not impede cleavage crack propagation. The ITT equation that was used is the following:

$$ITT = - 19 + 0.26*(\sigma_p + \sigma_b + \sigma_d) - 11.5*d^{-1/2} \quad \dots(2.15)$$

where d is the mean linear intercept of high angle boundaries, i.e. 'packet' or prior austenite grain boundaries, σ_p is the precipitation strengthening due to carbides, σ_b is the low angle lath boundaries strengthening and σ_d is the strengthening by random forest dislocations. This equation assumes that all the strengthening factors will have the same embrittling effect.

The suggested equation for the proof stress of low carbon bainite/acicular ferrite was developed by Gladman [37] and is the following:

$$\sigma_y = 88 + 15.1*d_L^{-1/2} + \sigma_d + \sigma_p \quad \dots(2.16)$$

where d_L is the mean linear intercept of the bainitic ferrite grain size (mm). The various strengthening factors are described by the following equations:

$$\sigma_d = \alpha*\mu*b*\rho^{1/2} \quad \dots(2.17)$$

$$\sigma_p = \frac{0.015}{\lambda_c} * \ln \frac{D}{2|b|} \quad \dots(2.18)$$

$$\sigma_b = 15.1*(d_L^{-1/2} - d^{-1/2}) \quad \dots(2.19)$$

where α is a constant, μ is the shear modulus of the matrix, b is the Burgers vector of the slip dislocations, ρ is the dislocation density, λ_c is the carbide spacing (μm) and D is the carbide particle diameter (\AA).

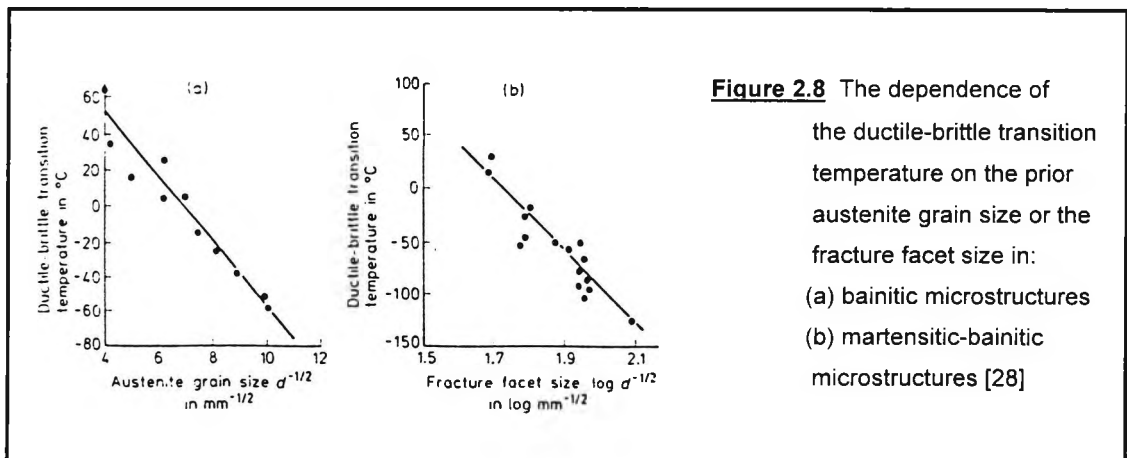
The above approach to the structure-property relationships was reported to predict yield strength and transition temperatures with good accuracy, except in the case of

some low carbon bainitic steels which contain coarse carbides at the bainitic ferrite laths [28].

2.3.3 Martensitic steels

The high hardness and brittleness of rapidly quenched steels is the result of the formation of martensite, but as in the case of acicular ferrite and bainitic microstructures, there is also great difficulty in determining the yield strength and the impact transition temperature of martensitic microstructures through structure-property relationships.

Pickering [28] quotes that Equation 2.15 was used with good agreement between observed and calculated ITT values, provided that the austenite grain size was used as a measure of d . As can be seen in Figure 2.8 there is a clear relationship between the impact transition temperature and the martensite fracture facet size, i.e. the 'packet size'.



The lack of quantitative and predicting equations regarding the strength of martensite has also been reported [18,28] and is attributed to the complexity of the structure, a tetragonal lattice with interstitial carbon in solid solution, formed by shear which leads to high densities of dislocations and fine twins. There are, as a result, several possible strengthening mechanisms:

- substitutional and interstitial solid solution
- dislocation strengthening, i.e. work hardening
- fine twins which restrict dislocation movement

- fine grain size
- segregation of carbon atoms which interact with dislocations
- precipitation of iron carbides

2.3.4 Tempered bainitic/martensitic microstructures

The tempering of martensite results to a fine dispersion of carbides in an α -iron matrix which often bears little structural similarity to the original as-quenched martensite [18]. The microstructure and mechanical properties of the steel depend on the time and the temperature of tempering; Honeycombe [18] separates the tempering of plain carbon steels into four distinct but overlapping stages:

- Stage 1, up to 250°C - precipitation of ϵ -iron carbide ($\text{Fe}_{2.4}\text{C}$); partial loss of tetragonality in martensite.
- Stage 2, between 200 and 300°C - decomposition of retained austenite.
- Stage 3, between 200 and 350°C - replacement of ϵ -carbide by cementite; martensite loses tetragonality.
- Stage 4, above 350°C - cementite coarsens and spheroidises; recrystallisation of ferrite.

The tempering stages mentioned above are shown in Figure 2.9. It can be seen that the carbon level is of great importance at the initial stages of tempering, and as Pickering [28] quotes, in medium-high carbon steels tempered at low temperatures, fine dispersions of ϵ ($\text{Fe}_{2.4}\text{C}$) and η (Fe_2C) carbides will be formed in the matrix and the coherency of these carbides with the matrix will vary for different tempering parameters.

The presence of alloying elements is also very effective in altering the tempering stages of complex alloy steels in the following ways [18]:

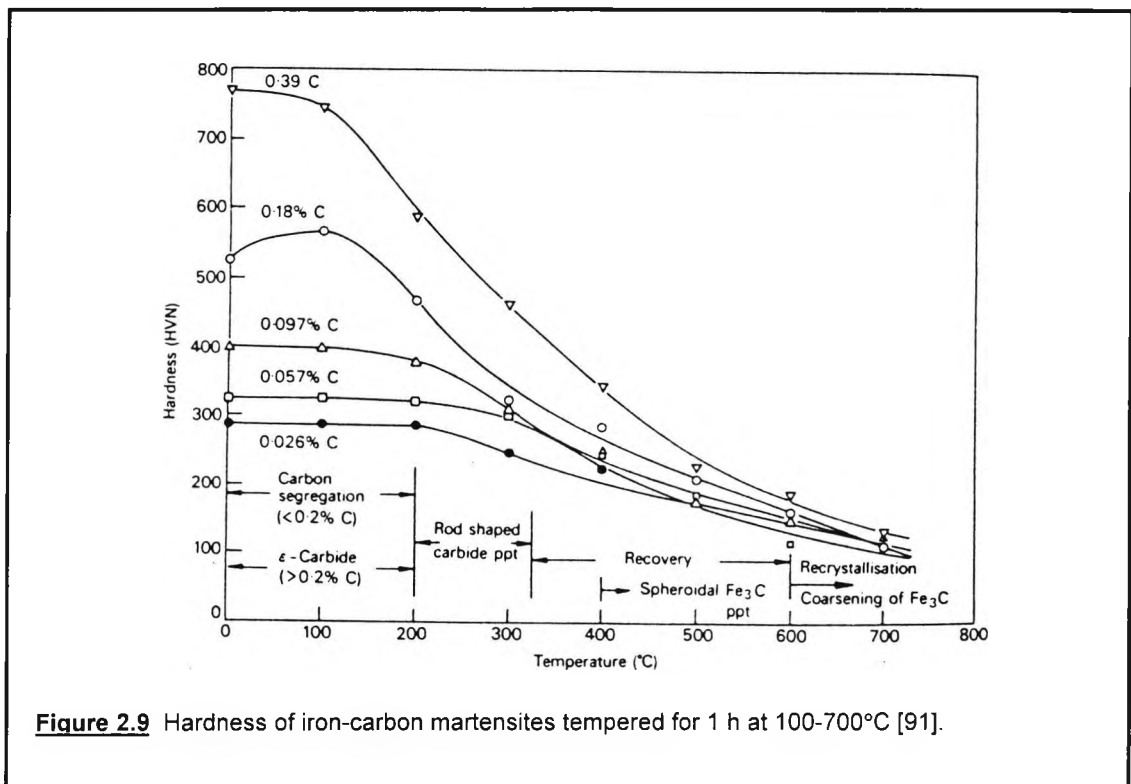
- Alloys such as Cr, Mo, W, V, Ti and Si, can increase the stability of supersaturated iron-carbon solid solution and as a result the disappearance of the tetragonality of martensite is delayed, whereas Mn and Ni decrease it.
- The proportion of austenite retained on quenching may be increased, and this austenite decomposes on tempering to give high concentrations of grain boundary cementite and thus cause *tempered martensite embrittlement* in the range 300-350°C.

- The coarsening of cementite is restrained and in the range 400-700°C and at temperatures above 500°C alloy carbides are formed. As a result, the reorganisation of dislocations is slowed down and softening is retarded.
- The formation of alloy carbides which are sometimes coherent with the matrix and remain very fine after prolonged tempering, causes the so called phenomenon *secondary hardening*. This is a type of age-hardening reaction and is both time and temperature dependent, so both variables are often combined in one parameter, usually referred to as the *Holloman-Jaffe* parameter and is described by the following equation:

$$HP = T \cdot (k_h + \log t) \quad \dots(2.20)$$

where T is the absolute temperature ($^{\circ}K$) and t the tempering time, while k_h is a constant which is about 20 for alloy steels. This parameter can be plotted against hardness to give one typical curve for a particular steel.

All the above considerations make the development of quantitative relationships between the complex tempered structures and their properties extremely difficult.



Work on heavily tempered plain carbon martensites by Onel and Nutting [38], has thrown considerable light on these more simple microstructures [28]. In the case when the carbides are exclusively at the ferrite grain boundaries, the carbides contribute no strengthening and the yield stress is predominantly controlled by the tempered ferrite grain size, d :

$$\sigma_y = 108 + 18.2*d^{-1/2} \quad \dots(2.21)$$

Both σ_i and k_y are rather higher than for polygonal ferrite, probably due to a contribution from residual dislocations to σ_i , which will also increase k_y as indicated for strained structures [28].

Structures that contain carbides within the matrix showed an additional strengthening effect, σ_p :

$$\sigma_y = 77 + 23.9*d^{-1/2} + \sigma_p \quad \dots(2.22)$$

where σ_p is described by Equation 2.18.

The toughness of tempered martensite and bainite decreases with increasing strength although alloying elements very substantially improve the toughness, when compared with plain carbon steels of similar strength levels [18]. Figure 2.10 shows the relationship between tensile strength and impact value.

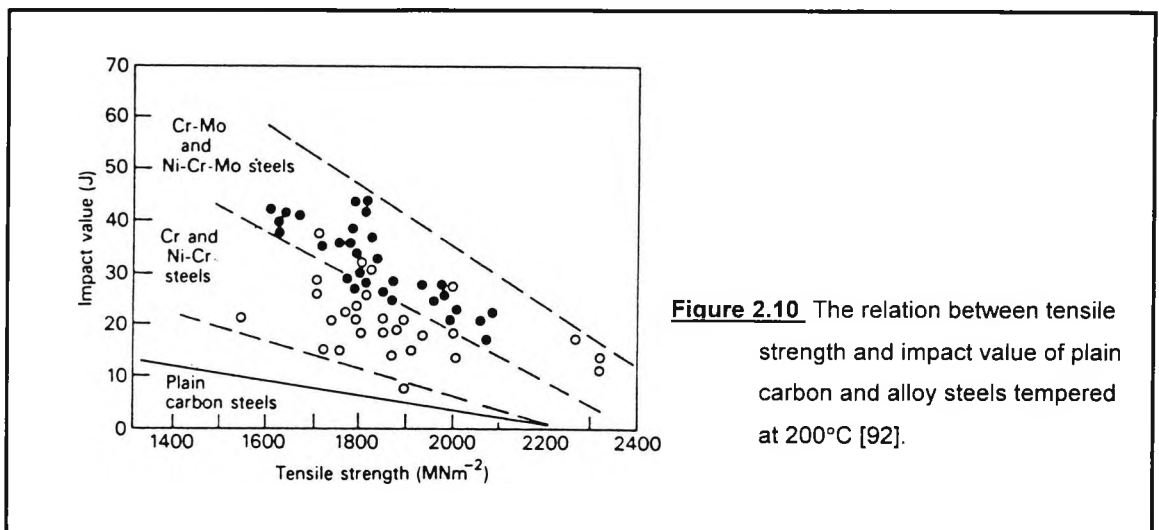
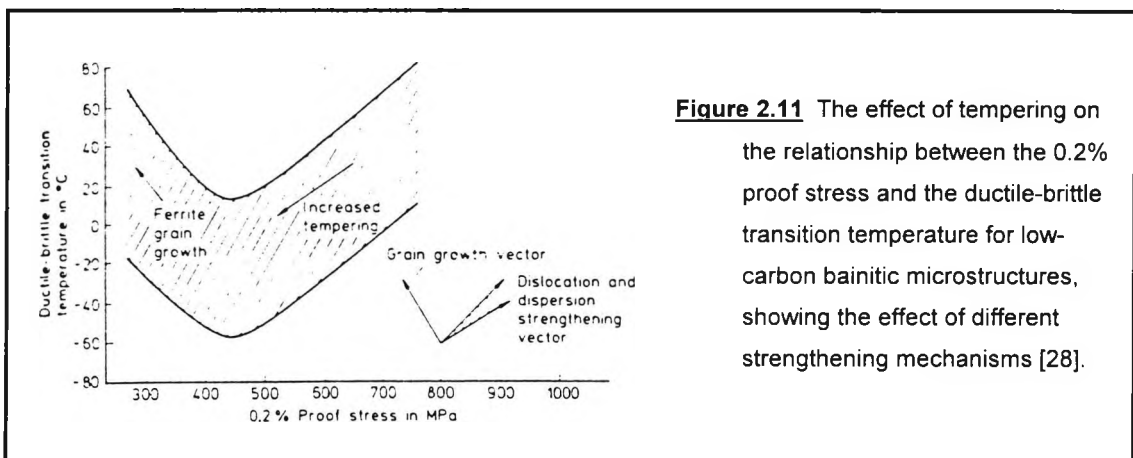


Figure 2.10 The relation between tensile strength and impact value of plain carbon and alloy steels tempered at 200°C [92].

In the case of tempered martensite and bainite, there is evidence that the transition temperature increases with increasing the carbon content, and in the case of tempered bainite the transition temperature decreases with tempering due to the decrease in both σ_p and σ_d , [28]. The effect is virtually linear, ITT decreasing by 0.2/0.3°C for each MPa decrease in σ_y , Figure 2.11. At higher tempering temperatures, towards the A_1 temperature, the recrystallisation and grain growth of the ferrite matrix results in an increase in ITT, Figure 2.11. This behaviour has also been reported by other investigators [36,39].

As in bainite and martensite, there is evidence that an increase in the prior austenite grain size of tempered martensite, causes an increase in the ITT. Pickering [28] has suggested, that provided no anomalous embrittlement occurs during tempering and with the appropriate modifications, the analysis that can be used to relate the microstructure to the transition temperature in tempered martensite could be based on the analysis of polygonal ferrite-pearlite microstructures.



2.3.5 Dual phase steels

The dual phase steels were developed to provide a reasonably high strength with enhanced formability and this was achieved by introducing a hard second phase into a ferrite matrix. This second phase is a martensite-austenite (MA) constituent, usually formed after annealing in the $\alpha+\gamma$ region for several minutes to allow the formation of small regions of austenite, followed by rapid cooling in order to promote the transformation of the newly formed austenite into martensite. These steels contain

0.08-0.2% C, 0.5-1.5%Mn, with microalloying additions such as Cr (0.5%) and Mo (0.4%).

The yield strength of the dual phase steels can not be simply given by the polygonal ferrite-pearlite microstructures because the presence of the hard MA particles promotes continuous yielding at much lower stresses than those predicted by ferrite-pearlite structure-property relationships [28]. Work by Lanzillotto and Pickering [40] has related stress and formability to the volume fraction of MA particles and to their size, favouring a high volume fraction and a refined MA size.

Rigsbee and VanderArend [41] have examined the structure-property relationships in dual phase HSLA steels and found that the yield strength depends on the volume fraction of martensite, Figure 2.12. It can be seen that the yield strength initially decreases rapidly as the martensite volume fraction increases, but after the martensite reaches a critical value (4%) the yield strength starts to increase. This increase is more pronounced for higher carbon contents.

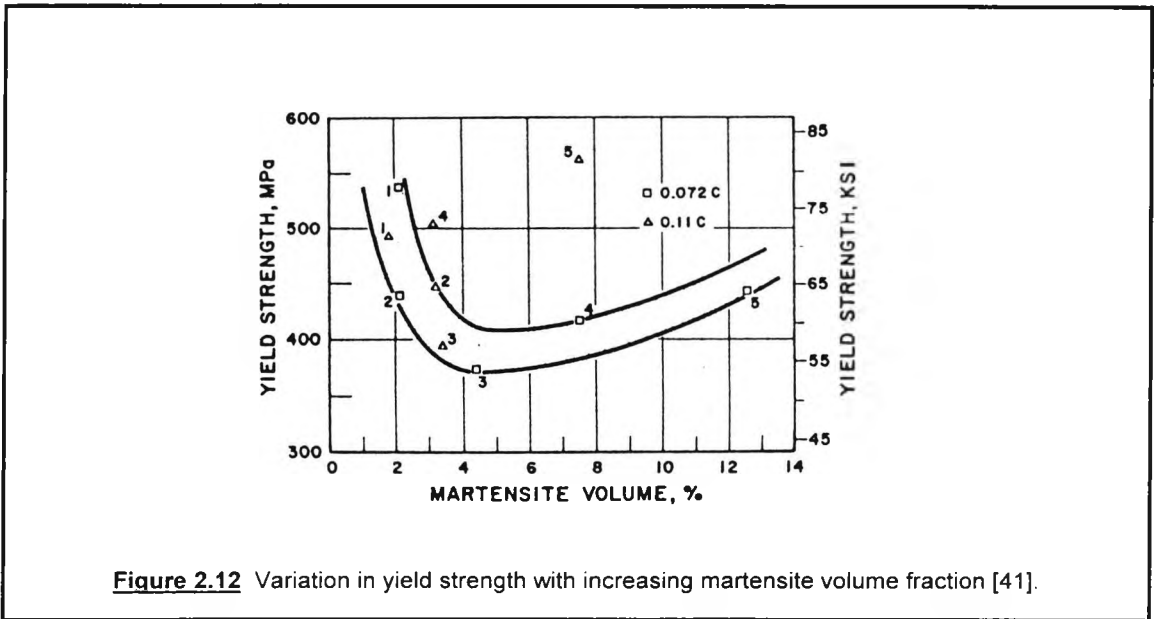


Figure 2.12 Variation in yield strength with increasing martensite volume fraction [41].

2.4 Age-hardening of plain low-carbon steels

It is appropriate before entering into the domain of HSLA-steels, to discuss the development work and the age-hardening potential of plain carbon steels as the

principles underlying the effect and control of precipitation hardening are similar to those used in the age hardenable Cu containing steels.

The aim is to create an age-hardening model in the Fe-C system similar to that of Al-Cu, which will provide information on the precipitation of carbides in steel and their effect on properties. It is known that the solubility of carbon is much less in ferrite than it is in austenite as can be seen from the expanded portion of the low-carbon end of the Fe-C diagram [42] showing the temperature-composition range of ferrite and the decreasing solubility of carbon in ferrite with decreasing temperature, Figure 2.13. A supersaturated solid solution consisting of carbon atoms in ferrite can be achieved by soaking the low-carbon steel close to the eutectoid temperature ($\alpha \rightarrow \gamma$ phase change) and subsequently quenching in ice/brine. The resultant non-equilibrium structure can then undergo ageing treatment.

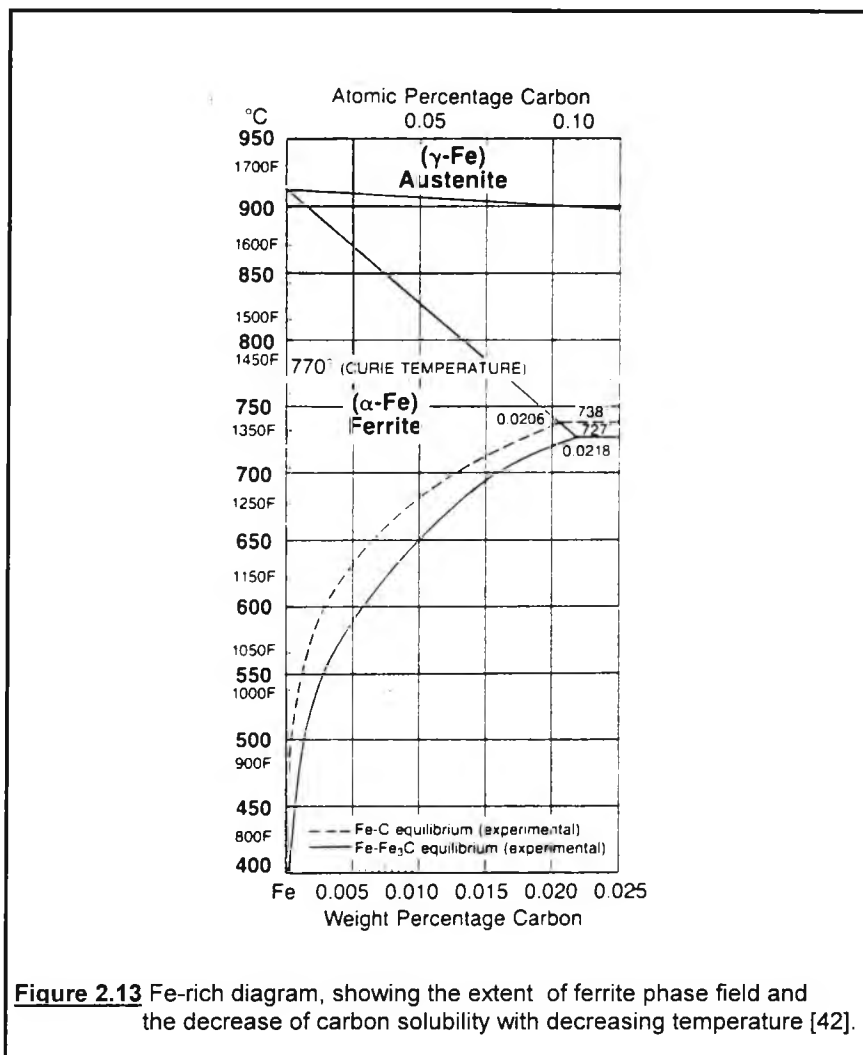


Figure 2.13 Fe-rich diagram, showing the extent of ferrite phase field and the decrease of carbon solubility with decreasing temperature [42].

Investigation on this subject dates back to the 1950's when several studies were made [23,24,43,44]. Initially, investigators looked on the effect of age-hardening on the mechanical properties of commercial carbon steels with particular emphasis on the ductile-brittle transition. As Leslie *et al.* [23] have quoted, the results of their predecessors could be summarised as follows:

- Cementite, Fe_3C , precipitated from ferrite at elevated temperatures (400-700°C) raises the transition temperature after quenching from 700°C.
- Ageing at room temperature after a solution quench also raises the transition temperature of a 0.02%C iron or steel, but over-ageing can lower the transition.
- Precipitated carbides make the transition from ductile to brittle fracture less abrupt.
- A finely dispersed carbide precipitate can promote ductility at low temperatures.
- The exponent of strain hardening decreases with increasing carbon content and with decreasing temperature.

Undoubtedly the above observations are correct because of the number of investigators involved and the variety of compositions and heat treatments used, but, it was soon realised that any findings had to be investigated in terms of detailed examination of carbide nucleation, growth and distribution in an attempt to determine how precipitated carbides interact with slip in ferrite. Leslie *et al.* [23] followed up to the foregoing work by examining the tensile properties of high purity low carbon and manganese iron alloys. It was first verified that Fe-C alloys (0.013-0.07%C) that are quenched from 720°C and then aged at 200-500°C do not exhibit any change in their tensile properties at room temperature or in the carbide particle spacing. They concluded that it was obvious that these samples were in the over-aged condition which does not allow any hardening according to the Orowan's relation. In contrast, ageing for 48 h at 40°C after quenching, produced large increases in yield strength, tensile strength and hardness, and large decreases in ductility.

Cold rolling of over-aged samples revealed that the carbide precipitates (cementite) were seldom deformed plastically. With a few exceptions, they are either completely shattered by a slip band or they remain undeformed. However, it has also been indicated [23] that carbon in the proper amount and distribution can improve the low-temperature ductility of ferrite, as measured by the amount of uniform elongation. That carbon amount, should be less than 0.02% and the carbide particles should be finely dispersed within the grains. The reason that has been given for this conclusion, is that

the finely dispersed carbide precipitate increases the uniform elongation because of the possibility that the particles serve as sources of dislocations at low temperatures, thus distributing slip more uniformly; an effect similar to that produced by decreasing the grain size. This is opposite to the situation at room temperature, where the presence of the fine carbides increases the non-homogeneous deformation (yield-point elongation). Secondly, the particles, in being shattered by slip, decrease the energy available for the formation of cracks. Thirdly the presence of the precipitate probably inhibits twinning, thus eliminating cracks that can be formed at the junction of twins.

As there had been enough evidence to justify a more detailed investigation of the precipitate nucleation and growth, Leslie [43], extended the above work to an electron transmission study aiming to correlate the mechanical properties to the microstructure. In this study, the kinetics of the nucleation, growth and type of the precipitates together with their interaction with dislocations were examined. The effect of manganese and silicon was also investigated.

Detailed examination of the precipitates had been carried out [43] after ageing at 60, 100, 150-175 and at 200 °C. and was observed that when carbon activity was low, i.e. at low temperatures or at short ageing periods, the carbide precipitated on the $\{100\}_\alpha$ plane and its chemical composition could not be identified, whereas at higher temperatures and longer ageing times the carbon precipitated on the $\{110\}_\alpha$ plane and was identified to be cementite. It was also concluded that the carbon activity can be controlled by changing the carbon content or by addition of substitutional solutes. By lowering the carbon activity, manganese decreases the temperatures at which changes occur; silicon raises the activity and therefore increased the temperature at which changes occurred.

Leslie [43] has considered nucleation and growth of precipitate to be complex thus prohibiting the development of a general expression. Depending on factors such as ageing temperature and composition, nucleation would occur within the matrix, on dislocations or at both. At low ageing temperatures nucleation occurs within the matrix only and is time dependent. In addition, an anomalous increase in the rate of precipitation was observed at these low temperatures i.e. the rate of precipitate growth is proportional to the fraction of carbon precipitated. In contrast, at high ageing temperatures nucleation of carbides occurs only on dislocations and the rate of growth of the carbides is inversely proportional to the fraction of carbon precipitated. The

examination of strained samples showed that fine precipitated particles can be sources of dislocations during plastic straining of the matrix and that cementite precipitates do not shear but fracture. The principal unknowns that remained after this particular piece of work were the identification of the carbide which was formed at low ageing temperatures, the nature of the matrix nucleation sites and the mechanism of strengthening by the unidentified carbide.

In a further work by Leslie and Rauch [44], the work of other investigations has been reviewed, and it has been concluded that the precipitate that had the $\{100\}_\alpha$ habit plane is an ϵ -carbide and has been indicated as "low-temperature" ϵ -carbide. The premium objective of their work [44] has been the examination of the effect of the aluminium (up to 5.8%) in low carbon steels and it has been concluded that aluminium like silicon also increases the cementite initiation temperature for a given ageing time, and greatly increases the time required for cementite formation at a given temperature. In an attempt to determine whether the effects of Mn, Si and Al can be explained on a common basis, Leslie *et al.* [44] have stated that the ways in which the solute can act to modify carbide precipitation can be considered in two categories; those affecting the relative thermodynamic stabilities of the various precipitated carbides, and those affecting the precipitation kinetics. These two areas are not unrelated, since the thermodynamic driving force or free energy change will influence the critical nucleus size for precipitation.

Another interesting piece of work is that carried out by Allen *et al.* [24] in which a variety of low carbon steels have been examined after double heat treatments at 950 and 700 °C in order to study the effects of carbon in solution in the ferrite and of carbon present as carbide films on the yield (or proof) stress and the transition temperature. Having examined more than 15 steels of carbon levels varying from 0.0025% to 0.117%, Allen *et al.* [24] have observed that the alloys that had all the carbon in solution, i.e. those with carbon levels between 0.0096% and 0.013% had the lowest transition temperatures amongst all the other steels.

All the alloys in Allen *et al.*'s work [24], have also been examined after heat treating at 950°C and at various conditions such as water quenched, air-cooled and furnace-cooled. Those that had been previously water-quenched were left to age at room temperature and their mechanical properties have also been examined. This revealed that the yield properties remained constant whereas the impact behaviour was very

much affected. Transition temperatures increased considerably after ageing, thus implying that the cleavage strength at the transition temperature is lowered by ageing. This, as has been suggested by Allen *et al.* [24], could arise from two causes: either the cleavage strength of the ferrite is reduced because of the decrease in the amount of carbon in the solution, or the effect is due to the carbide that is precipitated, or both.

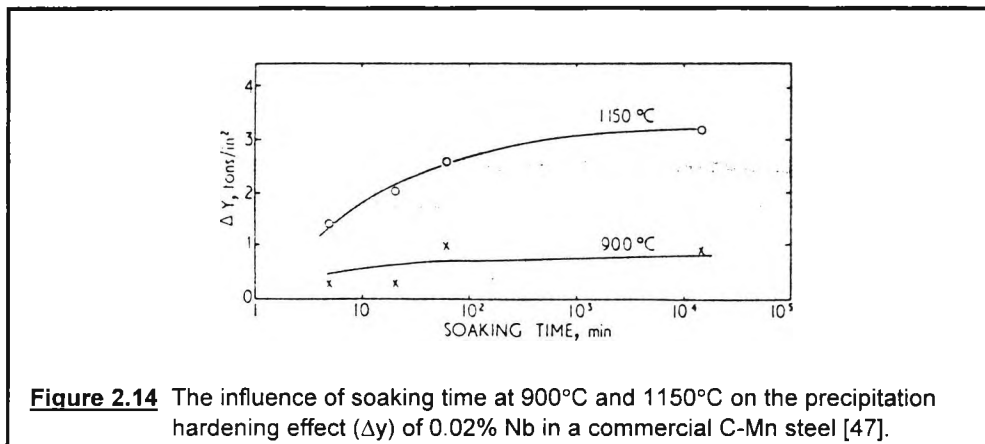
Work by Gladman *et al.* [45] has also shown that quench ageing steel can considerably increase the strength as well as causing the impact behaviour to deteriorate. Their observations have been explained in terms of normal dispersion strengthening.

2.5 Precipitation hardening of HSLA-steels

Although precipitation hardening is mainly used in light alloys, most HSLA-steels take full advantage of their ability to age-harden due to the presence of microalloying additions such as, niobium, vanadium mainly, and titanium. Microalloying elements are added singly or in combination to carbon-manganese steels, to produce the HSLA-steels and their premium effect on steel is to refine the grain size. Their ability to age-harden the steel is often referred to as “secondary hardening” and this is achieved by tempering a super-saturated solid solution in the temperature range 500-700°C for a certain period of time.

The precipitates that form upon phase transformations are nitrides and carbides the most common of these are: TiN, NbN, TiC, VN, NbC and VC. As a consequence of the importance of precipitate size and volume fraction, the intensity of precipitation strengthening depends on the stoichiometric ratio of the precipitating microalloy carbide/nitride in austenite and on the $\gamma \rightarrow \alpha$ transformation temperature[46].

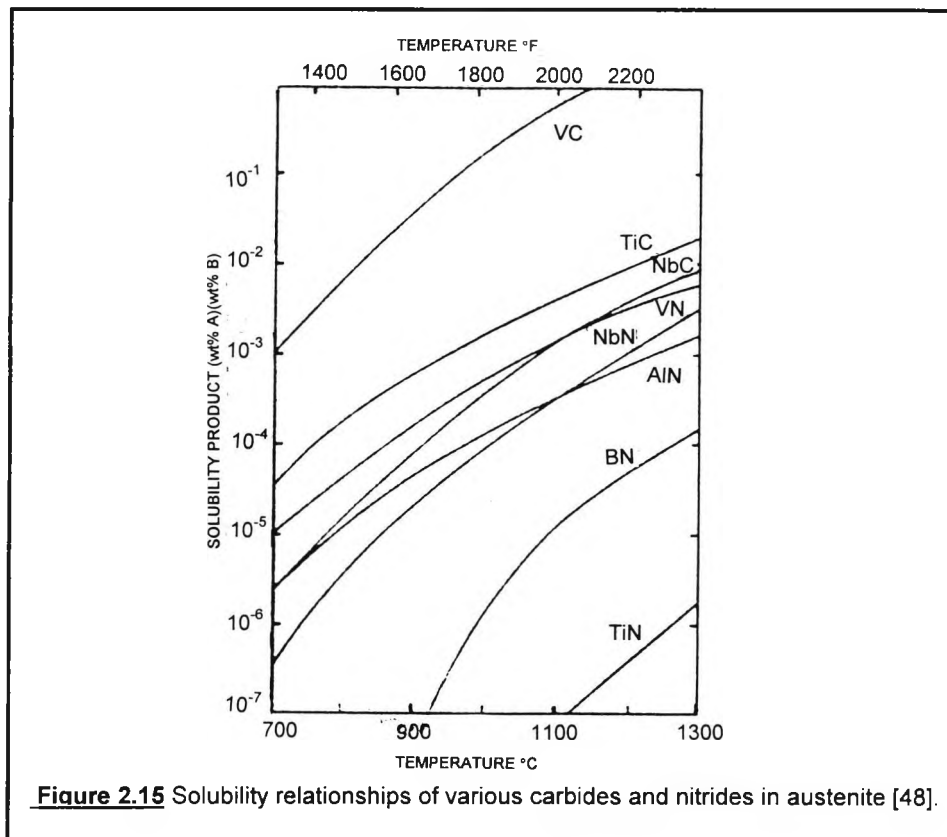
The influence of small niobium additions on the properties of carbon-manganese steels has been examined by Morrison [47] and has been found that niobium dissolves when heated at high austenitising temperatures and precipitates during the transformation to ferrite as a very fine and coherent niobium carbide. When the material had been cooled rapidly from the austenite region some niobium was retained in solution and this caused secondary hardening after tempering, Figure 2.14. Slowly cooled material, or material that had been austenitised at lower temperatures than 1100°C did not show any response to tempering.



In Nb steels the strengthening precipitates are predominantly Nb(CN) and in Ti steels they are predominantly TiC. Due to the restricted solubility of TiC in the austenite, strengthening by TiC requires higher Ti additions than those required for optimum grain refinement, and higher austenitising temperatures; thus Ti additions are used in the form of TiN for grain refinement and not for precipitation strengthening. On the other hand, the VC precipitate has a much higher solubility in austenite and V steels are therefore extensively used for precipitation strengthening. Moreover, the strengthening by VC can be enhanced by increased N contents, either due to additional VN precipitation or by N being dissolved in VC as V(CN). Vanadium forms nitrides preferentially to carbides, especially at higher temperatures, but even with the enhanced nitrogen contents VN can be dissolved in the austenite to produce increased precipitation strengthening. Niobium however, is not used with enhanced nitrogen due to the low solubility of NbN (even less than TiC but higher than TiN) and does not offer any substantial precipitation strengthening [46]. Typical solubility relationships are shown in Figure 2.15, [48].

In general, the precipitation strengthening potential of microalloyed carbides/nitrides increases as their solubility in austenite increases. To increase this, manganese is usually employed at a level of 0.7 to 1.5 wt.%. This element together with the others mentioned above, actually suppresses the transformation temperature and increases strengthening. As Pickering has quoted [46], the reason that these microalloying additions lower transformation temperatures is due to their effect on hardenability of the steel, but he has also added that this effect is difficult to quantify. The difficulty arises from the fact that these elements segregate to the austenite grain boundaries to

an extent dependent on the C and N contents and because the grain boundaries are pinned, grain boundary segregation can be increased thereby increasing hardenability to an unknown degree.



It is to be noted that, in addition to the solubility considerations, the volume fraction and size of the precipitate particles are obviously important factors that affect grain boundary pinning [48].

An early attempt to quantify the effect of microalloying additions on the transformation temperatures of steels was made by Andrews [49], but he also refers to considerable doubt on the effect of Ti, Al and As. It is however essential to have knowledge of the A_{e3} and M_s temperatures in the present work and his equations are quoted below:

$$\begin{aligned}
 A_{e3}, (^\circ\text{C}) = & 910 - 25*\%Mn - 11*\%Cr - 20*\%Cu + 60*\%Si \\
 & - 60*\%Mo + 40*\%W + 100*\%V + 700*\%P + 3 \\
 & - (+250*\%Al + 120*\%As + 400*\%Ti) - \Delta T \quad \dots(2.23)
 \end{aligned}$$

where: **3** refers to S and is assumed to give a constant rise in A_3 .

the figures in brackets are particularly doubtful, and

ΔT is a function of carbon and nickel and is included in reference [49].

$$M_s, (^\circ\text{C}) = 512 - 453*\%C - 16.9*\%Ni + 15*\%Cr - 9.5*\%Mo \\ + 217*(\%C)^2 - 71.5*(\%C)*(\%Mn) - 67.6*(\%C)*(\%Cr) \quad \dots(2.24)$$

Repas [48], in his review of metallurgical fundamentals for HSLA steels, has referred to a more recently developed equation for the Ae_3 temperature:

$$Ae_3, (^\circ\text{C}) = 910 - 310*\%C - 80*\%Mn - 20*\%Cu - 15*\%Cr - 55*\%Ni - 80*\%Mo \\ \dots(2.25)$$

As has been mentioned by Repas [48], the cooling rate through the transformation range is also extremely important to the development of the final microstructure and the precipitation reactions that can occur, are either simultaneously with (interphase precipitation) or subsequent to (general matrix) the formation of ferrite.

2.6 Copper in steels

As was mentioned in the introduction, the main aspect of this research is to examine the effect of copper on HSLA steels. Bearing in mind that the main contribution of copper in the strength of these steels would result from precipitation hardening, it is reasonable to concentrate on this and on its effect on impact behaviour.

Research on copper steels originated in the early thirties, initially concentrating on the solubility of copper in iron and in lattice changes during ageing [50]. In the sixties, Hornbogen *et al.* [51], have examined the precipitation of copper from iron, this being mainly a metallographic study. After that, many investigators have worked on this subject covering a wide range of copper steels [1-3,5-7,36,39,52-76].

As Jesseman and Murphy [64] have quoted, copper in steel differs from the more conventional precipitation hardening elements such as niobium, vanadium or titanium in that it has a high solubility at conventional 870 to 950 °C austenitising temperatures. High solubility makes copper ideal for hardening thick low carbon steel plates, which must be hot formed or heat treated by normalising or quenching and tempering to develop the necessary strength and toughness.

Irani, Dulieu and Tither [5], have pointed out the positive effects of copper in low-alloy steels. These include not only the so favourable age-hardening effect, but also the resistance to corrosion by atmospheric and chemical environments and its strong effect in increasing the plastic anisotropy of cold-rolled sheet. Its main disadvantage is the cause of a surface hot shortness during rolling of ingots and slabs.

The first commercial copper steel was developed by INCO and is specified as IN-787. Its composition is given in Table 2.1. Modifications of this steel have often been made to improve properties such as weldability, by reducing the carbon content and to minimise hot shortness, by adding nickel [77]. Further research by ARMCO has led to the development of, as specified, ASTM A710 steel. This steel is used for high strength welded fabrications. This has been widely used for the construction of both offshore oil drilling platforms and U.S. Navy ships [78]. Table 2.2, contains the chemistry of this steel as specified by the ASTM standard. Grade A, class 3 of ASTM A710 is often referred to as HSLA-80 and is a replacement of the higher carbon HY-80 steel.

ELEMENT	PERCENT WEIGHT
Carbon, max	0.060
Manganese	0.400-0.650
Phosphorous	0.010
Sulphur	0.009
Silicon	0.200-0.350
Chromium	0.730
Nickel	0.70-1.00
Molybdenum	0.180
Copper	1.00-1.30
Niobium, min	0.020
Aluminium	0.050
Iron	balance

Table 2.1 Typical composition of IN-787 steel.

ELEMENT	PERCENT BY WEIGHT	
	GRADE A	GRADE B
Carbon	0.070	0.060
Manganese	0.400-0.700	0.400-0.650
Phosphorous, max	0.025	0.025
Sulphur, max	0.025	0.025
Silicon, max	0.400	0.150-0.400
Nickel	0.700-1.000	1.200-1.500
Chromium	0.600-0.900
Molybdenum	0.150-0.250
Copper	1.000-1.300	1.000-1.300
Niobium, min	0.020	0.020

Grade A, Class 1 - As rolled and precipitation heat treated
Grade A, Class 2 - Normalised and precipitation heat treated
Grade A, Class 3 - Quenched and precipitation heat treated
Grade B - As rolled and precipitation heat treated

Table 2.2 ASTM A-710, Grades A and B chemistry specification [93].

Copper and nickel are the principal alloying elements. Copper is the strengthening precipitate and nickel modifies the ferrite matrix to reduce the potential adverse effects of copper on the hot working properties of steel. Rather than providing traditional hardenability characteristics, chromium and molybdenum are present to strengthen the ferrite matrix, control grain size, and supplement the precipitation hardening mechanism. Typical yield strength and impact transition temperature values of steel A-710 Grade A can be viewed in Table 2.3.

Plate thickness (mm)	Class	Transverse Tensile Properties		
		0.2% Yield Strength , (MPa)	Tensile Strength (MPa)	% Elongation in 50 mm, (%)
4.8 - 7.9	1	585	655	20
over 7.9 - 19	1	550	655	20
4.8 - 25	2	450	495	20
over 25 - 51	2	415	495	20
over 51	2	380	450	20
4.8 - 51	3	515	585	20
over 51	3	450	515	20
All Thicknesses	Class	Charpy V-notch Impact Property		
		Test Temp. (°C)	Impact Energy, (J)	
			longitudinal	transverse
	1	-45	27	20
2	-45	69	47	
3	-62	69	47	

Table 2.3 Minimum tensile and charpy V-notch impact property requirements for ASTM A-710 Grade A steels [3].

Many investigators [57,60,61,66], have experimented on the composition and properties of copper steels and new families of low-carbon copper-steels have emerged such as the Cu-B steels for pressure vessel application and Cu-Si-Ti-Nb-B steels for hydrogen resistant applications [65].

Another type of copper containing HSLA steels, is the HSLA-100 which is a further development of the HSLA-80 steel [36,39,73,79]. The chemical composition of this steel is similar to that of the A710 steel, with a higher Nickel level. With an appropriate temper, the recently developed HSLA-100 meets the Navy specifications for 100 ksi (689 MPa) yield. The Navy HSLA-100 steel with increased copper (~2.0% Cu), not only meets the 100 ksi yield strength requirement, but also meets all the Naval specifications for the 130 ksi (896 MPa) yield strength plate.

Other pieces of work [54,80,81] include investigations of copper containing steels which have a higher content of carbon and therefore higher strength. These higher carbon steels usually have martensitic microstructures.

2.6.1 Solubility of copper in steels

It was mentioned earlier that precipitation hardening depends on the solubility of an alloying element in the austenite. It is therefore inevitable that the solubility of copper in steels must be examined prior to any attempt to explain the precipitation hardening of copper containing steels.

The phase boundaries in the Fe-C system are affected by the presence of additional alloying elements, and these also affect the transformation characteristics on cooling, the strength of the various phases present, and the possibility of strengthening by subsequent heat treatment procedures such as ageing. Copper is one of the alloying elements which have been added in the past to a small extent, often in the form of a residual or tramp element in the scrap comprising part of the charge used to produce the melt, although today it is becoming much more widely used as a deliberate addition in order to produce the copper steels. Hence it is appropriate to examine the phase equilibria for Cu in Fe and steels in order to appreciate its consequent effects on the microstructure and strength, as well as on the processing variables.

Figure 2.16, shows the Fe-Cu diagram, and it is seen that irrespective of the exact solubility values, the diagram illustrates the substantial decrease in solubility with decreasing temperature. Generally speaking, the maximum solubility of Cu in α -Fe is 2.1% at $\sim 850^\circ\text{C}$, and decreases to 0.5% at 700°C , ($\sim 0.35\%$ or less at room temperature) [56]. The decreasing solubility of copper in iron provides the opportunity for subsequent precipitation or age hardening to be employed. The products of the eutectoid reaction are ϵ -phase, i.e. FCC copper with a small amount of iron in solution, and ferrite or α -phase Fe which contains a small quantity of Cu in solution. Figure 2.17 shows an extended part of the iron-rich portion of the Fe-Cu phase diagram [82].

The relatively low melting point of the ϵ -phase ($\sim 1090^\circ\text{C}$) means that potential problems exist where there has been extensive segregation of Cu in an ingot or in the case of higher Cu-containing alloys on which subsequent reheating and hot working are to be carried out. In order to prevent the formation of primary or hypoeutectoid ϵ -phase and minimise hot shortness, the quantity of Cu added should normally be kept below $\sim 2.5\%$ [16].

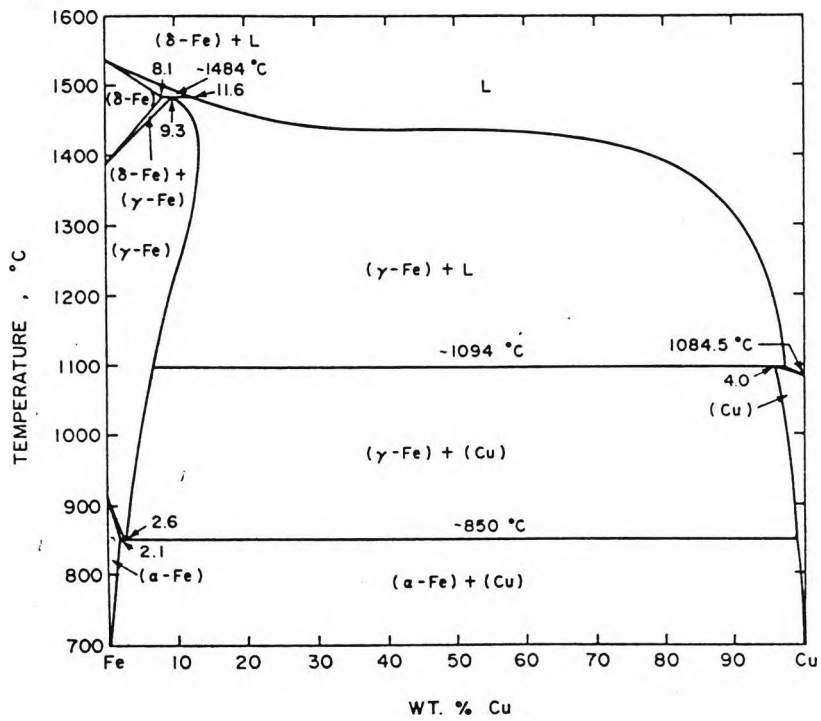


Figure 2.16 The Fe-Cu diagram (based on data from ref.[12].)

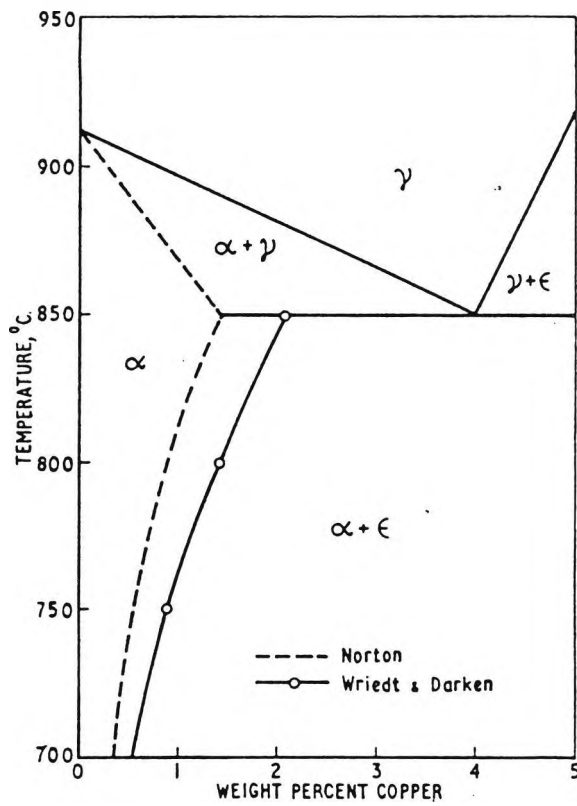
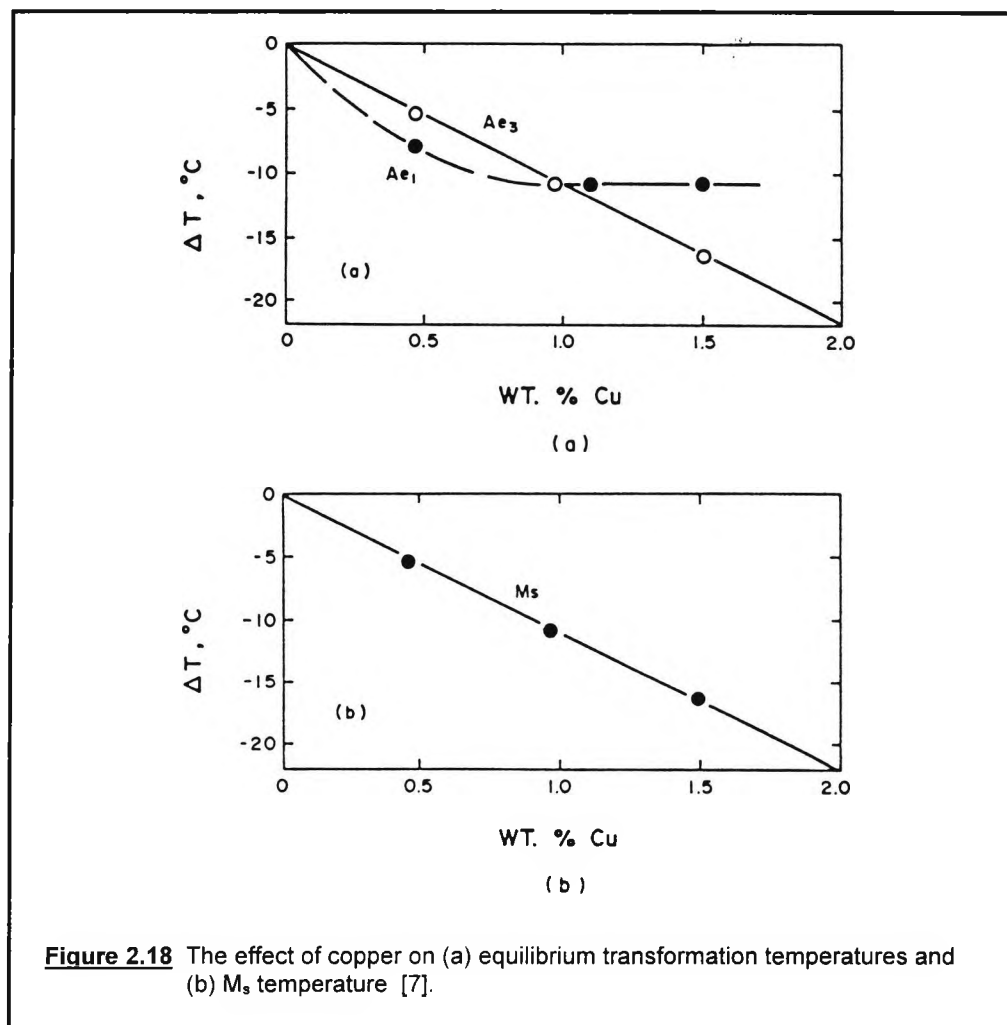


Figure 2.17 Fe-rich side of the Fe-Cu diagram (based on data from ref.[82]).

2.6.2 Hardenability and transformation kinetics

Only limited information is available regarding the effect of Cu on the hardenability and transformation kinetics of steels. It is known that copper slightly lowers the allotropic and M_s temperatures [7], the extent of the decrease being proportional to the Cu content as show in Figure 2.18. Copper delays the decomposition of austenite as it is a mild austenite stabilising element. Grange *et al.* [83] have observed that, in a medium carbon steel, Cu additions retarded the transformation of austenite more or less equally at all temperatures, this being shown in Figure 2.19. Habraken and Greday [7] have reported a continuous cooling transformation diagram for a Cor-Ten steel (0.32% Cu) of a thickness between 5 and 15 mm, using dilatometry and thermal analysis measurements, Figure 2.20. This diagram exhibits a fairly large bainitic domain. Metallographic examinations verified that the structure was composed mainly of ferrite, pearlite and granular bainite.



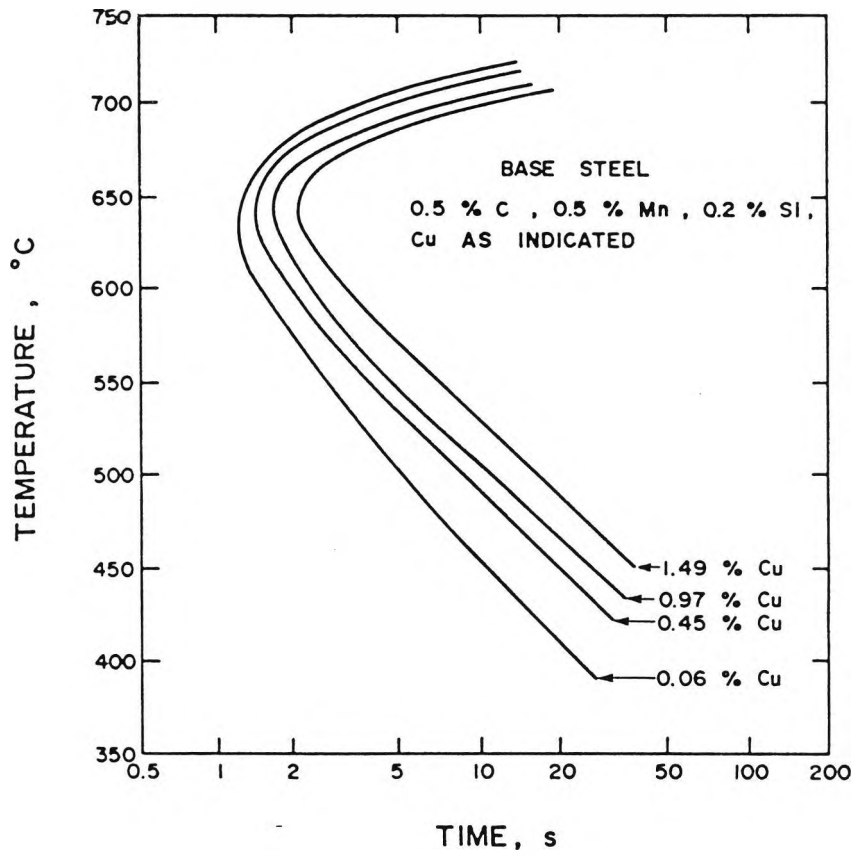


Figure 2.19 The effect of copper on the time for 50% isothermal transformation in a medium carbon steel [83].

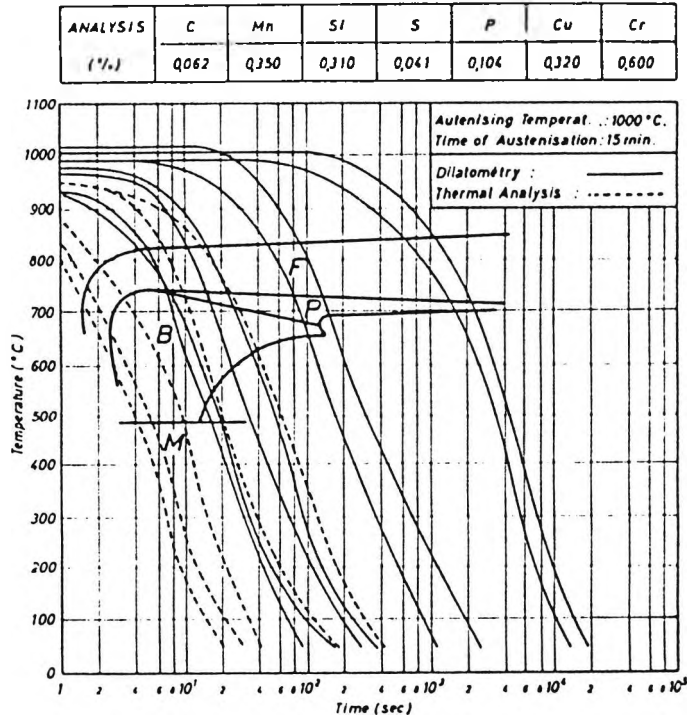


Figure 2.20 CCT diagram of COR-TEN steel [7].

Krishnadev [16] has reported that the combined additions of Cu and B to low carbon steels resulted in a lowering of the transformation temperature to a greater extent than expected from a summation of the individual effects.

The definition of hardenability is concerned primarily with microstructure and it is therefore important to mention the effect of different cooling rates on the microstructure of Fe-Cu alloys and Cu-containing steels. Martensitic transformation and massive transformation are two terms describing the mechanisms of transformation[12]

Martensitic transformation is a completely diffusionless transformation. Once the stable nucleus is formed, the interface is propagated by means of the systematic coordinated shear of large regions of the parent phase containing many atoms, in such a way as to create an entirely new lattice. The distance through which any single atom moves relative to its neighbours is less than one atom spacing. No interchange of position is possible and so the compositions of parent and product phase are identical. The most characteristic feature of this type of transformation is the shape change produced by a shear deformation[12]

Massive transformation occurs by the rapid movement of an incoherent interface which is capable of propagating across parent grain boundaries. Although the transformation is diffusionless in the macroscopic sense, advancement of these interfaces is accomplished by an atom rearrangement [84]. Although requiring short-range diffusion at the interface, propagation still occurs so rapidly that the reaction can not be suppressed with normal cooling rates. The resulting microstructure shows massive, irregular grains with faceted boundaries. Hence this transformation has been termed massive transformation[12]

The combination of various alloying elements in the Fe-Cu system has a significant effect on the transformation kinetics. Thompson *et al.* [34] have recently studied the Continuous Cooling Transformation (CCT) and the microstructures in a low-carbon, HSLA plate steel with slightly higher alloy additions than ASTM A710 steel (0.06% C, 1.45% Mn, 0.032% Al, 1.25% Cu, 0.97% Ni and 0.42% Mo) and found that the CCT diagram, Figure 2.21 showed significant suppression of the polygonal ferrite formation and a prominent transformation region, normally attributed to bainite formation, at temperatures intermediate to those of polygonal ferrite and martensite formation [34].

In the intermediate region, ferrite formed in groups of similarly oriented crystals about 1 μm in size and contained high density of dislocations produced by the transformation of austenite during continuous cooling. The ferrite grains assumed two morphologies, elongated or acicular and equiaxed or granular. Austenite regions, some transformed to martensite, were enriched in carbon and retained at interfaces between ferrite grains. At slow cooling rates, polygonal ferrite formed, containing low dislocation densities and incoherent ϵ -copper precipitates that had formed by an interphase transformation mechanism.

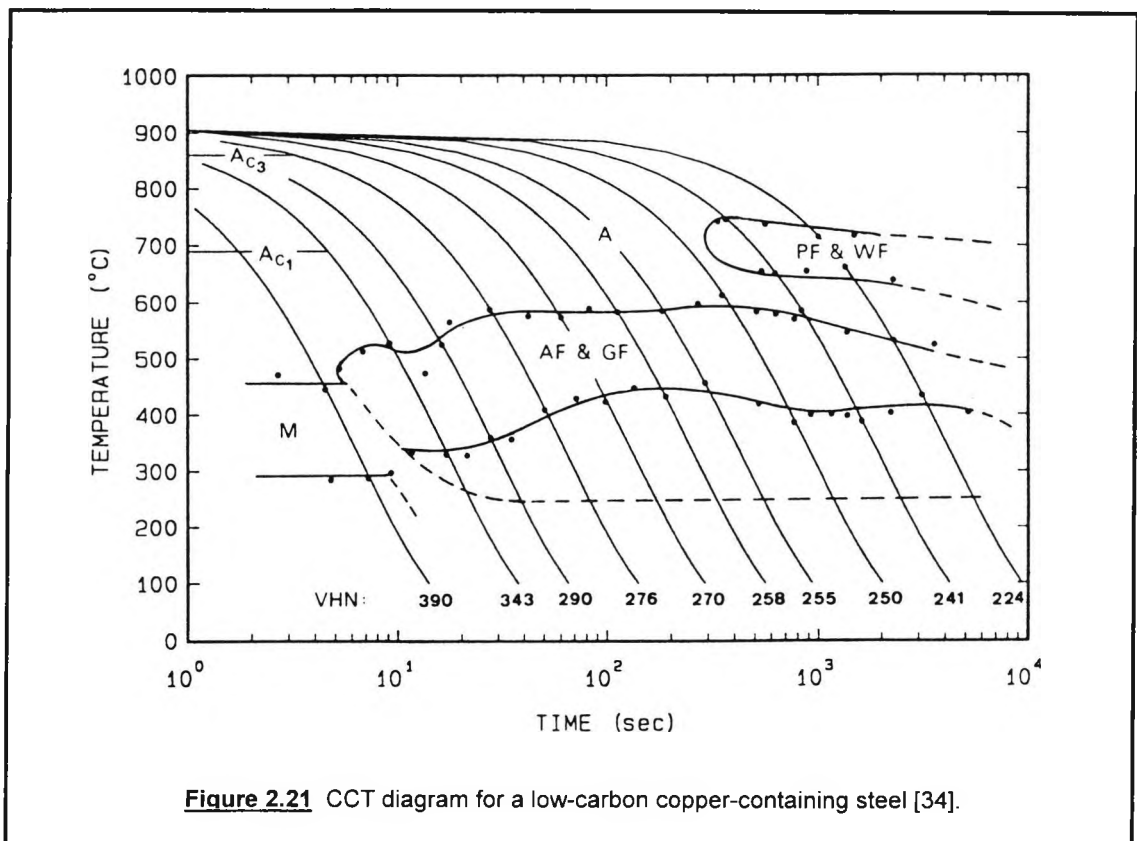


Figure 2.21 CCT diagram for a low-carbon copper-containing steel [34].

2.6.3 Copper precipitation in steels

Because of the decrease in solubility of Cu with decrease in temperature, in the iron-copper system, ϵ -phase can be precipitated by ageing supersaturated α -phase which has been previously formed upon rapid cooling. The process can be described in terms of the formation and growth of coherent BCC Cu-rich clusters, the transformation of these to FCC ϵ -phase particles, and the subsequent growth of these to form rod-like precipitates after prolonged ageing [16].

The precipitate morphology and its nucleation sites vary with respect to the type of heat treatment, the alloy composition and the cooling rate from the austenitising temperatures.

Krishnadev and Le May [56] have examined the microstructure of a water-quenched commercial low-carbon copper-bearing steel (0.05%C, 2.14%Cu, 1.45%Ni) and observed that after prolonged ageing, ϵ -phase precipitation took place both along dislocations and uniformly around the matrix. This was in contrast to the predominant nucleation along dislocations observed by Cox [54] in a 0.3%C, 1.5%Cu steel, but the greater carbon content may have increased the degree of supersaturation sufficiently to alter the criterion for nucleation [16].

Uniform precipitation has also been reported by Hornbogen and Glenn [51,85]. In their work they have concentrated on a pure metallographic study of the precipitation of copper from α -iron and they separated precipitation into three stages. In the first stage shortly after ageing at 500 and 600 °C, spherical particles with diameters less than 100Å have been observed to form at a high rate. During the second stage, the particles grew at a different rate, proportional to the square root of time (i.e. slower) and in the third stage, growth was observed to be much slower; rod-shaped particles formed after long ageing times at 700°C.

Limited information is available regarding the ageing kinetics of Fe-Cu alloys and Cu-containing steels. Hornbogen and Glenn [51] have reported that the only experimental evidence for clustering was the time dependence of the appearance of particles of measurable size. After their appearance the ϵ -particles have been observed to be growing slowly by normal volume diffusion. The rate of growth has been found [51] to obey Zener's equation:

$$d_p = \alpha \cdot (D_f \cdot t)^{1/2} \quad \dots(2.26)$$

where d_p is the particle diameter, D_f the volume diffusion coefficient and α a constant that depends upon the concentration distribution inside and outside the growing particle and t is the time. This equation can be applied for particles that are almost spherical.

In contrast to Hornbogen's and Glenn's findings, Cox [54] has observed copper precipitation mainly on dislocations in a 0.3%C-1.5%Cu steel that had been previously austenitised at 870°C for 1 hour and quenched in water and then tempered for 1 hour in the range of 100-700°C. These copper precipitates were spherical and have first been observed after tempering at 600°C; the rate of growth was then reduced and at 700°C began to grow into rods. Possible reasons for precipitation at dislocations were the following: 1) the precipitation of copper at dislocations would be favoured if the carbon increased the supersaturation since the rate of precipitation depends upon diffusion in the matrix and 2) the increased number of dislocations arising from the martensite transformation should offer more sites for the precipitation of copper.

Hornbogen and Glenn [51] have also made an attempt to explain the transition from spherical to rod shape during the growth of the particles. For the particles of a size from 50 to 300Å, surface energy may be the factor that determines the spherical shape. When the particles grow larger, this factor becomes less important. Reference has also been made to Nabarro, who showed that the strain energy of a noncoherent ellipsoidal particle will decrease in the following sequence: sphere → needle → disc, which could explain the rod shape of particles with a major dimension of more than 300Å. Disc-shaped copper particles might be observed after very long periods of ageing at high ageing temperatures.

In the study that was carried out by Hornbogen [85], the role of strain energy during the precipitation of copper and gold from α -iron was examined, and was found that little strain energy is required for the nucleation of copper rich particle, because the atomic volume of the matrix and that of the precipitate are about equal. The nucleation barrier was found to be determined only by the surface energy between the FCC particle and the BCC matrix. The following equation was taken as a starting condition for nucleation if the solution becomes supersaturated:

$$\Delta G = \alpha \cdot \gamma \cdot \nu^{2/3} + \beta \cdot \nu \cdot (\Delta G_C + G_E) \quad \dots(2.27)$$

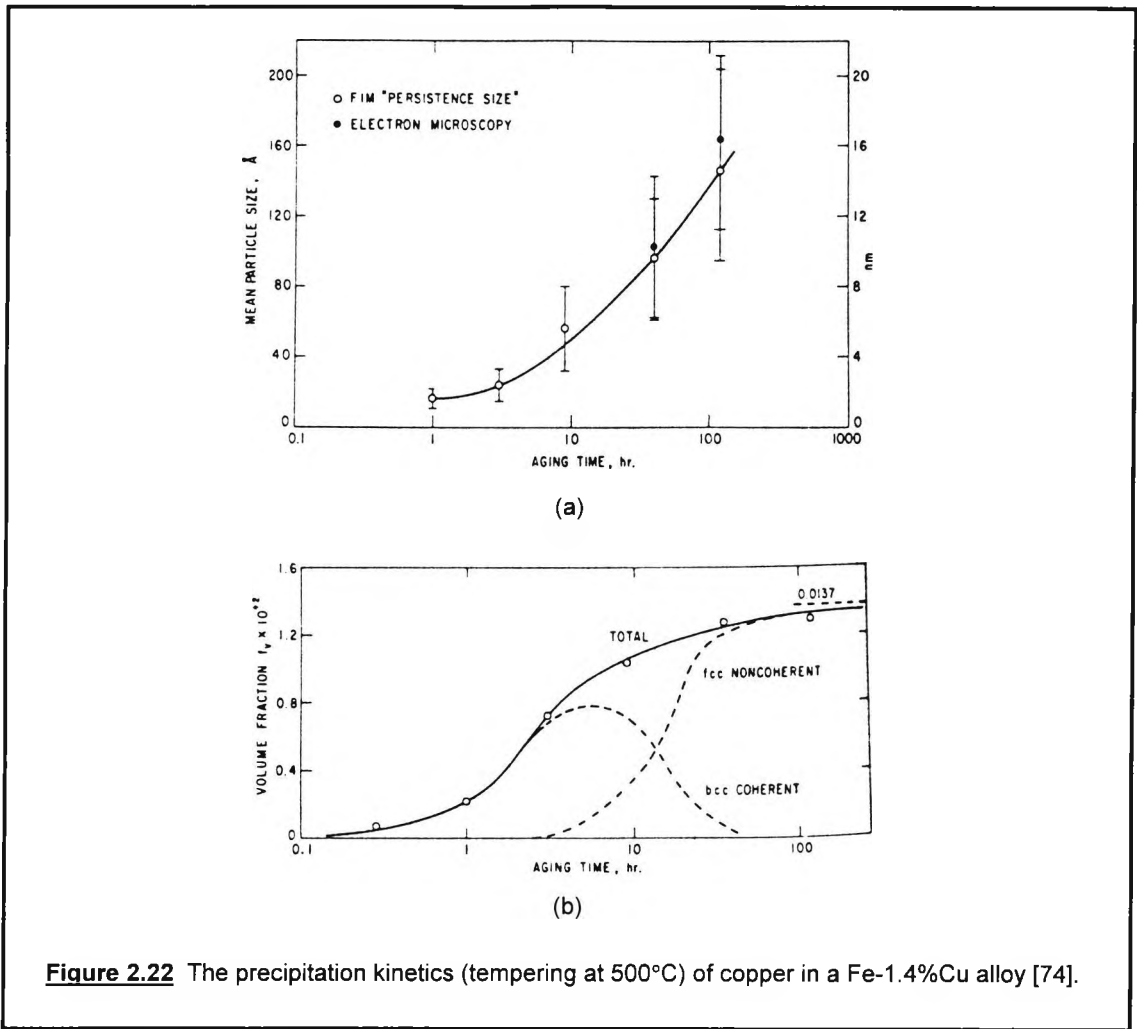
where G_E is the strain energy needed for formation of the nucleus, ΔG_C is the chemical energy gained from the formation of the nucleus, ν is the number of atoms in the nucleus and α and β are constants that depend on its shape. Although uniform precipitation was observed, the largest number of nuclei were those that formed

without visible relation to imperfections and these determine the precipitation behaviour of the alloy. Growth of the particles was however, difficult to estimate on the basis of the depletion of the matrix; the reason is that larger particles tend to grow at the expense of smaller particles, even long before the matrix is depleted. The nucleation and growth of gold particles in the iron matrix was found to be difficult due to the large difference in size between gold atoms and iron atoms in contrast to the small size difference between copper and iron atoms. This led to the favoured nucleation site for gold particles being at dislocations. This difference between the two systems illustrated the effects of a very low and a very high strain energy barrier to nucleation.

The change from initial spherical to rod-like morphology on prolonged ageing is due to either the minimisation of strain energy [85] or the anisotropy of the surface energy [53]. Speich [53] has reported the length to radius ratio in a heavily over-aged Fe-Cu alloy as being constant and about 10, however Krishnadev [56] has reported the observations of precipitates with ratios in the range 20 to 50.

The copper precipitates that are coherent with the matrix are very difficult to observe because the lattice structure is continuous across the interface and into the precipitate. In addition to this, the atom sizes of copper and iron are similar. However, Goodman et al. [74,75] in a field-ion microscope (FIM) atom probe study of a quenched and aged (at 500°C) Fe-1.4%Cu-0.016%C alloy, have examined the morphology of copper precipitates and reported the presence of a fine coherent copper precipitate no larger than 5 nm. They have also observed that contrary to previous theories, the coherent precipitates did not consist solely of Cu atoms, but were a mixture of Fe and Cu atoms (50% each). The precipitation kinetics of copper have also been studied, Figures 2.22 (a) and (b). It has also been reported that the size of the coherent particles was 2.4 nm at peak hardness (~10 h at 500°), and that the particles lost their coherency with the matrix and transformed to the FCC ϵ -phase when they had grown above 5 nm in diameter.

It must be mentioned however, that most of the above investigations have been performed on high purity Fe-Cu alloys that were solution-treated at very high temperatures (~1000°C), for long times (3~20 h) and rapidly cooled in order to ensure that all the copper had been kept in solution. The morphology and the ageing kinetics of copper precipitation will certainly change when commercial alloy compositions and economic manufacturing processes are being employed [5].



Mclvor [55] have reported that in a normalised mild steel (0.16%C, 0.52%Mn, 1.5%Cu) of ferritic structure, copper precipitation was characterised by the formation of parallel rows of ϵ -Cu precipitates. This type of precipitation, termed as *interphase precipitation*, is usually found in low alloy steels containing strong carbide forming elements and it has been found to occur at the advancing ferrite/austenite interface [86]. This type of precipitation has also been reported [86] to result in the formation coherent Cu particles.

Wada *et al.* [66], have observed that if the cooling rate from austenitising temperatures is not too fast to retain all the copper in solution, then the equilibrium state will not be obtained. According to the adopted cooling rate, the steel at room temperature will consist of supersaturated ferrite matrix and ϵ -phase precipitates. They [66] have

referred to this phenomenon as “cooling precipitation” and derived the following equation to predict the minimum cooling rate, **CR**, required in order to retain copper in solid solution:

$$\ln CR (\text{°C/s}) = 1.983 (\%Cu) - 0.077 \quad \dots(2.28)$$

Krishnadev and Galibois [60] have observed very limited precipitation in a Cu-Ni-Nb-Mo low carbon steel after it had been air-cooled from a finish rolling temperature of 760°C. The explanation that has been given, is that the alloying elements, Mo, Ni, Mn and Cr, retard the precipitation of copper because of their effect in delaying the austenite to ferrite transformation.

2.6.4 The influence of copper on the tensile strength of steels

Considerable increases in the strength of ferrite can be obtained from Cu precipitation through grain refinement and precipitation hardening, without having too much influence on the impact transition temperatures.

An interesting question is why a softer phase, like copper, can have a hardening effect on iron [51]. There are three possibilities:

1. the particles do not share plastic deformation and the strengthening effect is given by the average spacing of the particles,
2. the particles cause coherency stresses in the matrix and inhibit the motion of dislocations, or
3. the zones or particles are sheared and the strengthening is given by the energy necessary to shear a particle or zone.

Experiments by Hornbogen and Glenn [51] showed that ϵ -particles are sheared after 10% plastic deformation. Dislocation pile-ups outside a particle, leading to the deformation of the particle on its own system of plastic deformation, seemed more probable than dislocations cutting through the particle. The experiments gave some evidence that two dimensional defects (twins or stacking faults) form, rather than one-dimensional defects, when these particles are sheared. The spherical copper particles seemed to be unchanged by small amounts of plastic deformation, however close observation showed that they contained an increasing number of straight lines, probably due to stacking faults or thin twins.

Goodman *et al.* [74,75] have also attempted to relate the conventional precipitation hardening theories to their observed strength increases and concluded that the theory of dislocation interactions with coherent particles were not sufficiently well developed to make a quantitative comparison.

An interesting strengthening model has been suggested by Knowles and Kelly [87] and is the so-called *elastic modulus hardening*. The model that has been developed, predicted that in the Fe-Cu system, dislocations in the deformed, aged structure should thread through the copper particles. The explanation for this, is that copper has a lower shear modulus than iron and the dislocations will therefore prefer to lower their energy by threading their way through as many particles as possible. This model had also been verified by experiment and applies both for coherent and incoherent precipitation. In that study the results for the over-aged condition have been found to agree with the Orowan criterion for dispersion strengthening. Russel *et al.* [88] who have developed a dispersion strengthening model based on differing elastic moduli for the Fe-Cu system, have also observed that their results were so close to those predicted from the Orowan model, that it was impossible to detect the difference. In an examination of two normalised and over-aged low carbon copper containing steels (0.53 % Mn, 1.05~2% Cu), MacIvor [57] has also found that the strengthening effect is in accord with the Ashby-Orowan strengthening mechanism. However, MacIvor's [57] metallographic observations have suggested that dislocations bow between, rather than thread through, the copper particles.

In a different approach of the subject, Hornbogen and Staniek [59], have investigated the grain size dependence of the mechanical properties of a plastically deformed, age-hardened Fe-1%Cu alloy and observed that for copper particles larger than 15 nm in radius the yield stress is independent of grain size. For particles with a radius of less than 5 nm, an additive behaviour of grain boundary and precipitation hardening has been found. For the intermediate particle sizes, a transition has been found, with grain size dependence for small grain size and independence for large grain sizes.

A series of laboratory Fe-Cu steels with very low carbon content have been investigated by Wada *et al.* [66], the copper content increasing in 0.2% steps, up to 2%. In their work which generally refers to the strengthening effects of copper in steel, various aspects such as solid solution hardening and precipitation hardening have

been examined, as well as the grain refinement effect of copper and the effect of alloying elements on the strength of commercial copper-containing steels. Finally a series of composition-property relationships were established. In their study of quasi binary Fe-Cu alloys, they have found that there is a linear relationship between the copper content and the inverse square root of the mean grain diameter, both for the water quenched and air cooled condition.

2.6.5 Commercial copper-containing steel alloys

In commercial copper containing steels, the strengthening that is induced by alloying elements is enhanced by the precipitation effect of copper. The work that has been carried out in the past is concerned with the effect of different chemical compositions on the strength and on the ageing kinetics of the commercial copper containing steels.

Krishnadev and Galibois [89] studied the combined effect of Cu and Nb on the age-hardening response of a 0.02%C, 1.88%Mn, 0.11%Nb, 1.52%Ni, 1.86%Cu steel and found that the duration of the peak hardness plateau was greater than that of a similar Nb-free steel, Figures 2.23 (a) and (b).

In a comparison between the ageing characteristics of a low carbon Cu-Ni-Nb steel with those of a Cu-Ni-Nb-Mo steel, both in the as-quenched (1250°C for 1 h, water quenched) and normalised conditions, it has been found [5,60] that the addition of Mo has a great effect in intensifying the strengthening response due to Cu precipitation, figures 2.24 (a) and (b). Krishnadev and Le May [12] have explained that because Mo and Cr additions retard the premature precipitation of copper, further strengthening can be achieved by ageing. Krishnadev and Galibois [60] also suggest that Nb and Mo may prevent the segregation of copper to grain boundaries and therefore improve impact properties.

The structure and properties of the commercially developed Armco "Ni-Cop" alloy which has a chemical composition as specified by ASTM A710 Grade A, has been the subject of several studies [2,63,64,67-69,78]. The observed strength and impact transition temperatures have been found to be in good agreement with the A710 designated properties. Krishnadev *et al.* [67] have observed a maximum yield strength of 640 N/mm² and a 54J ITT of -100°C, in a 19mm plate steel that had been heated at 900°C for 1 h, water quenched and tempered at 600°C for 1 h. Miglin *et al.* [2], in a

study of the same alloy, have obtained very high yield strength results and excellent impact properties, Table 2.4, over a wide range of heat treatments, Table 2.5. The best combination of strength and impact properties has been obtained from heat-treatment C6, i.e. the water quenched (980° for 4 h) and over-aged condition (675° , 4 h), Table 2.4. In an attempt to explain the impact behaviour of the steel, the authors [2] have suggested that the decrease of ITT's is consistent with the resistance of the material to shear localisation. The observation of higher ITT's at peak strength has been attributed to the presence of microstructures that contained a shearable coherent copper precipitate. These structures would be expected to be more susceptible to shear instability than those containing the larger semi-coherent precipitate.

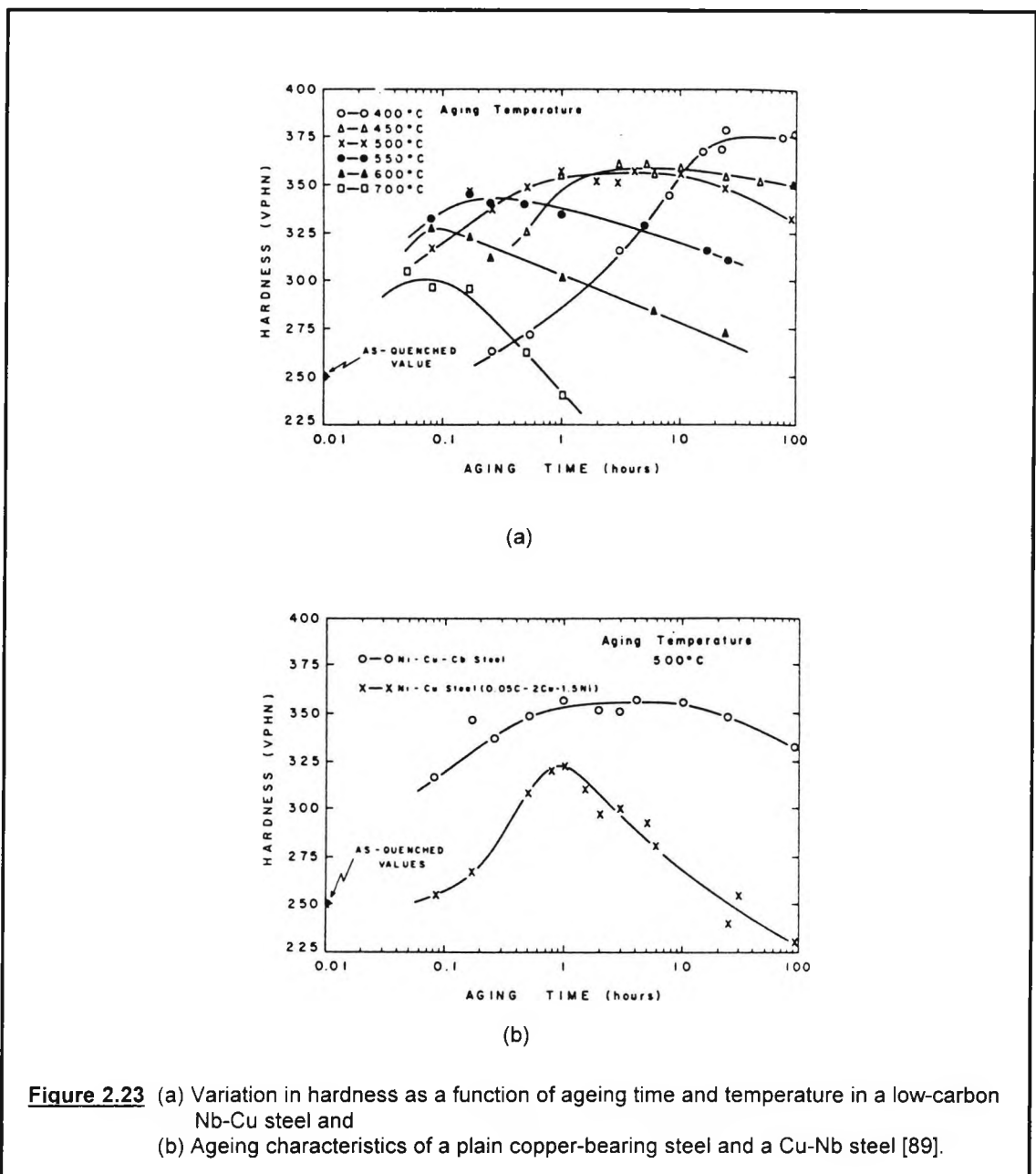
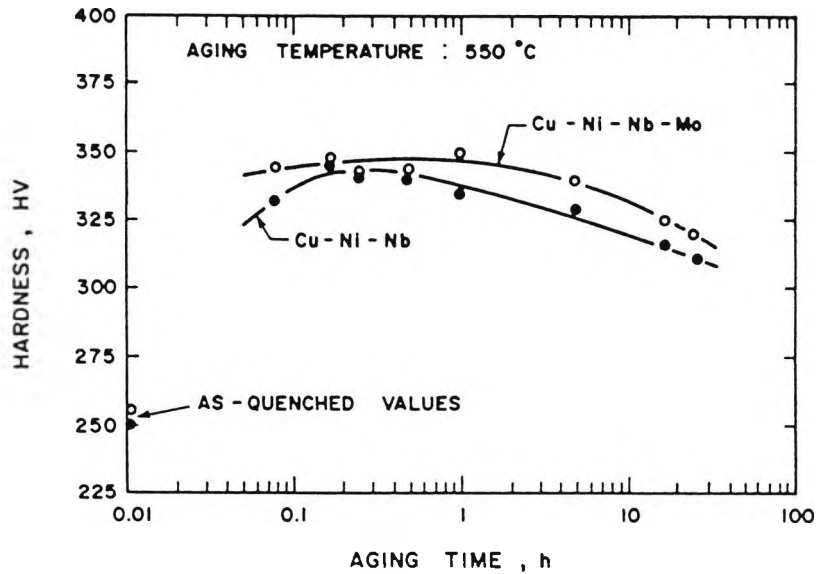
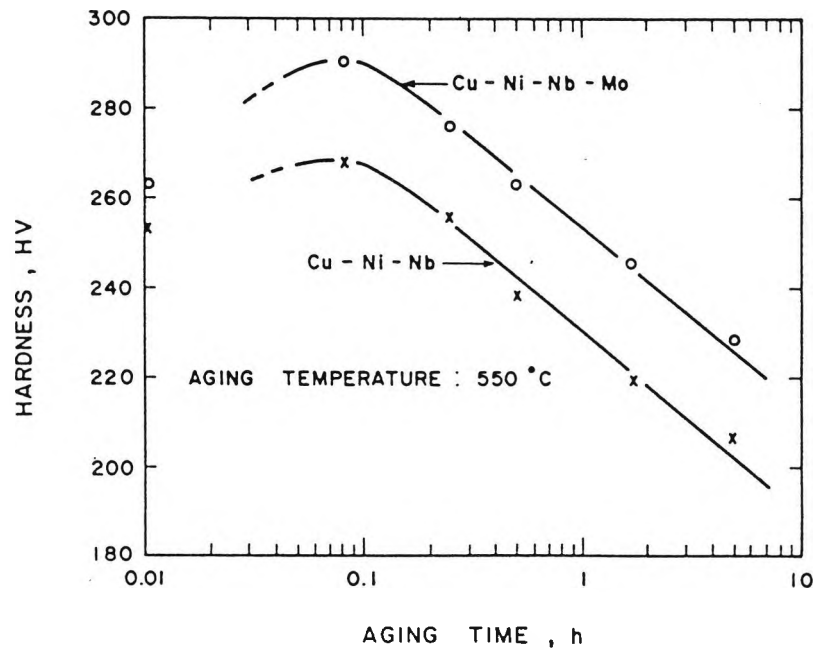


Figure 2.23 (a) Variation in hardness as a function of ageing time and temperature in a low-carbon Nb-Cu steel and (b) Ageing characteristics of a plain copper-bearing steel and a Cu-Nb steel [89].



(a)



(b)

Figure 2.24 The effect of 0.3%Mo addition on the ageing characteristics of a Cu-Ni-Nb steel
 (a) water-quenched (from 1250°C) and tempered at 500°C and
 (b) normalised (at 950°C for 1/2 h) and tempered at 500°C.

Tensile Properties and Charpy V-Notch Impact Data

Heat Treatment	0.2 Pct Offset Yield Strength, (MPa)	Ultimate Tensile Strength, (MPa)	Total Elongation in 25 mm, (Pct)	Strain-Hardening Exponent, n	Charpy 47-J Transition Temperature, ($^{\circ}$ C)
AR	601	682	20	0.129	-56
C1	501	661	34	0.216	-105
C2	572	695	33	0.159	-66
C3	411	475	48	0.213	-157
C4	653	737	32	0.135	-106
C5	715	806	23	0.102	-51
C6	486	544	36	0.118	-175

Table 2.4 Mechanical properties of an ASTM A710 steel [2].

Microstructures and Heat Treatments

Heat-Treatment Number	AR (As-Received)	C1	C2	C3	C4	C5	C6
Austenitizing temperature, C	(Control rolled)	900	1095 ^(a)	900	980	1095	980
Austenitizing time, hours	—	8	1 ^(a)	8	4	1	4
Cooling	—	Air cool	Furnace cool	Air cool	Water quench	Water quench	Water quench
Tempering temperature, C	595	535	535	675	535	535	675
Tempering time, hours	1	1	1	4	0.5	1	4
Ferrite morphology	Polygonal	Polygonal	Coarse acicular	Polygonal	Polygonal	Fine acicular	Polygonal
Ferrite mean-intercept grain size, μ m	5.0	4.5	—	5.6	2.9	—	2.3
Fraction of Nb in interphase precipitates ^(b)	0.25 ^(d)	0.25	1.00 ^(c)	0.25	~0.5	1.00 ^(c)	~0.5
Fraction of Nb in austenite-nucleated precipitates	0.75 ^(d)	0.75	—	0.75	~0.5	0	~0.5
Coherency of Cu precipitates	Coherent	Coherent	Coherent	Coherent and semi-coherent	Coherent	Coherent	Coherent and semi-coherent
Structure of Cu precipitates	bcc	bcc	bcc	bcc and fcc	bcc	bcc	bcc and fcc

(a) Followed by two-hour solution treatment at 815 $^{\circ}$ C and water quench.(b) Nb (C, N) precipitates that form by precipitation at the α - γ interface during transformation are finer (1 nm diameter) and more closely spaced than those that remain as primary carbides during austenitization and grow somewhat on cooling (10 to 20 nm diameter).^(c)

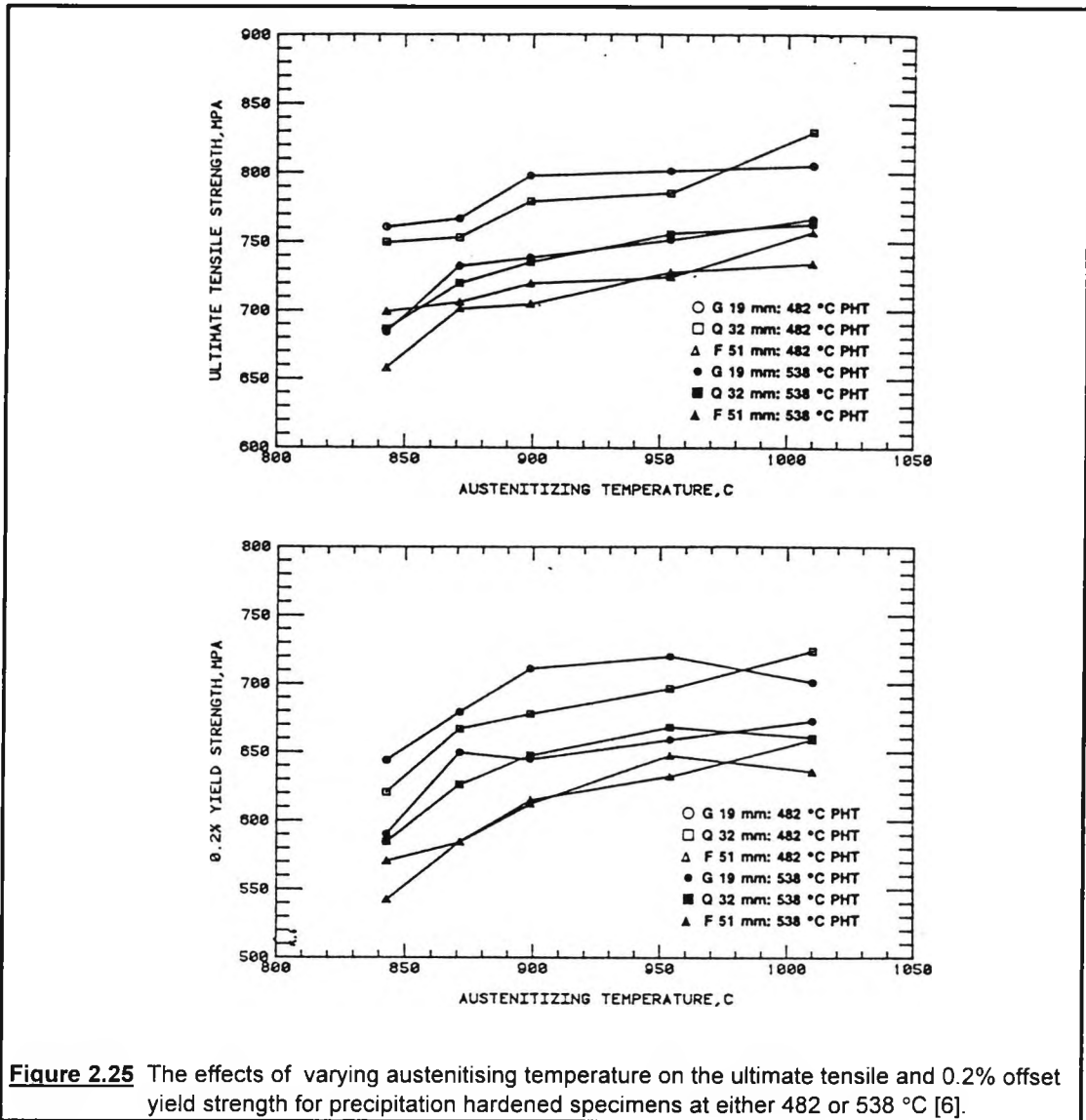
(c) Estimated from solubility data.

(d) Estimated from grain size.

Table 2.5 Heat treatments of an ASTM A710 steel [2].

In a study that has been carried out by Hicho *et al.* [63], the examination of the effect of thermal processing variations on the mechanical properties and microstructure of an ASTM A710 grade A class 3 steel, has been involved and it has been found that a variation of +/- 30 minutes in the austenitising time at 900 $^{\circ}$ C had very little effect on the mechanical properties. Any variation of the properties has been attributed to the changes in the precipitate distribution. However, precipitation kinetics have not been studied quantitatively. In another study [6], the same authors have examined the same steel, concentrating on the optimisation of the austenitising treatment and the cooling rate. Three steel plates of different thicknesses have been examined (19, 32 and 52 mm) and the best results observed for the 19 and 32 mm steel plates when these had been treated at very high austenitising temperatures (~1066 $^{\circ}$ C) and water quenched, Figure 2.25. Referring to the strength properties, the authors [6] have suggested that if

the size and coherency of the precipitates are such that the dislocations can easily move past the precipitate, rather than shear it, then cross-slip occurs and/or the number of dislocations increases. This produces a more uniform slip distribution throughout each grain and results in good toughness in the material.



A modified A710 steel with increased Mn and Mo additions was the subject of an investigation which was carried out by Thompson, Colvin and Krauss [90] in order to examine its structure. The heat treatments involved water quenching of plates that had been previously hot rolled to a final thickness of 31.75 mm and 50.8 mm and austenitised at 900°C. Additionally some plates of 50.8 mm thickness were tempered at 604°C for 1 hour. Transmission Electron Microscopy of the as quenched sample

revealed that the structure was comprised of laths and interlath elements and was initially believed to be upper bainite. The interlath second-phase particle however was not cementite as it should be, but was found to consist of 50% martensite and 50% austenite, a most unusual structure which was defined as granular bainite. After ageing, some cementite was present which was presumed to have formed from pools of austenite. Most of the austenite was however found to be stable during high-temperature (1 h at 604°C) tempering treatments.

More recent work [36,39,79,73] involves the study of the HSLA-100 steel and its modifications. As mentioned at the beginning of this section, the HSLA-100 steel has a composition similar to that of A710 Grade A, but with higher Ni additions (~3.5% Ni). In a study of the effect of the decomposition of the austenite in Fe-Cu alloys, Ricks *et al.* [86] have suggested that the addition of Ni lowers the transformation temperature, therefore favouring the production of Cu-supersaturated ferrite. It has also been found that the presence of Ni in the structure promotes the formation of faceted equiaxed ferrite, Widmanstätten ferrite and bainitic ferrite. Nickel also increases the isothermal reaction time, thereby making it possible for copper to be redistributed in the interphase boundary.

Fox *et al.* [36] have examined the microstructures and the mechanical properties of two HSLA-100 steels, one having a higher copper amount (2% Cu). The two steels were austenitised at 899°C, water quenched and then tempered for 1 hour at various temperatures. As can be seen from Figure 2.26, the maximum 0.2% PS that can be obtained, is 1050 N/mm² after tempering the steel at 450°C for 1 hour. The impact transition temperatures have been observed to be exceptionally low for the as-quenched and over-aged conditions, Figures 2.27 (a) and (b). The as-quenched structures were found to consist of lath martensite with thin films of retained austenite at the lath boundaries and some bainitic ferrite especially at the centre of the plates. After tempering, the retained austenite transformed to bainite.

In a similar study to that described in the above paragraph, Foley and Fine [73] also obtained very good yield strength results after tempering in the 600-700°C region, Figure 2.28. The authors managed to derive a linear relationship between the -84°C impact energy value and the 800-1110 MPa yield strength region, Figure 2.29. It must however, be pointed out that the tempering of high-Ni Cu-containing steels at

temperatures such as 600 to 700 °C ($\alpha+\gamma$ region) results in the formation of *new austenite* which as a consequence influences the age hardening kinetics of copper.

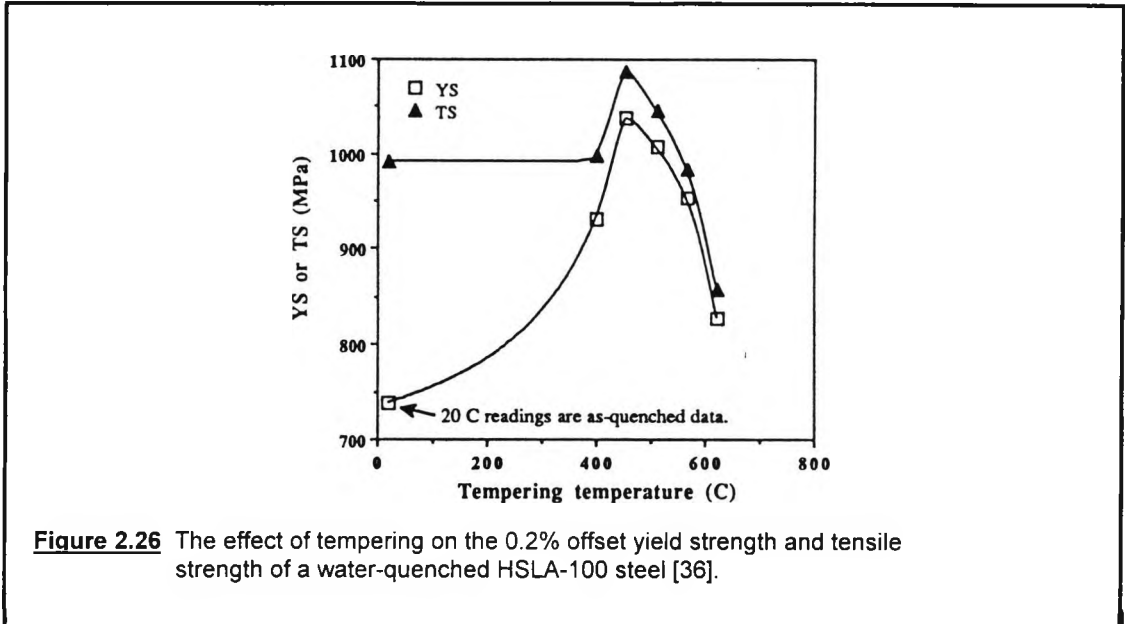


Figure 2.26 The effect of tempering on the 0.2% offset yield strength and tensile strength of a water-quenched HSLA-100 steel [36].

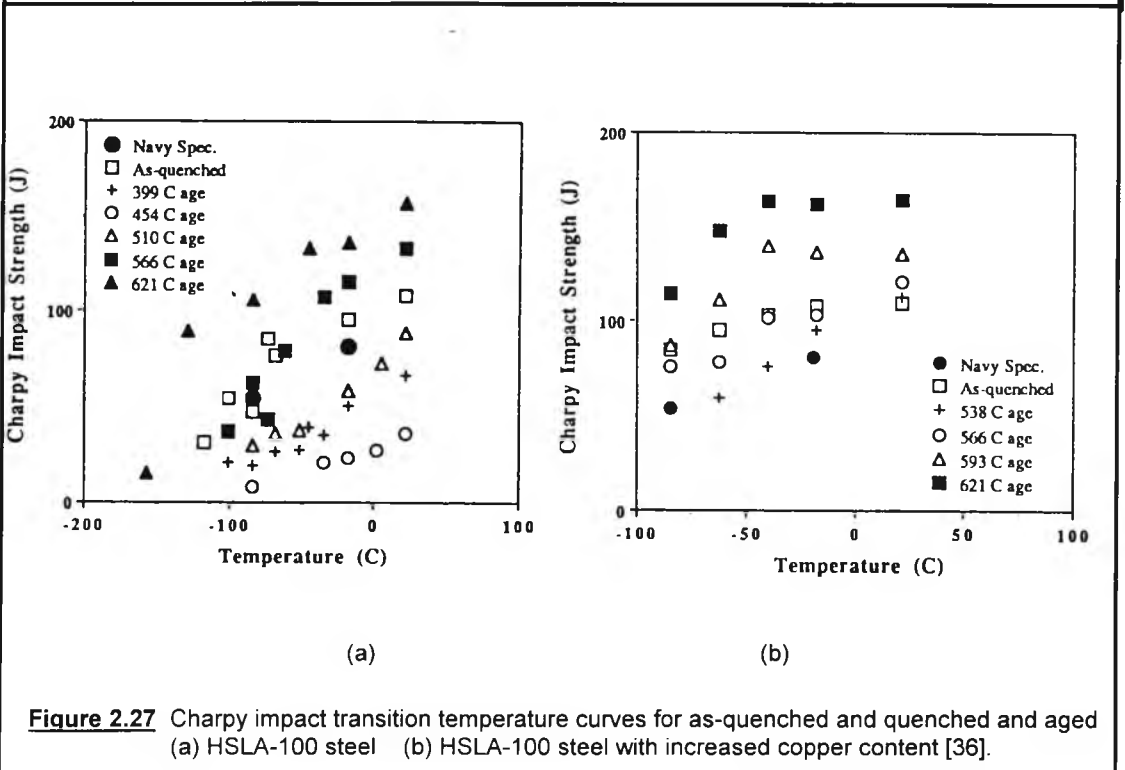


Figure 2.27 Charpy impact transition temperature curves for as-quenched and quenched and aged (a) HSLA-100 steel (b) HSLA-100 steel with increased copper content [36].

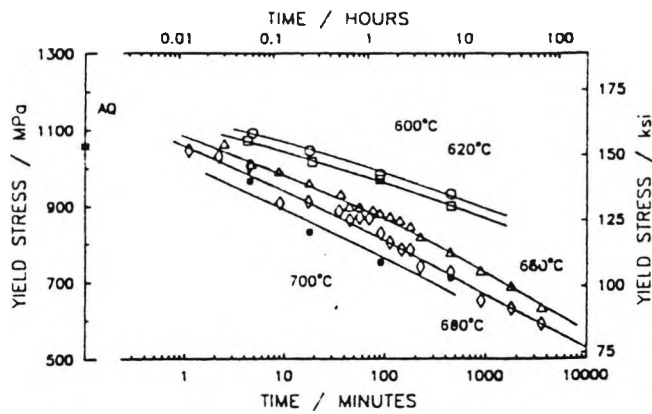


Figure 2.28 The effect of tempering on the 0.2% offset yield strength of a water-quenched (1 h at 950°C) HSLA-100 steel plate (19 mm in thickness) [73].

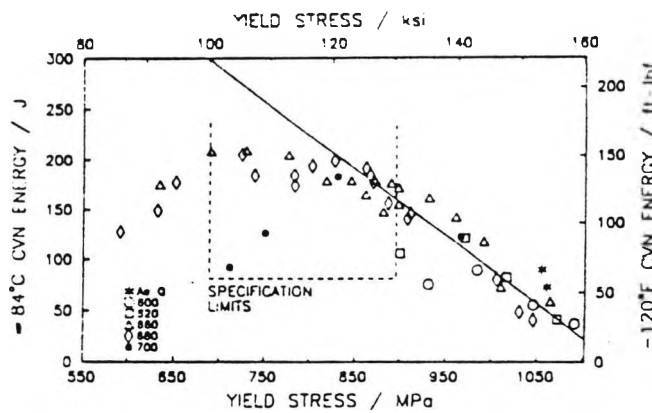
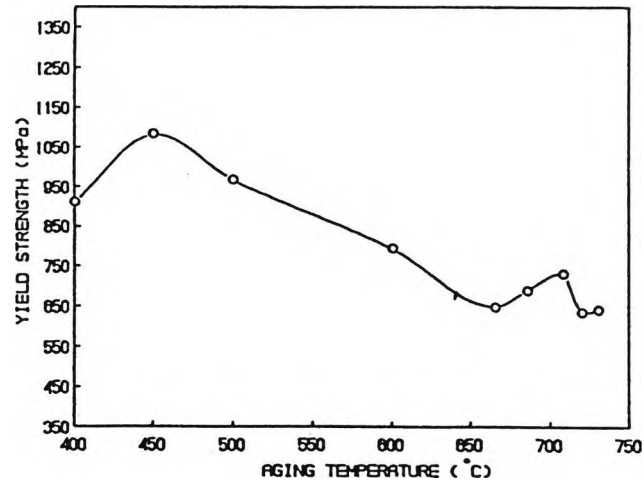
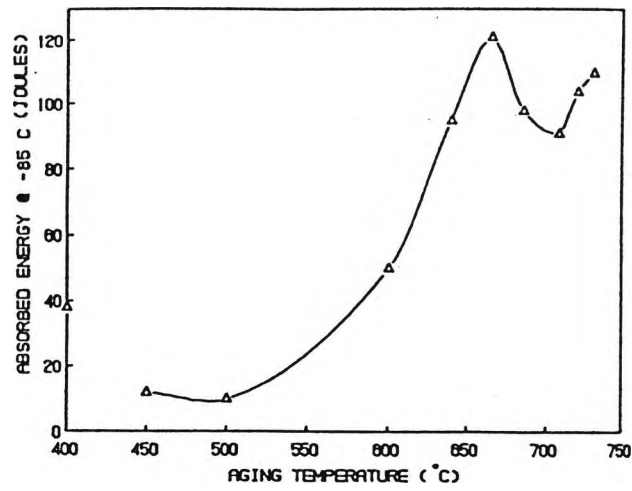


Figure 2.29 The relationship between the -84°C impact strength and the yield strength of a water-quenched and tempered HSLA-100 steel plate [73].

Mujahid, Garcia and DeArdo [39], in an attempt to explain the impact behaviour of HSLA-100 steel, Figures 2.30 (a) and (b), attributed the ITT improvements to the formation of new austenite which has been found to be rich in alloying elements and free of dislocations and starts to occur at 630°C. At tempering temperatures above 660°C, the growth of the new austenite caused the dilution of solutes and finally transformed to martensite or bainite on cooling, therefore leading to the deterioration of the impact behaviour. However, no reference was made to the influence of copper on the impact behaviour of the steel.



(a)



(b)

Figure 2.30 The effect of tempering (1 h) of (a) the yield strength and (b) -84°C impact strength, of a water-quenched (1 h at 900°C) HSLA-100 steel plate (19 mm in thickness) [39].

3

EXPERIMENTAL PROCEDURES

3.1 Introduction

Nine steel plates were received from British Steel Corporation, and their compositions and condition (as received) are shown in Table 3.1. The experimental work consisted of the following:

- Heat treatments (solution treatment, austenitising treatment, ageing /tempering treatment)
- Mechanical tests (hardness tests, tensile tests, impact tests)
- Metallography (optical microscopy, scanning electron microscopy, transmission electron microscopy)

3.2 Heat treatments

A number of plates from steels No1, 2P1H and 4P28H were solution treated near the A_{e1} temperature (between 700 and 720 °C) for 1 hour and were then quenched in ice/brine. An Isoheat air-circulatory electric furnace, equipped with a EURO THERM controller/programmer type 815, was used for all the solution treatments and care was taken to ensure minimum period of time elapsing between opening the furnace and

quenching. Some of the above plates were left in the as-quenched condition and some were aged at temperatures not exceeding 100°C. Ageing treatments for steels No1 and 2P1H were carried out using a B&T UNITEM electric oven. In the case of steel 4P28H, a GALLENKAMP Hotbox electric oven, equipped with a fan and a GRANT ageing bath were used. A 70:30 ethanol/water solution was used for the ageing bath. All the material concerning this exercise was kept in a freezer when not in process since ageing at room temperature would occur.

For steels 2P1H and 4P28H, trial heat treatments were carried out prior to the actual heat treatments to check the structure and hardness and to investigate the age-hardening behaviour of each steel before any decisions were made concerning heating times and temperatures. For these trial heat treatments a plate from each of the two heats, having the same dimensions as the actual plates, was solution treated and quenched. Then this plate was cut into strips (≈ 15 mm in thickness), followed by slicing into smaller pieces (15-30 mm in length). These small pieces were aged at various temperatures for various periods of time and the age-hardening behaviour of the steels was determined.

Age-hardening trials were also carried out for steel No1, but only at a small scale because there was limited material quantity.

For steels 1P140M, 2P148H, 2P149H and 2P150H, heat treatments involved austenitising, quenching, normalising and tempering. Austenitising treatments were carried out in an Isoheat electric furnace equipped with a EURO THERM controller, for a period of 1/2 hour. Several cooling rates were examined such as oil-quenching, for which a synthetic quenching oil was used as the quenching medium. Normalising was also examined as well as a slower cooling rate, which was achieved by surrounding the austenitised plate with vermiculite. The tempering treatments were carried out in the EURO THERM furnace mentioned above. Trial heat treatments were also carried out prior to any actual heat treatment. Full-size samples were used for the trial austenitising treatments, and small ones for the trial tempering treatments, in order to obtain the most suitable tempering temperature/time combinations.

During all the heat treatments mentioned above a thermocouple consisting of nickel-chromium and nickel-aluminium was used for monitoring the plate temperature. The nose of the thermocouple were inserted in a hole (50 mm long) that had been drilled at

the centre of the plate along the rolling direction and its two ends were connected to a potentiometer. The voltage reading was converted into temperature from appropriate voltage/temperature tables for that particular thermocouple.

Cooling curves of temperature against time, were constructed for each plate in order to check the cooling rates. The time taken to cool from 800 to 400 °C was used to obtain the average cooling rate.

Care was taken to keep heating and cooling conditions as uniform as possible. This was achieved by:

- Keeping plate dimensions the same, Figure 3.1.
- Keeping the volume of the cooling medium constant when this was required.
- Recording every possible information concerning each individual heat treatment.
- Monitoring of furnace heat-up time and avoiding furnace overheating. Furnace overheating was achieved by eliminating the number of heat treatments in the same furnace, to once a day.

3.3 Mechanical tests

The mechanical tests that were used to determine the mechanical properties of the steels that were examined, were impact, tensile and hardness tests. These are generally the most frequent tests that are used in accordance with metallography in order to establish structure-property relationships.

Plastic deformation of certain pieces of steel 2P150H was carried out in order to examine deformed microstructures and particles on the microscope. A 10 to 20% deformation was achieved by stretching 4 mm rods on a LLOYD floor model M30K tensile test machine.

3.3.1 Impact tests

Impact or notched bar tests measure the ability of a material to resist brittle fracture i.e. its toughness. Notches produce triaxial tension stresses which increase the ratio of tensile to shear stresses. There are two types of notched bar tests and these are the Izod and the Charpy test. In both tests the test piece is placed on a vice and a weighted pendulum, swinging on ball bearings, is raised to a standard height and allowed to strike the specimen at a certain speed. The energy that is absorbed is indicated by a pointer and gives an assessment of the ductility of the material. Test

pieces have a 10 mm² section with a standard V-notch. Izod specimens have a cylindrical section while Charpy specimens have a square one (see Figure 3.2). In Izod tests, the striking velocity is slow and tests are usually performed at room temperature and this type of test is therefore used for the classification of a material as tough or brittle. Charpy tests are almost universally used now in determining the Impact Transition Temperature (ITT) of steels, since their geometry allows them to be tested over a wide range of temperatures.

In this study, standard Charpy samples with a 45° V-notch, 2 mm deep and a 0.25 mm radius, were machined and checked to B.S.131 part 2. The Charpy samples were taken from the longitudinal direction of the steel with the notch being machined across the thickness (transverse direction). Each heat treated plate was wide enough to provide enough material for at least 8 specimens (see Figure 3.1) and these were tested over a wide range of temperatures.

An AVERY-DENISON impact test machine, No. 6703/A/31045, was used which was calibrated to B.S.131 part 4. Samples were placed on the machine vice in a horizontal position by the use of a metal holder/carrier and these were struck by the pendulum at a speed of 5 m/s with a maximum capacity of 300J.

In order to achieve the wide range of temperatures that was mentioned above, various cooling or heating baths were used and these are summarised as follows:

- **Ethanol / dry ice mixture:** this bath was used for obtaining temperatures in the range of 20 to -60 °C. The solution was prepared in a stainless steel container which is manufactured to be used for cryogenic products.
- **Liquid nitrogen / isopentane:** Liquid nitrogen was poured to an AMSLER Tv742 cooling chamber and this would circulate around a smaller chamber containing isopentane. The samples were placed in the isopentane chamber where a thermostat and a stirring mechanism would maintain the temperature constant. This cooling method is capable of achieving temperatures from 20 to -140 °C.
- **Water:** warm and hot water baths were used for very brittle samples that had to be heated if a 100% ductile fracture was required. A hot plate would be used for heating a beaker full of water and temperatures from 20 to 100 °C were obtained using this method.

- **Electric furnace:** for obtaining test temperatures higher than 100°C, the charpies were first warmed up in boiling water and then inserted into a hot furnace. The temperature was monitored with a thermocouple. As this is an unusual technique, a sufficient number of test trials were carried out prior to the actual tests, in order to calibrate the furnace temperature and the heating period.

For all the above methods several types of thermometers were used to monitor the temperature. These were manufactured according to B.S.1704 and are the following:

1. 20 to -140 °C alcohol thermometer encased in a steel tube.
2. +30 to -120 °C alcohol thermometer.
3. +20 to +120 °C mercury thermometer.
4. -150 to +800 °C battery operated DIGITRON digital thermometer type 3204Pt, B.S.1904.

In order to comply with B.S. 131, part 2, in all cases the period of immersion of the test sample and the holder in the cooling bath at the required temperature must not be less than 10 minutes and the test piece must be broken within 5 seconds from the time of removal from the bath.

The percentage fibrous/brittle fracture was estimated by observing the fractured surfaces under an optical microscope which had a 10x10 mm² square grid.

3.3.2 Tensile tests

Tensile tests were carried out on various testing machines at room temperature. A HOUNSFIELD (horizontal type), a LLOYD (vertical type, floor model W30K) and an INSTRON (vertical type, floor model 4204) tensile testing machines, were used. Most of the tests were carried out on the last two of the machines mentioned above, of which the INSTRON was preferred since an extensometer (10 and 25 mm) could be fitted onto the gauge length of the tensile sample so that the strain could be measured accurately. The Lloyds machine was however more user-friendly since it was remotely operated with the aid of a PC (80386 microprocessor) and test results could be stored on a floppy disk and were of course nicely presented. Tensile test machines were always calibrated before any testing was done.

The sample geometry can be observed in Figures 3.3 (a) and (b). Sample type (a) was rarely used (only when insufficient material was available) because of its poor design as compared to (b). At least two samples from each plate were tested. Before placing the specimen in the machine its diameter was measured with a micrometer and two small 'pop' marks were made at a distance apart corresponding to the gauge length on which the extension was going to be measured.

The test speed was set so that a strain rate of 1.2 to $1.4 \times 10^{-3} \text{ s}^{-1}$ which complies with the B.S.18, part 2, which specifies the maximum strain rate to be $2.5 \times 10^{-3} \text{ s}^{-1}$. After breaking the sample the reduction of area was measured using a device specifically designed for this purpose. Elongation was also calculated, after examining the final length (a magnifying lens was used for accuracy). As some samples did not exhibit a yield point, a 0.2% and a 2% proof stress was calculated.

3.3.3 Hardness Tests

Hardness tests were carried out at various stages, on a VICKERS-ARMSTRONG pyramidal diamond hardness machine using a 10 kg load. At least five hardness impressions were made on each sample and an average value was calculated. Tests were carried out after heat treatments, on broken charpies and on broken tensile samples. Surface preparation was carried out on grinding wheels before testing.

The presence of more than one phase in most of the steels examined and the difficulty in identifying those phases made the use of micro-hardness tests necessary. These were carried out mainly on broken charpies with the use of a SHIMADZU microscope equipped with a pyramidal diamond indenter. The samples were mounted in thermosetting material, ground, polished and etched (see optical microscopy below), prior to micro-hardness testing.

Hardness and micro-hardness equipment were always calibrated against standard blocks with known hardness, before the tests took place.

3.4 Metallography

Metallography is the science of studying, interpreting and recording detail of the physical structure of metals by means of the microscope. The purpose of a metallographic study is to determine the structure of a metal, such as phases, grain

size, phase volume, particles and in the end correlate all this information with the mechanical properties. All the information mentioned above, can be recorded, illustrated and studied with the aid of photomicroscopy.

Metallography was the main core of the experimental part of this study and proved to be very tedious, since steel specimens that contained copper were difficult to prepare as they oxidised rapidly and their structures were difficult to identify. Almost all of the samples had to be prepared a number of times, measurements repeated and photographs retaken, redeveloped and reprinted, before deemed satisfactory. These tasks took an enormous period of time.

The main aspects of metallography are therefore, sample preparation and microscopy.

3.4.1 Sample preparation

Samples for micro-structural examination were cut from the broken charpies. The surface that was examined was that opposite to the notch (i.e. along the rolling direction). Below, the main stages of sample preparation are described for samples that were examined using the optical and scanning electron microscopes.

- **Cutting:** this was performed with the use of two METASERV cut-off abrasive wheel machines. Sufficient coolant was used to prevent burning or deformation of the metal. The samples to be mounted, were cut at a length of 20 mm. Those to be fitted in the scanning electron microscope holder, were cut to 10 mm in length, so that the surface could be set flush with the top of the holder ensuring that the magnification on the screen needed no correction.
- **Mounting:** two mounting presses were used for this purpose, one being a BUEHLER manual mounting press, model SIMPLIMET 2 and the other a METASERV automatic mounting press. BUEHLER transoptic powder was used for the optical microscope moulds and a conductive powder (bakelite) the as used for the SEM samples.
- **Grinding:** this was carried out on a series of progressively finer grades of waterproof abrasive papers over which a stream of water was allowed to flow. Automatic grinding wheels and/or METASERV hand grinders were used in this study. The former had a diameter of 8" (203 mm) and were used in accordance with self adhesive discs of P-120 (coarse) and P-1200 (fine) grit size. The latter

consisted of four rolls of grinding paper of 600, 400, 320 and 240 grit size. On changing from one grade to the next, the specimen was rotated through an angle of 90° so that the fresh scratches run at right angles to the previous ones.

- **Polishing:** after the samples were ground, they were polished to reach a mirror finish. This was done on COOK-TROUGHTON & SIMMS and STRUERS rotating wheels which were covered with a suitable cloth (Selvyt) and impregnated with abrasive. The abrasive pastes that were used were KEMET 6, 1 and 1/4 μm diamond compounds in conjunction with KEMET lubricant.
- **Etching:** when the required mirror finish had been obtained, the microstructure of the sample was revealed by swabbing the sample with, or immersing it in, etching reagent. For samples that were going to be examined under the optical microscope a 2% nital solution (2 ml of 70% nitric acid in 98 ml of alcohol) was used. Samples that were going to be examined on the scanning electron microscope were either etched with a saturated picral solution (≈ 25 g of picric acid in 100 ml of alcohol) or with a mixture of 70% picral solution (saturated) and 30% nital (2%) solution. Sometimes alterations of this mixture were made in order to achieve better results.

Thin foil preparation and extraction of replicas were carried out in order to examine samples on the transmission electron microscope (TEM). These techniques were carried out in the following steps:

- **Thin foil preparation:** 3 and 4 mm rods were machined from broken charpies. The 4 mm ones were strained to an approximate diameter of 3 mm, to give at least a 10% strain. Chemical thinning in a 50:50 mixture of 100 vols. hydrogen peroxide and 7% H_2SO_4 saturate with oxalic acid, was sometimes performed in order to achieve the required thickness. The steel rods were then sliced into thin discs of an approximate diameter of 20/1000" (0.5 mm) using a precision cut-off lathe. They were then ground down to a thickness of 4-7/1000 in (0.101-0.177 mm) and stored in pure alcohol. Finally foils were electropolished using a STRUERS Tenupol-2 apparatus, until a very small hole was produced at their centre, indicating that thin electron penetrable areas would now be present close to this hole. The electrolyte used, had the following composition:

100 ml ethanol
50 ml 2-butoxyethanol
12.5 ml perchloric acid.

Electrothinning was performed under the following conditions:

Temperature : 5-15 °C

Voltage : 40 ±5 volt

Current : 60-100 mA depending on temperature

- **Extraction replicas:** samples that had been previously used for the optical microscope were used for extracting replicas from them. All samples were polished with great care, since minor surface scratches would make replica extraction impossible. Then they were etched with 2% nital, repolished, re-etched very lightly and ultrasonically cleaned. Then, they were placed in an EDWARDS VACCUM HIGH "SPEEDVAC" coating unit, operating at 10^{-4} torr., until a layer of carbon film was deposited on the surface. The thickness of the carbon film was approximately 20 Å, to allow optimum extraction. To judge the thickness of the film it was useful to place a clean glass slide with a drop of oil on it, on a piece of white paper alongside the specimen. Since the carbon had not form a film on the oil droplet, the whiteness of the paper would continue to show through the droplet during the evaporation process. When the colour of the carbon film would change to golden yellow, the carbon film would be approximately at the required thickness. Non-conductive film was then applied onto the mounting disc to define the area that was going to be examined. The carbon film was then scribed into 3 mm squares. The replica was removed by immersion in a solution that consisted of 10% hydrochloric acid and 90% ethanol until the carbon film started to crack. When that happened, samples were carefully immersed in distilled water so that the thin replicas floated on the water surface. With the aid of tweezers these replicas were transferred onto copper and/or silicon grids of 3 mm in diameter, left to dry and stored in capsules.

3.4.2 Microscopy

Three different types of microscopes were used in order to give a thorough understanding of the structure/property relationship of the steels that were examined.

These were the following:

- Optical Microscope (O.M.)
- Scanning Electron Microscope (S.E.M.)
- Transmission Electron Microscope (T.E.M.)

3.4.2.1 Optical Microscopy

A NIKON 'Optiphot' and a VICKERS microscope were used for optical examination of the samples. The microscopes were equipped with objective lenses capable of the following magnifications: x5, x10, x40, x100 and x95 (oil-immersion). A further eyepiece capable of a magnification of x10, was attached in combination with one of the above lenses for the NIKON microscope, thus resulting in higher magnifications. This eyepiece formed part of a Nikon AFX-II photographic camera.

All photographs were black&white and were developed and printed using the dark room and photographic equipment of the Department.

Using the optical microscopes mentioned above, valuable information was obtained concerning the structure of the steels examined, such as ferrite grain size and volume fraction of phases. This was done using the following procedures:

- **Volume fraction of phases:** The volume fraction of phases present, was measured with the aid of a SWIFT point counter, model F.415C attached to the stage of the microscope. At least 1000 counts were made for each sample (100 at a time). For samples that exhibited banding, the counts were performed along the direction of the grains, at right angles and at 45° to the bands.
- **Ferrite grain size measurements:** The average ferrite grain size was calculated by the mean linear intercept method. A stage micrometer was used and the distance traversed for a 100 grain boundary interceptions was measured. This was repeated ten times and the average value was then taken to obtain the mean linear intercept. When a second or a third phase was present, this was taken into account in the calculations for ferrite grain size. As with volume fraction measurements, possible directional effects were also taken into account.

All the results from the measurements mentioned above are within the 95% confidence interval.

3.4.2.2 Scanning Electron Microscopy

A JEOL JSM T100 scanning electron microscope was initially used which was later replaced by a JEOL JSM T200. The microscopes were operated at the maximum acceleration voltage of 25kV and generally at x10000 magnification. A JEOL T20-CSI

photographic camera, equipped with a 6x7 MAMIYA roll film adapter, was attached to the microscopes. Black&white photographs were taken, developed and printed.

The measurements made, were grain boundary carbide thickness and grain boundary carbide linear density. On occasions, ferrite and martensite grain size and the volume fraction of martensitic particles were also measured. SEM photographs were also used to confirm the size of coarse incoherent copper particles, as on some occasions these were clearly observable.

- **Grain boundary carbide thickness measurements:** the technique that was used was developed by Mintz *et al.* [4]. For each sample the average thickness was calculated after taking 100 measurements at 0° stage tilt (sometimes a 10° tilt was used). The thickest part of the carbide, perpendicular to the grain boundary, was always measured at X10000 magnification, using a mm ruler on the screen of the SEM. Carbides at triple grain boundary intersections were measured across their thickest limb. When a number of carbides occurred in close proximity, only the largest two were measured. Isolated carbides at the tail and around pearlite colonies were also measured. Because Mintz *et al.*'s readings [4] were taken at 45° stage tilt, all the readings that were taken during the present exercise were corrected by a 10% reduction.
- **Grain boundary carbide linear density measurements:** the stigmator of the SEM was used to create a grid on the cathode ray screen. The stage micrometer of the microscope was moved along the X and Y direction, at a magnification of x10000, until 100 grain boundary carbides were counted. The readings of the micrometer were taken and the linear density was calculated.
- **Volume fraction measurements of martensitic particles:** in some occasions, the optical microscope magnification was inadequate to measure the martensite volume fraction of very fine steel micro-structures, therefore these measurements were repeated on the SEM. The stigmator was again used for creating a grid on the SEM screen and the stage was moved at 0.05 mm steps until 100 counts were made. This was repeated 5 times along the X and 5 times along the Y direction. A constant magnification of x3500 was used. In some cases however, it was difficult to distinguish between martensitic particles and carbides.
- **Coarse incoherent copper precipitate size measurements:** these were occasionally carried out when the SEM photograph image was clear and sharp. A

magnifying lens was always used in accordance with a 10 mm ruler (0.1 mm scale divisions) and at least 100 readings of the particle thickness were taken from each photograph. The average particle thickness was then calculated for each steel condition.

As in the case of the optical microscope results, SEM results satisfy the 95% confidence interval criterion too.

3.4.2.3 Transmission Electron Microscopy

Several transmission microscopes were used, for the examination of thin foils and extraction replicas. The thin foils were examined using a PHILLIPS 400 electron microscope operating at 100 kV, at British Steel Corporation and the extraction replicas were examined using a JEOL T100 electron microscope operating at 60 kV, at St. Bartholomew's hospital. Both microscopes were equipped with an EDAX analyser. Black & white photographs were taken, that were used for measuring the precipitate dimensions by the use of a magnifying lens. Unfortunately, the 95% confidence interval criterion could not be satisfied at all the instances, therefore it was decided that it is essential to mention the number of the particles that were counted during the recording of the results.

Code	Plate thickness (mm)	Composition (% by weight)														
		C	Si	Mn	P	S	Al	Cr	Ni	Nb	Sn	Cu	Mo	B	V	N
No1	13	0.020	0.006	0.230	0.016	0.027	0.012	0.010	0.020	0.001	0.005	0.030	---	---	---	0.0030
2P1H	12	0.013	<0.005	0.280	0.011	0.005	<0.005	---	---	---	---	---	---	---	---	0.0050
4P28H	12	0.022	0.013	0.280	0.012	0.004	0.005	---	---	---	---	---	---	0.0015	0.038	0.0030
1P138M	15	0.059	0.345	1.440	0.012	0.001	0.056	0.158	0.480	---	---	0.020	0.169	---	---	0.0440
1P139M	15	0.046	0.370	0.550	0.012	0.005	0.043	0.610	0.710	0.040	---	0.020	0.210	---	---	0.0066
1P140M	15	0.046	0.380	0.540	0.013	0.003	0.041	0.600	0.710	0.042	---	1.260	0.210	---	---	0.0040
2P148H	15	0.045	0.320	0.770	0.016	0.003	0.015	<0.02	<0.02	<0.005	---	<0.01	<0.005	---	<0.005	0.0056
2P149H	15	0.042	0.300	0.780	0.015	0.003	0.022	<0.02	<0.02	<0.005	---	1.220	<0.005	---	<0.005	0.0097
2P150H	15	0.044	0.310	0.780	0.016	0.003	0.022	<0.02	<0.02	<0.005	---	2.020	<0.005	---	<0.005	0.0048

Table 3.1 Chemical composition of steel plates.

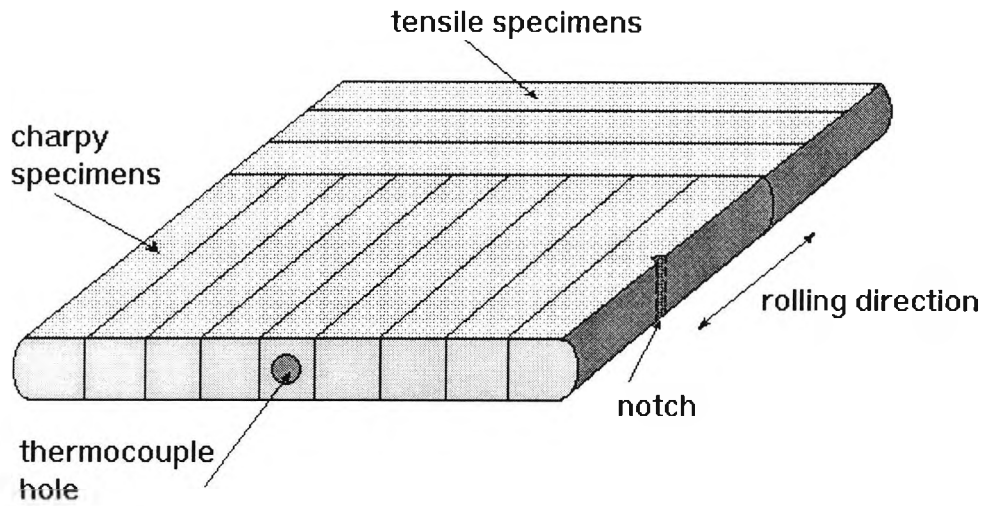


Figure 3.1 Standard outlook of steel-plates used for heat treatments.

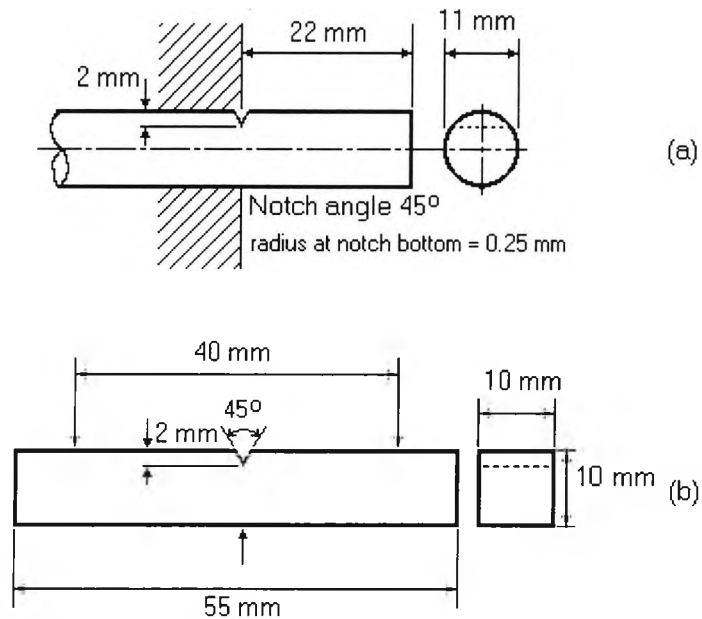


Figure 3.2 V-notch impact test specimens: (a) Izod (round) and (b) Charpy (as used in the present exercise).

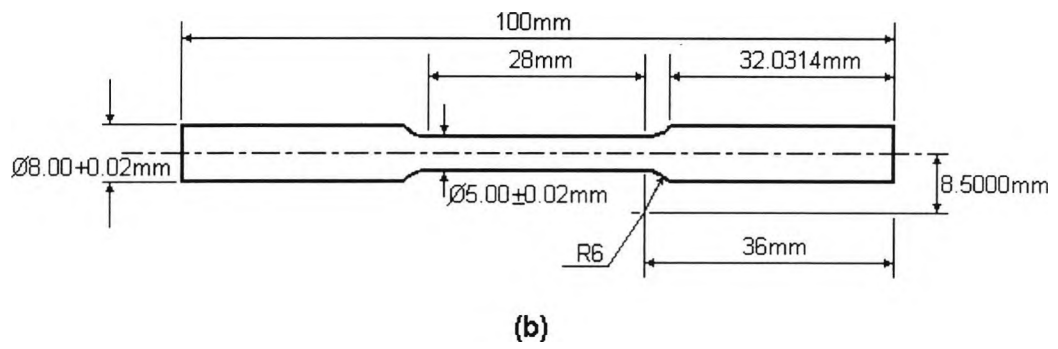
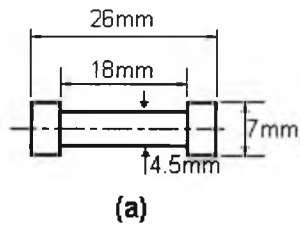


Figure 3.3 Tensile test pieces.

4

THE STRENGTH AND IMPACT PROPERTIES OF LOW-CARBON QUENCHED-AGED STEELS

4.1 Introduction

This quench-ageing study of low carbon steels forms part of a detailed examination of age-hardenable steels. The impact and strength properties in relation to the microstructure, are the main aspects of this investigation. The carbon levels of the steels which were examined range from as low as 0.013% to 0.022% and as a consequence of this, a ferritic structure is obtained.

The principal idea of this study is to introduce a fine coherent precipitation into the matrix, in order to examine its effect on the mechanical properties. It is useful to establish knowledge of a simple system before proceeding to the more complex commercially interesting Cu age-hardening steels. In addition, there has been no work which has combined sophisticated microstructural examinations with changes in strength and impact behaviour.

In this chapter, the effect of ageing on steels that have been ice-quenched after solution treatment at 700-720°C (α -phase) is examined. Ageing at 60°C was chosen for one of the steels because Leslie [43] has shown that the precipitates formed at this

temperature are coherent with the matrix (fully-aged condition). Ageing at 100°C was chosen for the over-aged examination of another steel of this study, as precipitation at this temperature, has been shown by Leslie to be incoherent. The impact and tensile test results are supported by optical, scanning and transmission electron microscopy work. The results that are obtained from this exercise are studied in accordance with the work of previous investigators who have either examined the micro-structure, hardness and strength of low carbon steels [23,24,43,44], or the impact behaviour of steels in general [4,20,29,94,95].

Previous work by Gladman *et al.* [45], has shown that quench ageing steels with 0.1%C, can result in considerable strengthening by the formation of fine incoherent cementite particles. This strengthening however results in an increase in the ITT in a similar manner to that given by normal precipitation hardening.

Allen *et al.* [24], also stress that the production of carbide films at grain boundaries has a deteriorating effect on the impact transition temperature, but found that in some instances a raising of the yield point is not necessarily accompanied by an increased susceptibility to brittle fracture.

In the present instance, the effect of strengthening via coherent precipitates which can shear has been examined.

4.2 Experimental

The exercise involved three different steels whose chemical compositions are given in Tables 4.1. In the first exercise steels No1 and 2P1H were used. Steel No1 was cut into two halves, of sizes 135x160 and 120x160 mm². These were solution treated at 700°C for 1 hour and then quenched in ice-brine. A small piece was cut out of one of the plates and was aged at 60°C for various periods of time, checking its hardness after each ageing treatment. Peak hardness was observed after 16 hours. The conditions that were chosen to be examined were the as-quenched and quenched and aged at 60°C for 16 hours, (QA60). The heat treated plates were kept in the freezer to inhibit room-temperature ageing and V-notch charpy specimens were machined out of them. Unfortunately, there was not enough material to machine full size tensile samples, Figure 3.3 (b), therefore smaller sub-standard samples were machined, Figure 3.3 (a). However, these gave considerable scatter, which was attributed to their

poor design. This led to the need to repeat heat treatments on two plates of similar size, that were cut from the lower carbon steel plate, 2P1H, and were used for the production of the tensile specimens.

Tensile, hardness and impact tests were carried out and microstructural examination was carried out on the optical microscope.

The exercise described above, formed the basis of a final year student project and all the experiments were carried out in co-operation with the student. It can be seen from the results of this exercise that the solution heat-treatment had little influence on the impact behaviour, but after fully-ageing a considerable increase in the strength and hardness occurred. However, due to differences in the chemical compositions of the tensile and charpies, it was decided to repeat the work using steel 2P1H and that the work would form the basis of another final year students project. Yet again the experiment was unsatisfactory due probably to the lower C content of the steel and possibly poor quenching by the student. Long and frequent periods of defrosting took place during the machining of the steel, all encouraging softening of the steel. The results are shown in Figure 4.1(b), indicating that again the impact behaviour was insensitive to the heat-treatment, but this time little increase in strength was noted, probably due to the poor quenching.

The necessity of repeating the work was therefore strong, if any serious conclusions were to be produced. This time ageing trials were performed at 60 and 100°C after quenching in ice-brine from 720°C and the work was carried out on another steel of similar C content (0.022%), coded as 4P28H (see Table 4.1 for composition).

This steel's ageing trials revealed that peak hardness was reached after 10 and 3 hours of ageing at 60 and at 100°C respectively, Figure 4.2. In this exercise, the use of a methanol/water bath at 60°C and an air-circulated oven at 100°C ensured accurate results. Also, special care was taken to minimise the time that the steel had to be left outside the freezer.

In the latest exercise, the as-quenched (Q), quenched and fully-aged at 60°C (QA60) and quenched and aged at 100°C (QA100) were examined and mechanical test results were supported by optical and scanning electron microscopy.

4.3 Test results

4.3.1 Hardness and tensile test results

For steels 1 and 2P1H the plate hardness was found to be 166 and 180 HV10 respectively, and these figures increased after ageing to 199 and 190 HV10, Table 4.3. As expected, ageing at peak hardness also increased the tensile strength at the expense of ductility, Table 4.3. The lower yield stress and ultimate tensile stress of steel 2P1H increased after full-ageing from 333 to 380 N/mm² and from 461 to 490 N/mm², respectively and elongation decreased from 24 to 21%. All the tensile samples exhibited a yield point, although it was not sharp for some of them.

Although the tensile test results of steel No1 are not very reliable, they appear to show similar behaviour to that of steel 2P1H, only the increase in strength on ageing was much smaller. The as-quenched steel showed a LYS of 409 N/mm² and this value increased to 431 N/mm² after ageing at 60°C for 16 h, Table 4.3. The ultimate tensile strength however, did not show too much change after ageing, and was maintained at the same level as in the as-quenched condition, Table 4.3. Little change in ductility took place on ageing, Table 4.3.

For steel 4P28H, the quenching and ageing trials revealed an average plate hardness of 145 HV10 for the as-quenched condition, a value that was successfully matched after quenching the three plates. Further hardness tests after ageing two of the three plates at 60 and at 100°C showed that peak values, as indicated by age-hardening curves, Figure 4.2, were obtained and these were 190 and 165 HV10 respectively. However, tests on broken tensile and charpy specimens revealed hardness values of 179 HV10 after ageing at 60°C, but only 139 HV10 after ageing at 100°C. The low hardness for the samples aged at 100°C, was attributed to overheating during machining and this condition was subsequently taken as being over-aged.

As far as tensile behaviour is concerned, there was no sign of a yield point and 0.2% and 2% proof stress values are indicated, Table 4.4. The as quenched sample gave a 0.2% proof stress of 279 N/mm². A marked increase of 100 N/mm² in terms of 0.2% proof stress was observed after fully-ageing at 60°C, whereas ageing at 100°C caused the yield strength to fall back again to the as-quenched value (again suggesting that the sample was over-aged). Ultimate tensile stress values behaved in a similar pattern.

Ductility decreased after ageing the steel at 60°C but was restored after ageing at 100°C.

4.3.2 Impact test results

Whereas the strength was very much affected by the ageing treatments, the impact behaviour hardly changed, such changes being within the scatter for ITT curves.

In the as-quenched condition, steel No1 showed impact transition temperatures of -16 and -20 °C at absorbed energies of 54 and 27 J respectively, Table 4.3. At 50% fibrous appearance, the temperature was -13°C. All the transition temperatures decreased slightly after ageing by approximately 8°C, Figure 4.1(a). Shelf energies were low and of the order of 216 and 192 J for the as-quenched and the quenched and aged condition, respectively.

In contrast to steel No1, the impact transition temperatures were found to increase slightly after fully-ageing steel 4P28H at 60°C and were restored after ageing at 100°C, Table 4.5. Very high impact transition temperatures were observed, for all the conditions, the 54 J ITT being +88°C for the as-quenched and quenched and over-aged conditions and +100°C for the fully-aged condition. All the samples fractured in a brittle manner at room temperature and exhibited a sharp transition from brittle to ductile fracture. Despite the deterioration of the impact behaviour, the shelf energies were high, 290-300 J. The ITT curves for steel 4P28H are shown in Figure 4.3.

4.4 Metallography

All the samples were examined with the optical microscope. The samples from steel 4P28H were also examined with the scanning electron microscope and the thickness of the carbides situated at the grain boundaries and in the matrix, was measured.

4.4.1 Optical microscopy

When steel No1 was examined, an equiaxed fully ferritic structure was observed, Figure 4.4. The ferrite grain size was found to be $6.5 \text{ mm}^{-1/2}$ for the as-quenched sample and $6.2 \text{ mm}^{-1/2}$ (24 and 26 μm , respectively) for the quenched-aged sample, Table 4.2. The presence of sulphides was also observed. The micro-structure of a tensile sample made from steel 2P1H was also examined and found to be fully ferritic. Its grain size was however, much coarser than that of steel No1, this being measured

to be $4 \text{ mm}^{-1/2}$ ($62 \text{ }\mu\text{m}$). It must be mentioned that the grains of steel 2P1H were slightly elongated.

Examination of steel 4P28H, revealed a coarse ferritic structure, Figures 4.5, 4.6 and 4.7, in which however, some finer grains were also present, Figure 4.5 (a). The average ferrite grain size was measured in the normal way and was found to be $3.5 \text{ mm}^{-1/2}$ ($82 \text{ }\mu\text{m}$) for all conditions.

When examining the samples at high magnifications using the x40 and x100 lens, large cementite particles were observed at grain boundaries and also within the ferrite matrix, Figures 4.6 and 4.7.

4.4.2 Scanning electron microscopy

When steel 4P28H was examined, it was almost instantly observed that there are two kinds of grain boundary particles:

1. fine carbides with average thickness values of the order of 0.11, 0.15 and 0.14 μm for the as-quenched, fully-aged and over-aged conditions, respectively; and
2. coarser particles with average thickness values increasing, from 0.46 to 0.49 and 0.51 μm for the three conditions as listed above, Table 4.6.

Figure 4.8 (a) shows some of the finer particles, whereas Figure 4.9 (a) shows some of the coarser particles situated at grain boundaries. The large difference in thickness between the fine and the coarser particles suggests that they have a different origin. The coarser particles are probably carbides which did not dissolve at 720°C and the finer have formed on cooling during the quench.

In addition to the above, it was also observed that particles did not only form at grain boundaries but also within the matrix. Again there was a variation in the size of the matrix particles and an average value has been taken, Table 4.6. These particles are shown in Figures 4.8 (b), 4.9 (b) and 4.10.

It should be noted that the exercise was again repeated on the same steel, this time at British steel, by a final year student working under Dr Crowther's supervision [96]. These results are also shown in Table 4.7 and Figures 4.11 and 4.12 and can be seen to be broadly in agreement with the present work.

4.5 Discussion of results

4.5.1 The influence of ageing on hardness and tensile properties

The most evident change after ageing, was the increase of the hardness and the tensile strength. The hardness increased by 30 units on the HV10 scale, for steels 1 and 4P28H after fully-ageing, but only by 10 units for steel 2P1H. This is most likely due to the lower carbon level of steel 2P1H which provides the supersaturated ferrite phase with less carbon atoms for precipitation. However, despite the fact that the 0.013% carbon steel (2P1H) did not show a large hardening effect, it was generally harder than the other two 0.02% carbon steels and this may be due to its higher Nitrogen level and possibly due to age-hardening having occurred prior to testing.

Ageing after quenching had a similar effect on the yield stress of steels 2P1H and 4P28H as it had had on their hardness measurements. The increase in the yield strength of the 0.022% carbon steel was 100 N/mm² at peak hardness, Table 4.4, whereas for the 0.013% carbon steel the equivalent increase was only 47 N/mm². This smaller increase may again be related to the lower C content of steel 2P1H, thus reducing the amount of C that can be precipitated out of the solution. Although there is considerable variation in the strengthening that occurs on ageing, in all cases the strength was observed to increase and often by a very large amount (50 to 100 N/mm²). However, the yield strength of steel No1, which has a carbon content very similar to steel 4P28H also increased, but only by 22 N/mm². The variability in the strengthening that occurs on ageing, probably arises as a result of the variability in quenching.

The steels mentioned above, cannot be compared on the basis of actual stress values, as there are compositional and structural differences. However, the individual tensile behaviour of each steel is typical of an age-hardenable steel. Changes in tensile yield strength and ductility are purely due to age-hardening, since there was no change of grain size after the ageing treatments. The highest change of yield strength after ageing, 100 N/mm², was observed for steel 4P28H (0.022% C) when this was aged at 60°C for 10 h.

The ability of the steel to impede dislocation movement is lost after over-ageing the steel, because the coherent precipitate thickens and the total elastic force becomes

too large to be resisted by the atomic register forces between precipitate and the matrix and it breaks away from the matrix (i.e. it becomes incoherent). The atomic fit and the elastic stresses are destroyed and the yield stress falls [15]. This explains the sharp fall of tensile strength and hardness of the 0.022% carbon steel (4P28H). At this stage, interparticle spacing and precipitate size become important factors in controlling the strength of the metal rather than coherency stresses. In the case of steel 4P28H, the strength and hardness fell below the as quenched values after over-ageing the steel at 100°C. This may signify that the increase in the precipitate thickness occurred at the expense of smaller precipitates. A large interparticle spacing is then obtained which gives space for the dislocations to move freely between particles.

As mentioned earlier, the steels that are examined in this exercise cannot be compared on the basis of their actual stress values, as there are compositional and structural differences. For this reason the expected lower yield strength values were calculated using Equation 2.10. That equation had been developed for air-cooled 12 mm thick, ferrite/pearlite steels plates [4]. Those plates had been shown by internal friction to contain very low carbon and nitrogen levels in solution ($\leq 0.001\%$ C and 0.001% N), even though the C and N content of the steels was high, $\sim 0.2\%$ C and $\sim 0.005\%$ N. It can be seen that the yield strength for the as quenched steels, is always in the region of 100-200 N/mm² higher than the expected one, Table 4.8. This indicates that a large part of the carbon and probably all the Nitrogen is in solution, in the ferrite. The multiplying factor to account for solid solution hardening by carbon and nitrogen, is generally taken as 5000, [31]. Thus, the very high values suggest that nearly all the carbon is in solution, certainly for steels No1 and 2P1H. However, it is clear from the microstructure observations, that for steel 4P28H there is also a fair amount of carbon which has been taken out of solution as carbides.

In the over-aged condition, steel 4P28H lost all the strength that came from coherent precipitation, but maintained the initial δLYS , 98 N/mm², Table 4.8. This is probably due to dispersion strengthening, caused by incoherent carbon precipitates. This behaviour has been expected, since complete over-ageing would only be achieved after 100 hours of ageing at 100°C.

4.5.2 The effect of ageing on the impact properties of low carbon steels

The general appearance of the situation in this exercise, is that despite the fact that the strength and hardness are influenced by ageing, the impact behaviour is only slightly affected, Figures 4.1 and 4.3. This is not in accord with conventional precipitation hardened steels [24,97], whose impact properties are profoundly related to the tensile strength changes.

4.5.2.1 The impact behaviour of steels No1 and 2P1H

Ageing steel No1 at peak hardness (i.e. full-ageing) had a favourable effect on the impact transition temperatures as these were lowered. There was a negative shift of all transition temperatures by 8°C, Figure 4.1 (a). Generally, increasing strength would be expected to cause a deterioration in impact behaviour, by particle hardening, therefore this improvement in toughness was not expected. In the present case, ageing causes the strength to increase by 22 N/mm² which should also cause the impact transition temperatures to increase by approximately 10°C (Equation 2.8). If this value is added to the 8°C observed decrease in the ITT, it then follows that the impact properties in the fully-aged condition have improved by, approximately, 20°C.

Steel 2P1H showed an even greater increase in yield stress of the order of 47 N/mm². Again the impact behaviour of this steel was found to be relatively insensitive to ageing, Figure 4.1 (b). Increasing the strength on fully-ageing, thus has little influence on the impact behaviour.

A possible explanation for this behaviour, is that the coherent precipitates that form, do not fracture but encourage cross slip [6]. In this way, deformation is dispersed uniformly giving high ductility and strength. The rapid build up of dislocations which normally causes crack nucleation is therefore prevented from occurring.

In accord with the changes in hardness, the ductile shelf energy in steel No1 was slightly reduced by 24 J after ageing, Table 4.5. The reason for this, is that ductile shelf energy is influenced by the presence of precipitates and inclusions and by the dislocation density. Ductile fracture occurs by voiding at the matrix/particle interface and these cavities link up to give failure under the action of shear stresses. In the fully-

aged condition a higher shear force is required than in the as-quenched condition and this encourages voiding, thereby resulting in a lower shelf energy.

The majority of the investigators [4,20,24] have related the impact behaviour to the changes in grain size and grain boundary carbide thickness. In this exercise for each of the steels, there was no change of grain size and the grain boundary carbide thickness and density were below the level which is able to influence impact behaviour and did not vary with ageing. It was therefore concluded that the unusual impact behaviour, related to the carbon precipitated in the matrix rather than at the boundaries. Scanning electron microscopy, indicated that there were only a few grain boundary carbides and those present were very thin, so it is unlikely that they would influence impact behaviour.

4.5.2.2 The impact behaviour of steel 4P28H

This steel gave the greatest increase in strength on ageing of all the steels. Impact behaviour was again insensitive to the changes in strength, Table 4.5. The toughness of the material in all the conditions was very poor, with a slight increase in the impact transition temperatures after ageing at peak hardness and the restoration of those, after over-ageing.

In contrast to steels No1 and 2P1H, in which there was no trace of grain boundary carbides, the grain boundaries of steel 4P28H were full of carbides many of which are coarse. Although, this aspect does not seem to affect the ageing behaviour, it certainly affects the impact transition temperatures. It is therefore necessary to assess the impact behaviour on the basis of the difference between observed and predicted ITT values.

The equations that were used for the prediction of the impact transition temperatures are those derived by Mintz *et al.* [4] and are given in chapter 2 (Equations 2.7, 2.8 and 2.9). Δy in this case was taken to be the difference between calculated and observed lower yield stress values (δLYS), i.e.,

$$\Delta y, (\text{N/mm}^2) = LYS_{\text{observed}} - LYS_{\text{calculated}} \quad \dots(4.1)$$

The calculated values of lower yield stress were derived using Equation 2.10, [4]:

$$\text{LYS, (N/mm}^2\text{)} = 43.1 \% \text{Mn} + 83 \% \text{Si} + 15.4 d^{-1/2} + 1540 \% \text{N}_f + 105$$

As it can be seen from Table 4.8, the calculated LYS is approximately 100 N/mm² lower than the observed value for the as quenched condition. The most reasonable explanation for this, is the presence of a large amount of carbon atoms in solution. If the vector of 5000 is used for C and N from Morrison's Equation (2.11) [31], then 0.017% C and 0.003% N would have been quenched in solution. Also, Allen *et al.* [24] suggest that water-quenching from 700°C, would cause about 0.015% of the carbon to be retained into solution in the ferrite. The presence of the very coarse grain size probably accounts for the absence of yield point.

Before proceeding to the calculation of transition temperatures, it had to be decided which particle thickness was going to be used. Because it is the coarser carbides distribution which controls the impact behaviour, only these measurements were used for the ITT calculations.

Based on the equations mentioned above, the ITT values were calculated. However, the present steels contain lower S and C levels than the steels that were used by Mintz *et al.* [4] to develop the original regression equations. Recent work [30] has shown that these lower S and C levels will lead to higher ductile shelf energies as well as to lower transition temperatures. A further 40°C has therefore been subtracted from Equations 2.7, 2.8 and 2.9 in order to compensate for these differences. This deduction gives the best fit, for all the steels that were used for the present exercise and those in the next two chapters. The predicted transition temperatures for the as-quenched condition were found to be +83 and +44 °C for the 54 and 27 J ITT criteria, respectively. The 54 J ITT is in excellent agreement with the observed value, and at 27 J the observed value is only 16°C higher than the predicted value, Table 4.9.

For the quenched and fully-aged condition, the predicted values diverged from those that were observed in the sense that they were higher by 37 and 10 °C for the 54 and 27 J criteria, respectively. Thus again, it can be seen that fully-ageing at 60°C, provides a better combination of strength and impact behaviour, and other things being equal, the impact transition temperatures are 10 to 37 °C better.

In the quenched and over-aged condition, the predicted value for the 54 J ITT, is in good agreement with the observed one. At 27 J the observed value is higher than that calculated by 14°C. It is clear that the impact behaviour of the over-aged condition is very much the same as that of the as quenched condition.

The above observations confirm the findings for the other two steels that had been previously examined in this exercise, i.e. the increase in yield strength that occurs on age-hardening, had no significant influence on the impact behaviour and as mentioned in the previous section, the suggested cause for this event, is the ability of the coherent particles to encourage cross slip. McMahon and Cohen [20] who have examined the initiation of cleavage in polycrystalline iron of very low carbon content (0.007 and 0.035% C) all deposited at grain boundaries as carbides, have found that the majority of cleavage microcracks in ferrite is initiated by carbide-cracking during plastic straining of the ferrite. If the cracks in the carbides are large enough, they will enter the ferrite and propagate until they encounter a barrier strong enough to stop them, or until sufficient relief of stress (or absorption of energy) by slip or twinning occurs at the advancing crack [20]. In the present case, it seems that the microcracks initiate at coarse carbides, but the presence of coherent particles which of course do not crack, may somehow reduce the energy of the advancing cracks and provide stress relief. This ability of the coherent iron-carbide particles is probably attributed to their soft nature.

As mentioned earlier, the work was again repeated at British Steel using the same steel. In this latest piece of work, the ageing treatment for the 100°C temperature was carried out for 12 hours, to ensure that the steel was well and truly over-aged. This resulted in the yield strength falling back again to the as-quenched value, but no changes in the impact behaviour were observed [96]. The results were very similar to those obtained in the present exercise on fully-ageing, in that the strength increased by the same amount, 100 N/mm², but the impact behaviour was little affected. Some limited TEM work was also carried out on samples aged at 60°C and these, as in Leslie's work [43], indicate that the precipitates were most likely to be coherent, Figure 4.11. As can be seen from the TEM micrographs, Figure 4.11, the coherent particles were mainly situated at dislocations and their diameter was measured to be of approximately 30 nm.

To summarise, although there have been great problems experimentally, in examining the quenched-aged low C-steels and the experiments had to be repeated many times, there is no doubt that the overwhelming evidence indicates that the presence of coherent precipitation benefits strength without materially influencing impact behaviour.

steel element	No1	2P1H	4P28H
C	0.020	0.013	0.022
Si	0.006	<0.005	0.013
Mn	0.230	0.280	0.280
P	0.016	0.011	0.012
S	0.027	0.005	0.004
Al _{tot}	0.012	<0.005	0.005
Al _{soln}	0.008	--	--
Cr	0.010	--	--
Ni	0.020	--	--
Nb	0.001	--	--
Cu	0.030	--	--
Sn	0.005	--	--
N	0.0030	0.0050	0.0030

Table 4.1 Chemical composition of steels No1, 2P1H and 4P28H (% by weight).

Steel	Condition	Heat treatment		Soaking time (hr)	Cooling medium
		Type	Temp(°C)		
No1 & 2P1H	Q	solution treatment	700	1	ice-brine
	QA60	solution treatment	700	1	ice-brine
		ageing	60	16	air
4P28H	Q	solution treatment	720	1	ice-brine
	QA60	solution treatment	720	1	ice-brine
		ageing	60	10	air
	QA100	solution treatment	720	1	ice-brine
		ageing	100	3	air

Table 4.2 Heat treatments of steels No1, 2P1H and 4P28H.

Steel	Condition	Grain size		Hr (HV10)	LYP (N/mm ²)	UTS (N/mm ²)	ϵ (%)	RA (%)
		μm	$\text{mm}^{-1/2}$					
	Q	24	6.5	166	409	485	16	81
No1	QA60	26	6.2	199	431	477	17	84
	Q	62	4	180	333	461	24	73
2P1H	QA60	62	4	190	380	490	21	71

Table 4.3 Hardness and tensile properties of steels No1 and 2P1H.

Condition	Grain size		Hardness (HV10)	0.2% PS (N/mm ²)	2% PS (N/mm ²)	UTS (N/mm ²)	ϵ (%)	RA (%)
	μm	$\text{mm}^{-1/2}$						
Q	83	3.5	146	279	325	417	27	76
QA60	84	3.5	179	379	456	516	22	73
QA100	80	3.5	139	275	324	420	24	79

Table 4.4 Hardness and tensile properties of steel 4P28H.

Steel	Condition	Impact transition temperature (°C)			Energy absorbed (J)		
		at 54 J	at 27 J	50%FATT	at 0 °C	at RT	Shelf
	Q	-16	-20	-13	190	208	216
No1	QA60	-25	-28	-21	178	192	192
	Q	+88	+60	+94	8	6	300
4P28H	QA60	+100	+75	+122	8	8	292
	QA100	+88	+64	+92	8	10	300

Table 4.5 Impact properties of steels No1 and 4P28H.

Condition	Grain boundary particle thickness (μm)			Matrix particle thickness (μm)			linear density of coarse carbides (particles/mm)
	t_f	t_{co}	t_{avg}	t_f	t_{co}	t_{avg}	
Q	0.11	0.46	0.28	0.13	0.48	0.30	5
QA60	0.15	0.49	0.32	0.15	0.35	0.25	5
QA100	0.14	0.51	0.32	0.14	0.47	0.30	3

f: fine carbide particles
co: coarse carbide particles
avg: average carbide size (i.e. $(t_f + t_{co})/2$)

Table 4.6 Scanning electron microscopy of steel 4P28H.

Condition	LYS (N/mm ²)	UTS (N/mm ²)	ϵ (%)	RA (%)	54J ITT (°C)	27J ITT (°C)	Shelf energy (J)
Q	249*	379	34	86	+90	+75	281
QA60	347*	488	25	84	+98	+97	210
QA100	310	400	27	87	+90	+75	276

* 0.2% Proof Stress

Table 4.7 Mechanical properties of steel 4P28H, as the have been recorded at British Steel by Dr Crowther and Thulaseetharan [96].

Steel	Condition	LYS (N/mm ²)		
		obs	calc	δ LYS
No1	Q	409	220	189
	QA60	431	216	215
2P1H	Q	333	187	146
	QA60	380	187	193
4P28H	Q	279	177	102
	QA60	379	177	202
	QA100	275	177	98

Table 4.8 Comparison between observed and calculated (Equation 2.10) lower yield strength values, of steels No1, 2P1H and 4P28H.

Steel	Condition	Impact Transition Temperatures (°C)								
		at 54 (J)			at 27 (J)			50% FATT		
		obs	calc	δ ITT	obs	calc	δ ITT	obs	calc	δ FATT
4P28H	Q	+88	+83	+5	+60	+44	+16	+94	+96	-2
	QA60	+100	+137	-37	+75	+85	-10	+122	+144	-22
	QA100	+88	+88	0	+64	+49	+15	+92	+99	-7

In ITT equations, t_c was taken to be the average thickness of the coarser grain boundary particles.

Table 4.9 Comparison between observed and calculated impact transition temperatures, of steel 4P28H.

ITT curves

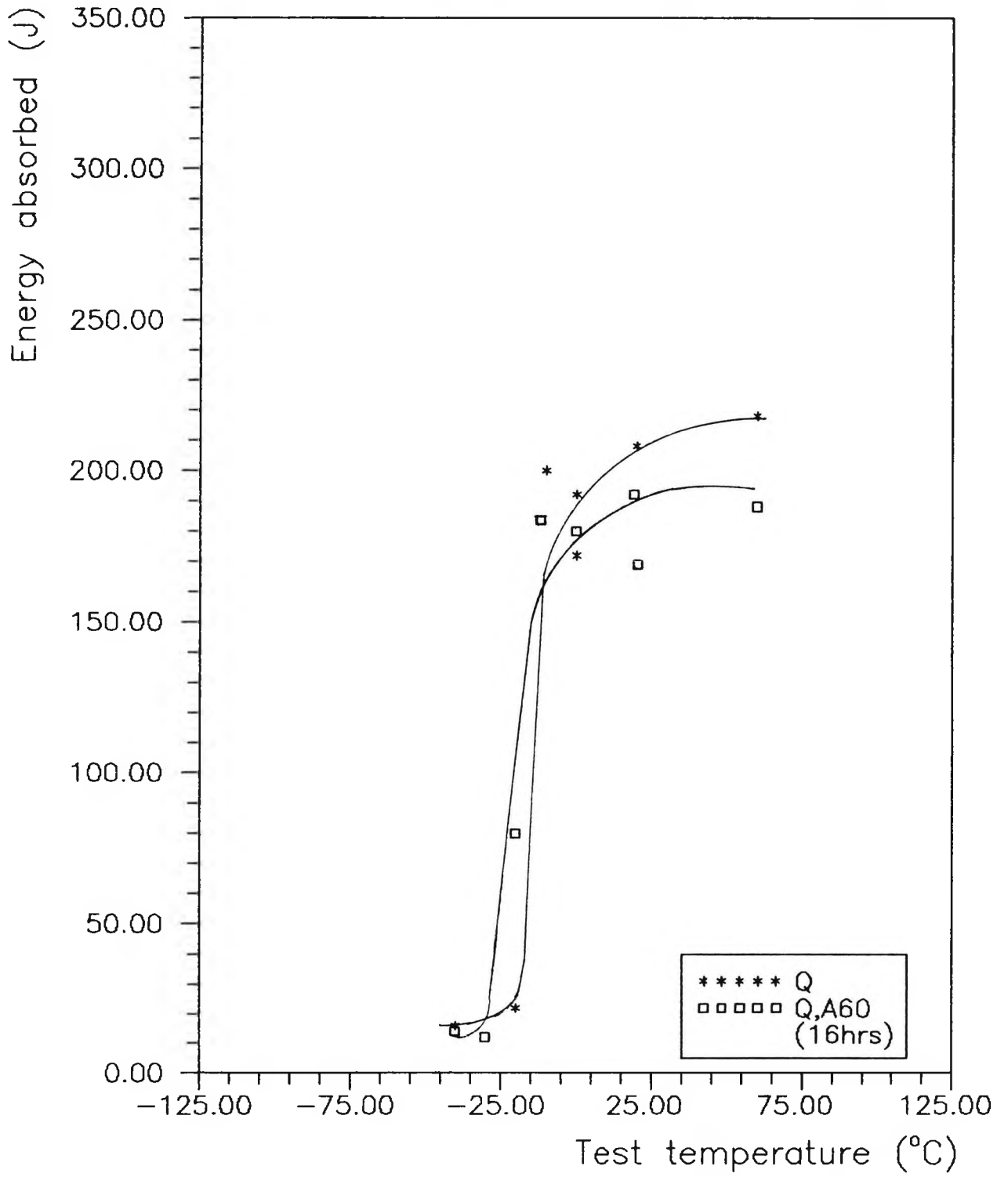


Figure 4.1 (a) Impact transition temperature curves, for quenched and aged steel No1.

ITT curves

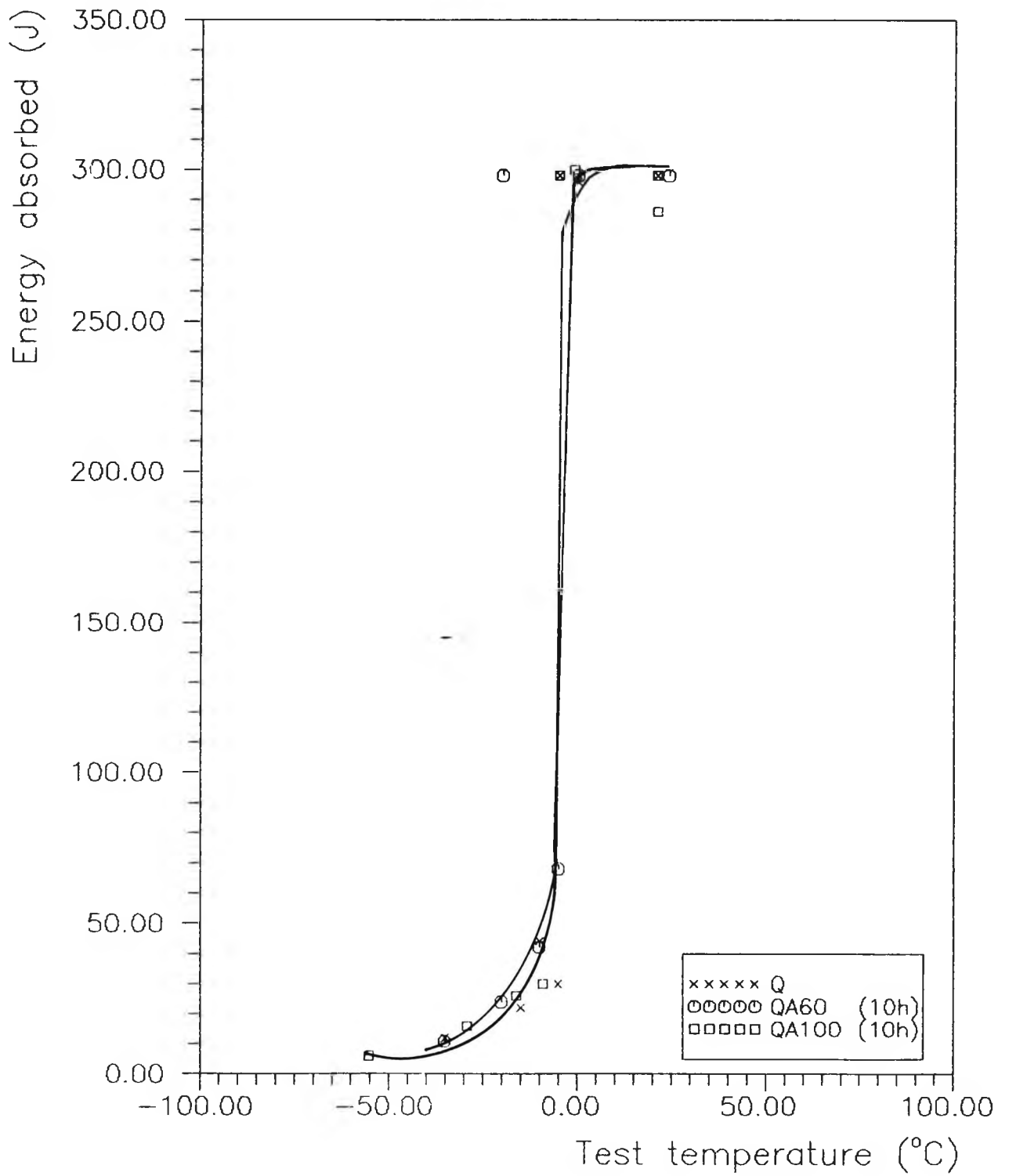


Figure 4.1 (b) Impact transition temperature curves, for quenched and aged steel 2P1H.

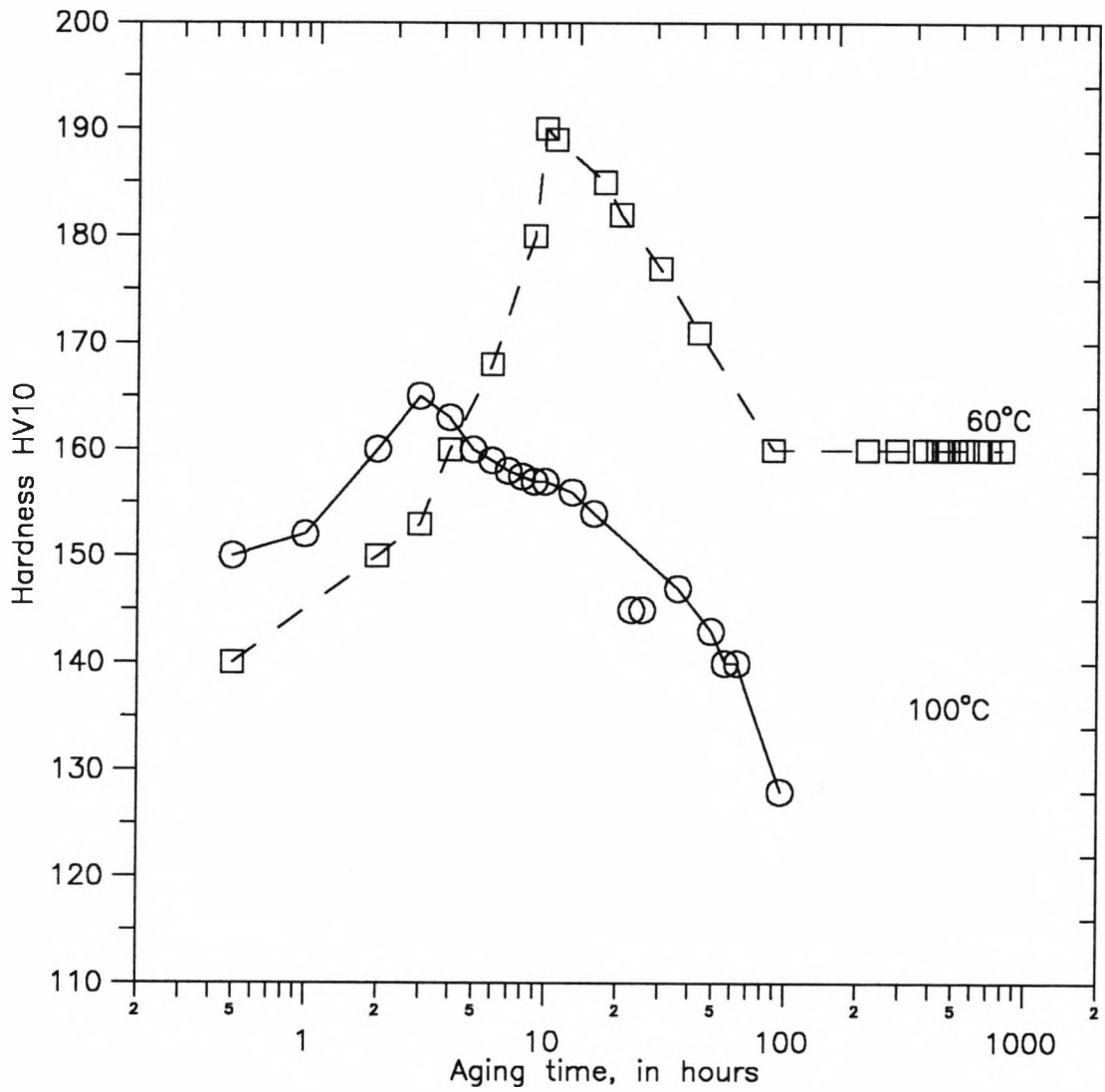


Figure 4.2 Age-hardening behaviour of steel 4P28H, quenched from 720°C and then aged at 60 and at 100 °C for various periods of time.

ITT curves

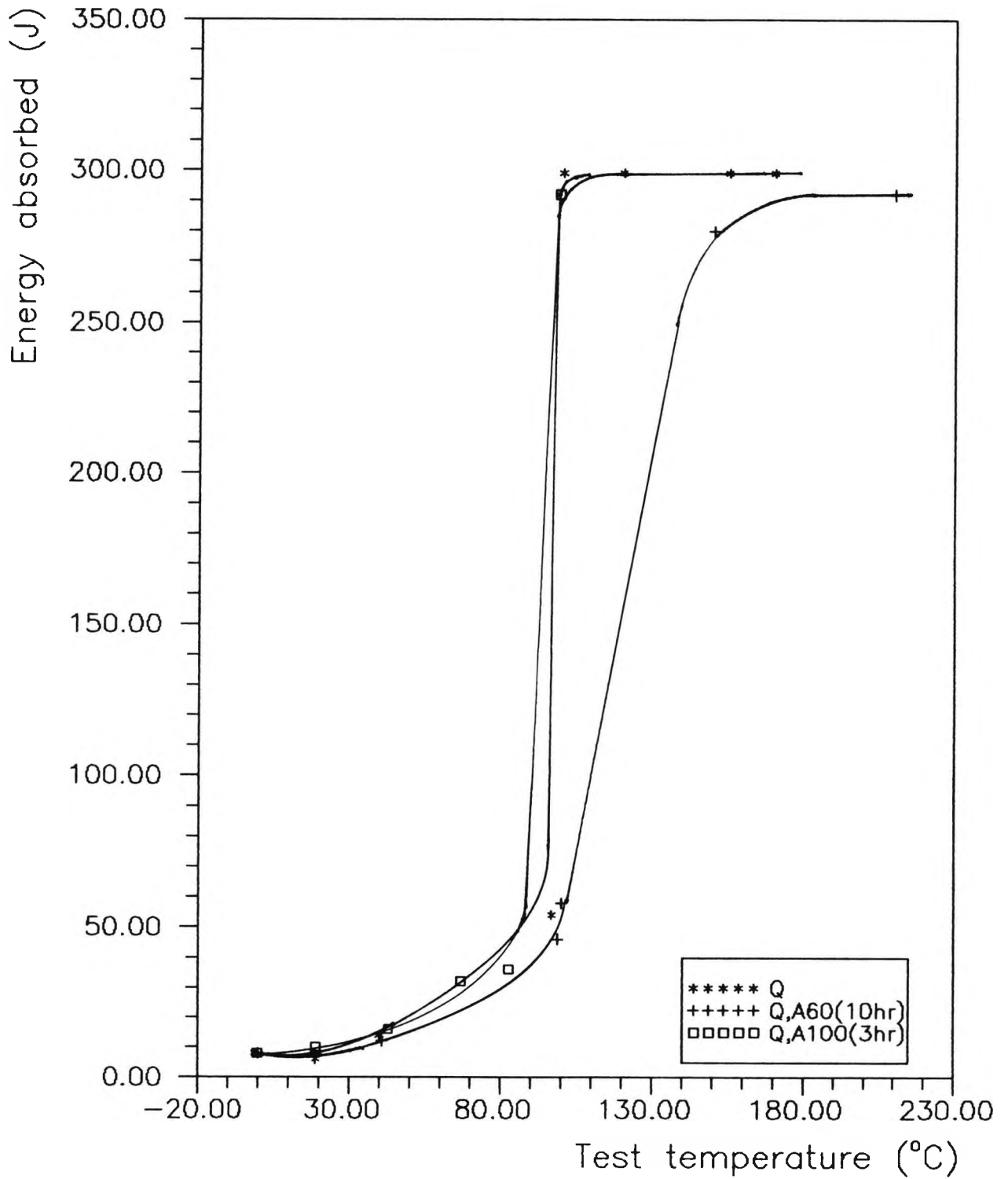


Figure 4.3 Impact transition temperature curves, for quenched and aged 4P28H steel.

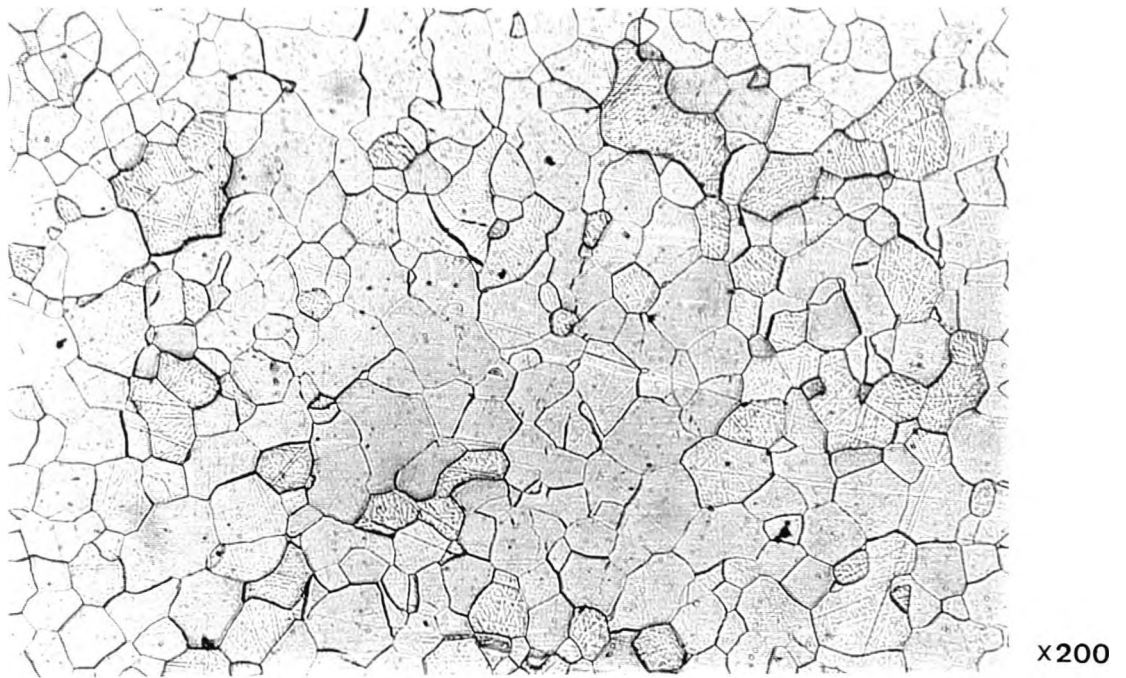
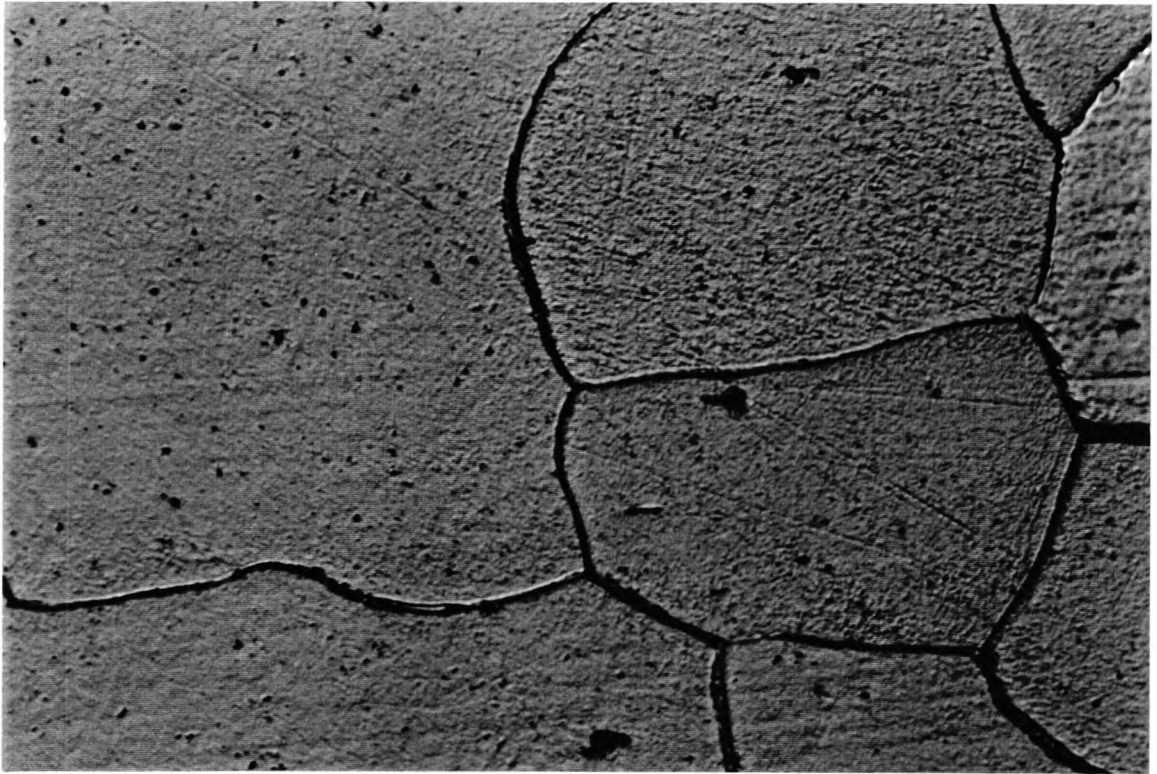


Figure 4.4 Optical micrograph of steel No1, solution treated at 700°C for 1 h and ice-quenched and then aged at 60°C for 16 h.



Figure 4.5 (a) Optical micrograph of steel 4P28H, as-quenched from 720°C.



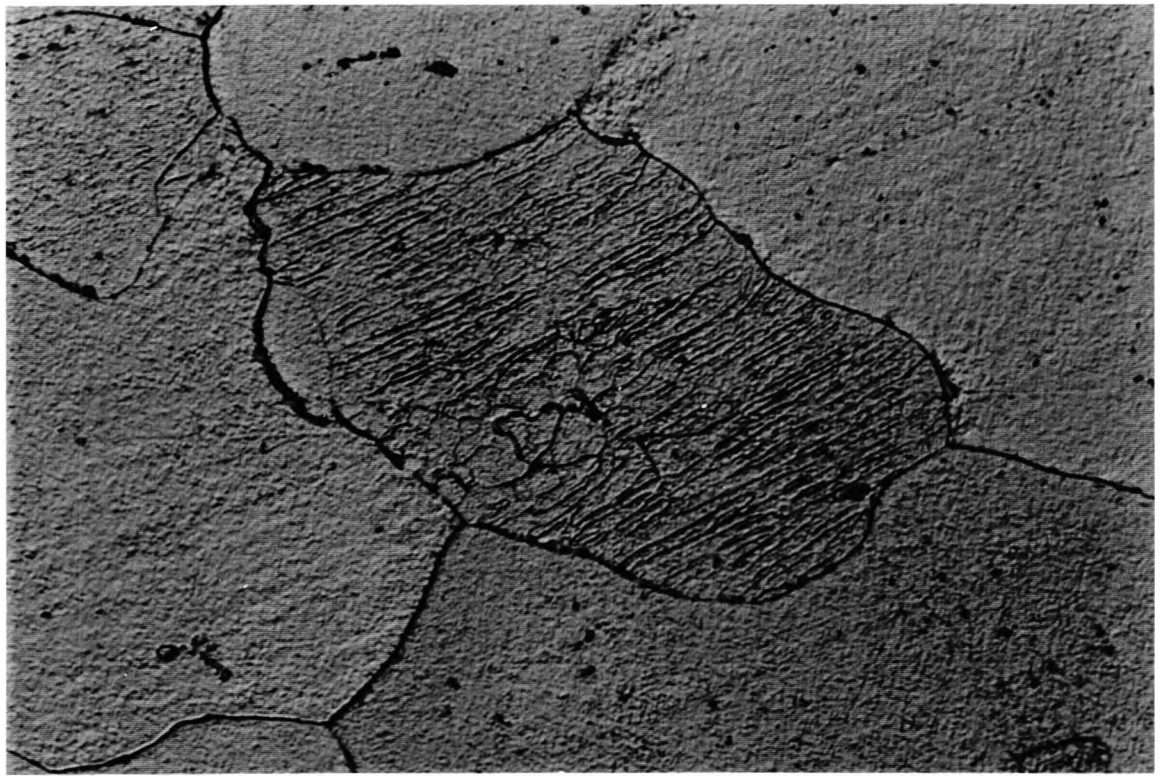
x1000

Figure 4.5 (b) Optical micrograph of steel 4P28H, as-quenched from 720°C, showing carbide precipitation in ferrite.



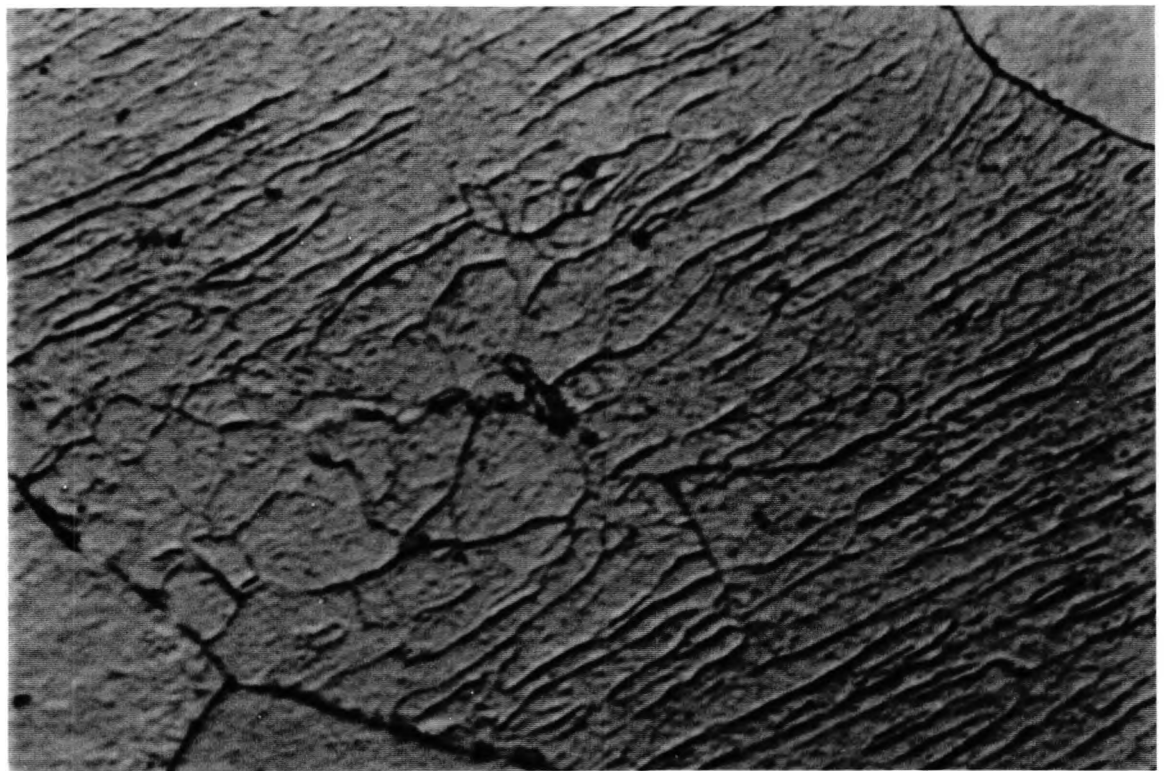
x1000

Figure 4.6 Optical micrograph of steel 4P28H, quenched from 720°C and aged at 60°C for 10h, showing carbide precipitation in ferrite.



x1000

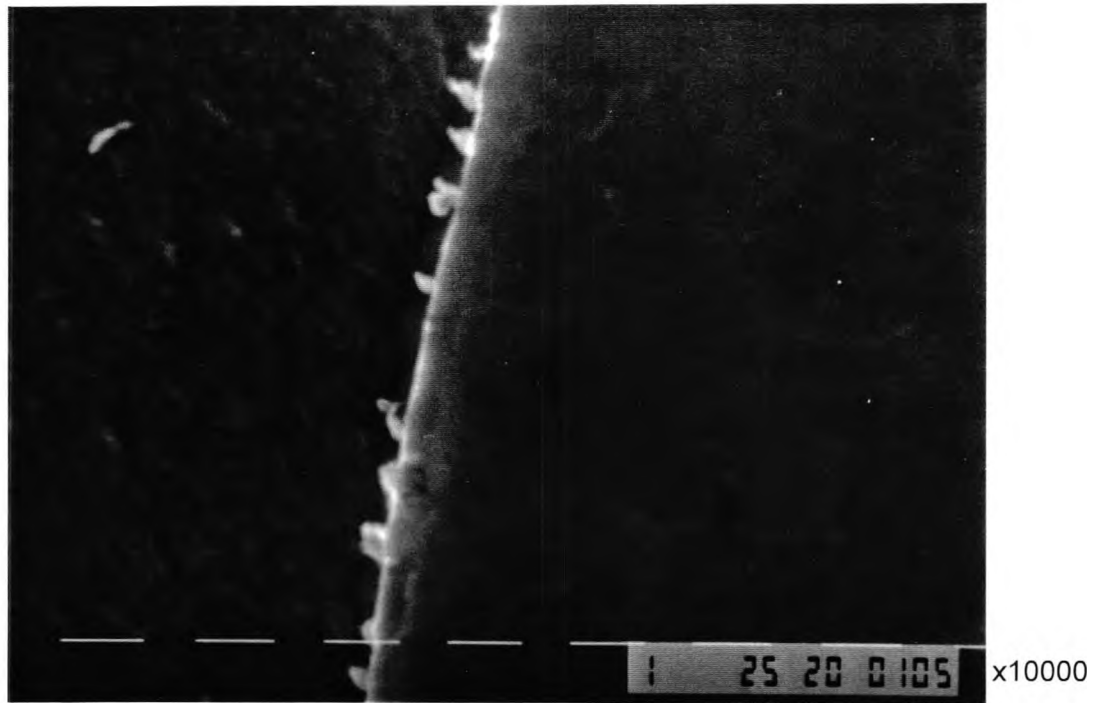
(a)



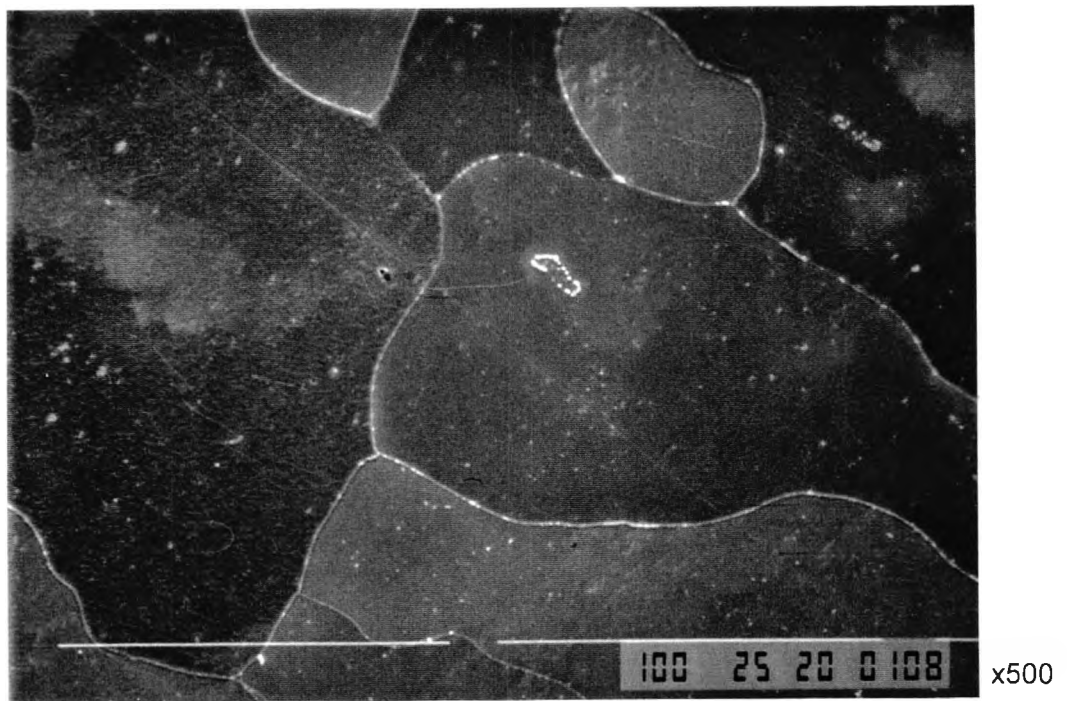
x2500

(b)

Figure 4.7 (a), (b) Optical micrographs of steel 4P28H, quenched from 720°C and aged at 100°C for 3 h, showing carbide precipitation in ferrite.

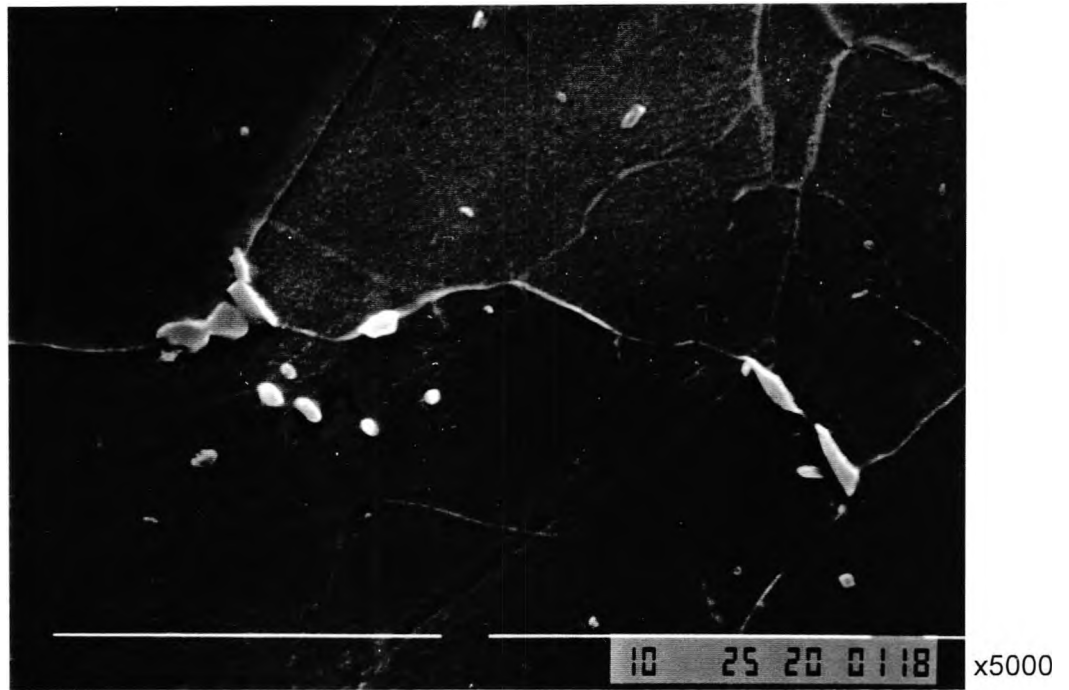


(a)



(b)

Figure 4.8 (a), (b) Scanning electron micrographs of steel 4P28H, as-quenched from 720°C.

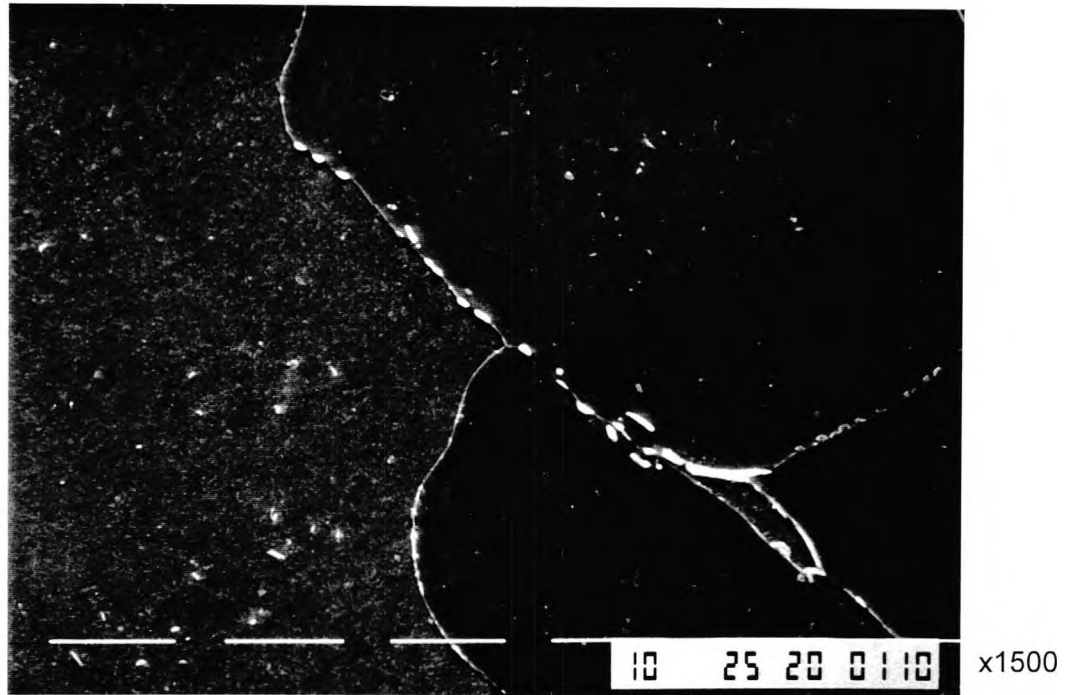


(a)

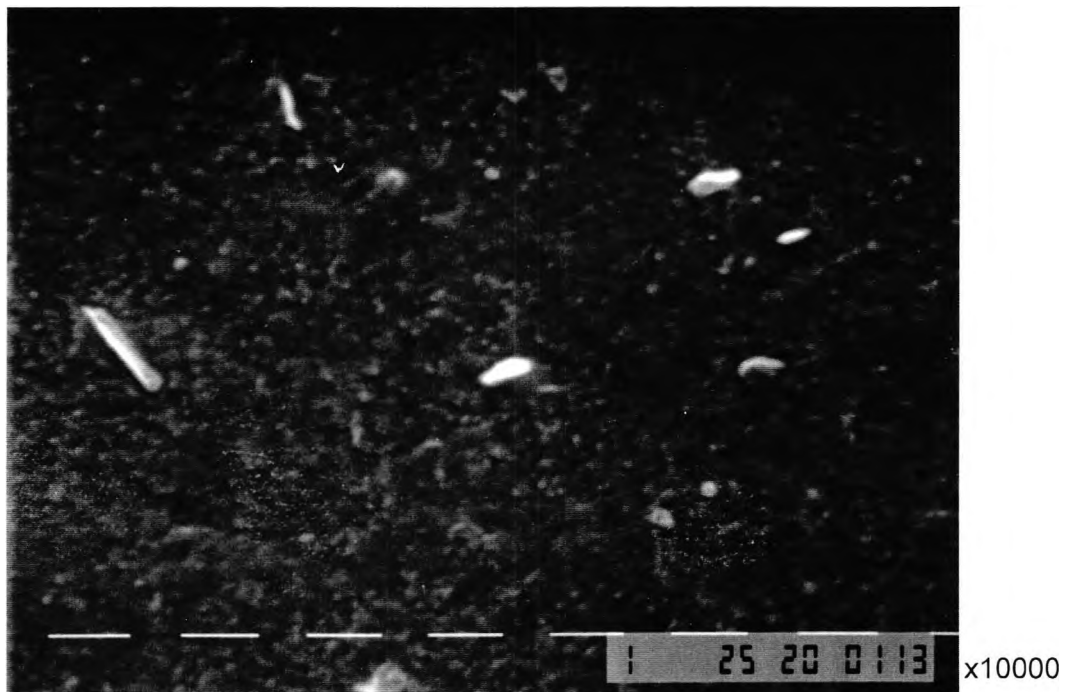


(b)

Figure 4.9 (a), (b) Scanning electron micrographs of steel 4P28H, quenched from 720°C and aged at 60°C for 10 h, showing: (a) coarse carbides at grain boundaries and (b) carbide precipitation in ferrite matrix.

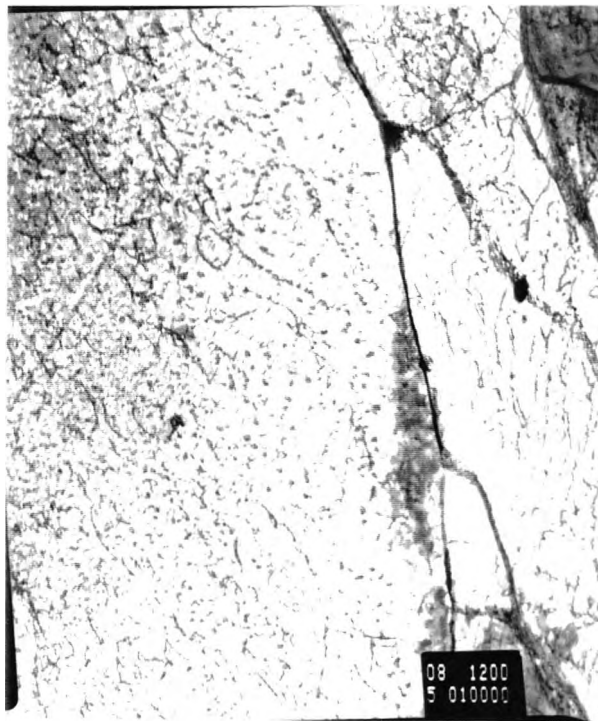


(a)



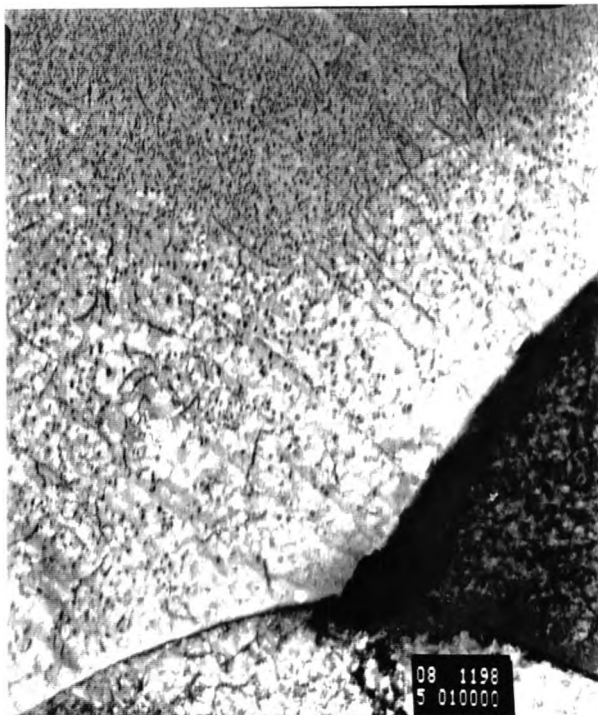
(b)

Figure 4.10 (a), (b) Scanning electron micrographs, of steel 4P28H, quenched from 720°C and aged at 100°C for 3 h, showing: (a) carbides at grain boundaries and in ferrite matrix and (b) coarse carbide precipitation in ferrite matrix.



x10000

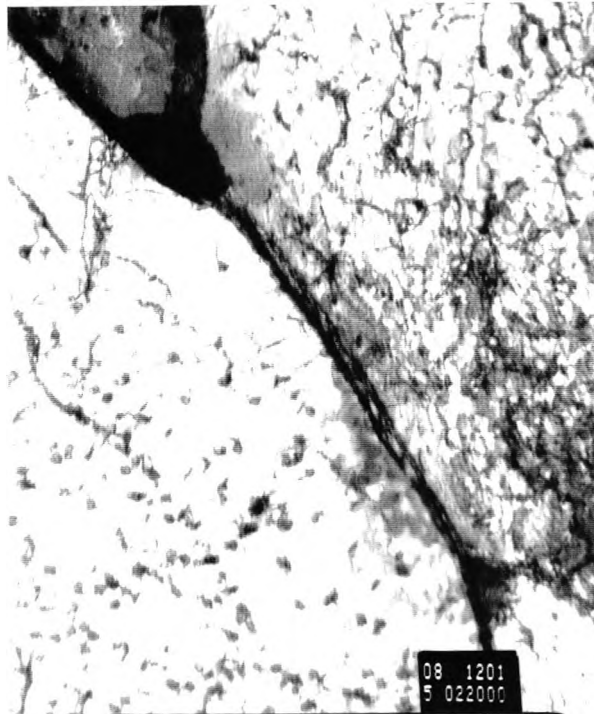
(a)



x10000

(b)

Figure 4.11 (a), (b) Transmission electron micrographs of steel 4P28H, quenched from 720°C and aged at 60°C for 10 h, showing very fine precipitation of iron carbides in ferrite matrix. Coarser particles can also be observed at grain boundaries [96].



x22000

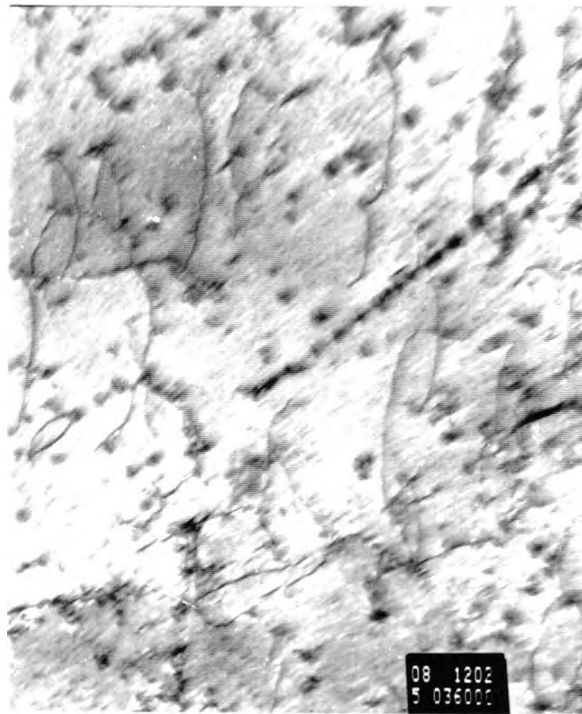
(c)



x28000

(d)

Figure 4.11 (c), (d) Transmission electron micrographs of steel 4P28H, quenched from 720°C and aged at 60°C for 10 h, showing grain boundary carbides and fine iron-carbide precipitates, probably coherent with the matrix.



x36000

(e)



x60000

(f)

Figure 4.11 (e), (f) Transmission electron micrographs of steel 4P28H, quenched from 720°C and aged at 60°C for 10 h, showing fine iron-carbide precipitates and dislocations, in the ferrite matrix.

Transition curve

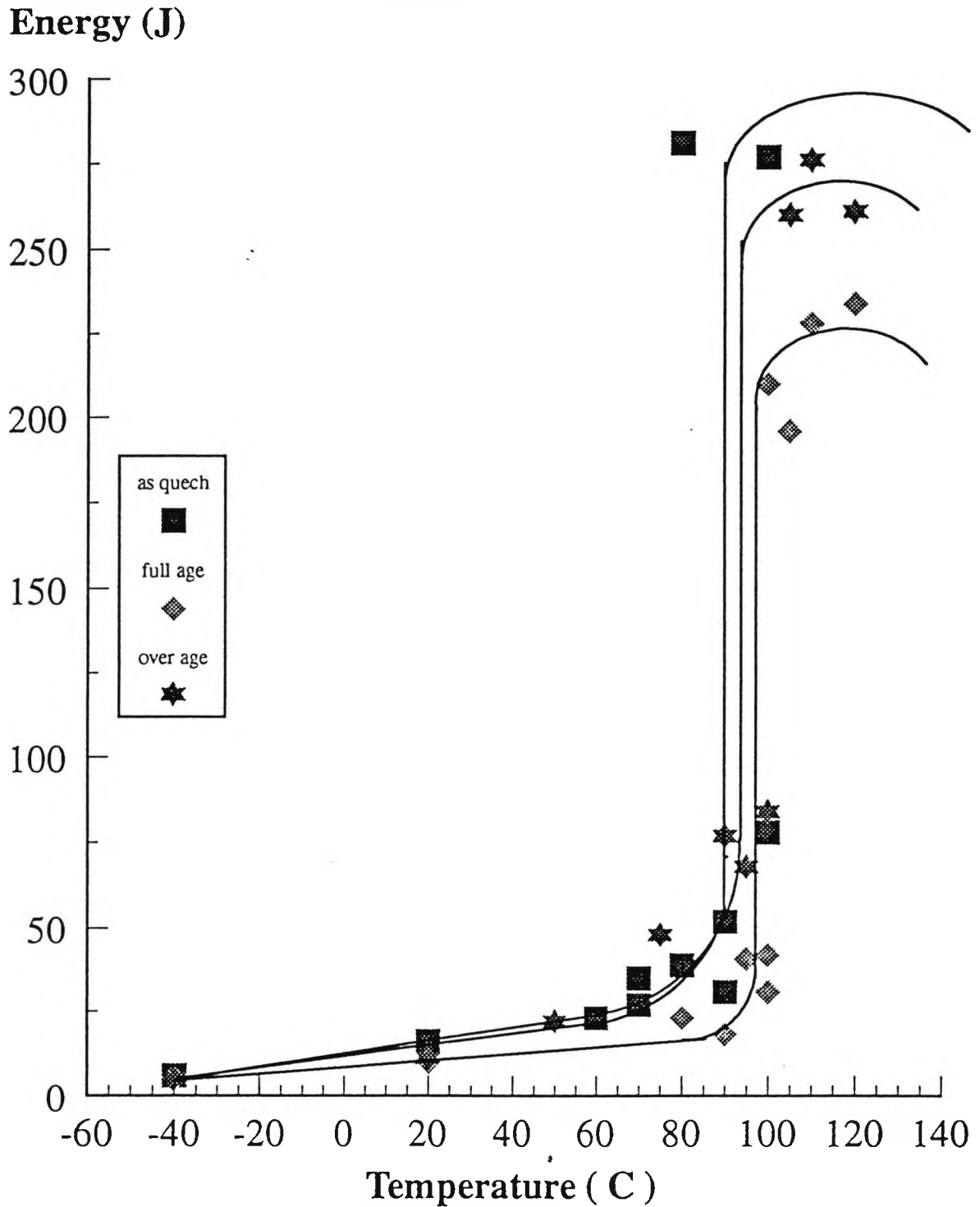


Figure 4.12 Impact transition temperature curves, for quenched and aged, steel 4P28H (the tests have been carried out at British Steel [96]).

5

THE STRENGTH AND IMPACT PROPERTIES OF LOW-CARBON COPPER-CONTAINING FERRITE-PEARLITE STEELS

5.1 Introduction

Prior to this exercise, a similar one had taken place which aimed to look into the structure-property relationships of a commercial copper containing steel and investigate the effect of copper precipitation on these relationships, chapter 6. However, the complexity of the composition resulted in structures that were difficult to relate to the properties and therefore imposed limits in the assessment of the copper effect and it was decided that the exercise should be repeated, this time using simpler laboratory steels. For simplicity, it was decided to present and discuss the results of the simpler steels prior to those of the commercial steel.

Three steels were chosen, all having the same alloy composition but different copper levels. These steels were to be given the same heat treatments as the commercial steels, only this time a slower cooling rate would be applied in order to avoid martensite formation.

The steel compositions are shown in Table 5.1. It can be seen that in comparison to the commercial steels, Table 3.1, several alloying elements such as chromium,

niobium and nickel are absent all of which decrease the transformation temperatures. This leaner composition, combined with the slower cooling rate would thus eliminate the possibility of martensite formation.

5.2 Experimental

The three steel plates, Table 5.1, were sectioned into smaller plates which were used for the trial and the actual heat treatments. All the plates were austenitised at 910°C, the γ -region, for 30 min and then cooled in vermiculite. This resulted in an average cooling rate of 5 °C/min, in the temperature range of 800 to 400 °C, Table 5.2. The trial plates were then sectioned into smaller pieces which were consequently tempered at temperatures ranging from 300 to 650 °C for one hour. Vickers hardness tests were then performed on the trial pieces, using a 10 kg load and the age-hardening behaviour of each steel was determined by plotting the hardness values against the Holloman parameter values, Figure 5.1. It can be seen that except for the Cu-free steel in which the hardness remained essentially constant, the hardness remained low until the Holloman parameter reached 15, then increased to a peak (Holloman par.=16) and then fell.

The three following conditions were finally selected to be examined in detail for steels 2P148H and 2P149H: "normalised" (N), "normalised" and fully-aged at 525°C for 1 h and "normalised" and over-aged at 650°C for 1 h, Holloman parameters of 16 and 18.5 respectively. The conditions for steel 2P150H were slightly different; "normalised", "normalised" and fully-aged at 550°C for 1 h and "normalised" and over-aged at 650°C, Holloman parameters of 16 and 18.5 respectively.

It must be mentioned that steel 2P148H, which was free of copper, was not expected to show any variation in hardness or any other property upon ageing. It was, nevertheless, decided that heat treatment procedures similar to those followed for steel 2P149H (1.22% Cu) would be followed for the sake of comparison. Although vermiculite cooling was used instead of air cooling, the term "normalising" has been used for simplicity.

Three tensile samples were tested for each condition, one on the LLOYD tensile test machine and two on the INSTRON machine. A 20 mm extensometer was used for

tests carried out on the INSTRON machine. The tests were carried out at a strain rate of $1.4 \times 10^{-3} \text{ s}^{-1}$.

Standard V-notch charpy tests were carried out to determine the impact transition temperatures. The test temperatures ranged from -100 to +80 °C.

The structures of the three plates in the three conditions were examined on the optical, scanning electron and transmission electron microscope. The hardness was also measured in all stages, i.e. on the tempering trials, the broken charpies, the broken tensiles and on the rods that were going to be used for thin foil preparation.

In addition to the transmission electron microscopy that was carried out on all steels in the three conditions, some further experiments were carried out so as to obtain some information regarding the influence of strain on these copper precipitates. A higher tempering temperature of 700°C was chosen, so as to coarsen the precipitates and make it easier for observations to be made under the TEM. Steel 2P150H (2.02% Cu) was chosen to be examined. One steel plate was austenitised at 910°C for 30 min, cooled in vermiculite and then tempered at 700°C for one hour (coded as NT700). Then part of it was cut and machined into a 4 mm rod, which was then strained by 15% on the INSTRON machine (NT700 + 15% straining). Another steel plate was austenitised at 910°C for 30 min but cooled in air, i.e. normalised so as to give some indication as to the difference in precipitation between air and vermiculite cooling. All these conditions were examined on the TEM.

5.3 Test results

5.3.1 Hardness test results

The age hardening behaviour of the three steels was determined after performing tempering trials and this is shown in Figure 5.1. The hardness of the 1.22 % Cu steel, was 191 after “normalising” and reached a peak of 236 HV10 after ageing at 525°C for one hour, and then dropped below the initial value, to 173 HV10 after ageing at 650°C for one hour.

The hardness of the 2.02 % Cu steel was found to be 167 HV10 after “normalising” i.e. softer than the steel with 1.22% Cu, and increased to 204 HV10 after tempering at

550°C for one hour. This value dropped to 177 HV10 after ageing the steel at 650°C for one hour.

The steel that was free of copper showed only very slight variations in hardness after tempering above 450°C.

As it can be seen from Table 5.3, hardness tests were also performed on all the tested specimens and an average value was calculated for each condition. Those values are lower than those obtained from the tempering trials, but trends are always the same. The variability may be due to the hardness gradient across the centre of the plate. It should be noted that except for the over-aged condition, when there was little difference between the two steels, the higher Cu containing steel gave lower hardness values than the lower Cu containing steel.

5.3.2 Tensile test results

The steel that is free of copper, showed an initial LYS of 228 N/mm² and this value increased slightly to 244~246 N/mm² after tempering at 525 and at 650 °C for one hour. Other tensile parameters such as ultimate tensile strength, elongation and reduction in area, did not show any variation. The percentage elongation was found to be 42~44, and the reduction in area 76%.

Steel 2P149H, the 1.22% Cu containing steel, gave a lower yield point of 400 N/mm², which rose to 487 N/mm² after tempering at 525°C and then fell back to 394 N/mm² on tempering at 650°C. The changes in the ultimate tensile stress followed a similar pattern, rising from 492 to 586 and then falling to 454 N/mm², whereas the elongation dropped from 31 to 26 and then rose to 32% respectively for the (N), (NT525) and (NT650) conditions.

The lower yield stress of the 2.02% Cu steel 2P150H, was found to be 376 N/mm² in the normalised (N) condition, and increased by nearly 80 N/mm² after tempering at 550°C for one hour. In the over-aged stage it was found to be 415 N/mm². The ultimate tensile strength values were found to be 454, 520 and 472 N/mm² for the respective (N), (NT550) and (NT650) conditions. Thus, again except for the over-aged state, the higher Cu containing steel gave lower strength levels than the 1.22% Cu

containing steel. The elongation values for the (N), (NT550) and (NT650) conditions, were found to be 39, 32 and 36%, respectively.

In all cases a clear yield point was obtained rather than a proof stress. The ductility was at its highest for the copper-free steel, and at its lowest for the 1.22% Cu steel, whereas the reverse behaviour applied to the strength. All results can be looked at in more detail in Table 5.4.

5.3.3 Impact test results

The main observation concerning the impact properties of the copper-free steel, is the similarity of the test results for the three conditions. The only plate which showed a small deterioration in the impact behaviour, was the fully-aged (525°C for one hour).

For all the steel conditions a steep transition from ductile to brittle fracture was observed, resulting in similar values for the 27, 54 J ITT and 50% FATT impact criteria, Figure 5.2. These values were all found to be between the -23 and -25 °C for the (N) and (NT650) samples. For the (NT525) sample, the ITT at 54 J and 50% FATT values were found to be -11 and -10 °C respectively, and the 27 J ITT was found to be -19°C, Table 5.5. Shelf energies were at the maximum obtainable with the machine, for all steel conditions, i.e. 300 J.

The ductile to brittle transition curves of the 1.22% Cu steel were neither so abrupt as that of the copper-free steel, nor so well defined, Figure 5.3. For the “normalised” condition (N), transition temperatures at 54 and 27 J were found to be -33 and -47 °C, respectively. The 50% FATT was found to be -15°C. The shelf energy was lower than in the copper-free steel, being 240 J at room temperature, which decreased even further down to 160 J after ageing to peak hardness. The impact shelf energy in the fully-aged condition at room temperature was even lower, 110 J. The respective impact transition temperatures at 54 and 27 J, are -2 and -22 °C and the 50% FATT is 20°C.

After over-ageing the 1.22% Cu steel at 650°C for one hour, the impact strength was restored and the ITT values at 54 and 27 J were approximately the same as those of the “normalised” state. The 50% FATT was the lowest of all three conditions and this was -33°C. The shelf energy also increased to a maximum of 290 J at -10°C, although it later decreased down to 265 J at room temperature.

The impact behaviour of the 2.02% Cu steel was much better than that of the other two steels mentioned above, Table 5.5. In the "normalised" condition, the steel had an ITT of -84°C at 54 J and -89°C at 27 J. These values increased to -60 and -73 °C after ageing the steel to peak hardness. Over-ageing the steel however, did not succeed in recovering the impact strength completely, thus resulting in slightly higher transition temperatures than those of the N condition. The 54 and 27 J ITT values, were found to be -74 and -84 °C, respectively.

The changes of the 50% FATT value followed the same pattern as the ITT values, and were found to be -75, -45 and -65 °C for the respective steel conditions of (N), (NT550) and (NT650).

The shelf energy was at its maximum, 300 J, for the (N) and (NT650) conditions, and at its minimum, 273 J, for the (NT550) condition, at room temperature. The ITT curves for the higher Cu steel were also well defined, Figure 5.4.

5.4 Metallography

5.4.1 Optical microscopy

Optical examination of the copper-free steel revealed a polygonal ferrite structure in which there was 5% pearlite in accord with the steel's low carbon content, Figure 5.5 (b). The pearlite colonies tended to be in bands. The ferrite grain size was very coarse, although not uniform, with an average value of $6 \text{ mm}^{-1/2}$ or $27.5 \text{ }\mu\text{m}$, for all the three conditions. As can be seen from Table 5.6, there was no change in grain size or phase volume fraction upon tempering. The appearance of the three samples was also more or less the same for all the three conditions, Figures 5.5 (a), (b).

The 1.22% Cu steel had a similar structure to the copper-free steel, the main difference being the finer grain size which was measured to be approximately $14.2 \text{ }\mu\text{m}$ or $8.4 \text{ mm}^{-1/2}$ for all the three conditions. The grain refinement is probably related to the presence of copper which will lower the Ae_3 and thus gives less opportunity for the growth of ferrite. The pearlite volume fraction was again found to be 5% in all conditions and the line banding was present, Figure 5.6 (b). The main optical difference between the two steels is that the ferrite grains of the 1.22% Cu steel are not uniform in shade, Figures 5.6 (a) and (b). Efforts were made to measure this effect in terms of volume fraction but it was impossible to succeed, because shade

differences were small and etching time-dependent. This characteristic, has been observed by other investigators [57], but they gave no explanation as to its cause. It is most likely related to variations in the amount of coarser copper precipitation from grain to grain.

The shade effect mentioned above, was much more apparent as copper levels increase, Figures 5.7 (a) and (b). Volume fraction measurements revealed that 16% of the ferrite structure is much brighter than the rest of the ferrite. The etching time-dependency of the ferrite shade suggests that this effect could be attributed to the copper distribution among ferrite grains, although it was originally thought to be a grain orientation effect.

5.4.2 Scanning electron microscopy

5.4.2.1 Copper-free steel

SEM examination of the copper-free steel confirmed the ferrite-pearlite structure that had been observed under the optical microscope, Figures 5.8, 5.9 and 5.10. These photographs give an indication as to the morphology of pearlite and the effect that tempering has upon this phase. In the (N) condition, pearlite consists of densely packed, plates of ferrite and cementite, Figure 5.8, that do not spheroidise after tempering at 525°C for one hour, Figure 5.9. Partial pearlite spheroidisation only occurs when the steel is over-aged, that is after one hour of tempering at 650°C, Figure 5.10.

Carbides were present in all conditions, at grain boundaries, Figures 5.11, 5.12 and 5.13. A wide variation in the carbide thickness was noted, Figures 5.10 and 5.11 and Figures 5.12 and 5.13. Grain boundary carbide thickness measurements were performed for all conditions. For the "normalised" condition, the average carbide thickness was found to be 0.33 μm . In the (NT525) sample there was not much change of this value, Table 5.6. After over-ageing the sample, there was a slight increase in size, raising the thickness up to 0.37 μm .

In addition to the above comments on carbide morphology, the examination of the "normalised" sample revealed that on many occasions the grain boundary carbides were very long, Figures 5.12 (a) and (b), but broke into smaller lengths after tempering, Figure 5.13.

5.4.2.2 1.22% Cu steel

The addition of copper, had little influence on the carbide thickness, Table 5.6. The grain boundary carbide thickness values were found to be 0.4 μm for the (N) and (NT525) samples and 0.44 μm for the (NT650) sample. Typical grain boundary carbides can be seen in Figures 5.14, 5.18 (b) and 5.19. This insensitivity of the carbide thickness to the presence of copper is somewhat surprising, as lowering the transformation temperatures would be expected to cause the carbides to come out at lower temperatures. However, it is possible that most of the copper is taken out of solution at high temperatures, and by the time the transformation to pearlite occurs, there may be very little remaining to influence the $\gamma \rightarrow$ pearlite transformation temperature [34].

Another effect of copper on the steel structure is that precipitation is clearly observed, this precipitation having occurred during the slow cooling from 910°C, e.g. Figure 5.14. Although copper precipitation can be more readily resolved by transmission electron microscopy, the examination by the scanning microscope enables much larger areas to be examined. Using the SEM, the ferrite grains had a different appearance, as compared to that of the copper-free steel. All figures from 5.14 to 5.20 contain SEM photographs of the 1.22% Cu steel at all conditions and it can be clearly observed, that there is a plethora of fine particles within the ferrite matrix and more fine particles at the ferrite grain boundaries. The existence of these particles results in brighter ferrite grains than those pictured in Figures 5.8 to 5.13, i.e. the copper-free steel. There are however some grains that are darker than others, an indication that copper precipitation is not uniform. The difference between darker and brighter ferrite grains can be viewed in Figure 5.17, which shows two adjacent ferrite grains of different shade. This observation is in accord with optical microscope examination results. A detailed examination of the SEM photographs indicated that the copper particles (generally spherical in shape) had an average diameter of 57 and 70 nm, for the "normalised", and "normalised" and over-aged conditions, respectively.

There were also some very fine particles at the boundaries, Figure 5.20, later identified as carbides. These were not taken into account when the average carbide thickness was measured.

Another interesting but intriguing observation, is the presence of ghost boundaries which form finer grains irrespective of the well defined major ferrite grains, Figures 5.14, 5.16 and 5.20. This effect, which was observed in all conditions, is suspected to be a combination result of phase transformation and copper precipitation. Precipitate free zones on either side of these ghost boundaries are also observed, Figure 5.14. There are two possible reasons to account for these observations:

1. The coarse precipitates and boundaries formed on cooling during “normalising”. It may be that they formed at higher temperatures than the tempering temperature range and were thus able to grow to a stage when they were no longer able to pin the ferrite boundaries.
2. These coarse precipitates were present on heating up to 910°C and that the “normalising” treatment was not long enough to take them back into solution.

Finally, as in the copper-free steel, pearlite begins to spheroidise only after tempering at 650°C and even then, not all pearlite grains are affected, Figures 5.18 (a) and (b).

5.4.2.3 2.02% Cu steel

As in the steel with the lower copper level, the ferrite grains in all conditions are full of copper particles, Figures 5.21 (a) and (b), which are believed to form either on cooling from 910°C because of the low cooling rate applied, or were already present at the normalising temperature. The average size of these particles was measured from the SEM and their thickness was found to be approximately 75 nm for the “normalised” and the fully-aged conditions and 90 nm for the over-aged condition. These were coarser than those found in the 1.22% Cu steel. The grain boundary carbide thickness was also measured, this being 0.4, 0.42 and 0.44 μm for the respective (N), (NT550) and (NT650) conditions. Typical grain boundary carbides found in the “normalised” and over-aged conditions are shown in Figures 5.22 (a) and (b) respectively, the latter showing slight coarsening of carbides upon tempering. Some fine particles, subsequently identified as Fe_3C were also present at the ferrite boundaries, Figures 5.21 (a) and (b).

Also, in agreement with earlier optical microscope observations, the ferrite structure had different degrees of shading, Figure 5.23 (a). An enlarged section of the ferrite structure in Figure 5.23 (b), shows clearly this effect.

Figures 5.24 (a) and (b) show respectively a pearlite colony in the (N) sample, and a slightly spheroidised one in the (NT650) sample. It was generally observed, that as the copper level increases tempering becomes less effective on spheroidisation; possibly copper slows down the diffusion of carbon.

5.4.3 Transmission electron microscopy

Thin foils from the two copper steels were first examined, and the results were confirmed by the examination of replicas. The copper-free steel was excluded from the TEM study, as a brief examination of the (N) sample confirmed that there are no precipitates.

The mottled appearance of the thin foils made it difficult to infer whether there were any fine particles present.

5.4.3.1 1.22% Cu steel

Limited TEM examination of the thin foils revealed copper precipitates in the (N) and (NT525) samples, but failed to reveal them in the (NT650) sample, i.e. the over-aged condition. The precipitate size was approximately 60 nm for both (N) and (NT525) conditions. This came as a surprise, since the over-aged sample was the sample that was supposed to have the majority of precipitates. However, as mentioned in section 5.4.2.2, more detailed examination of SEM photographs of the “as normalised” and over-aged conditions made it possible not only to identify the copper particles, but also measure their thickness, Table 5.7 (a).

During the thin foil examination, a few of the particles that seemed to form ghost grain boundaries in earlier SEM investigations, were analysed and identified as aluminium nitride. However, the presence of precipitate-free zones indicates that the major precipitate at the ghost boundaries was the copper particles. Slow cooling however, gave rise to an increase in the local energy and possibly boundaries managed to migrate away from the pinning particles, or the particles were already present at 910°C prior to cooling.

The very fine grain boundary particles at the ferrite boundaries, were also analysed and were found to be composed mostly of Mn; they were therefore assumed to be very

fine carbides and not copper precipitates, as was first thought during the SEM investigation. EDAX analysis has shown that some Mn is also included in the composition of some of the coarser carbides, but of less proportion than in the finer ones.

The majority of the copper particles had a spherical appearance, Figures 5.25, and 5.26, their diameter being 58 nm for the "normalised" condition, as measured from TEM thin foil micrographs, Table 5.7 (a). However, the limited number of precipitates measured, means that results are not very reliable. To compensate for this, a clear SEM photograph was selected, Figure 5.16 (b), and the diameter of 100 particles was measured. This was found to be 57 nm, Table 5.7 (a), and is in good agreement with TEM results. Similar examination of SEM pictures of the over-aged condition, indicated a slight increase of precipitate diameter, this having been found to be 72 nm. Unfortunately this method was impossible to apply to the fully-aged condition, as there were not any clear photographs, but it can be assumed from the discussion section that ageing at 550°C was not likely to affect precipitate size, and the size would be that given by the "normalised" condition, 57 nm.

5.4.3.2 2.02% Cu steel

Thin foils of the over-aged sample, (NT650), were examined first and all were found to contain large amounts of copper precipitation. A similar precipitate density was observed in the (NT550) sample. However, the non-aged sample, (N), had a smaller precipitation volume fraction. These observations can be noticed in Figures 5.27, 5.28, 5.29 and 5.30. It is also noticeable, that the precipitate density is by far higher than that of the 1.22% Cu, compare Figures 5.25 and 5.26 with Figures 5.27 (b) and 5.28 (b).

The precipitate shape tended to be elliptical for most of the particles, for all conditions, rather than the spherical shape that dominated most of the copper particles of the 1.22% Cu steel. The precipitate size as measured from 27 thin foil particles, was found to be 45 nm in thickness and 75 nm in length in the normalised condition, Table 5.7 (a). Similarly, sample (NT550) was found to have elliptical precipitates that were of similar thickness i.e. 43 nm; but longer, 101 nm long (84 thin foil particles were measured). A slightly lower average particle size was measured for the elliptical-shaped precipitates in the over-aged sample, (NT650). This was found to be 39 nm in thickness, and 91 nm in length (49 particles were examined). This difference can be noticed if Figures 5.29 and 5.30 are carefully observed.

Commenting on the above observations, it can be said that part of the copper had already precipitated prior to ageing, as coarse elliptical-shaped precipitates. These, did not have a special nucleation site preference but were scattered all over the ferrite matrix. The rest of the copper atoms precipitates upon ageing to form a coherent precipitate that coarsens and becomes detectable after over-ageing.

Finally, it can be concluded that the plethora of particles that were observed in ferrite grains during the SEM examination are definitely copper precipitates. This can be seen by comparing SEM Figures 5.21, 5.23 and 5.24 with TEM Figures 5.28 (a) and (b), which were deliberately shot at the low magnifications of x6000 and x10000. The comparison shows that the particle density and size are identical between the two sets of photographs. As it was mentioned earlier in section 5.4.2.3, the precipitate size was measured from SEM photographs. The elliptical shape of the copper particles however, complicated measurements, because the particles were cut at various angles. This, in combination with the low magnification of photographs, might have introduced a slight inaccuracy of the readings. In all cases the thickness of the copper particles was measured, this being found to be approximately 75 nm for the (N) and (NT525) conditions and 90 nm for the (NT650) condition. The variation of these readings to those taken from the TEM photographs, is probably due to the reasons mentioned above. In addition, thin foils represent only a tiny fraction of the precipitate population, which was clearly observed to be non-uniform in size and distribution.

5.4.3.3 A TEM study on the effect of straining on the 2.02% Cu steel

Another plate that had been austenitised at 910°C for 1/2 h and cooled in vermiculite, was tempered at 700°C for 1 h, (NT700). This was found to have a dense population of precipitates, Figure 5.31 (a). These precipitates were elliptical in shape, Figure 5.31 (b) and had an average thickness of 63 nm and an average length of 111 nm, Table 5.7 (b). Spherical particles were also present and had an average diameter of 66 nm. As expected, these values together with particle density, are higher than the previous measurements for the sample aged at 650°C. Another significant observation, is that copper particles of the (NT700) sample, grow in all directions, Figure 5.31 (b).

Part of the plate that was cooled in vermiculite and was tempered at 700°C for one hour, was strained by 15% in order to examine the effect of plastic deformation on copper particles.

Thin foil examination of the strained (NT700) sample revealed the existence of dislocations, although these were in general difficult to find. Figures 5.32 and 5.33 clearly show copper particles surrounded by dislocations, whereas the observation of dislocations in Figures 5.34 and 5.35 is less clear. A large number of particles appear to have elongated, Figures 5.32, 5.34 and 5.35. Others seem to have suffered some degree of deformation, but their size did not change much, Figure 5.33. Particle size measurements indicate that straining caused a decrease in thickness, from 63 nm down to 39 nm, whereas the length remained approximately the same at 110 nm. The spherical particles that were present, may also have elongated after deformation, accounting for the low average length readings. Copper particles were not observed to be fractured by dislocations, except perhaps in one case, Figure 5.35. On the top right corner of Figure 5.35, there are two particles that each seems to be part of a single particle. The conical shape of the two particles suggests that the reason for them splitting apart is shear. However, no voiding was noted at any of these deformed particles and dislocation densities were very low, therefore putting some doubt as to this interpretation and more work is required to confirm these findings.

Figure 5.32 (a) shows dislocations that are pinned by other particles than the coarse copper particles. This observation is significant because it discloses the presence of very fine particles. These are probably fine carbides that precipitated during strain ageing.

5.4.3.4 A TEM study on the effect of cooling rate on the 2.02% Cu steel

As mentioned earlier in the experimental section, all the steels had been cooled in vermiculite after austenitisation, to avoid the formation of martensite. The result was that a large volume fraction of copper particles were present prior to ageing and it was difficult to subsequently separate these from those produced during ageing. As mentioned earlier, the precipitate could have formed as a result of the slow cooling or had already been present at the austenitising temperature of 910°C. To help sort this out, a further steel plate was austenitised at 910°C for 1/2 h and then air-cooled. Whereas vermiculite-cooling gave rise to spherical particles 57 nm in diameter, air-cooling resulted in finer particles 31 nm in diameter or 25 and 42 nm in thickness and

length respectively, Table 5.7 (b). Figure 5.36 shows TEM photographs of the air-cooled steel.

It would appear that cooling rate certainly has a big effect in influencing the size of these particles but it is still possible that undissolved particles were present at 910°C prior to cooling.

5.5 Discussion of results

5.5.1 The microstructures

A similar study to the present one, but concentrating only on over-aged samples, was carried out by Maclvor [57] and produced similar results as to the size of copper precipitation. The work carried out by Maclvor, concerned two low alloy steels of 1% and 2% copper contents that were normalised at 900 and 1000 °C and then tempered at 650°C for 4 h and at 700°C for 100 h. The precipitate thickness of the samples that were aged at 700°C is identical with that of the (NT700) sample of this exercise despite the differences of the ageing time, but the length was much greater (twice the present one). Also, as in the present study, an increase in the copper level is followed by an increase in the precipitate volume fraction. Surprisingly, Maclvor [57] did not observe marked differences in the precipitate size when the copper content was varied, whereas in this exercise, the 2.02% Cu containing steel resulted in coarser precipitation than the 1.22% Cu containing steel.

Deformation of Maclvor's [57] steel plates, after ageing at 700°C, produced slip dislocations that bowed between precipitates, but it was not clear whether these had entered or deformed the copper particles. In this study however, it is clear from photographs, Figures 5.32 and 5.33, that dislocations actually enter precipitates. It is also noticeable that dislocations are either absent or fade around precipitates that were observed to deform, Figures 5.34 and 5.35.

5.5.2 The influence of tempering on hardness and tensile properties

An interesting observation is that steel 2P150H which has the highest copper level and the finest grain size of the other two steels, gives lower hardness values than the 1.22% Cu steel, Figure 5.1. Initially it was thought that this might have been the result of an error in calculating the Ae_3 temperature and therefore austenitising the steel at an inadequate temperature. To check this, another piece of the 2.02% Cu steel was

austenitised, this time at a higher temperature of 950°C, for 1/2 hour and was consequently cooled in vermiculite. Further tempering trials were performed and the hardness was tested. Hardness results verified the correctness of previous results, indicating that there must be some other explanation for this event.

The lower yield strength, behaved in a similar manner to that of hardness and was lower for the 2.02% Cu steel than that of the 1.22% Cu steel in all conditions, Table 5.4 and Figure 5.37. On the other hand, in the over-aged condition, the 2.02% Cu steel retained half of the strength due to precipitation hardening, whereas the other copper steel lost all of it, Table 5.11.

Bearing in mind that some degree of dispersion strengthening has occurred in the copper containing steels during cooling of the samples from the austenite region (or prior to "normalising"), it is necessary to use theoretical equations in order to calculate the expected LYS values. This will help to appreciate the exact contribution of copper to the strength of each steel. There are many empirical equations which can be used to do this, such as Equations 2.10 and 2.11, [4,31].

$$\sigma_y = 43.1*\%Mn + 83*\%Si + 15.4 d^{-1/2} + 1540*\%N_f + 105 \quad \dots(2.10)$$

$$\begin{aligned} \sigma_y = & 70 + 32*\%Mn + 84*\%Si + 680*\%P - 30*\%Cr + 38*\%Cu \\ & + 33*\%Ni + 11*\%Mo + 5000(\%C + \%N) + 18.1 d^{-1/2} \quad \dots(2.11) \end{aligned}$$

Equation 2.11 is in some ways more accurate than Equation 2.10, because it takes into account the influence of copper in solution, whereas Equation 2.10 is for plain C-Mn steels. In practise because much of the copper is taken out of solution, even Equation 2.11 is not exact. However both must be used, as calculated ITT values will be derived from equations that rely upon the results of Equation 2.10.

A LOTUS spreadsheet was created for the calculation of expected LYS values and the results are displayed in Table 5.8. It can be seen that if copper is taken into account for the calculation of the expected LYS values, in "normalised" samples, there is a better agreement with observed LYS values than if Equation 2.10 were used. For the copper-containing steels, the latter equation gives much lower calculated figures than the observed ones.

There are two possible explanations to account for the age-hardening behaviour. The first, is that coarse, dispersed particles, such as incoherent precipitates, do not allow dislocations to cut their way through, but force them to bow out until they pass them by looping (Orowan mechanism [15]). This is termed as dispersion strengthening and could be a possible reason for the present age-hardening behaviour, since the slow cooling rate or the short austenitising treatment, would allow -as has been observed- marked precipitation of relatively coarse copper particles.

Maclvor [57], has shown that because the volume fraction of copper precipitates in the over-aged Cu-containing steel is so high, the changes in strength and hardness can often be explained in terms of changes in dispersion strengthening. Dispersion strengthening increases with the volume fraction of particles and decreases with their size and is generally satisfactorily accounted for by the Orowan-Ashby relationship. It might therefore be argued, that on "normalising", not all the Cu is precipitated out and ageing encourages more precipitation, thus increasing strength until the equilibrium volume fraction is achieved which corresponds to peak-hardness; then further increase of the ageing temperature, causes the copper precipitation to coarsen and over-age. Because of the large volume fraction of precipitation in this system, it is permissible to have quite large particles (30~100 nm) and still get considerable strengthening.

The second explanation of this age-hardening behaviour, is to assume that the curve shows normal age-hardening behaviour and the peak of the curve corresponds to the point just before the change from coherent to incoherent precipitation. In this case, in the fully-aged condition it will not be easy to see the coherent precipitate which is fine, even when over-aged.

Maclvor [57] was able to interpret his results for the over-aged state, entirely in terms of dispersion strengthening. In that particular study several models were explored, these being the following:

$$\text{Orowan,} \quad \tau = \frac{1.2\mu b}{2\pi} \left[\frac{1}{x(\sqrt{\pi/4f} - 1)} \right] * \ln \left[\frac{x(\sqrt{\pi/4f} - 1)}{2b} \right] \quad \dots(5.1)$$

$$\text{Ashby,} \quad \tau = \frac{1.2\mu b}{2\pi} \left[\frac{1}{1.18x(\sqrt{\pi/4f} - 1)} \right] * \ln(x/2b) \quad \dots(5.2)$$

Ansell,
$$\tau = \frac{\mu}{120(\sqrt{\pi/4f} - 1)} \quad \dots(5.3)$$

where τ is the shear stress, assumed to be one half of the tensile strength σ , μ , the shear modulus (8.03×10^4 N/mm² for a ferrite matrix); b , the burger's vector (0.24 nm); x , the mean intercept diameter of precipitates; and f , the total fraction of precipitates. Of the three equations, Ashby's model gave the best agreement with experimental observations [57]. The mean diameter of precipitates, x , is calculated as follows:

for spherical particles of diameter d_p ,

$$x = d_p * \sqrt{2/3} \quad \dots(5.4)$$

for elliptical particles of thickness t_p , and length l_p ,

$$x = \sqrt{2 * t_p^2 * l_p / (t_p + l_p * \sin 54)} \quad \dots(5.5)$$

In that study [57], the particle volume fractions were very high (0.007 for the 1% Cu containing steel and 0.016 for their 2% Cu containing steel) and particle size was also large, spherical particles being 38 nm in diameter and rod-shaped 62 and 240 nm in thickness and length, respectively. A large degree of strengthening nevertheless occurred, this being much greater for the higher Cu containing steel in accord with its higher volume fraction of precipitated copper. The estimated dispersion strengthening at their lower ageing temperature of 650°C was 100 N/mm² for the lower copper containing steel and 150 N/mm² for the 2% copper containing steel. These values fitted in well with the calculated values from the Ashby-Orowan relationship using their measured particle size (38 nm) and the calculated volume fraction of precipitation (0.007 and 0.016 for the 1% and 2% copper steels, respectively).

However, Crowther [52], working on commercial Cu containing steels with complex compositions, again found considerable strengthening on ageing, but could detect no precipitation at the peak hardness in the ageing curve and had to overage in order to coarsen the precipitates (10~30 nm) and to be able to observe them under the

microscope. Crowther interpreted his results in terms of normal age-hardening behaviour that the coherent fcc, ϵ -copper precipitation was too fine to be detected readily with TEM and only when it coarsened could the precipitation be identified.

It seems likely in the present instance that both mechanisms, dispersion strengthening and age-hardening, are required to interpret the changes in strength. In the present study, it is clear that considerable precipitation of copper particles has occurred either on cooling, or at 910°C, as can be seen from the SEM photographs, Figures 5.16 and 5.21 (a). The slow cooling would be expected to encourage precipitation and the high copper addition would be expected to promote precipitation at higher temperatures during cooling, producing a coarser precipitation as can be seen from Figures 5.16 (b) and 5.22 (a), for the low and high Cu containing steels, respectively. This justifies why the strengthening effect is greater for the low copper containing steel.

The Ashby model (Equation 5.2) was used in the present study to calculate the expected dispersion strengthening effect, Table 5.9. The size of copper particles that was used, was that measured from SEM photographs and the equilibrium volume fraction was calculated from the solubility data of Wriedt and Darken [82], given by the following equation:

$$\text{Log}_{10} \text{ wt \% Cu} = 4.335 - 4499 * (1/T^{\circ}\text{K}) \quad \dots(5.6)$$

This equation predicts that at 525, 550 and at 650 °C, there will be 0.05, 0.07 and 0.29 % Cu in solution. Subtracting these values from the total Cu additions and allowing for the difference in density between Cu and Fe and small variations in lattice parameters between Cu and the ϵ -Cu particles (3.615 and 3.625 Å for Cu and ϵ particles respectively), the precipitate volume fraction and thus the dispersion strengthening, was calculated for the two steels assuming equilibrium conditions, Table 5.9. It can be seen from this table that a considerable amount of the copper would have been precipitated out during cooling prior to tempering. It must be noted however, that the results of Equation 5.6 correspond to equilibrium conditions at the temperatures mentioned above. The actual values will be different. This will be certainly so for the "normalised" condition, but equilibrium conditions may well be appropriate for the tempered and fully-aged (NT500), (NT525) condition and most likely for the tempered and over-aged (NT650) condition.

The small difference in strength for the “normalised” condition between the 1.22 and 2.02 % Cu containing steels is due to the coarser precipitation in the 2% Cu containing steel being balanced by its larger volume fraction.

In the case of the 1.22% copper containing steel, dispersion strengthening was calculated from the Ashby model to be between 60 and 82 N/mm² for all the steel conditions. These values are slightly lower than the calculated δ LYS values for the “as-normalised” and “normalised and over-aged” conditions using Equation 2.10, Table 5.8, but much lower for the fully-aged condition as would be expected if coherent precipitation is to make a substantial contribution to the strength.

Bearing in mind that a lot of copper must have precipitated out in a coarse form in the “normalised” condition, it is clear that the dispersion strengthening component given by Equation 2.11 (which contains a term for copper in solution) must be too low (46 N/mm²) and because some copper remains in solution, the precipitation hardening contribution given by Equation 2.10 (which has not a term for the copper) is too high (99 N/mm²), i.e. neither equation gave a satisfactory value for the dispersion strengthening component .

If for example the precipitation hardening component, δ LYS, given by Equation 2.10 is used (99 N/mm²) with the precipitate diameter of 57 nm, then using the Ashby equation the volume fraction f of precipitate would be 0.0152 (i.e. 1.71% Cu) which is in excess of the copper present in the steel. Using Equation 2.11 with a much smaller δ LYS of 46 N/mm², the precipitate volume fraction would be 0.0038 (i.e. 0.43% Cu), which seems very low when the SEM photographs are examined.

Although the δ LYS value that is derived from Equation 2.11 should be the one that is used in conjunction with the Ashby equation, it does not give a correct f value; the reason being that copper which has precipitated out, reduces the amount left in solution and if this had been taken into account, it would result in a higher δ LYS value and therefore in a higher precipitate volume fraction. If one assumes, for example, that 80% of the copper is precipitated out, then the δ LYS in Equation 2.11 would increase from 46 to 84 N/mm². Such a precipitation hardening component would be in accord with a precipitate volume fraction approximately 0.01008. If this volume fraction and the precipitate size (57 nm) are then used in conjunction with the Ashby equation, then

the dispersion strengthening (i.e. δLYS) is calculated to be 79 N/mm^2 , which is not too far from the value that was estimated from Equation 2.11, i.e. 84 N/mm^2 . This leads to the conclusion that the actual δLYS values lie between $\delta\text{LYS}^{(1)}$ and $\delta\text{LYS}^{(2)}$ (slightly towards $\delta\text{LYS}^{(2)}$). If such values had been used, then more meaningful f values would have been derived. It also appears that for the 1.22% Cu-containing steel, probably 80% of the copper is precipitated out and only 0.25% Cu remains in solution available for further precipitation hardening on ageing.

For the aged conditions, in which equilibrium conditions are most likely to exist, it can be assumed that nearly all of the copper had indeed precipitated out and Equation 2.10 gives better results than Equation 2.11. The results are displayed in Tables 5.8 and 5.9.

As can be seen, on fully ageing, further strengthening occurred, indicating that further precipitation of copper had taken place. There was little indication from the SEM photographs that ageing at peak hardness had enhanced the coarser precipitation and certainly particle size did not change. The particle size increased slightly after over-ageing (approximately by 10~15 nm for both steels). In order to explain the increased strength that occurs on ageing at peak hardness, i.e. 80 to 90 N/mm^2 (which results in $\delta\text{LYS}^{(1)}$ and $\delta\text{LYS}^{(2)}$ values of 137 and 190 N/mm^2 , respectively for the 1.22% Cu steel), in terms of dispersion strengthening, then for the lower copper containing steel and for a particle size of 57 nm the increase in precipitate volume fraction corresponding to $\delta\text{LYS}^{(1)}$ should be 0.025 which is clearly impossible (in such case the copper content should be 2.8%). For $\delta\text{LYS}^{(2)}$ the f value was calculated to be 0.0433 which is even more impossible. Hence, the additional strengthening that is noted in the fully-aged condition must come from normal age-hardening coherency strains rather via dispersion strengthening. The actual amount of copper available for precipitation to give this marked strengthening can then be very small.

Thus, it is not surprising that no change in particle size or in volume fraction can be discovered on ageing at peak hardness, as the coherent precipitation is too fine to be observed. However, on ageing at 650°C , the coherent precipitation will have coarsened off and may be approaching the size of the coarser precipitation obtained on vermiculite-cooling from 910°C . MacIvor [57] found for example, that ageing at

650°C for 4 hr after air-cooling from 900°C, produced particles similar in size to those found in the present exercise.

It is indeed interesting to note that some of the precipitation present in the over-aged condition was finer than that present in the fully-aged condition. This suggests that this was the over-aged precipitation derived from the coherent precipitation. Because of the relatively small size of volume fraction of copper available for precipitation on ageing, it is not surprising that the over-aged state had very similar strength to the as-"normalised" one, as any extra dispersion strengthening would be small.

To summarise:

- In the non-aged condition, the strengthening that was observed, which is 99 and 55 N/mm² for the 1.22% and 2.02% Cu steels, respectively (according to Equation 2.10), is an effect of dispersion strengthening, the precipitation arising either during cooling from the austenitising temperature or being present on "normalising".
- In the fully-aged condition, strengthening is a combination of coherency strengthening and of dispersion-strengthening.
- In the over-aged condition, dispersion strengthening, is the major contributing strengthening vector.

5.5.3 The effect of precipitation hardening on impact properties

Of most interest in the present work is the influence of copper on impact performance. Copper has been shown to refine the grain size and so is beneficial to impact behaviour. However, this in itself would not be sufficient grounds for adding copper to steel. The other feature which copper has, is that it has been suggested that it can strengthen steels via precipitation hardening without influencing the impact behaviour.

In order to examine this, it is necessary to use conventional structure-property relationships for steels which show normal precipitation hardening behaviour (HSLA microalloyed steels) and to see whether the observed impact transition temperatures are better than would have been predicted from the equations developed for the conventional age-hardening steels. Such Equations (2.7, 2.8 and 2.9), were developed by Mintz *et al.* [4] for steels with average C and S contents of 0.2 and 0.025 % respectively. In order to use these equations for the analysis of the results in the present work, it was necessary to account for the higher shelf energies observed in

this study due to lower C and S levels, and a further reduction of 40°C was made to the calculated ITT's. In these equations, δy was calculated as a function of Equation 2.10 and the results are displayed in Table 5.10 (a).

The above correction can be justified in terms of the more recent work of Mintz, Peterson and Nassar's ITT equations [30] which were derived for steels with sulphur and carbon levels in the range of 0.002 - 0.021 wt.% S and 0.065 - 0.22 wt.% C. To account for this difference, the carbon and sulphur levels of the present exercise were deducted from these high values and the products were multiplied by the equivalent carbon and sulphur vectors of Mintz et.al.'s ITT equations [30]. The combined effect of the two vectors was found to be ~40 °K at 27 J and ~50 °K at 54 J. It must be clarified that it was not possible to use the more recent ITT equations for the assessment of the impact behaviour of the copper containing steels, because they do not take precipitation hardening into account.

According to the results, Table 5.10(a), the calculated transition temperatures for the copper-free steel are slightly lower than the observed values at 54 and 27 J and slightly higher than the observed 50% FATT values. The copper steels showed improvements in transition temperatures of the order of 55 to 80 °C at 54 J, 40 to 65 °C at 27J and 40 to 60 °C at 50% FATT.

Another set of calculated results was produced, this time attempting to modify the constant that should be added to the ITT equations, in order to achieve the best fit. This constant was calculated on the basis that the calculated results of the copper-free steels should be corrected to agree with observed results. After such a process, it was concluded that -2, -15 and +16 °C should be added to Equations 2.7, 2.8 and 2.9, respectively. The corrected figures are shown in Table 5.10 (b) and according to these, the ITT improvements are between 60 to 75 °C at 54 J, 55 to 65 °C at 27 J and 25 to 45 °C at 50% FATT, for the 1.22% copper containing steel. The respective values for the 2.02% copper containing steel were found to be between 70 to 85 °C at 54 J, 65 to 80 at 27 J and 45 °C at 50% FATT.

It can be seen that in all cases the impact behaviour of the copper containing steels is better than would have been expected from conventional precipitation hardening structure-property predictions. The higher copper containing steel also gave the higher

δ ITT values, Tables 5.10(a) and (b) (by $\sim 10^\circ\text{C}$ better than the lower Cu steel). It can be also observed that the δ ITT values did not vary much with ageing. Although the observed ITT values were found to be lowest after over-ageing, the comparison between experimental and theoretical values indicates that the best improvement comes from the fully-aged condition although this is only small ($\sim 10^\circ\text{C}$ better than in the other conditions). However, scatter was greatest at the determination of the fully-aged curve, so without further work it would be unfair to place too much weight on these two observations (for the 1.22 and the 2.0.2% Cu containing steels). Presumably the presence of the coarse precipitation that was formed prior to tempering, is enough to always ensure good impact performance and the more that is present, as in the higher copper containing steel, the better. If there is any additional improvement above what would be expected, due to the coherent copper precipitation, it is likely to be small.

Higher copper level seems to have resulted in slightly better impact transition temperatures which points to the higher volume fraction of precipitation as being the key factor to impact property improvement. The 2.02% copper containing steel of this exercise has an outstanding combination of strength and toughness considering its relatively coarse grain size ($10\ \mu\text{m}$).

The differences between observed and expected impact transition temperatures, are best summarised and visualised in Figures 5.38, 5.39 and 5.40. Figure 5.41 expresses the graphical relation between observed lower yield strengths and observed impact transition temperatures and clearly indicates that this relationship is linear. It also shows clearly that introducing Cu into the steel improves the strength in the case of the 1.22% Cu steel, with little change in impact behaviour and for the 2.02% Cu steel both strength and impact behaviour are substantially improved.

The reason behind the present improvement of impact behaviour is most likely due to the coarseness of the copper precipitates that were present after "normalising". Those precipitates are able to deform rather than fracture and thus prevent stress concentrations occurring from pile-ups, which would then lead to crack nucleation and propagation.

MacIvor placed his explanation on the assumption that fracture propagation through the ferrite matrix can be blunted by the coarse soft copper particles [57].

steel element	2P148H	2P149H	2P150H
C	0.045	0.042	0.044
Si	0.320	0.300	0.310
Mn	0.770	0.780	0.780
P	0.016	0.015	0.016
S	0.003	0.003	0.003
Cr	<0.020	<0.020	<0.020
Mo	<0.005	<0.005	<0.005
Ni	<0.020	<0.020	<0.020
Al	0.015	0.022	0.022
Cu	<0.010	1.220	2.020
N	0.0056	0.0097	0.0048
Nb	<0.005	<0.005	<0.005
Ti	<0.002	<0.002	<0.002
V	<0.005	<0.005	<0.005

Table 5.1 Chemical composition of steels 2P148H, 2P149H and 2P150H (% by weight).

Steel	Condition	Heat treatment		Soaking time (hr)	Cooling medium	Cooling rate (°C/min)
		Type	Temp(°C)			
2P148H & 2P149H	N	austenitising	910	1/2	vermiculite	5
		austenitising	910	1/2	vermiculite	5
	NT525	tempering	525	1	air	--
		austenitising	910	1/2	vermiculite	5
2P150H	N	austenitising	910	1/2	vermiculite	5
		austenitising	910	1/2	vermiculite	5
	NT550	tempering	550	1	air	--
		austenitising	910	1/2	vermiculite	5
NT650	austenitising	910	1/2	vermiculite	5	
	tempering	650	1	air	--	

Table 5.2 Heat treatments of steels 2P148H, 2P149H and 2P150H.

Steel	Condition	Diamond Pyramid Hardness (at 10 kg)				
		Tempering trials	Broken charpies	Broken tensiles	Thin foil rods	Average value*
2P148H	N	131	118	120	115	118
	NT525	125	123	123	122	122
	NT650	125	120	120	142	127
2P149H	N	191	171	172	165	169
	NT525	236	209	206	201	205
	NT650	173	162	161	163	165
2P150H	N	167	151	156	149	152
	NT550	204	173	178	176	176
	NT650	177	158	165	159	161

* Hardness of "tempering trial" plates, was not taken into account for the calculation of the average values.

Table 5.3 Diamond pyramid hardness of steels 2P148H, 2P149H and 2P150H.

Steel	Condition	LYP (N/mm ²)	UTS (N/mm ²)	ε (%)	RA (%)
2P148H	N	228	376	44	76
	NT525	244	378	42	76
	NT650	246	373	42	76
2P149H	N	400	492	31	72
	NT525	487	586	26	67
	NT650	394	454	32	74
2P150H	N	376	454	39	74
	NT550	454	520	32	70
	NT650	415	472	36	75

Table 5.4 Tensile properties of steels 2P148H, 2P149H and 2P150H.

Steel	Condition	Impact transition temperature (°C)			Energy absorbed (J)		
		at 54 J	at 27 J	50%FATT	at 0 °C	at RT	Shelf
2P148H	N	-23	-25	-23	300	300	300
	NT525	-11	-19	-10	300	300	300
	NT650	-23	-25	-23	300	300	300
2P149H	N	-33	-47	-15	200	240	240
	NT525	-2	-22	+20	56	110	160
	NT650	-35	-45	-33	290	265	265
2P150H	N	-84	-89	-75	300	300	300
	NT550	-60	-73	-45	258	273	273
	NT650	-74	-84	-65	300	300	300

Table 5.5 Impact properties of steels 2P148H, 2P149H and 2P150H.

Steel	Condition	Ferrite grain size		Grain boundary carbide thickness, t_c (μm)	Phase volume fraction (%)			
		(μm)	$(\text{mm}^{-1/2})$		Ferrite			Pearlite
					dark grains	bright grains	total	
2P148H	N	26.9	6.1	0.33	--	95	95	5
	NT525	27.5	6.0	0.32	--	95	95	5
	NT650	27.8	6.0	0.37	--	95	95	5
2P149H	N	14.2	8.4	0.40	--	--	95	5
	NT525	14.8	8.2	0.40	--	--	95	5
	NT650	14.0	8.4	0.44	--	--	95	5
2P150H	N	9.5	10.2	0.40	81*	15	96	4
	NT550	9.4	10.3	0.42	80	17	97	3
	NT650	8.5	10.8	0.44	80	16	96	4

* dark grains have an average micro-hardness value of 180.2 (HV5g) and bright grains 167.1 (HV5g).

Table 5.6 Optical and scanning electron microscopy of steels 2P148H, 2P149H and 2P150H.

Steel	Condition	Copper precipitate size (nm)				
		Elliptical particles			Spherical particles	
		thickness, t_p		length, l_p	diameter, d_p	
		TEM	SEM	TEM	TEM	SEM
2P149H	N	--	--	--	58 _{(10)*}	57 ₍₁₀₀₎
	NT525	24 ₍₁₎	--	60 ₍₁₎	72 ₍₂₎	--
	NT650	--	--	--	--	70 ₍₄₀₎
2P150H	N	45 ₍₂₇₎	74 ₍₁₀₀₎	75 ₍₂₇₎	--	--
	NT550	43 ₍₈₄₎	75 ₍₁₀₀₎	101 ₍₈₄₎	--	--
	NT650	39 ₍₄₉₎	90 ₍₁₀₀₎	91 ₍₄₉₎	--	--

Table 5.7 (a) TEM (thin foil) and SEM copper precipitate size measurements.

Steel	Condition	Copper precipitate size (nm)		
		thickness (t_p)	length (l_p)	diameter (d_p)
2P150H	N (air-cooled)	25 _{(26)*}	42 ₍₂₆₎	31 ₍₁₁₎
	NT700 (slow cooling)**	63 ₍₂₄₎	111 ₍₂₄₎	66 ₍₇₎
	NT700 (slow cooling) + 15% straining	39 ₍₄₅₎	112 ₍₄₅₎	32 ₍₂₁₎

*Numbers in brackets indicate the sample size from which measurements were taken.

**slow cooling was obtained by using "vermiculite" as the cooling medium.

Table 5.7 (b) The effect of cooling rate and straining on the size of copper precipitates, on the 2.02% Cu steel (TEM-thin foils).

Steel	Condition	LYS (N/mm ²)				
		obs	calc ⁽¹⁾	δ LYS ⁽¹⁾	calc ⁽²⁾	δ LYS ⁽²⁾
2P148H	N	228	243	-15	259	-31
	NT525	244	241	3	257	-13
	NT650	246	241	5	257	-11
2P149H	N	400	354	46	301	99
	NT525	487	350	137	297	190
	NT650	394	354	40	301	93
2P150H	N	376	393	-17	321	55
	NT550	454	395	59	322	132
	NT650	415	404	11	331	84

(1) LYS is calculated by using equation 2.11, i.e. taking alloying additions into account.

(2) LYS is calculated by using equation 2.10, i.e. for plain ferrite-pearlite C-Mn steels.

Table 5.8 Comparison between observed and calculated lower yield strength values, of steels 2P148H, 2P149H and 2P150H.

Steel	% Cu available for precipitation			precipitate volume fraction at equilibrium "f"			dispersion strengthening effect $\sigma_{ds} = 2\tau$, (N/mm ²)		
	RT	NT _{FA}	NT _{OA}	RT	NT _{FA}	NT _{OA}	RT	NT _{FA}	NT _{OA}
1.22%Cu	1.22	1.17	0.93	0.0108	0.0104	0.0083	82	80	60
2.02%Cu	2.02	1.95	1.73	0.0179	0.0173	0.0154	66	64	52

FA : fully aged OA : overaged RT : room temperature

Table 5.9 Estimated dispersion strengthening effect (Ashby-Orowan), based on copper precipitate size as measured from SEM photographs.

Steel	Condition	Impact Transition Temperatures (°C)								
		at 54 (J)			at 27 (J)			50% FATT		
		obs	calc	δ ITT	obs	calc	δ ITT	obs	calc	δ FATT
2P148H	N	-23	-30	+7	-25	-45	+20	-23	-10	-13
	NT525	-11	-22	+11	-19	-39	+20	-10	-2	-8
	NT650	-23	-12	-11	-25	-31	+6	-23	+4	-27
2P149H	N	-33	+23	-56	-47	-5	-42	-15	+27	-42
	NT525	-2	+70	-72	-22	+30	-52	+20	+70	-50
	NT650	-35	+26	-61	-45	-2	-43	-33	+28	-61
2P150H	N	-84	-17	-67	-89	-37	-52	-75	-16	-59
	NT550	-60	+23	-83	-73	-7	-66	-45	+19	-64
	NT650	-74	-3	-71	-84	-26	-58	-65	-6	-59

Calculated values are based on δ LYS⁽²⁾, (table 5.8).

Table 5.10 (a) Comparison between observed and calculated impact transition temperatures, of steels 2P148H, 2P149H and 2P150H.

Steel	Condition	Impact Transition Temperatures (°C)								
		at 54 (J)			at 27 (J)			50% FATT		
		obs	calc	δ ITT	obs	calc	δ ITT	obs	calc	δ FATT
2P148H	N	-23	-28	+5	-25	-30	+5	-23	-26	+3
	NT525	-11	-20	+9	-19	-24	+5	-10	-18	+8
	NT650	-23	-10	-13	-25	-16	-9	-23	-12	-11
2P149H	N	-33	+25	-58	-47	+9	-56	-15	+11	-26
	NT525	-2	+72	-74	-22	+44	-66	+20	+54	-34
	NT650	-35	+28	-63	-45	+13	-58	-33	+12	-45
2P150H	N	-84	-15	-69	-89	-22	-67	-75	-32	-43
	NT550	-60	+25	-85	-73	+8	-81	-45	+3	-48
	NT650	-74	-1	-73	-84	-11	-73	-65	-22	-43

Calculated values are based on δ LYS⁽²⁾, (table 5.8) and are corrected for best fit according to calculated ITT values for the copper-free steel.

Table 5.10 (b) Comparison between observed and calculated impact transition temperatures, of steels 2P148H, 2P149H and 2P150H.

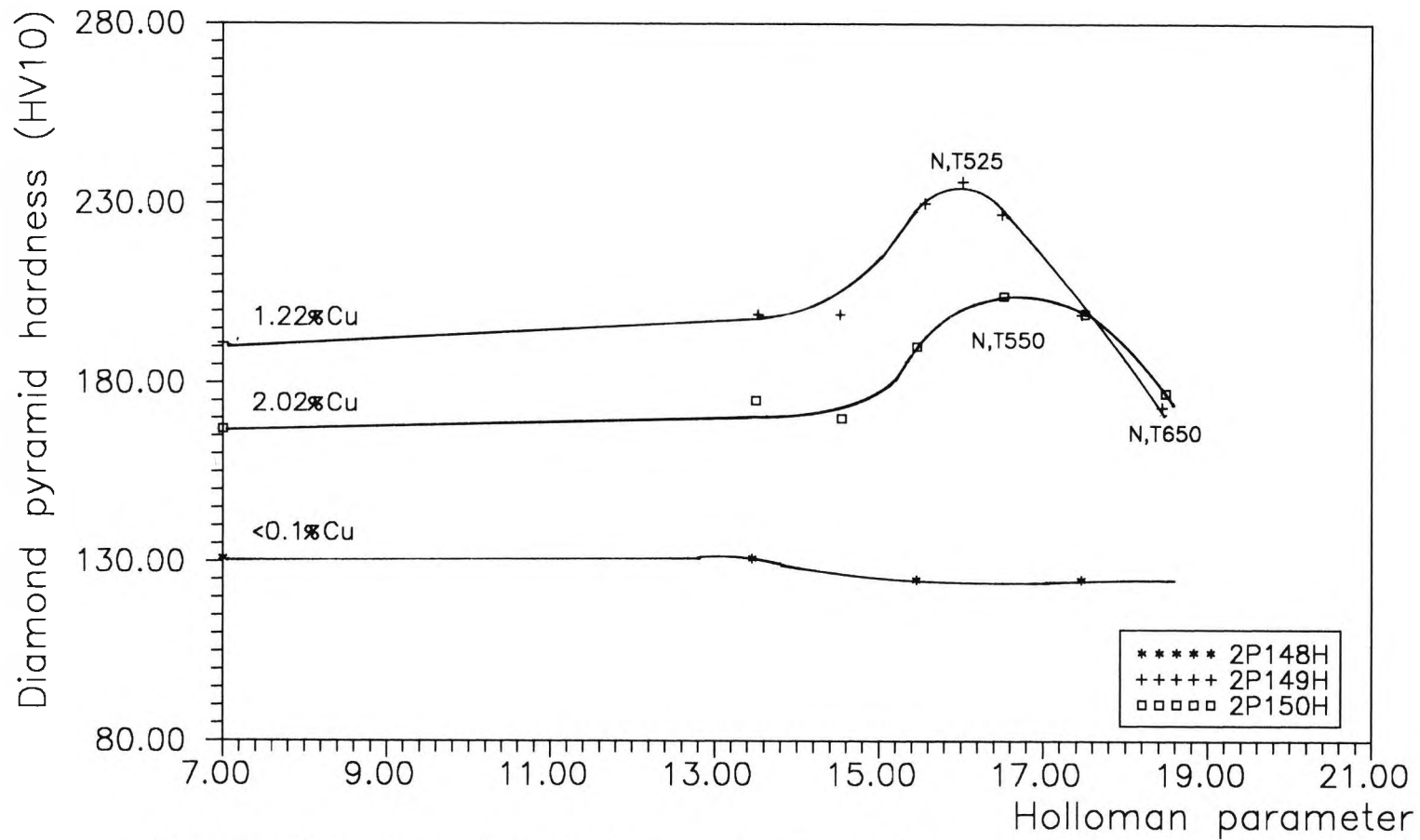


Figure 5.1 Age-hardening effect of tempering, on "normalised" 2P148H, 2P149H and 2P150H steels

ITT curves

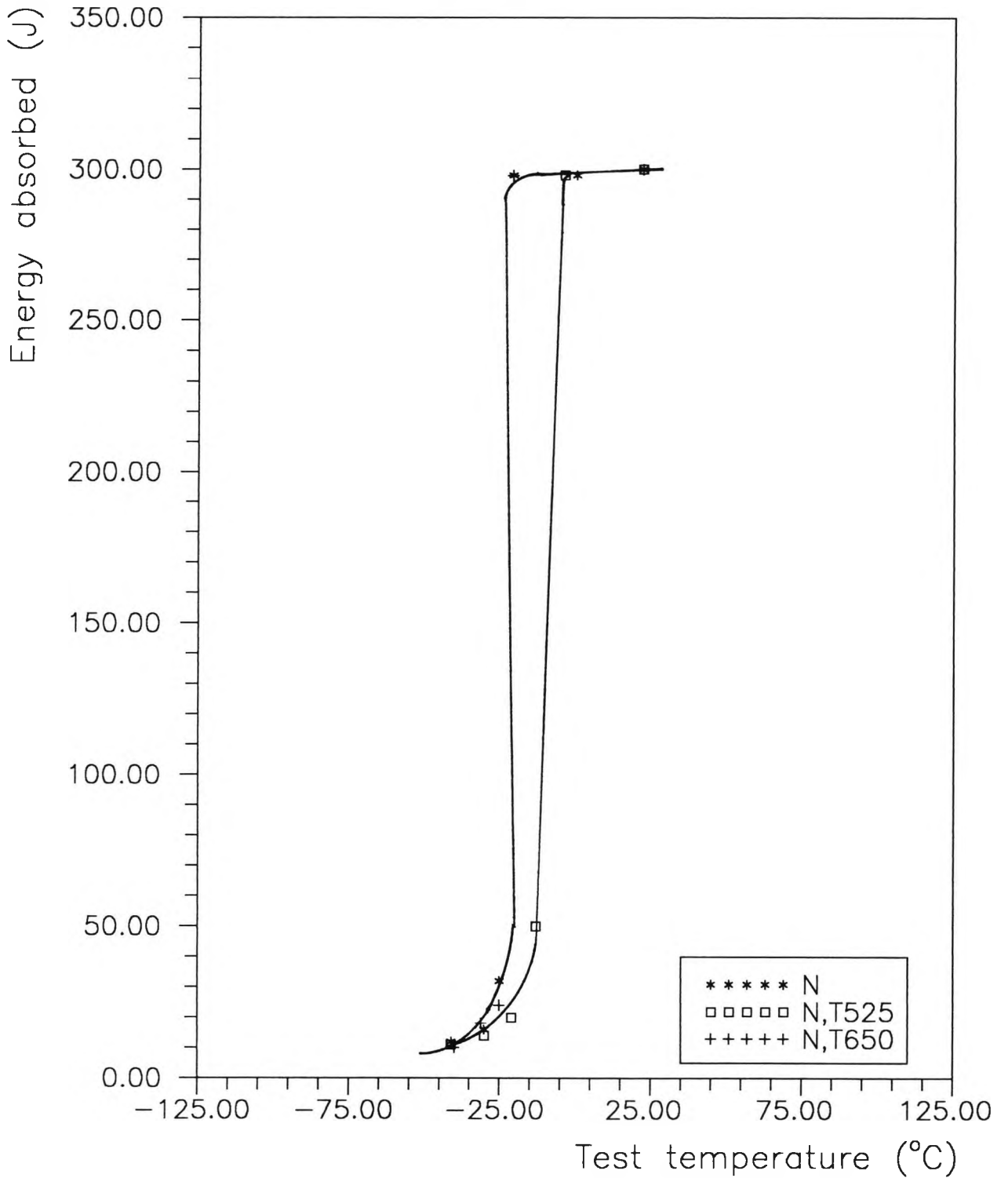


Fig.5.2 Impact transition temperature curves for "normalised" and aged 2P148H steel

ITT curves

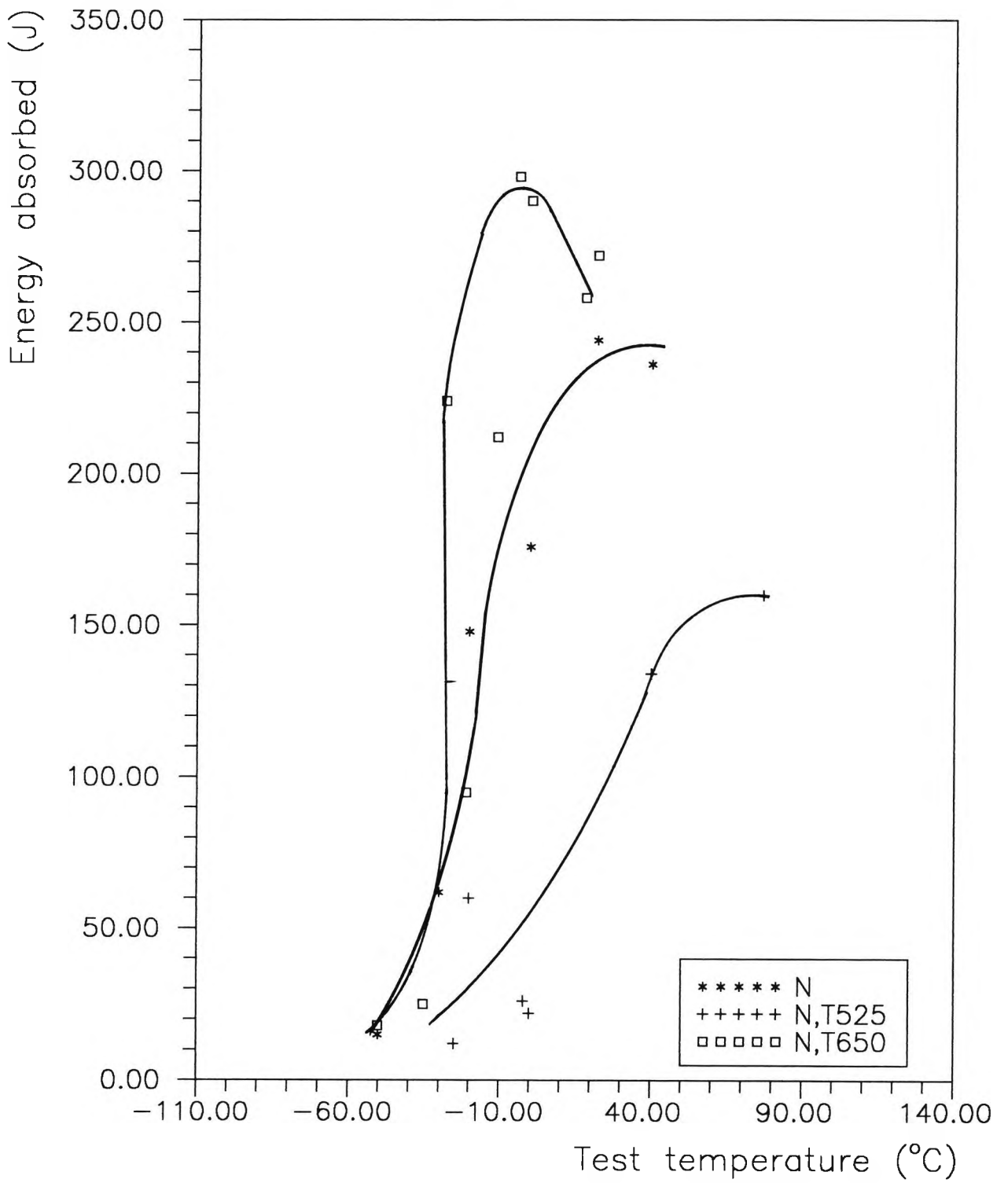


Fig.5.3 Impact transition temperature curves for "normalised" and aged 2P149H steel

ITT curves

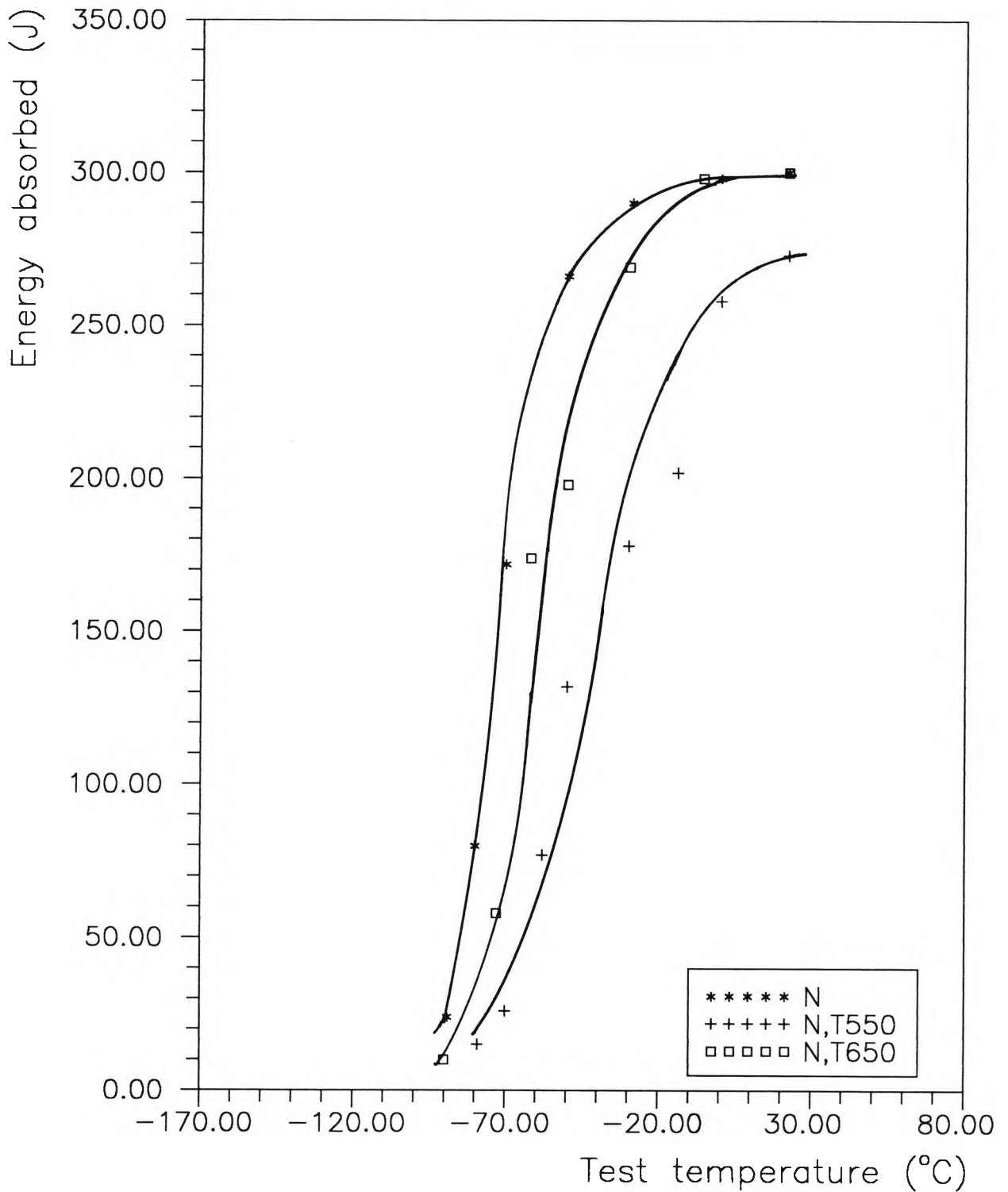
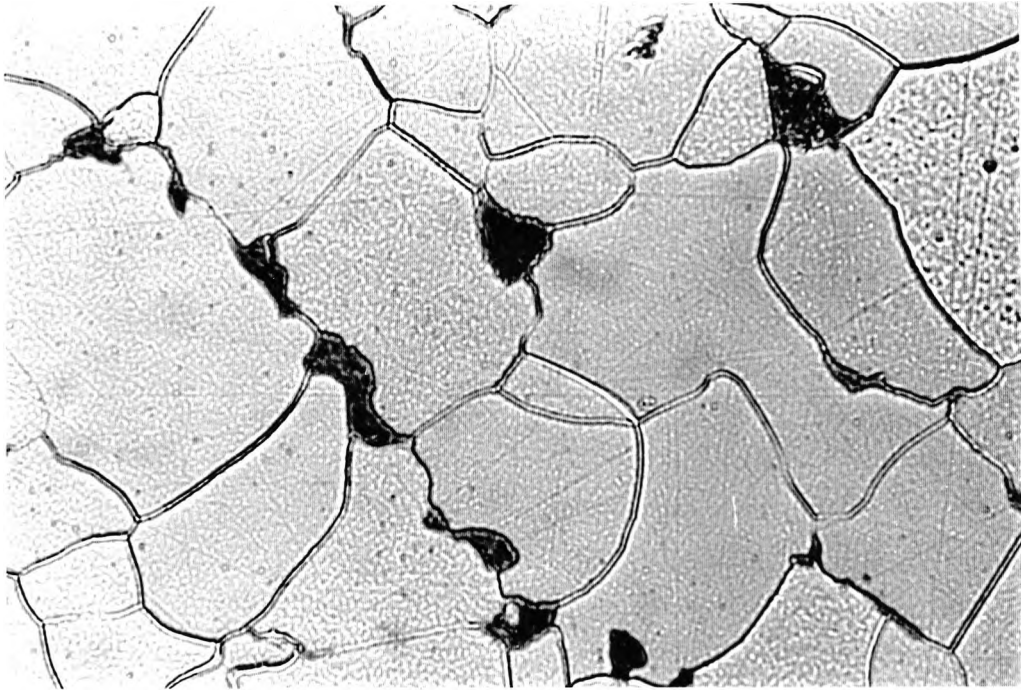
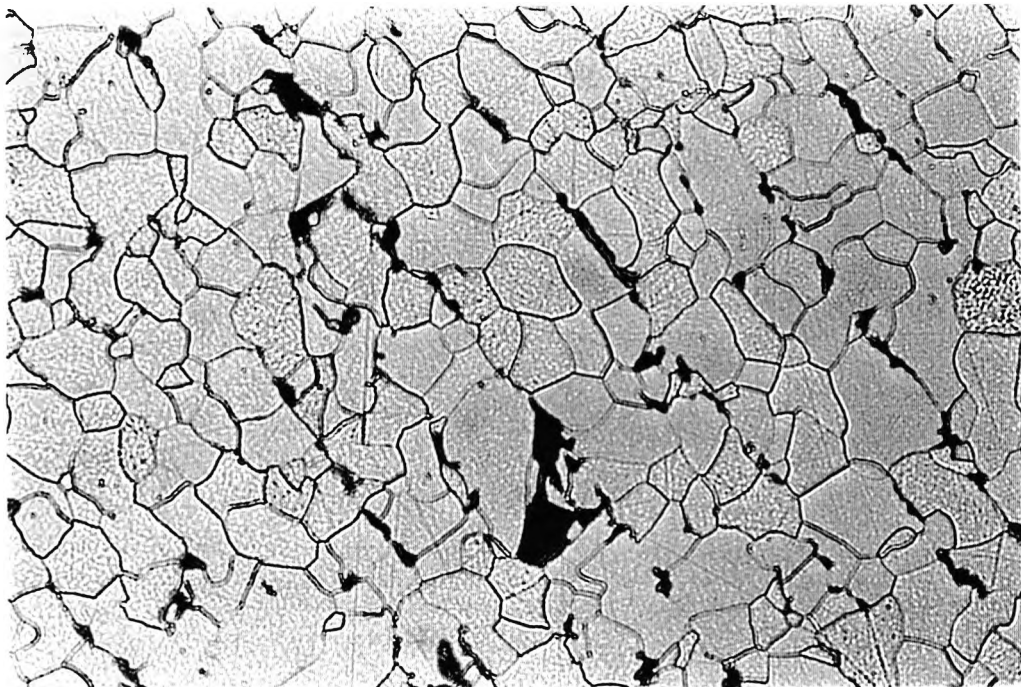


Fig.5.4 Impact transition temperature curves for "normalised" and aged 2P150H steel



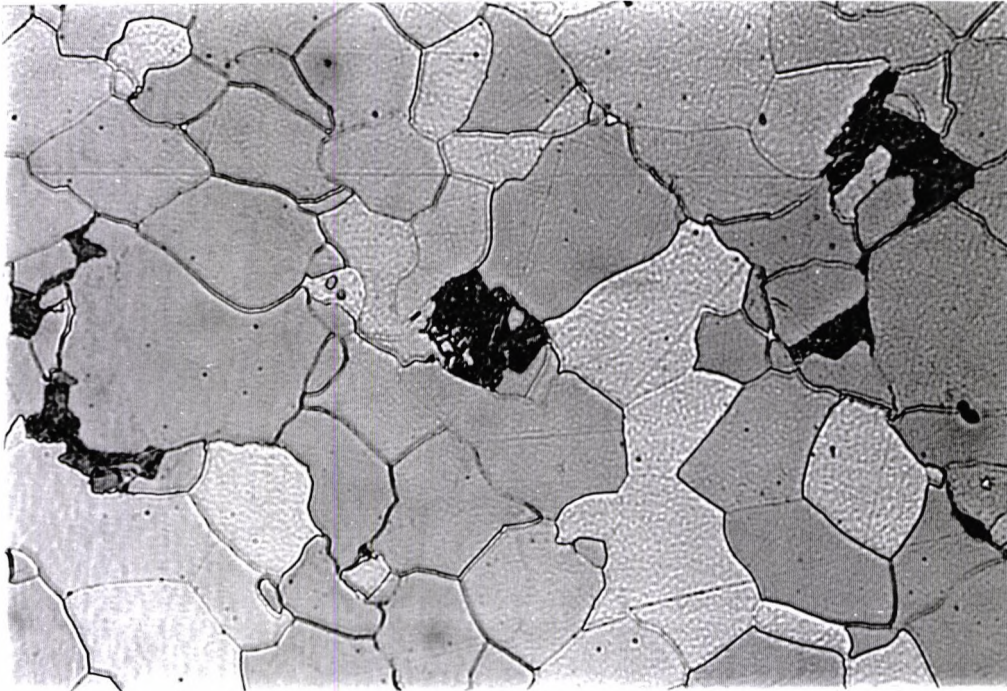
x800

Figure 5.5 (a) Optical micrograph of as "normalised" copper-free steel.



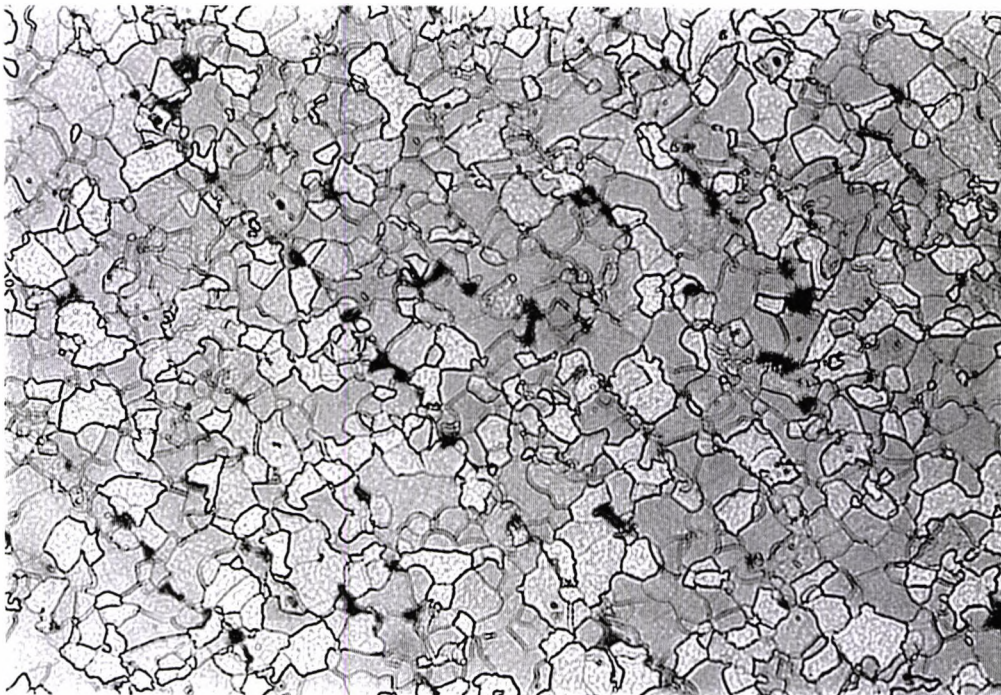
x200

Figure 5.5 (b) Optical micrograph of the NT525 copper-free steel, showing banding.



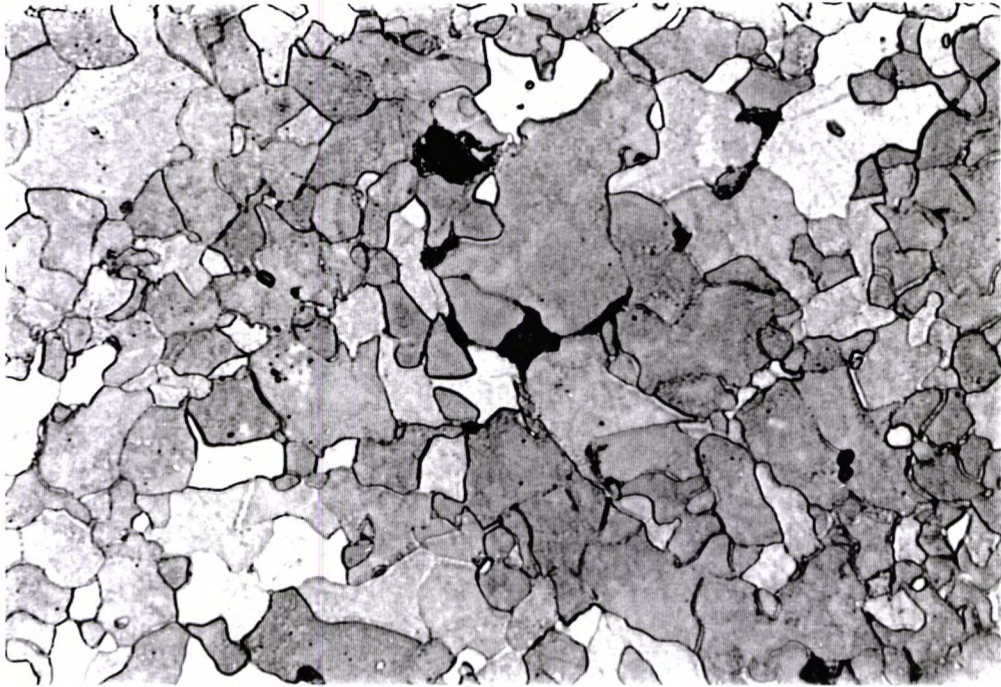
x800

Figure 5.6 (a) Optical micrograph of the NT525 1.22% Cu steel.



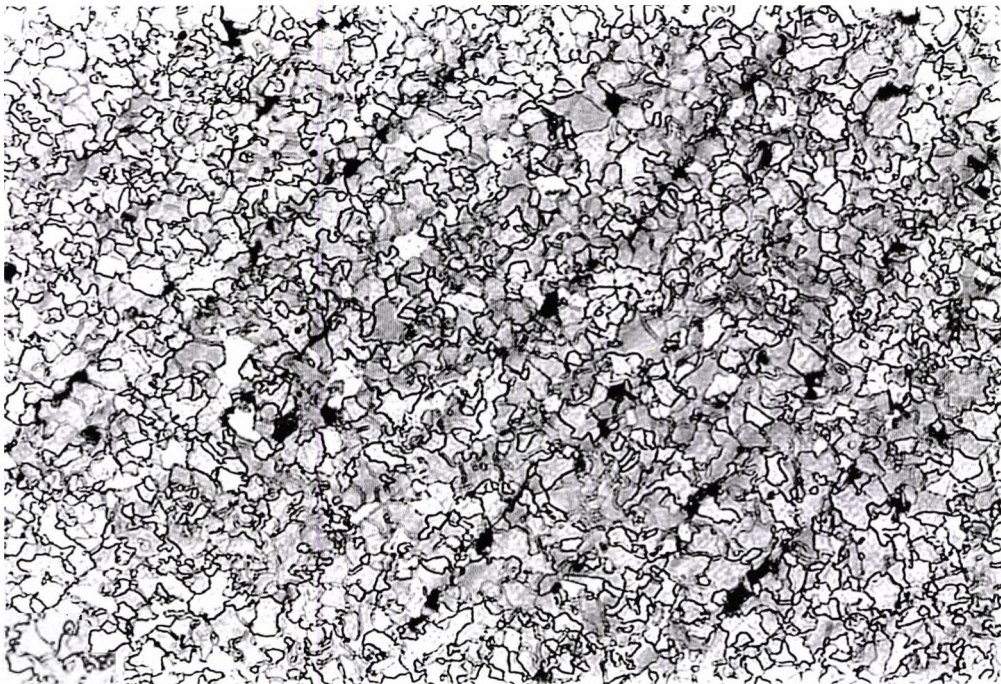
x200

Figure 5.6 (b) Optical micrograph of the NT525, 1.22% Cu steel.



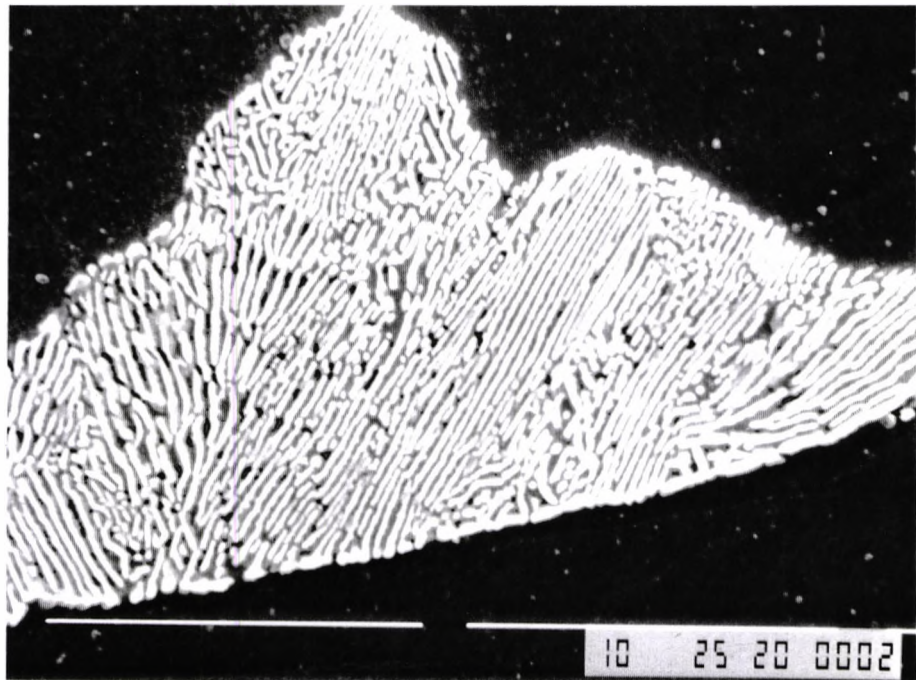
x800

Figure 5.7 (a) Optical micrograph of the NT650, 2.02% Cu steel.

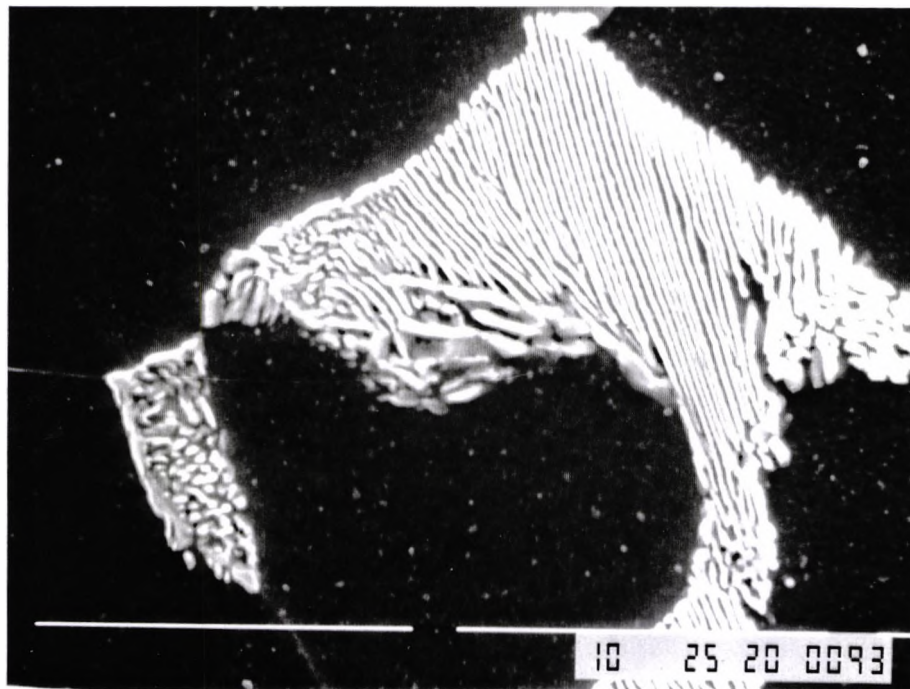


x200

Figure 5.7 (b) Optical micrograph of the NT650, 2.02% Cu steel, showing the banding effect and the variation in ferrite shade.



(a)



(b)

Figure 5.8 Scanning electron micrographs showing pearlite colonies of the as "normalised", copper-free steel.

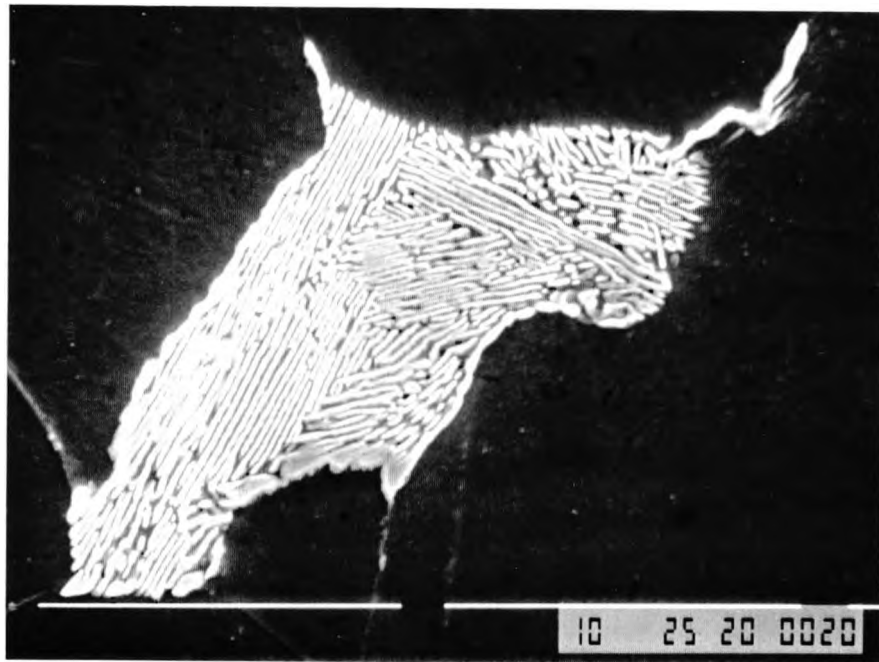


Figure 5.9 Scanning electron micrograph of the NT525, copper-free steel showing a pearlite colony.

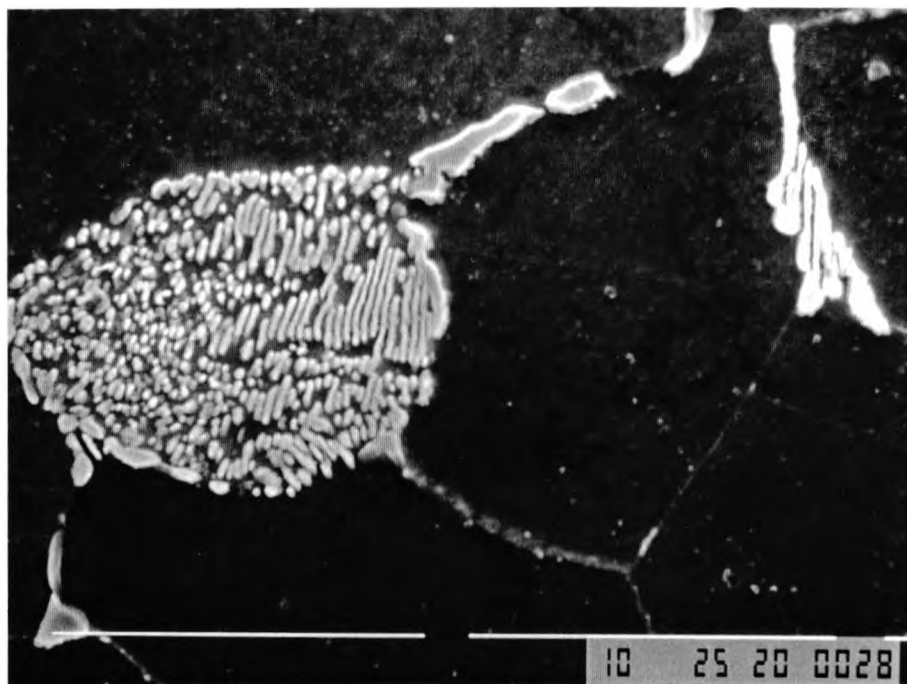


Figure 5.10 (a) Scanning electron micrograph of NT650, copper-free steel, showing spheroidised pearlite and carbides.

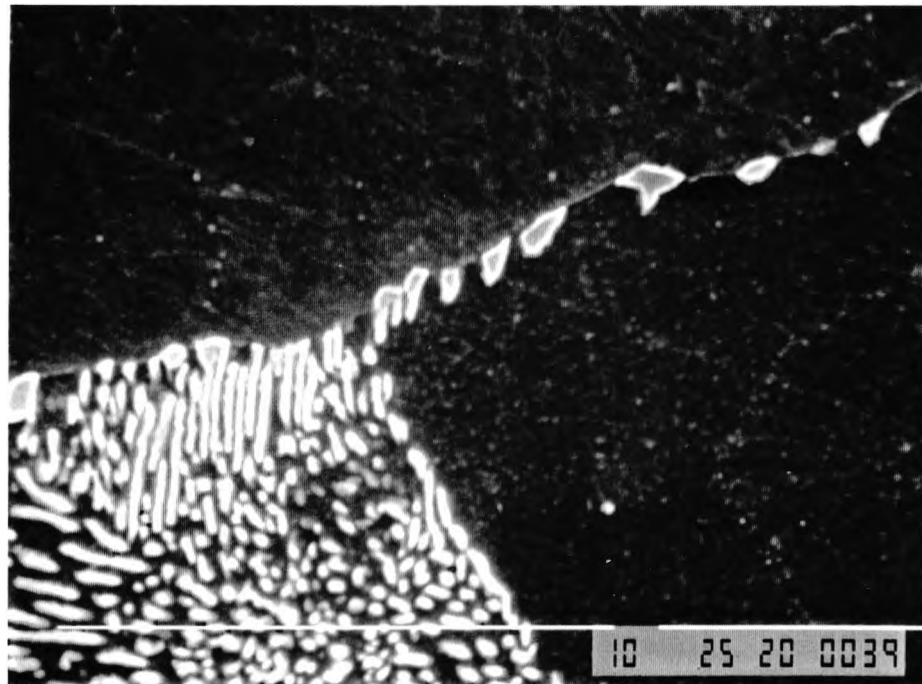


Figure 5.10 (b) Scanning electron micrograph of NT650, copper-free steel, showing spheroidised pearlite and carbides.

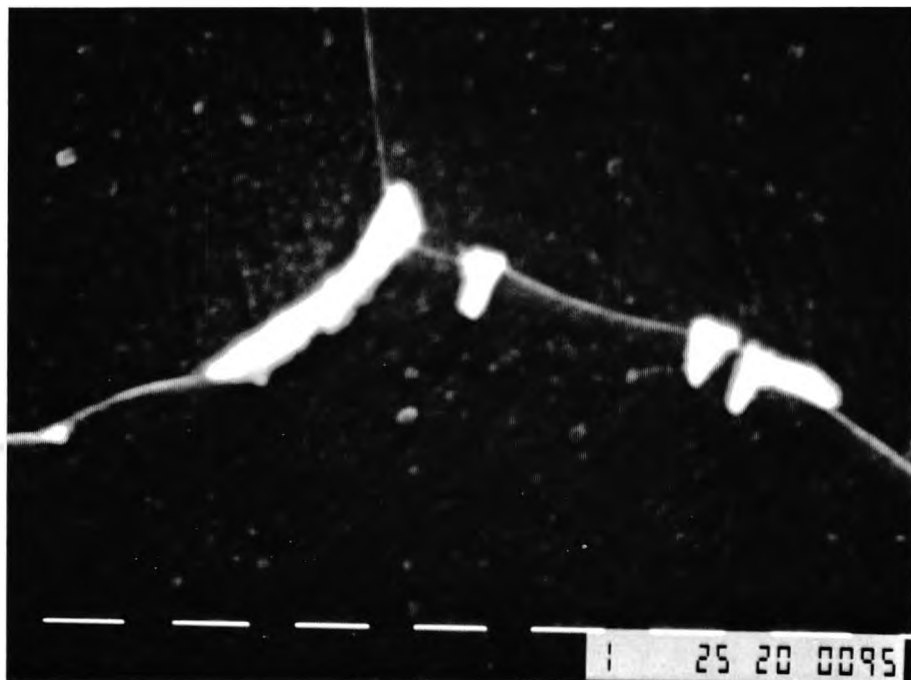
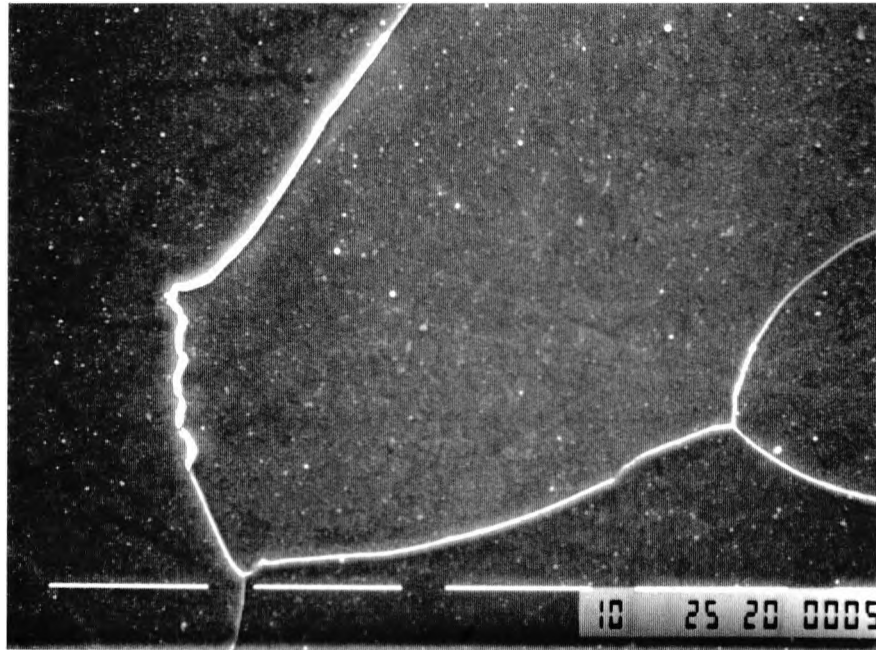
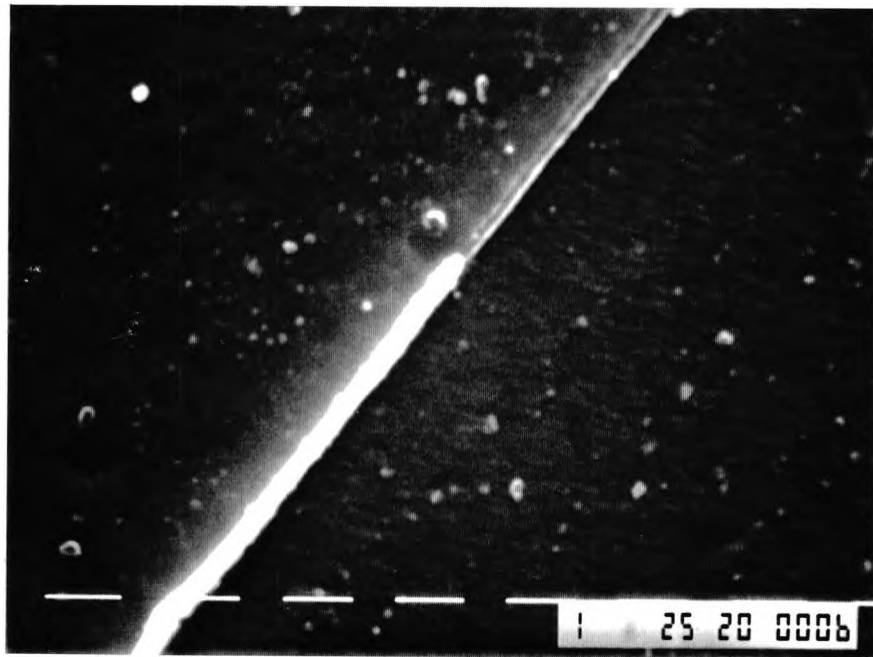


Figure 5.11 Scanning electron micrograph, showing carbides at the grain boundaries of the as "normalised", (N), copper-free steel.



(a)



(b)

Figure 5.12 (a) Scanning electron micrograph, showing a fine and long grain boundary carbide of the copper-free steel, in the as "normalised" condition. (b) Enlarged section of previous micrograph.

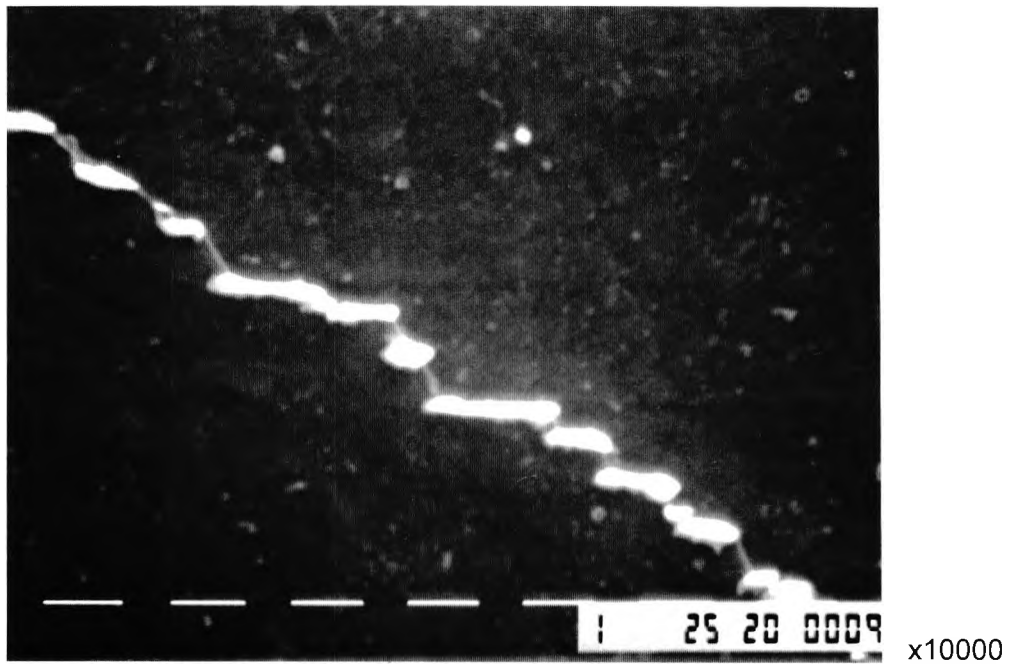


Figure 5.13 Scanning electron micrograph of NT525, copper-free steel; showing fine grain boundary carbides.

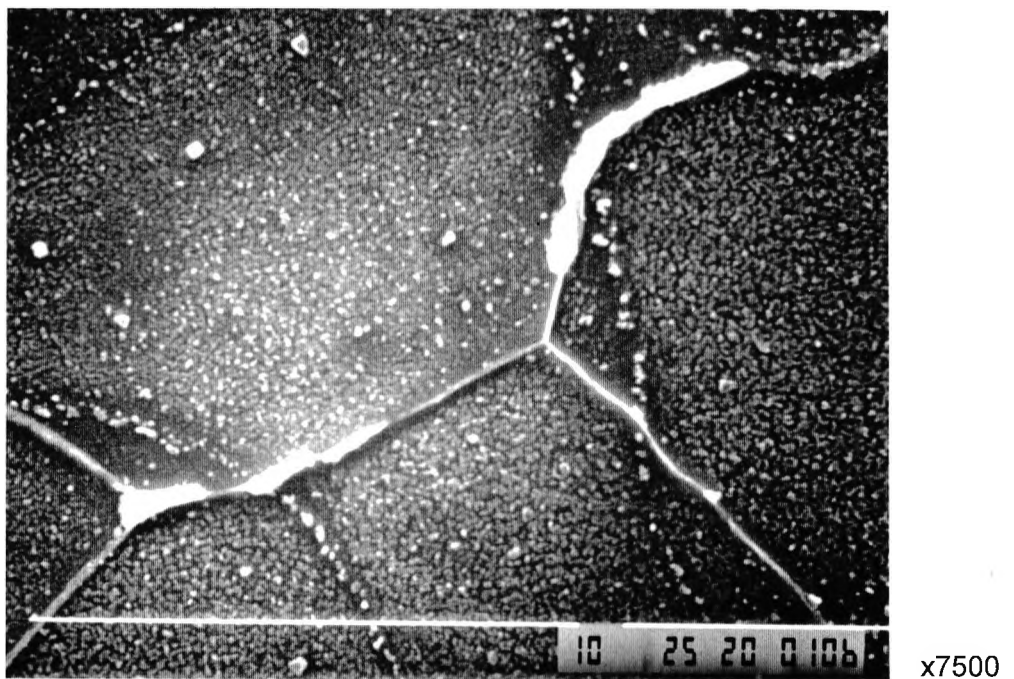


Figure 5.14 Scanning electron micrograph, showing grain boundary carbides of as "normalised", 1.22% Cu steel.

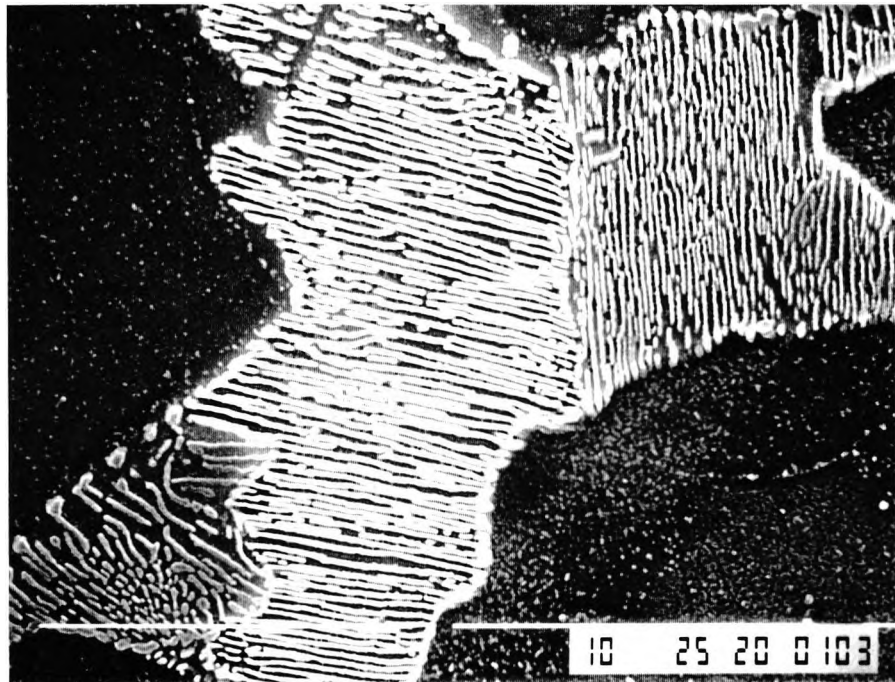


Figure 5.15 Scanning electron micrograph, showing pearlite colonies of the as “normalised”, 1.22% Cu steel.

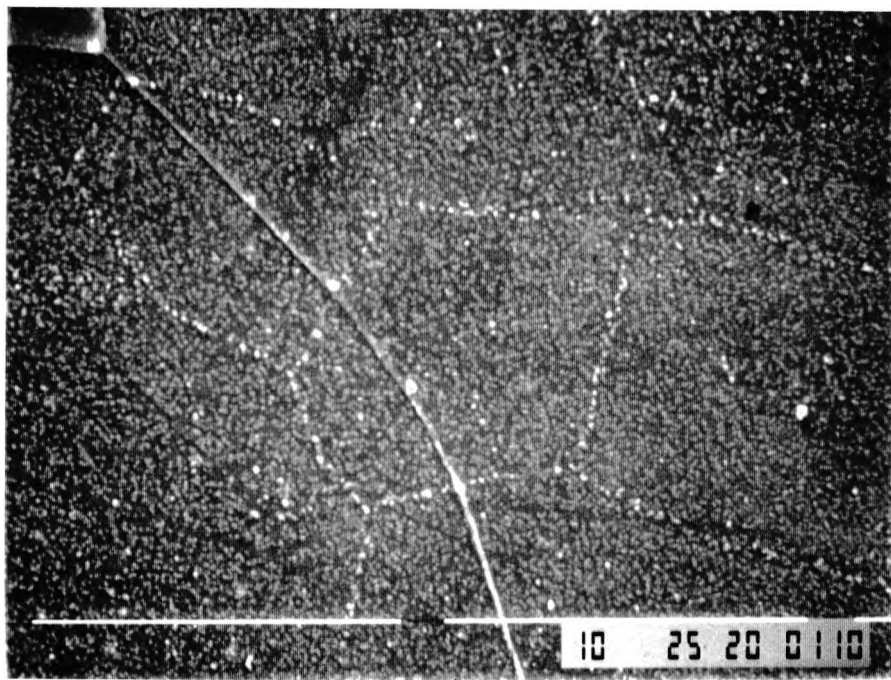


Figure 5.16 (a) Scanning electron micrograph, showing ghost boundaries formed by fine particles, on the ferrite matrix of as “normalised”, 1.22% Cu steel.

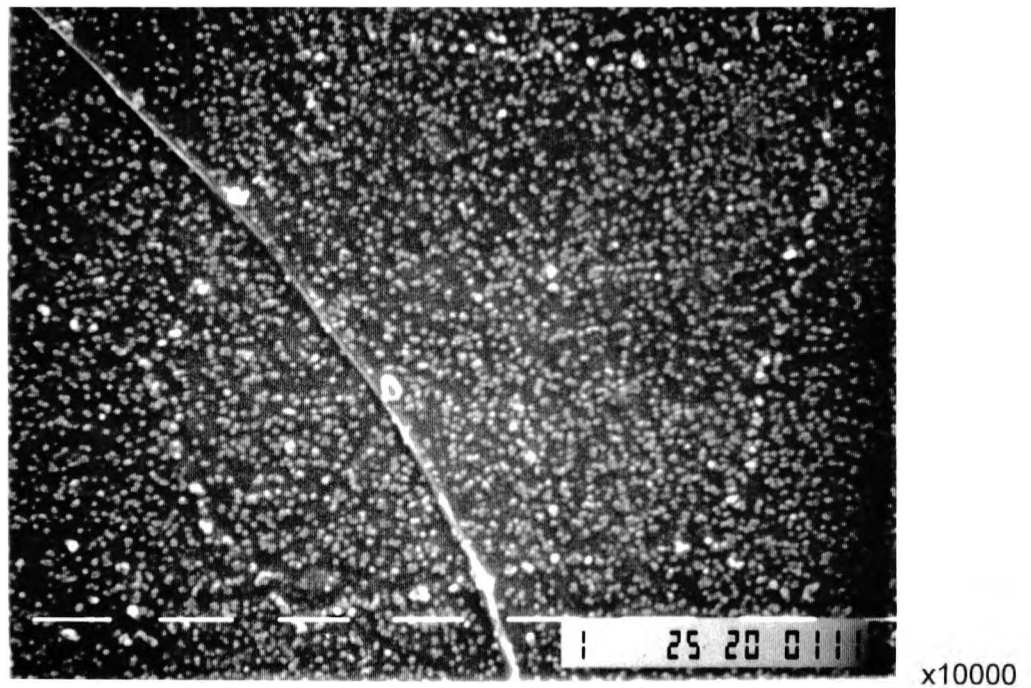


Figure 5.16 (b) Scanning electron micrograph, showing an enlarged area of figure 5.16 (a).

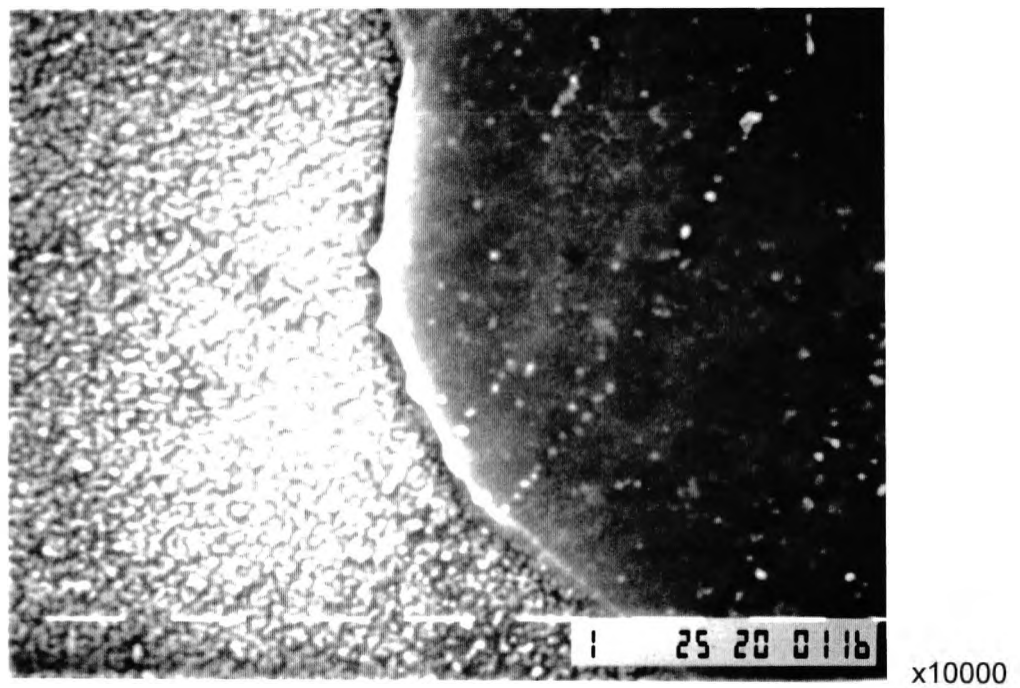
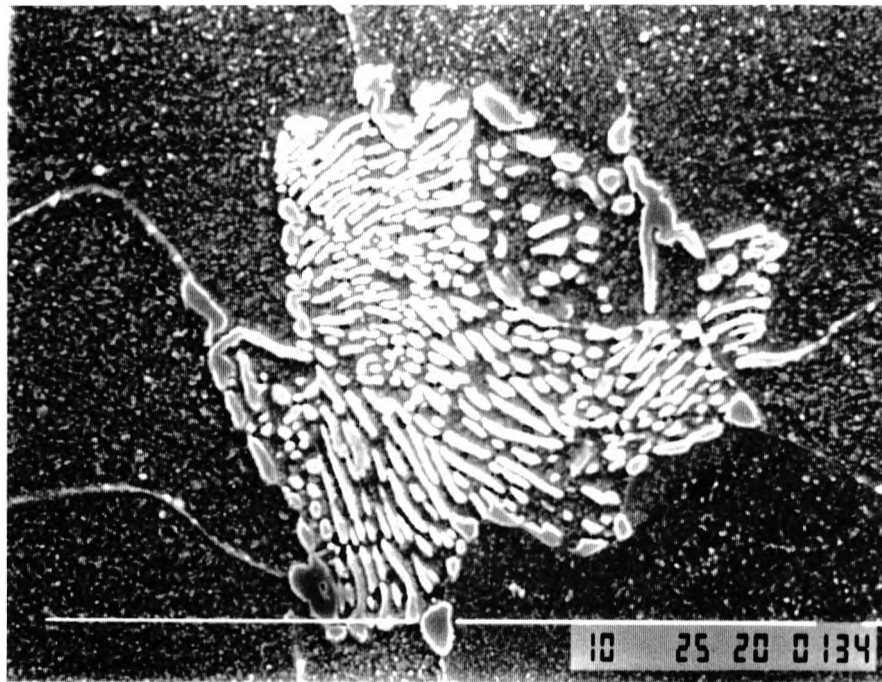
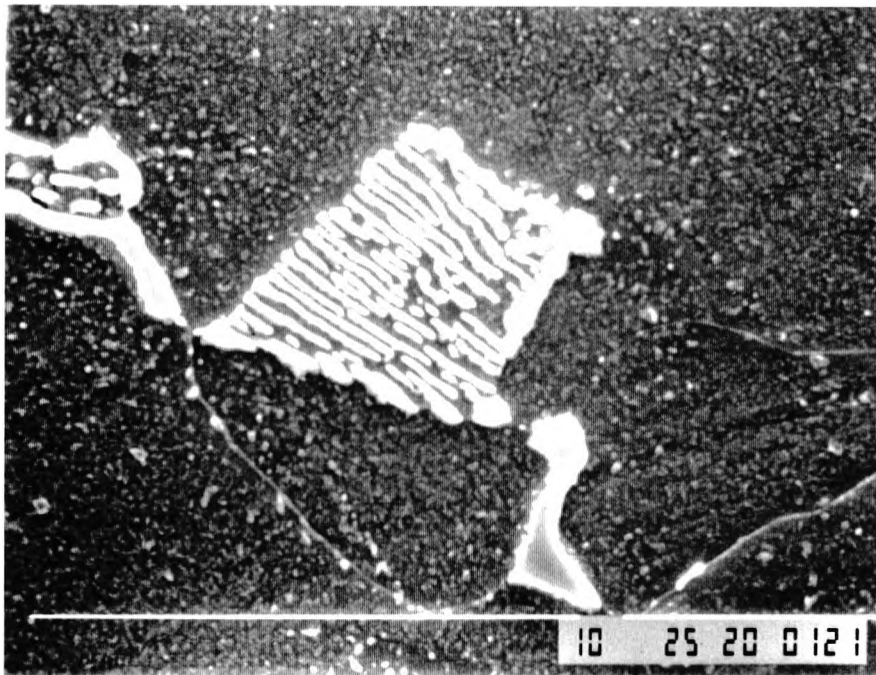


Figure 5.17 Scanning electron micrograph, showing the shade difference between adjacent ferrite grains, of "normalised" and fully-aged (NT525) 1.22% Cu steel.



x5000

(a)



x7500

(b)

Figure 5.18 Scanning electron micrographs of “normalised” and over-aged (NT650) 1.22% Cu steel sowing: (a) spheroidised pearlite, (b) Unaffected pearlite.

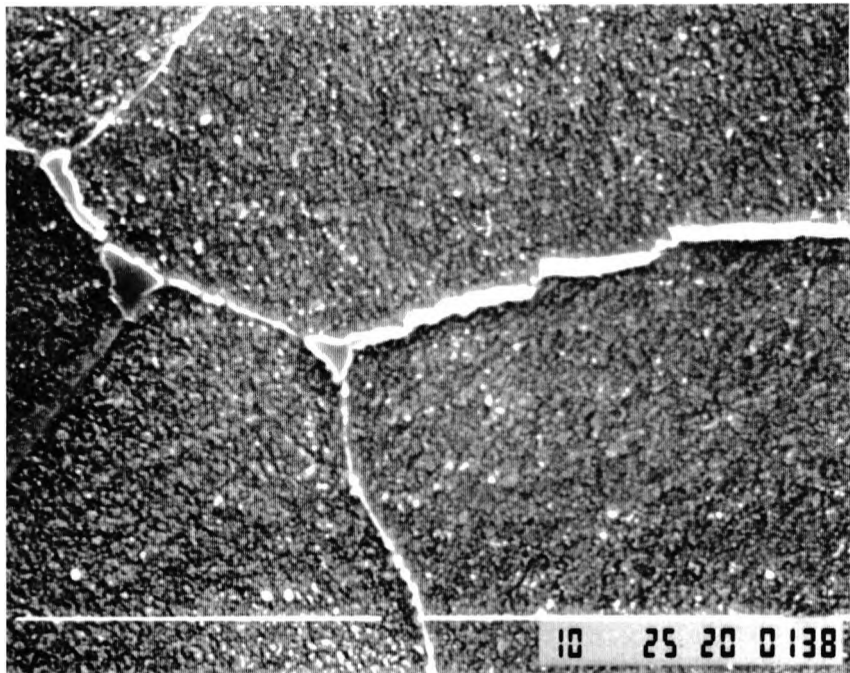


Figure 5.19 Scanning electron micrograph, showing grain boundary carbides of the 1.22% Cu steel, in the over-aged condition (NT650).

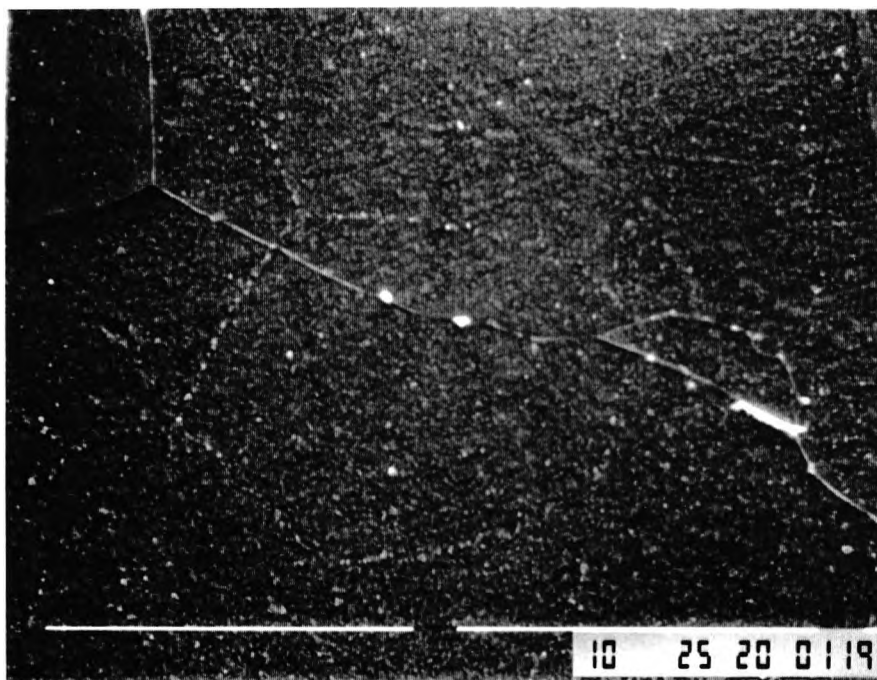
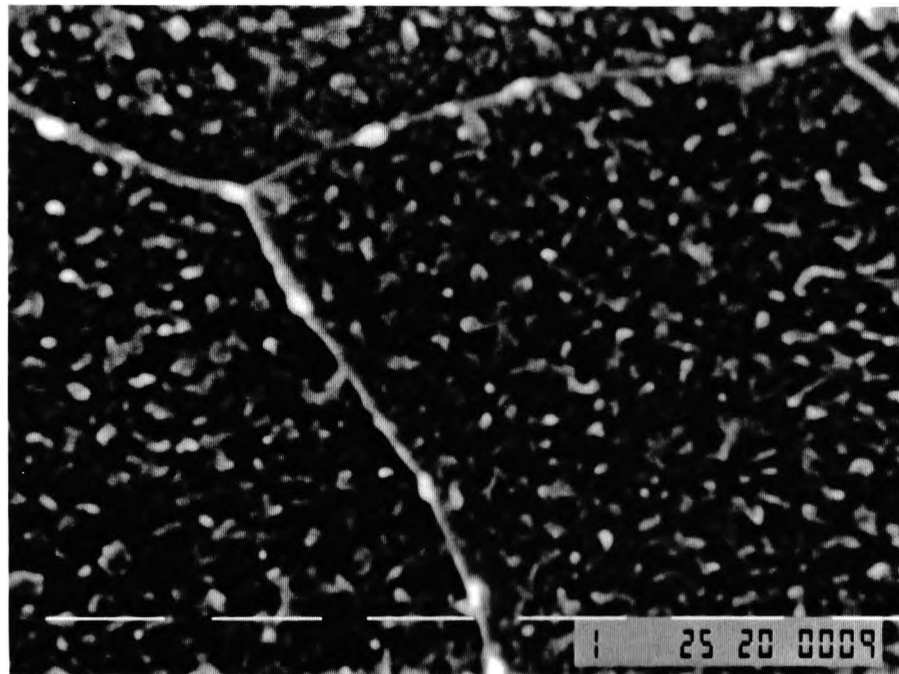
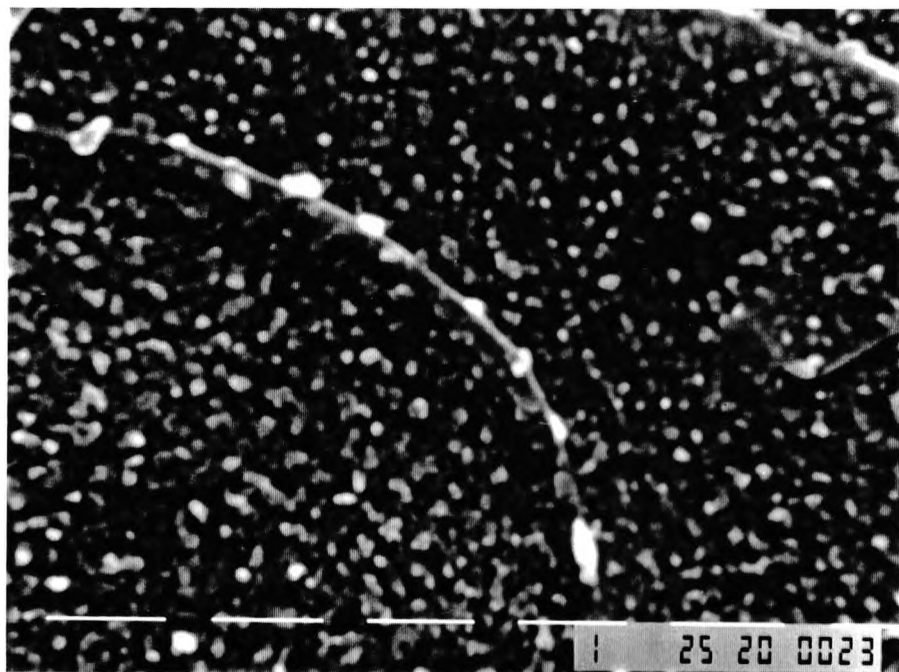


Figure 5.20 Scanning electron micrograph, showing a network of fine particles and very fine grain boundary particles, of the "normalised" and over-aged 1.22% Cu steel.



x15000

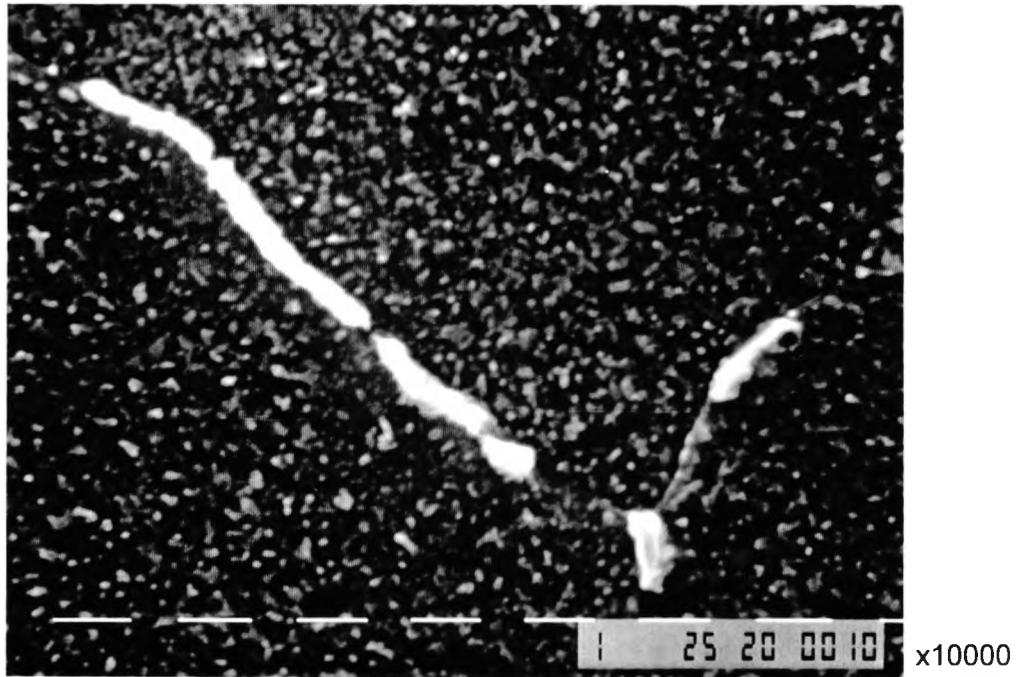
(a)



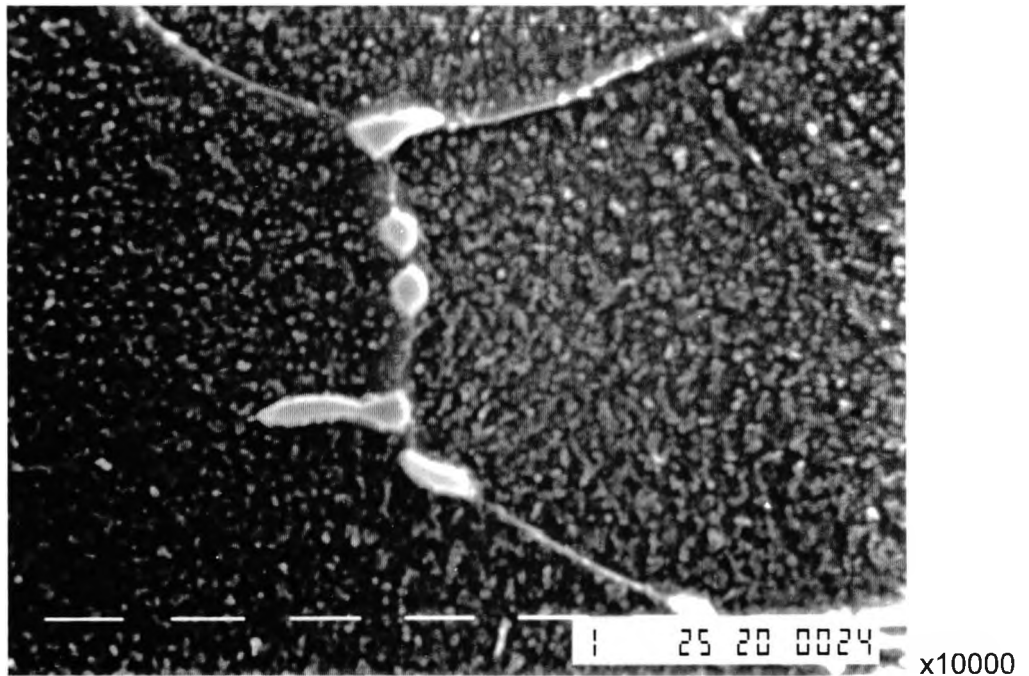
x15000

(b)

Figure 5.21 Scanning electron micrographs, showing very fine grain boundary particles and ferrite grains of the 2.02% Cu steel, saturated with precipitation particles: (a) N condition (b) NT550 condition.

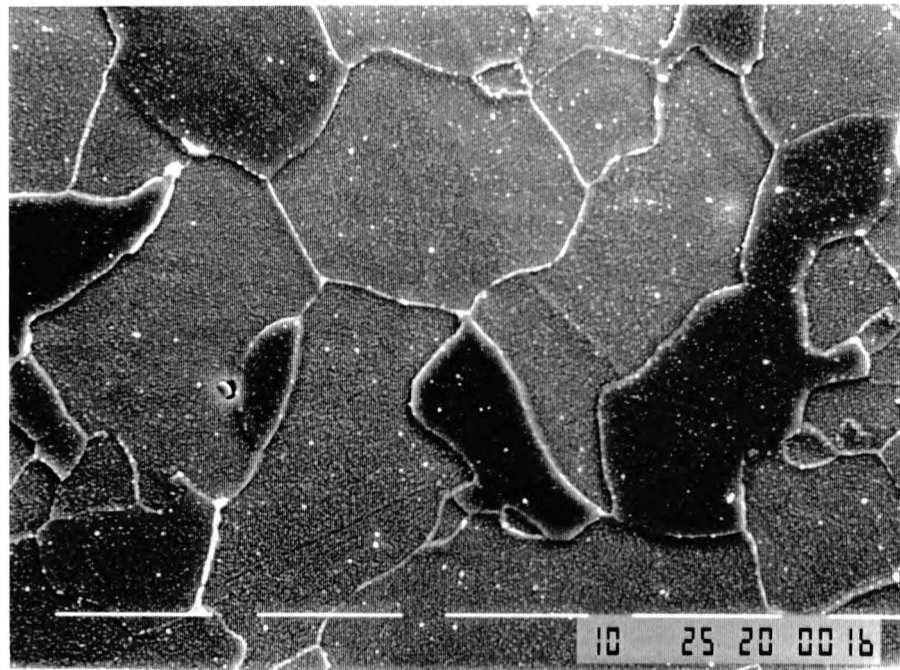


(a)



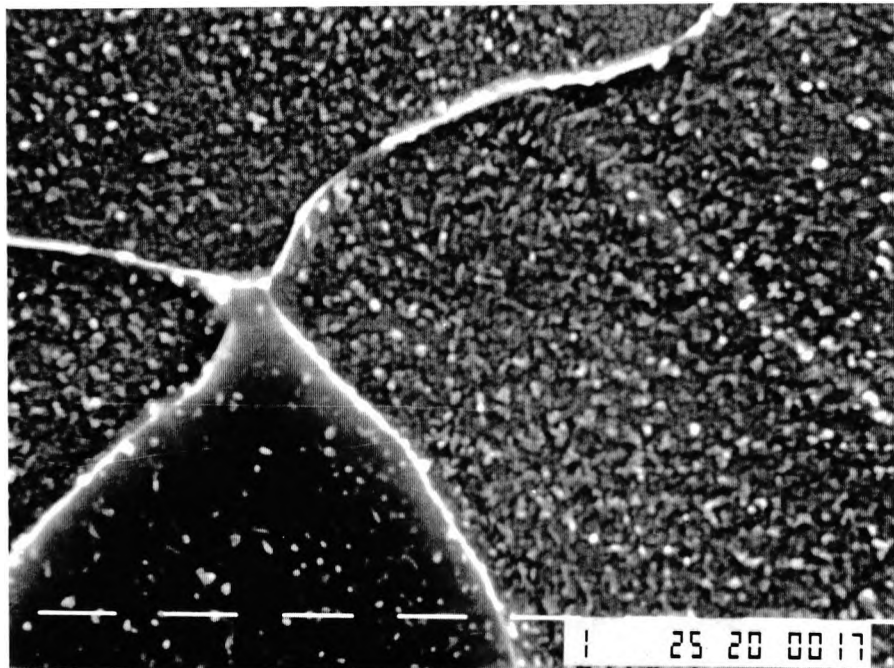
(b)

Figure 5.22 Scanning electron micrographs, showing carbides at the grain boundaries of 2.02% Cu steel: (a) N condition (b) NT650 condition.



x2000

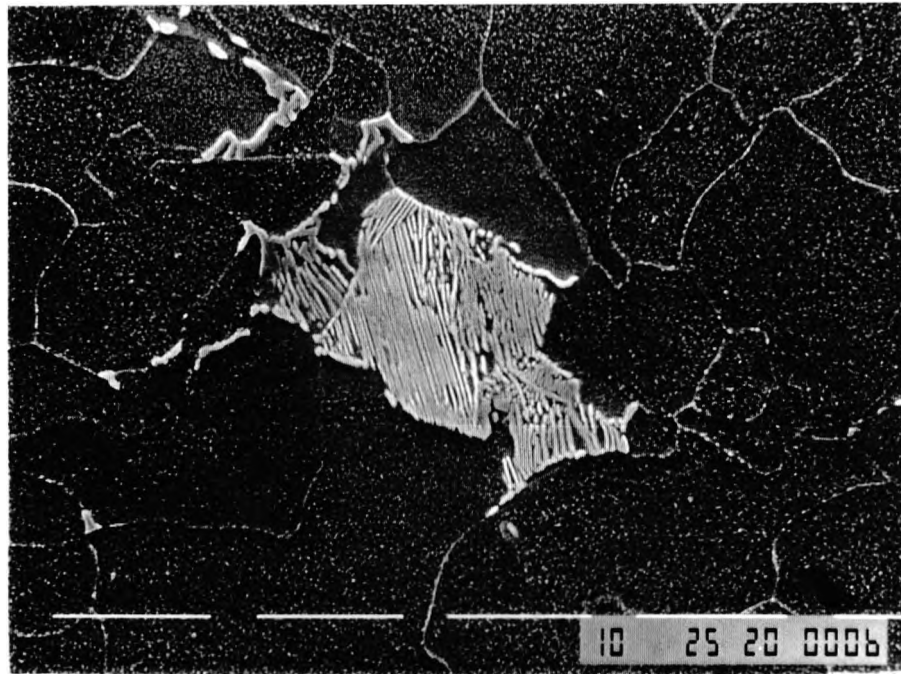
(a)



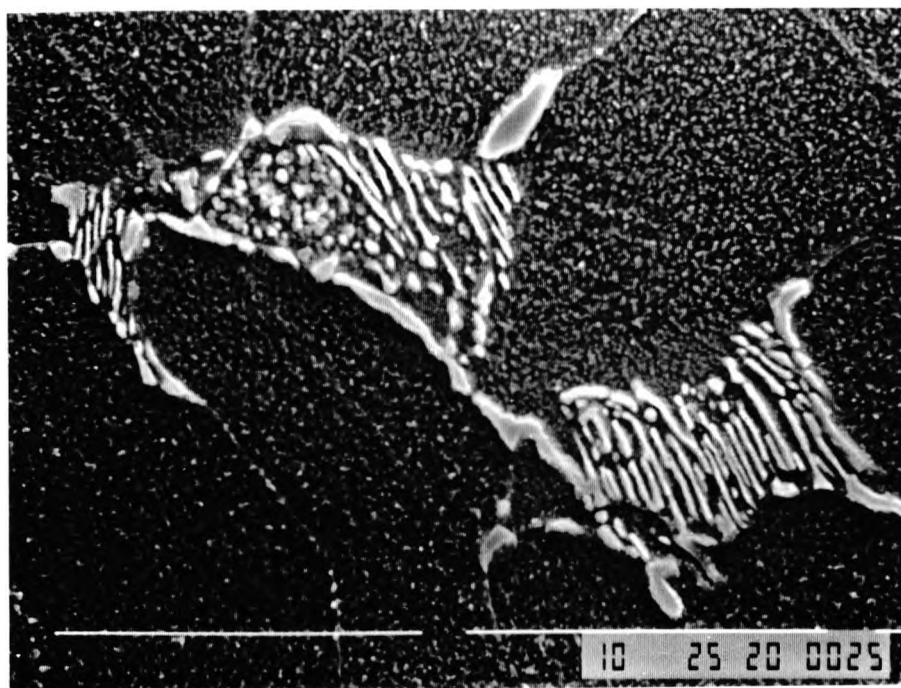
x10000

(b)

Figure 5.23 Scanning electron micrographs, showing ferrite grains of different shade, 2.02% Cu steel, the 'normalised' and fully-aged (NT550) condition.

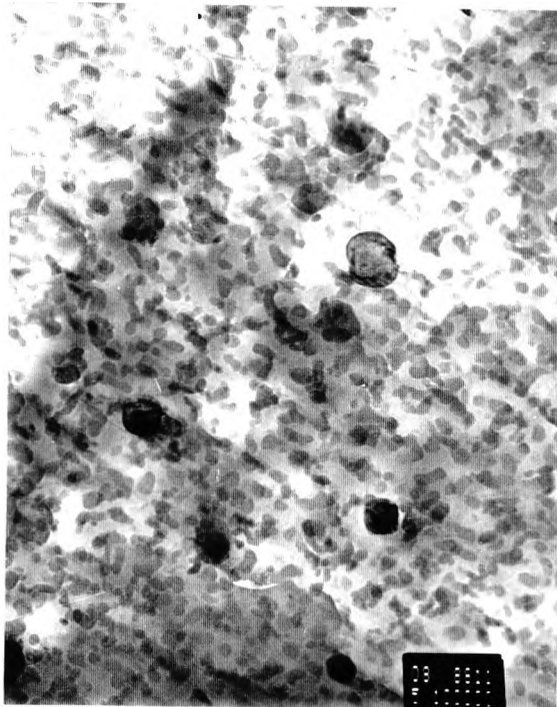


(a)



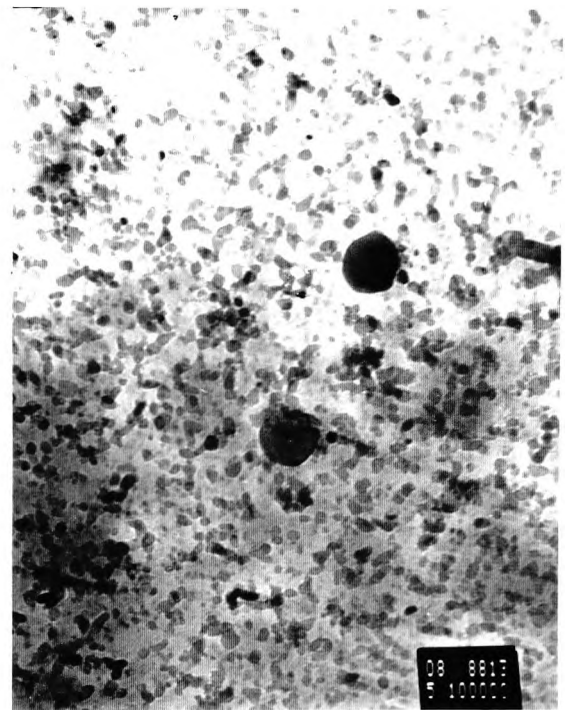
(b)

Figure 5.24 Scanning electron micrograph, showing the effect of tempering on the pearlite phase of 2.02% Cu steel: (a) as "normalised" (N) condition (b) "normalised" and over-aged (NT650) condition.



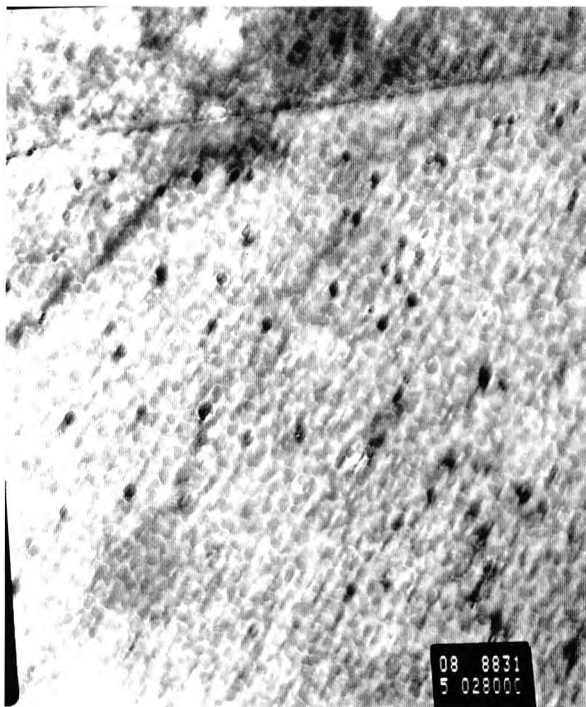
x100000

Figure 5.25 TEM of thin foil, showing copper precipitation, in the as "normalised" 1.22% Cu steel.



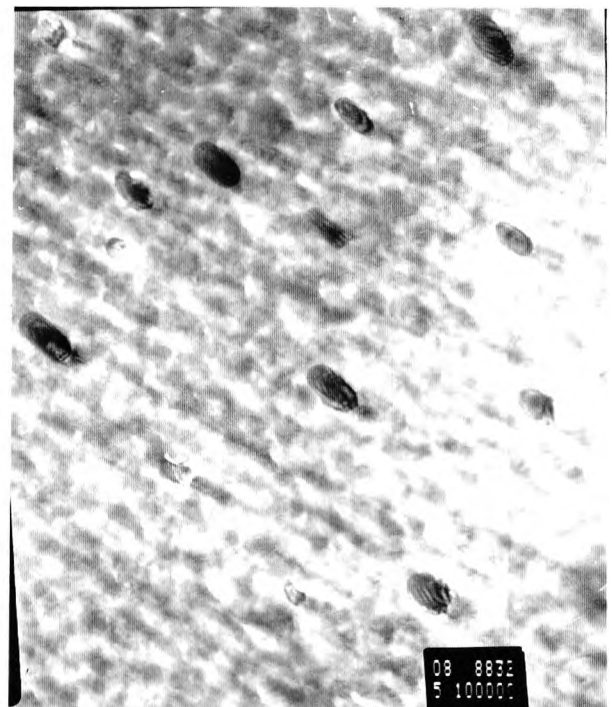
x100000

Figure 5.26 TEM of thin foil, showing copper precipitation, in the fully-aged 1.22% Cu steel.



(a)

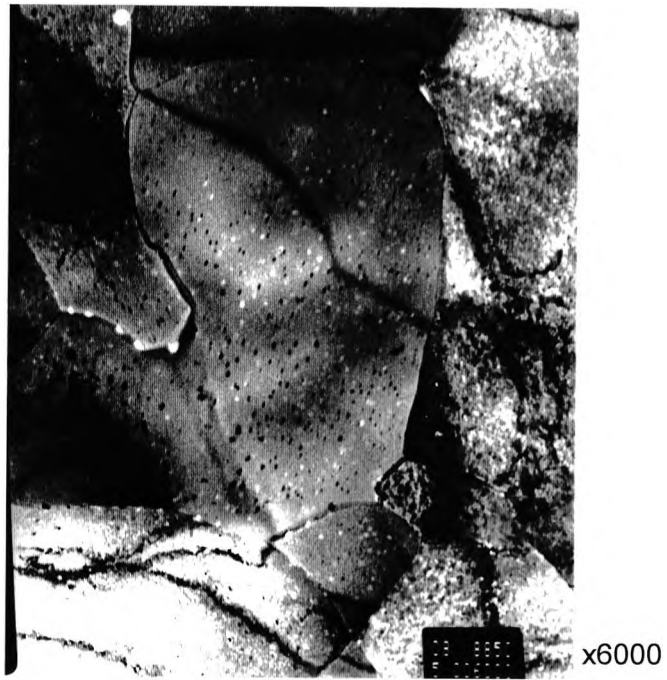
x28000



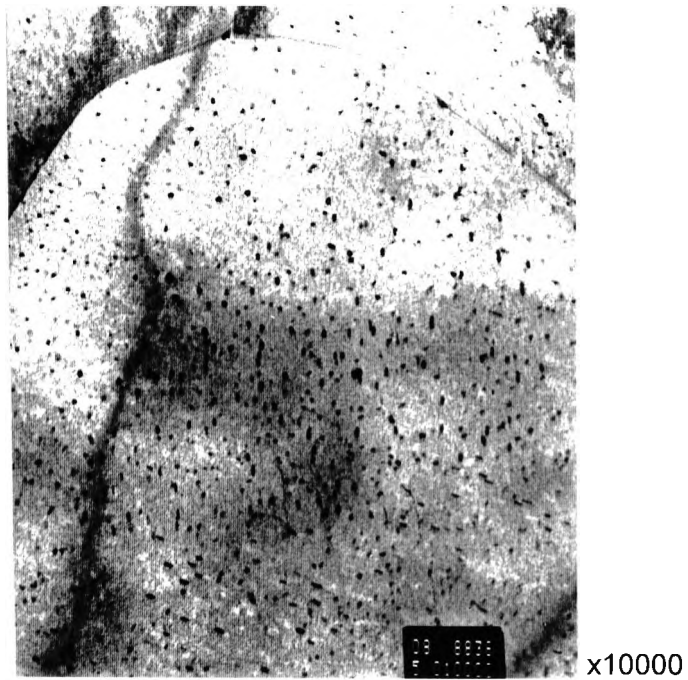
(b)

x100000

Figure 5.27 Transmission electron micrographs, showing copper precipitation in the as "normalised" 2.02% Cu steel (thin foils).

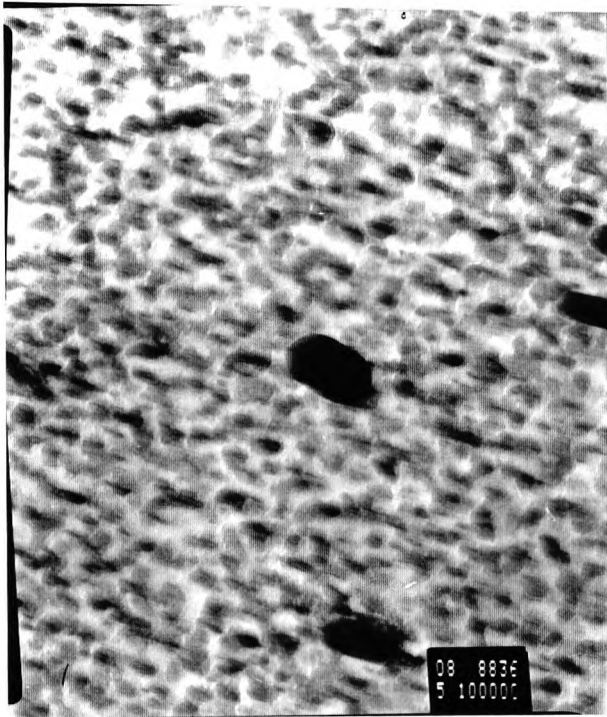


(a)



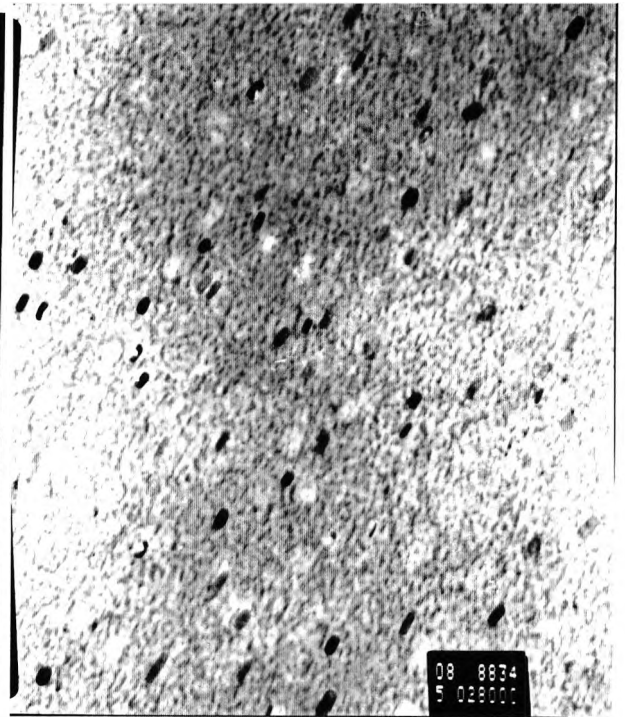
(b)

Figure 5.28 TEM of thin foils, showing the intensity of copper precipitation, in the NT550 condition of 2.02% Cu steel.



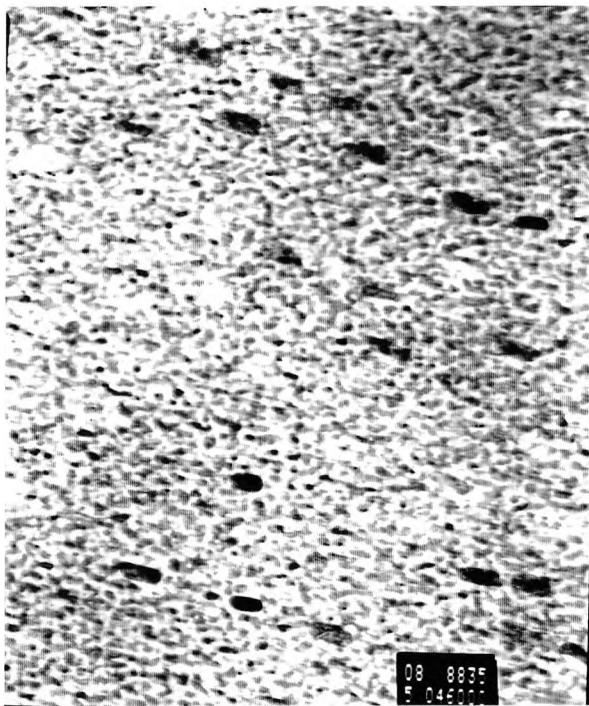
x100000

(a)



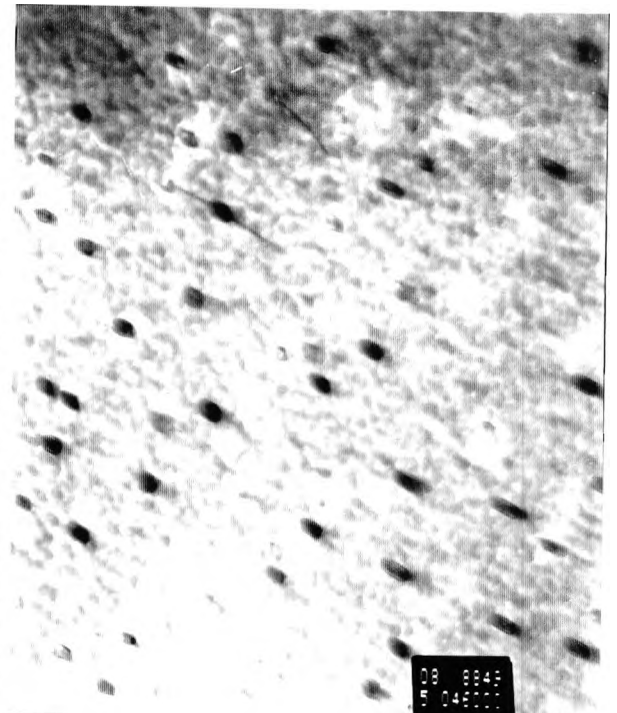
x28000

(b)



x46000

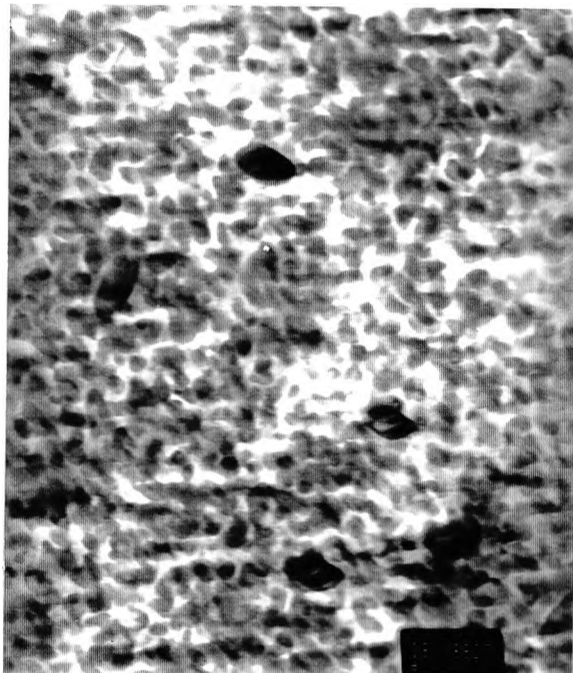
(c)



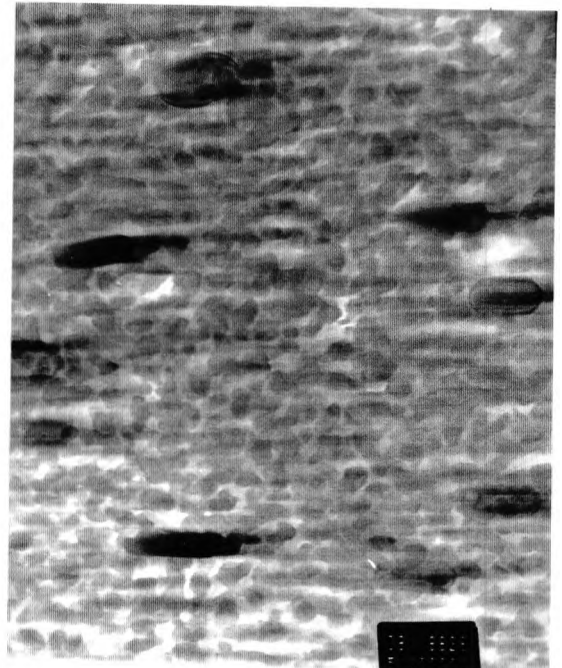
x46000

(d)

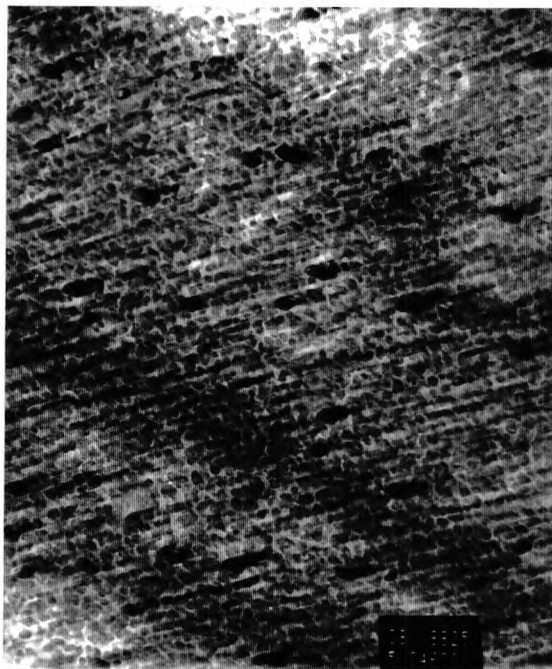
Figure 5.29 Transmission electron micrographs of thin foils, showing copper precipitates of the 2.02% Cu steel, in the fully-aged condition (NT550).



(a) x100000



(b) x100000



(c) x46000



(d) x28000

Figure 5.30 Transmission electron micrographs of thin foils, showing copper precipitation in the “normalised” and over-aged 2.02% Cu steel.

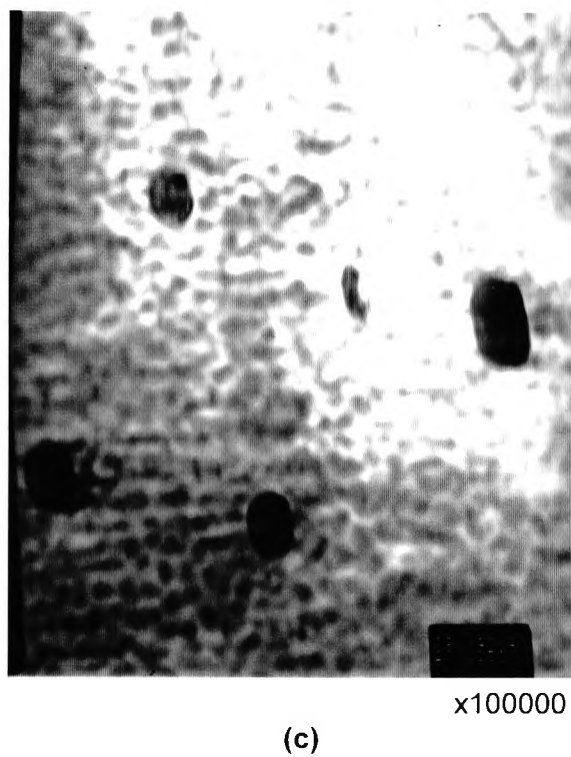
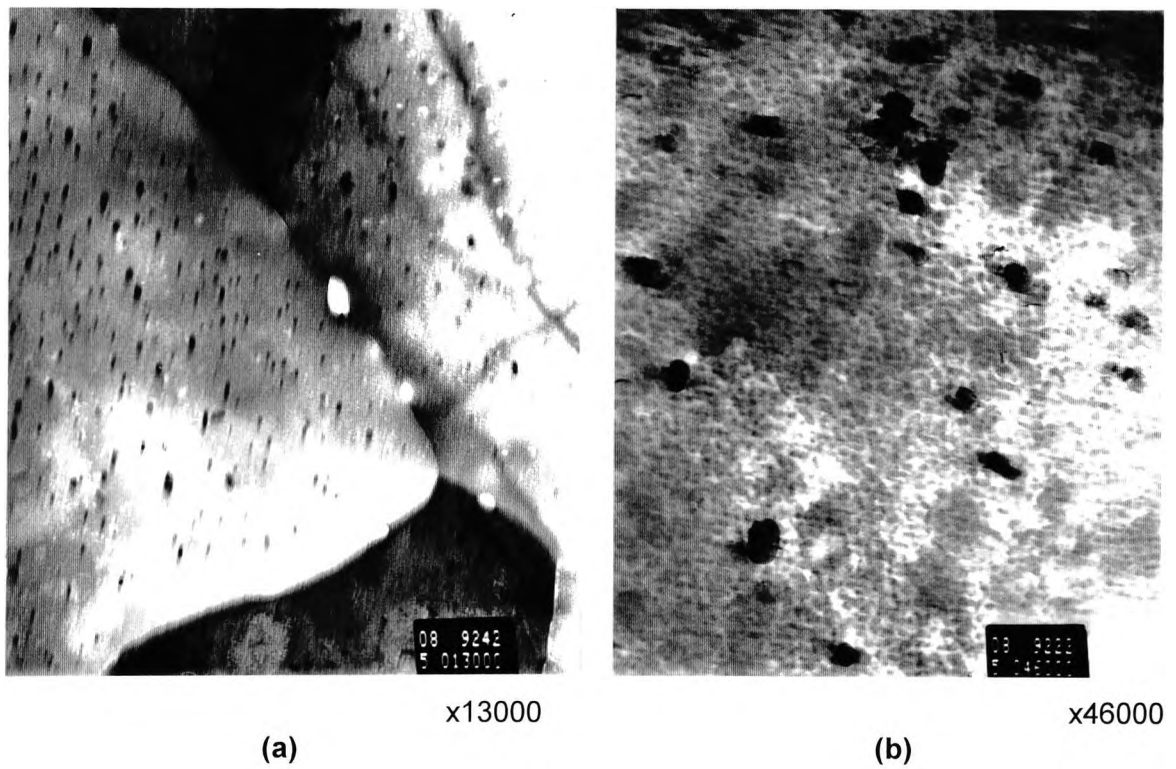
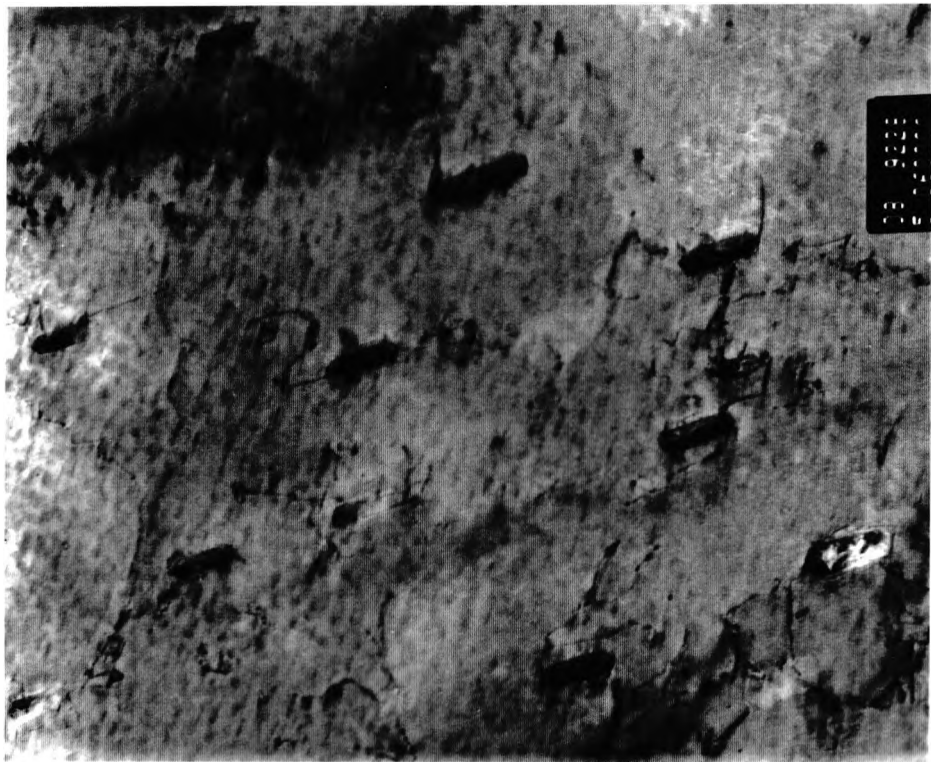
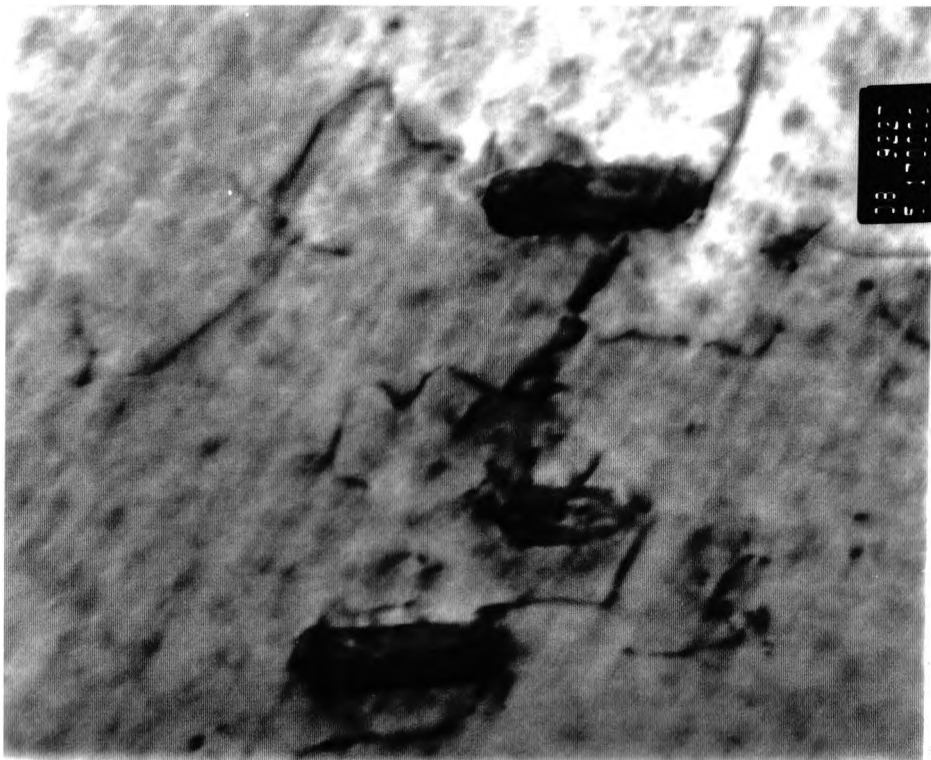


Figure 5.31 TEM of vermiculite-cooled and tempered, NT700, 2.02% Cu steel, showing (a) the intensity of precipitation (thin foil) (b), (c) the morphology of copper precipitates.



x81000

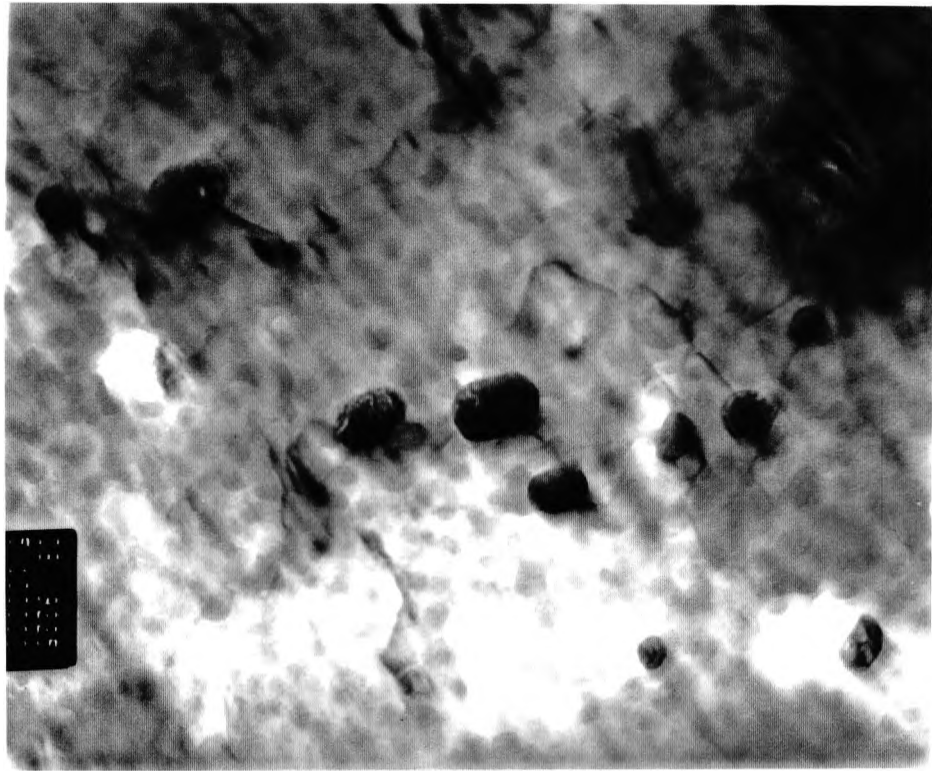
(a)



x230000

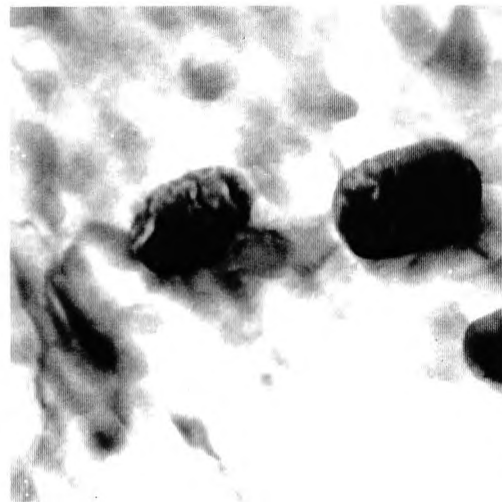
(b)

Figure 5.32 TEM of NT700, 2.02% Cu steel, that has been strained by 15%, showing precipitates surrounded by dislocations (thin foil).



x135000

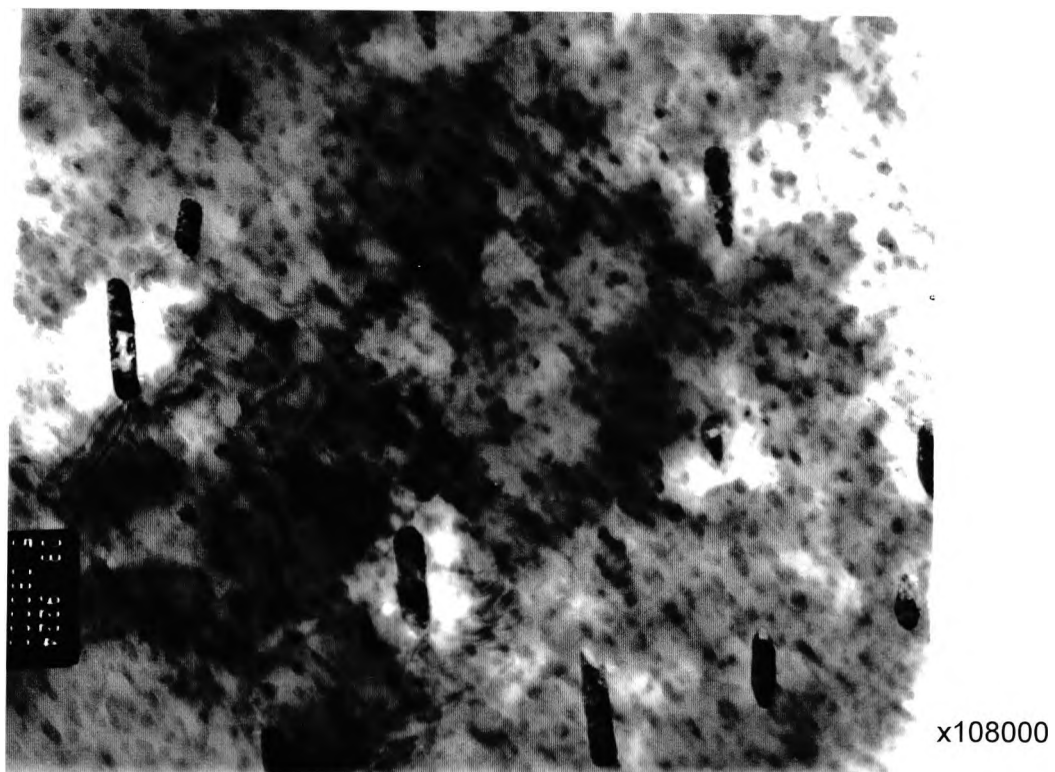
(a)



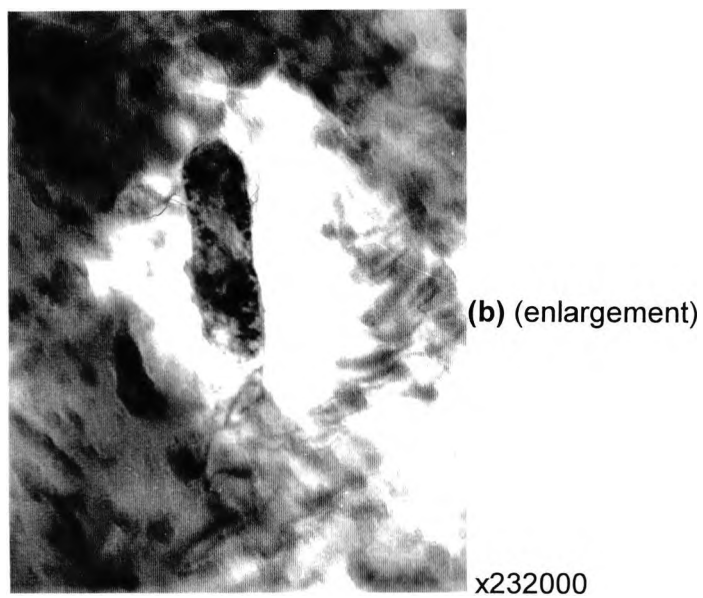
(b) (enlargement)

x230000

Figure 5.33 TEM of NT700, 2.02% Cu steel that has been strained by 15% (thin foil).



(a)



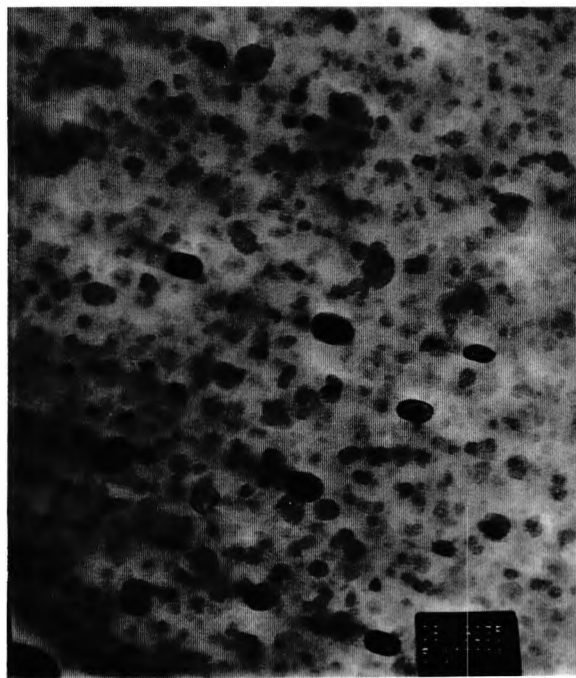
(b) (enlargement)

Figure 5.34 TEM of NT700, 2.02% Cu steel that has been strained by 15%, showing elongated copper particles (thin foil).

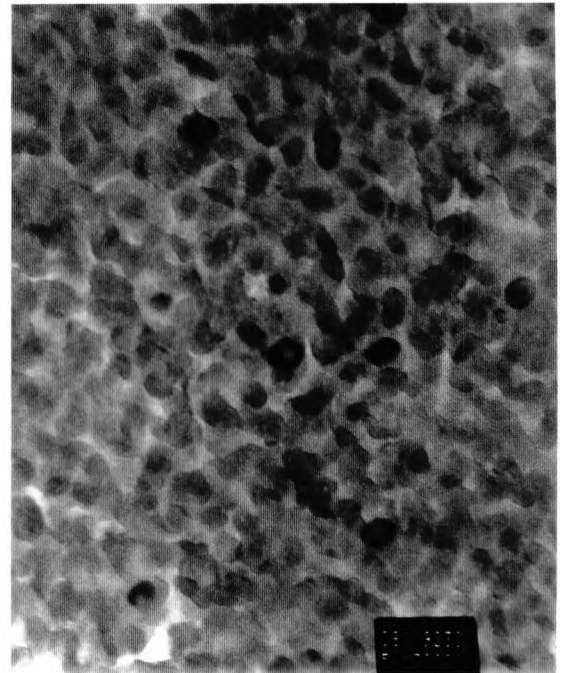


X135000

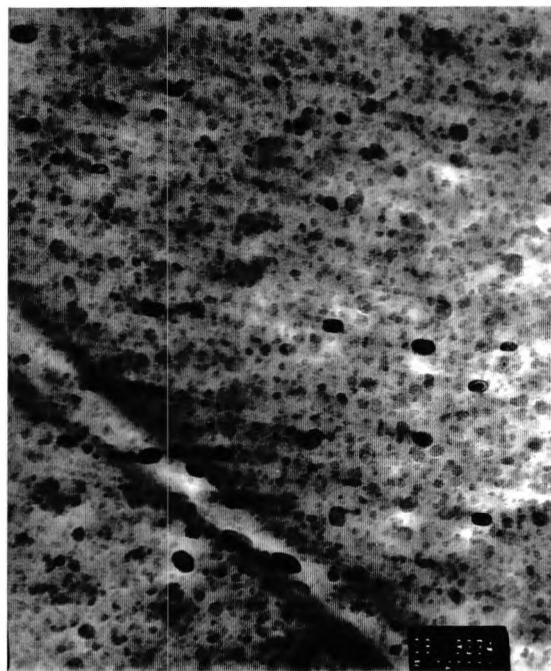
Figure 5.35 Transmission electron micrograph of NT700 2.02% Cu-steel that has been strained by 15%, showing deformed copper particles (thin foil).



(a) x100000



(b) x170000



(c) x60000

Figure 5.36 TEM of air-cooled (after austenitising at 910°C for 30 min) 2.02% Cu steel, showing copper precipitation (thin foil).

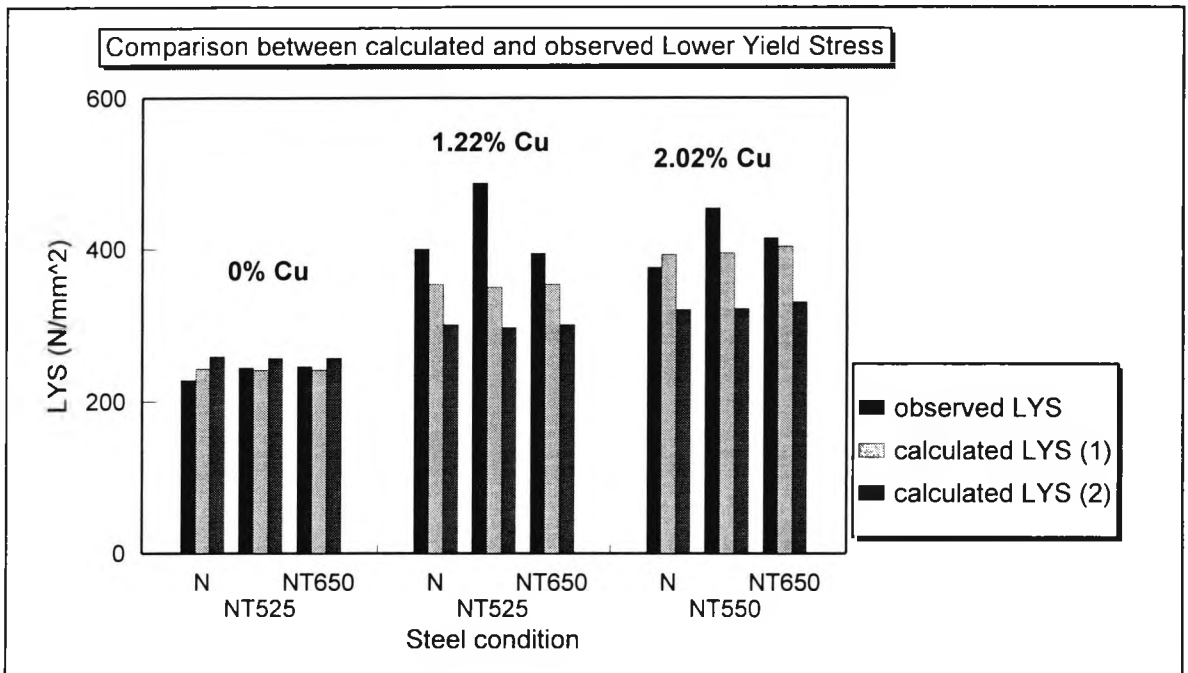


Figure 5.37 Comparison between calculated and observed LYS.

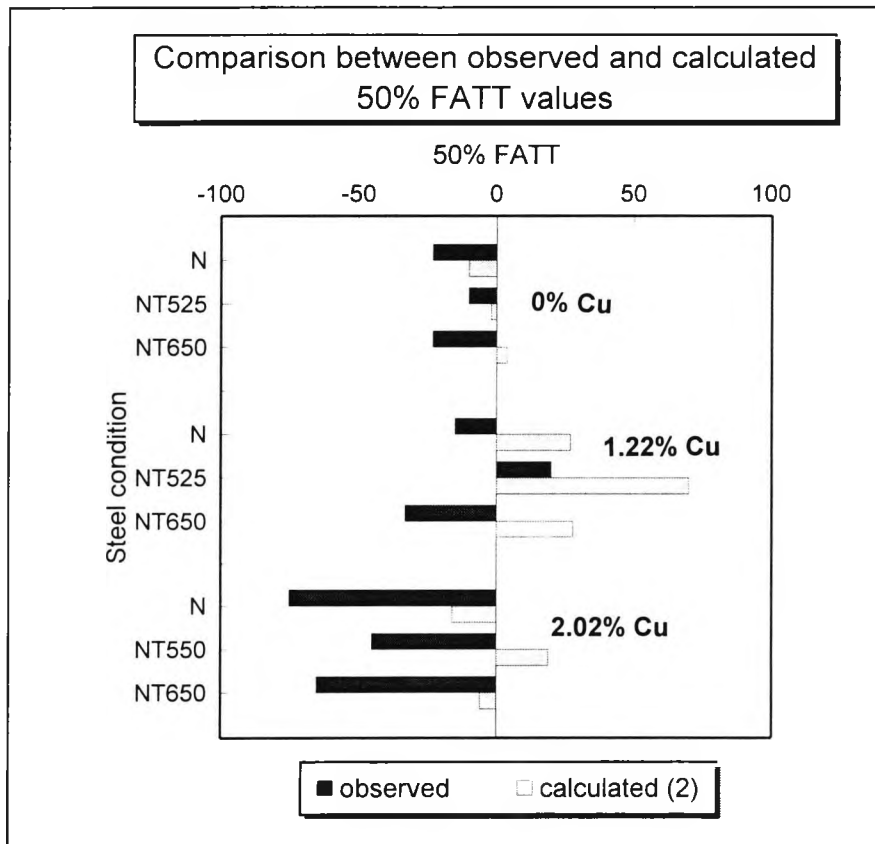


Figure 5.38 Comparison between observed and calculated 50% FATT values.

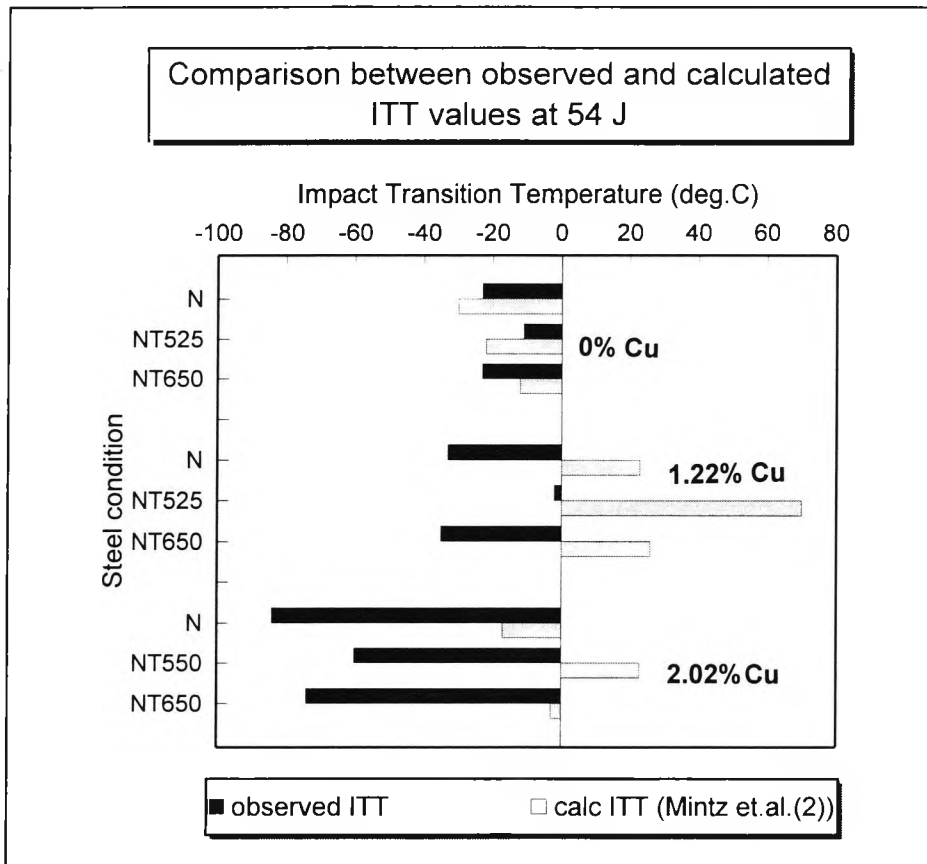


Figure 5.39 Comparison between observed and calculated 54J ITT values.

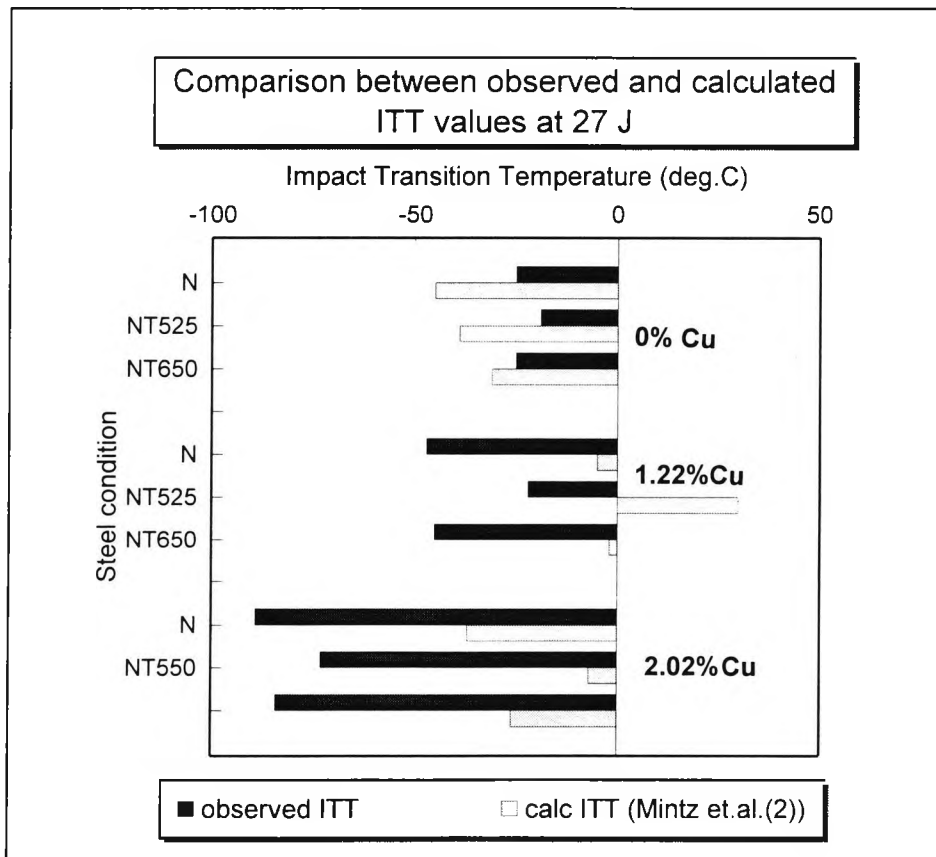


Figure 5.40 Comparison between observed and calculated 27J ITT values.

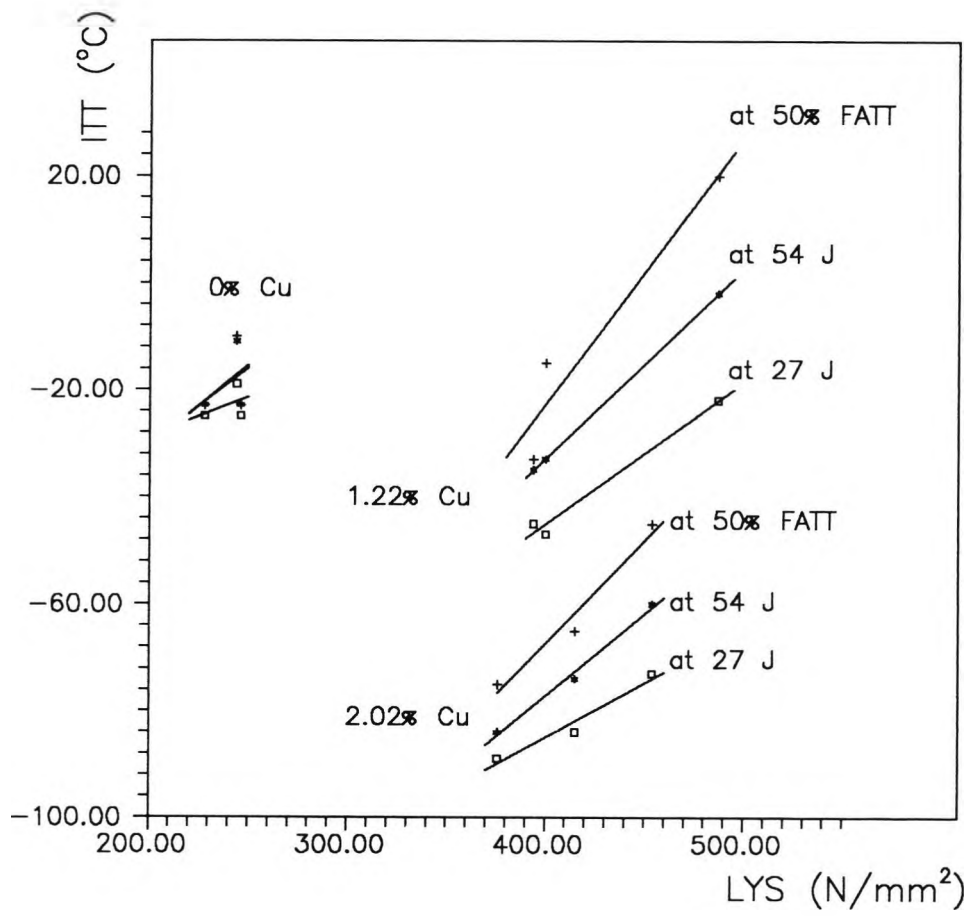


Figure 5.41 The variation of the observed impact transition temperatures as a function of the observed lower yield strength, of steels 2P148H, 2P149H and 2P150H.

6

THE STRENGTH AND IMPACT PROPERTIES OF LOW-CARBON COPPER-CONTAINING STEELS OF COMMERCIAL COMPOSITION

6.1 Introduction

The commercial need for strong, tough and weldable steels, for use in line pipes and naval applications, has led to the development of low carbon copper containing steels. These are age-hardenable and can combine good impact properties with high strength.

Research on copper steels originated in the early thirties, initially concentrating on the solubility of copper in iron and in lattice changes during ageing [50]. In the sixties, Hornbogen *et al.* [51,85] examined the precipitation of copper from iron, this being mainly a metallographic study. More recent work covers a wide variety of copper steels from low carbon [36,39,90] to medium carbon content and from simple to complex [7,52, 58] alloy additions.

The first commercial alloy IN-787, Table 6.1, was developed by INCO (International Nickel Company) and contained 1% Cu. Modifications to this steel have been made to improve properties such as weldability, by reducing carbon content and minimising hot

shortness by adding Ni. Such an improved steel is specified by ASTM A710 (plate), Tables 6.1 and 6.2.

A similar steel to the A710 specification Grade A, is being examined in the present study. This is a commercial steel developed by British Steel and contains 0.046% carbon, 1.26% copper and considerable amounts of alloying elements. The exercise is based on a previous investigation of an IN-787 modification, Table 6.1, carried out at British Steel [52] and aims at correlating tensile and mechanical properties to copper precipitation.

6.2 Experimental

Trial heat treatments were carried out, prior to the actual heat treatments. For these trials, two sample plates were cut from the steel. The two pieces were austenitised separately at 920°C for 30 min; one plate was left to cool in air (normalised), the other was quenched in oil. After the primary heat treatments the two trial plates were sectioned into smaller pieces and tempering treatments were carried out, in order to examine the age-hardening behaviour.

The tempering temperatures ranged from 200°C to 650°C for a soaking period of one hour, with the exception of one normalised sample which was tempered at 650°C for two hours. Vickers hardness tests were performed on polished surfaces across the plate thickness and age hardening curves were plotted as a function of Holloman parameter, Figure 6.1. For the normalised plate, maximum and minimum hardness was recorded after tempering for one hour at 550 and at 650 °C, respectively. For the quenched plate, the respective temperatures were 500 and 650 °C.

The six following conditions were finally selected to be examined in detail: normalised (N), normalised and fully-aged at 550°C for one hour (NT550), normalised and over-aged at 650°C for one hour (NT650), quenched (Q), quenched and fully-aged at 500°C (QT500) and quenched and over-aged at 650°C for one hour (QT650). Tempering at 500, 550 and 650 °C for one hour, corresponds to Holloman parameters of 15.46, 16.46 and 18.46 respectively. Cooling rates (for the austenitising treatment) were obtained for all the plates and are shown in Table 6.3.

The tensile tests were carried out on the INSTRON machine for the normalised specimens, using the 10 mm extensometer and at a strain rate similar to the one that was used for the previous exercises (chapters 4 and 5). The LLOYD tensile test machine was used to determine the tensile behaviour of the quenched samples.

Standard V-notch charpy tests were carried out to determine impact transition temperatures. Also, Vickers hardness tests on a 10 kg test load were performed after heat treatments and on tensile and charpy broken specimens.

Microstructural examination on broken charpies was carried out for trial samples and for the six conditions mentioned above.

6.3 Test results

6.3.1 Hardness test results

As mentioned above, the age-hardening behaviour of the steel was examined. Usually in ageing, temperatures are low and hardness is plotted as a function of time, drawing different graphs for various ageing temperatures. In this case however, the ageing temperature is nearer the higher tempering temperature range. For this higher ageing temperature range, the tempering time is usually kept constant while temperatures vary. To be able to assess hardness properly, the Holloman parameter is used. This is a function of both temperature and time, thus flexible to use. The equation governing the age-hardening or tempering process was mentioned in the literature review, Equation 2.20, and is as follows:

$$\text{Holloman parameter} = T * 10^3 (K_h + \log t)$$

where **T** is the absolute tempering temperature in °K, **t** is the tempering time in hours and **K_h** is a constant which is about 20 for alloy steels.

Tempering the normalised sample at 550°C and the quenched sample at 500°C for one hour resulted in respective increases in hardness from 175 to 227 and from 242 to 282 HV10, Table 6.4. Over-ageing the samples at 650°C for one hour causes a decrease in hardness. The hardness of the normalised plate, drops just above the original value, whilst that of the quenched plate drops below its original hardness value.

The hardness values of the trial plates, Figure 6.1, were found to be lower than those obtained for the actual plates, Table 6.1. The most likely cause is that trial steel pieces suffered some degree of decarburisation during the heat treatments because of their small size.

6.3.2 Tensile test results

The tensile properties of the steel in all conditions were obtained and are shown in Table 6.4. For both the normalised and the quenched samples, a 0.2% proof stress instead of a yield point was observed for the non-aged and the fully-aged conditions.

The 0.2% proof stress for the as-normalised sample was found to be 324 N/mm² and increased to 509 N/mm² after ageing at peak hardness. On over-ageing, the yield point was restored, the lower yield strength dropping to 455 N/mm² which was still considerably higher than that of the as-normalised sample. For the equivalent conditions of the oil-quenched sample, yield stress values were found to be 475, 625 and 560 N/mm².

The ultimate tensile stress (UTS) was also found to increase from 548 to 664 N/mm² after tempering the normalised sample at 550°C for one hour. It dropped down to 533 N/mm² after one hour of tempering at 650°C. The equivalent values for the quenched sample were found to be 638, 734 and 636 N/mm².

The ductility of the normalised and fully-aged sample, (NT550), was lower than that of the other two conditions, whereas for the quenched steel it remained the same for all conditions.

6.3.3 Impact test results

The impact strength fell when the steel was fully-aged, but was substantially improved upon over-ageing. The 27 J ITT values were observed to be -63, -40 and -104 °C, for the (N), (NT550) and (NT650) conditions, and -87, -69, -121 °C, for the (Q), (QT500) and (QT650) conditions, respectively.

The impact transition temperatures were also recorded at the impact energies of 54 and 69 J and at 50% fibrous appearance and as can be seen from Table 6.5, these approximately follow the same pattern of changes as those observed at 27 J.

Figures 6.2 and 6.3, show the ITT curves for the normalised and aged steel and the quenched and aged steel respectively. The ITT curves for the normalised samples, are well defined whereas points are widely scattered for the quenched samples at the (Q) and (QT500) conditions.

Figure 6.4, shows the 50% FATT curves for the normalised and the aged samples. As with the normalised samples ITT curves, a normal well defined curve was obtained.

Shelf energies were found to be generally high and maximum values were reached after over-ageing, for both normalised and quenched steels. The shelf energy of the as-normalised steel was at its minimum, 261 J, and was found to increase with ageing, whereas that of the quenched steel was at its minimum after full-ageing, 275 J, Figures 6.2 and 6.3, and Table 6.5.

6.4 Metallography

6.4.1 Optical microscopy

Optical microscopy was performed on all the trial samples and on the six selected conditions, i.e. the (N), (NT550), (NT650), (Q), (QT500) and (QT650) samples.

The structure of the normalised plate mainly consisted of equiaxed ferrite grains (88%), which had an average grain size of $10.3 \mu\text{m}$ ($9.9 \text{mm}^{-1/2}$), Table 6.6. Two different colour shades for ferrite were observed, Figures 6.5-6.10, suggesting that the material may be textured. The second phase of the structure was considered to be martensite with minute amounts of bainite and perhaps some retained austenite. It must be noted that initially and from previous work by Crowther [52] (working on a steel of a modified IN-787 composition, Table 6.1, an essentially ferrite/pearlite structure was expected. However, the smaller plate thickness of 15 mm in the present work compared to 20 mm [52], has resulted in a higher cooling rate upon normalising and this combined with the presence of Mo, has resulted in the formation of martensite. A lighter etch of one of the trial samples (normalised and aged at 200°C for one hour), Figure 6.7, identifies the martensitic phase more clearly.

After tempering the normalised plate at peak hardness, there was an apparent increase of the second phase from 12 to 13% which decreased down to 11% after over-ageing. The apparent increase in the volume fraction of the second phase, is due to the fact that ageing by allowing the carbon to precipitate as Fe_3C makes identification easier. The small decrease of the second phase on over-ageing probably reflects the growth of these carbides. The microstructure of sample (NT550) can be viewed in Figures 6.8 and 6.9. Also, Figure 6.10 shows the microstructure of sample (NT650).

As can be observed from the optical microscope photographs, there was a slight directional effect. This is most noticeable in Figure 6.9.

Optical microscopy of the oil-quenched samples revealed a fine microstructure which is a mixture of acicular ferrite and extremely fine martensite, Figures 6.11, 6.12 and 6.13. The fine grain size, the irregular grain shape and the difficulty in identifying martensite optically, prohibited the execution of accurate grain size or phase volume fraction measurements. It can be observed however, by visual comparison, that the quenched structures are approximately twice as fine as the normalised ones.

As in normalised material, ageing darkened the martensitic particles, Figures 6.12 and 6.13.

6.4.2 Scanning electron microscopy

Before any references are made on the photographs taken, it is worth mentioning that the preparation and observation of the SEM samples were quite tricky, partly because it was difficult to etch the ferrite-martensite combination and partly because the microscope itself was at that time causing problems with respect to the light contrast. Also, in the case of the quenched samples, the presence of very hard particles that are embedded in a very soft ferrite matrix, caused problems during the surface polishing.

6.4.2.1 Normalised microstructures

Scanning electron microscopy permitted a better and clearer observation of the martensitic grains than did optical microscopy. Figures 6.14, 6.15, 6.16 and 6.17 show micrographs of the as-normalised sample. Figure 6.14 was taken at a low

magnification in order to verify the structure in comparison to that of the optical micrographs.

Martensite was mainly in the form of islands, their size ranging from 0.5 to 10 μm ; 80% of this martensite was in the form of groups, Figure 6.15, whereas the rest was found at ferrite grain boundaries or in the form of single grains, as shown in Figure 6.16. The thickness of the islands that were concentrated at the grain boundaries, ranged from 0.5 to 1.5 μm , Figure 6.17.

The latter form of martensite mentioned above, made carbide thickness measurements difficult since its fine size made it look like the carbides, Figure 6.17. Measurements indicated that in the as-normalised condition, approximately 50% of the grain boundary particles were carbides, the rest being martensite, Table 6.7. The average grain boundary carbide thickness for this condition is 0.29 μm and the average grain boundary martensite thickness is 0.8 μm . The martensite-austenitic (MA) constituent appeared to be very shiny and resembled the MA constituent of the "dual-phase steels". However, the dual-phase steel structure is obtained through different processing routes, therefore any comparisons would not be reliable.

As in the simpler copper containing steels (chapter 5), normalising has allowed Cu precipitation. This appears to be quite coarse, since it can be detected in scanning electron microscope photographs, Figures 6.15, 6.16, 6.17. What is surprising in this case, is that these particles seem to have precipitated not only in ferrite, but also in the martensitic islands, Figures 6.15 and 6.17. In the simpler copper containing steels although there may have been some precipitation of copper in the pearlite colonies, it was very much less than observed in these martensite colonies. Again it is not too clear whether the Cu particles were present at the austenitising temperature or whether they formed on cooling through the transformation, although the former seems more likely.

After ageing at 550°C, the grain boundary carbides could easily be identified, since most of the martensite would break down into finer carbides on tempering, Figures 6.18, 6.19 (a) and 6.20. Detailed examination of the sample however, revealed that some areas containing martensitic particles were not affected by ageing, i.e. no carbide precipitation was observed, Figure 6.19 (b). Although this tendency was mainly observed for the smaller martensitic particles that were situated at grain boundaries,

there were enough untempered martensitic islands as large as 10 μm to suggest that the impact behaviour will be seriously impaired.

The average grain boundary carbide thickness, t_c , was found to be 0.13 μm (finer than after normalising) and its linear density was found to be approximately the same as that of the carbides of the normalised sample, Table 6.7. The grain boundary martensite thickness, t_m , was found to be 0.4 μm , Table 6.7, whereas the remaining martensite tempered into rod like particles of 0.3 μm in thickness. Of all the grain boundary particles, only 17% appeared to be untempered martensitic, but as it was mentioned in the previous paragraph, it is these particles that will influence the impact behaviour of the steel. Many of these were $\geq 1 \mu\text{m}$ as so would have a pronounced influence in raising the transition temperature.

After over-ageing at 650°C, the rod-like particles of the tempered martensite broke into finer particles of nodular shape, Figures 6.21 and 6.22, having an average diameter of 0.2 μm . The linear density of the grain boundary carbides doubled, Table 6.7, and they were approximately of the same thickness as those of the fully-aged sample. Figure 6.23 shows the marked increase in the number of grain boundary carbides. There was no observation of untempered martensite islands.

The reduction of grain boundary martensite thickness and volume fraction and the increase in the linear density of the grain boundary carbides after tempering, supports the suggestion that some of the grain boundary martensite had tempered into grain boundary carbides.

Unfortunately, the fully-aged and over-aged samples were not prepared as well as the normalised sample, and it was therefore difficult to observe the copper precipitates.

6.4.2.2 Quenched microstructures

Contrary to the scattered distribution and irregular size of martensitic particles that were observed in the normalised steel, the martensite present in the quenched steel is evenly sized and distributed, Figure 6.24. Unfortunately, because of the irregular and complex structure, it was impossible to make any accurate measurements of ferrite grain size or martensite particle thickness. The approximate size of the acicular ferrite grains is about half of that of the normalised structures, i.e. 5 μm . An indication of the

ferrite grain size and the martensite particle thickness, can be obtained from the photographs. For example, from Figure 6.25 (a), it can be observed that the martensite particle thickness ranges from 0.4 to 2.4 μm , although coarser particles than these have been observed in other instances. An indicative measurement of the martensitic particle thickness of the quenched samples, is shown in Table 6.7.

Thompson, Colvin and Krauss [90] have examined the water-quenched structure of a modified A710 steel with slightly higher amounts of Mn and Mo than in the present instance and classified the microstructures as "upper bainite". In upper bainite however, the ferrite laths are surrounded by cementite whereas in their investigation - as in the present exercise - the volume fraction of interlath second-phase particles was too large to be accounted for by cementite. TEM examination by Thompson *et al.* [90] of orientation relationships revealed that the second-phase, interlath particles are martensite/austenite. Previous investigators [35], have named this structure as "granular bainite". Thompson *et al.* [90], observed that about half of the volume fraction of second phase particles was austenite, and the other half was martensite. The smaller particles were completely austenitic, whereas the larger particles were mostly martensitic, but they were frequently surrounded by films of austenite. These observations probably explain why the martensitic particles of the present study, are surrounded by shiny edges, Figures 6.25 (a) and (b).

Another common observation, is that the ferrite grain boundaries are not developed by etching and the general appearance of the structure is therefore created by the arrangement and morphology of the second-phase particles. An interesting feature is shown in Figure 6.26, where a group of ferrite laths and second-phase (MA) particles is arranged in such a way that it seems to form a coarse grain that consists of both phases and is 47 μm wide and suggests transformation from a very coarse γ -grain.

Fox *et al.* [36] have also observed a similar microstructure in a water-quenched HSLA-100 steel plate. TEM work, revealed the existence of highly dislocated lath martensite with thin films of retained austenite at grain boundaries and occasional bainitic ferrite laths. In the centre of the steel plate the ratio of the bainitic ferrite to lath martensite was markedly increased and the bainite laths were often aligned or had a more equiaxed appearance [36]. This observation seems to be justified by the slower cooling rate at the centre of the steel plate, and seems to match the description of the

microstructure of the present steel. Fox *et al.* [36] have identified this sort of microstructure as “granular bainite”.

Ageing at 500°C for one hour, caused a slight degeneration of the coarser second-phase particles into smaller particles, probably cementite, Figures 6.27 and 6.28. This explains the darkening of some grains observed during optical examination of the samples. However, the tempering treatment left some large second phase particles unaffected, Figure 6.29. The average size of the second phase particles was measured to be 0.6 μm , Table 6.7.

The second phase particles were broken down further on ageing the quenched steel for 1h at the higher tempering 650°C, Figure 6.30, and their average thickness was found to be 0.4 μm , Table 6.7.

The ageing results are again in accord with Thompson *et al.*'s work [90], who have observed that some cementite had been formed from pools of austenite during ageing at 604°C for one hour.

Despite the fact that the structure was resistant to tempering, there was an effect on copper precipitation. As shown in Figure 6.28, ageing at 500°C for one hour, produced a fine copper precipitation. This appeared slightly finer than that observed in the normalised condition of the same steel, Figure 6.15 (b), and also finer than that of the as-“normalised” simpler 1.22% copper containing steel, Figure 5.16 (b).

6.4.3 Transmission electron microscopy

6.4.3.1 Normalised microstructures

Transmission electron microscopy was performed on replicas that were extracted from optical samples from all normalised conditions. As can be seen from Figure 6.31 (a) and (b), copper precipitates are either in spherical or in nodular form. The average diameter of round particles was found to be 41 nm whereas thickness and length of nodular precipitates was found to be 33 and 41 nm respectively, Table 6.8. There were however, numerous particles that were much finer, Figure 6.31 (b), these having a diameter of 4 to 8 nm, and were probably Nb(CN). EDAX analysis subsequently confirmed that these smaller particles contained Nb, and were therefore assumed to be Nb(CN) particles.

Unfortunately, the measured precipitate size does not agree with the limited SEM measurements which suggested that the average precipitate size of the normalised sample should be approximately 86 nm. Indeed SEM measurements were in general significantly higher than those of the TEM. However, only the TEM replica measurements will be used in this chapter, as they are more accurate than those of the SEM. One of the problems with measurements of the copper particles using the SEM, is that one is working at the resolution of the microscope. Focusing has to be very sharp, to accurately measure their size from the photographs and the quality of the photographs in this case is not as good as it was for the simpler Cu containing steels in chapter 5. In chapter 5, not only was the photographic quality better, but there was an excellent agreement between the TEM measurements and those from the SEM. In the present case this is not so, and the replica measurements have therefore been taken in preference.

Another observation in relation to the simpler Cu-containing steels, is that the copper precipitate size in the present case, is the same as that of the normalised (air-cooled) 2.02% Cu steel, Tables 5.7(b) and 6.8.

After ageing the sample at 550°C, the particle diameter, thickness and length increased to 51, 47 and 76 nm respectively. The thickness of finer particles, increased too, to 11~22 nm in diameter. An extraction replica of the steel microstructure is shown in Figure 6.32.

Over-ageing caused a further increase of the precipitate size, Table 6.8. The average diameter of round particles increased to 70 nm and the thickness and length of nodular particles to 50 and 102 nm respectively. Apparently, there were more fine particles than in the previous conditions, Figure 6.33 (a), (b) and (c), these having either round or nodular shape. Although there was an increase in the size of the coarser precipitates, the size of fine round particles stayed the same at a diameter of 10 nm. In addition to that, extra fine nodular particles were also observed having an average thickness of 10 nm and an average length of 17 nm. It is worth mentioning that there were some very coarse particles, Figure 6.33 (b) and (c), which are believed to be carbides and sulphides.

The conclusion drawn from the above observations, is that the coarse particles which are present in all normalised and normalised and tempered conditions, have been produced either on cooling from the austenitising temperature or were undissolved at 920°C, as was observed in the simpler copper-containing steels. The very fine particles must be Nb(CN).

6.4.3.2 Quenched microstructures

Replicas of the quenched samples show that there is a much higher density of precipitates compared to those of the normalised structures, Figure 6.34 (a) and (b) and these precipitates were also slightly finer. This is attributed to the much higher cooling rate during quenching. However, their general coarseness makes it possible that many of these precipitates were also present during the austenitising treatment. Although 920°C would be expected to be above the Ae_3 temperature (Andrew's equation, [49]), presumably the soaking time at that temperature may have been insufficient to allow the copper to go back fully into solution. Copper is a substitutional element and diffuses very slowly in the γ lattice. This possibility was checked in two ways: 1) The structure of the as-rolled material (i.e. as-received) was examined on the SEM and 2) a plate was austenitised at 920°C for 1/2 h followed by water quenching and then examined on the SEM. In both samples no precipitates could be traced and therefore somewhat surprisingly, has to be assumed that the precipitate that is visible in all these samples, is a result of cooling from the austenitising temperatures.

In the as-quenched condition only the coarser precipitates in the replicas could be detected. However, the quality of replicas for this sample was not very good. Measurement of the particle size indicates that the diameter of round particles is 30 nm (10 nm finer than those of the as-normalised condition of the same steel) and that the thickness and length of elliptical particles was 30 and 52 nm respectively. However, It is unlikely that any elliptical precipitates would form in the quenched condition [51]; their apparent elliptical shape is most likely due to having formed by the slipping and clustering of round particles during the replica preparation.

After one hour of tempering at 500°C, the precipitate diameter increased to 45 nm, Table 6.8. There were some particles that appeared to have an elliptical shape, although whether this was real -as already mentioned- is not clear. Their size is given in Table 6.8. Also, there was the appearance of some extra fine round particles, Figure

6.35, these having an average diameter of 9 nm. As in the case of the normalised steel, these are considered to be Nb(CN) particles.

After over-ageing the steel at 650°C for one hour, there was an apparent reduction in the size of the coarser precipitates, these having an average diameter of 34 nm, a thickness of 26 nm and a length of 49 nm, Table 6.8. The reason behind this size reduction, is probably due to the coarsening of the finer particles, Figure 6.36 (a) and (b) and some overlapping of precipitate size distribution for coarse and fine particles. The average diameter of the finer round particles was found to be 10 nm, whereas the thickness and the length of nodular particles was found to be 10 and 17 nm respectively.

Figure 6.36 (b) is an interesting picture which shows the emergence of some very fine particles again probably Nb(CN) particles.

6.5 Discussion of results

The analysis of the results of the commercial copper containing steel is complicated because of the presence of martensite. The presence of martensite prevents full realisation of the properties in all of the conditions but the over-aged, in which the martensite will be tempered off, the impact properties will be restored and the yield point will return. In the next few sections, the role of martensite in addition to the effect of copper on the strength and impact behaviour, will be discussed.

6.5.1 The influence of tempering on hardness and tensile properties

As in chapter 5, it is necessary to assess the large changes in the yield strength that occur on ageing, and this can only be done if the yield equations for ferrite/pearlite steels are used. However, the complex alloying composition of the steel that was used for this exercise, resulted in the presence of martensite which subsequently brings problems when it comes to interpreting the work in terms of structure-property relationships.

According to Mintz and Kolahi-Aval [98], small amounts of martensite have been shown to reduce the yield stress. This occurs because the volume expansion accompanying the martensite transformation causes pre-yielding and the mobile dislocations formed, are able to move at lower stresses. Work by Rigsbee and Vander

Arend [41], indicates that the yield strength decreases from 550 to 350 N/mm² with increasing percentage martensite up to 4% and then starts to increase again, reaching 450 N/mm² when 11% martensite was present. These authors [41] also noted that the Lüders strain decreased with increasing volume fraction of martensite and the change to continuous yielding occurred when the percentage martensite exceeded 4%. It is thought that the increase in strength for higher martensite volume fractions (>6%), occurs because at these levels the ferrite grain interiors become saturated with transformation induced dislocations [41].

Obviously, in the case of ferrite-martensite-carbide combinations, the use of structure-property relationships which were developed for ferrite-pearlite steels is limited. In particular, the regression equation for the yield strength applies to steels that show a distinct yield point. In the present instance, the only case in which these structure-property relationships can be strictly applied, is in the over-aged conditions when the martensite has been tempered and a yield point is again observed. However, the expected LYS values were calculated for all the conditions using both Equations 2.10 and 2.11. The calculated LYS and δ LYS values from Equation 2.11 (LYS⁽¹⁾ and δ LYS⁽¹⁾) will be mostly discussed in the following sections. The values that resulted from Equation 2.10 will only be used in conjunction with the ITT equations for the calculation of the predicted impact transition temperatures.

In the over-aged condition at 650°C, it is reasonable to assume that the volume fraction of copper precipitated out will conform to equilibrium condition so that f in Equation 5.2 can be readily calculated using the Wriedt and Darken Equation (5.6).

6.5.1.1 Normalised and over-aged condition (NT650)

For this condition the observed LYS was found to be 455 N/mm², whereas the predicted value, Equation 2.11, is 365 N/mm², i.e. the δ LYS⁽¹⁾ for dispersion strengthening is 90 N/mm². This δ LYS⁽¹⁾ value increases to 129 N/mm², Table 6.10, if one assumes that as in the case of the simpler copper containing steels, a large proportion of the copper has been precipitated out (i.e. removal of say 1% Cu from Equation 2.11). These δ LYS⁽¹⁾ values seem high, considering that it is unlikely to have any coherent precipitates at this stage of tempering (1h at 650°C). However, there is a large amount of precipitation, causing dispersion strengthening. Using the Ashby model for this condition, for a copper precipitate size of 50 nm wide and 102 nm long,

and an f value of 0.0086, assuming equilibrium, then the estimated value of dispersion strengthening is 58 N/mm^2 , Table 6.9. However, there is a large amount of niobium in the steel and this may be giving rise to some precipitation strengthening. Solubility data indicates that nearly all the Nb will be precipitated out at 920°C and one can therefore assume that f is 4.904×10^{-4} . Using the measured Nb(CN) precipitation size of 10 nm, Ashby's model would give another 56 N/mm^2 contribution to strength from dispersion strengthening. The overall dispersion strengthening then adds up to 114 N/mm^2 , which is not far away from the calculated value given by the yield strength equation.

6.5.1.2 Quenched and over-aged condition (QT650)

Considering the quenched and over-aged condition which also gave a distinct yield point and taking the ferrite grain size as $5 \mu\text{m}$, then the $\delta\text{LYS}^{(1)}$ is estimated to be 122 N/mm^2 when Equation 2.11 is used. This value rises to 162 N/mm^2 if 1% copper has been precipitated out in a coarse form and is therefore removed from the equation. Taking the copper precipitate size to be that given in Table 6.8, then the Ashby model calculates the dispersion strengthening from copper to be 96 N/mm^2 , Table 6.9. This, in addition to the Nb effect, results in a total dispersion strengthening of 152 N/mm^2 which again is agreeable with the calculated $\delta\text{LYS}^{(1)}$ for this condition, Table 6.10.

Although many assumptions have been made in this approach, it does seem to give a reasonable interpretation of the observed behaviour.

6.5.1.3 The influence of martensite and copper precipitation, on the yield properties other than the over-aged conditions

Having determined the strengthening mechanism of the over-aged condition, the analysis of the yield strength results of the other conditions will be attempted. In doing this, two problems exist and these are: 1) The presence of martensite and (2) the difficulty in determining the f value.

In order to overcome the problem that occurs due to the presence of the MA constituent, the present results must be compared with those of a similar work that has been carried out by Crowther [52] in which martensite was present in much smaller quantities and did not have any marked effect on yield properties.

The difficulty in determining the f value can be dealt with, if assumptions are made regarding the amount of copper that precipitated out of the solution in each condition. In the normalised and over-aged condition, where equilibrium conditions probably exist, it was estimated that the approximate maximum amount of copper that can be precipitated is 80% of the total copper content. This value was obtained using the Wriedt and Darken solubility equation (5.4).

For the non-equilibrium conditions such as the as-normalised and as-quenched structures, there is no doubt that the precipitated copper amount will be less than 80%. For these cases, the precipitated copper values were chosen to give the best fit to the data and were taken to be 50 and 30% of the total copper content for the as-normalised and as-quenched conditions, respectively. All of the niobium was considered to have precipitated out at the austenitising temperature, for the as-normalised and as-quenched conditions. After the above considerations, the $LYS^{(1)}$ and $\delta LYS^{(1)}$ values were corrected and the new values are presented in Table 6.10 and are marked with an asterisk, (*).

It is likely that ageing at 550°C will also result in equilibrium conditions so that most of the Cu will have been precipitated out. In any case, as for the fully-aged conditions of the normalised and quenched steel plates, it was found that the dispersion strengthening effect of copper does not vary significantly, when the assumed precipitated amount of copper is between 60 and 80% of the copper. For the ease of calculations, this value was taken to be 80%, i.e. as for the over-aged conditions, Table 6.9.

6.5.1.4 Normalised and fully-aged condition (NT550)

The analysis of the yield properties of the normalised and fully-aged condition is difficult, as the martensite that resulted during cooling from the austenitising temperature, is only partially broken down, Figures 6.19 (b) and 6.20. SEM observations confirmed that approximately 65% of the martensite had been tempered after ageing at 550°C for one hour, Table 6.7.

In the normalised and fully-aged condition of a modified IN-787 steel, Crowther [52] has reported a LYS value of 544 N/mm². When this value is corrected for the compositional and grain size differences between the steel of that exercise and the present one, drops to 523 N/mm² which is slightly higher than the observed yield

strength, 509 N/mm^2 , of the present exercise. Thus, when martensite is to a large degree tempered off, as in the present investigation for the normalised and fully-aged condition, there is no significant difference in the yield behaviour between the present work and that of Crowther's.

After taking the above observations into consideration, it may be concluded that for the fully-aged condition, the presence of a small amount of untempered martensite will cause a reduction of the LYS by only 15 to 30 N/mm^2 .

In this condition (NT550), it is apparent that the increase of LYS is due to the presence of coherent precipitates. Equation 2.11 estimates that the $\delta\text{LYS}^{(1)}$ is approximately 183 N/mm^2 , considering that approximately 80% of the copper has precipitated out. Noting that the total dispersion strengthening effect of copper and niobium is estimated to be 108 N/mm^2 , Table 6.9, then the precipitation hardening due to coherent copper precipitates can be considered to be 75 N/mm^2 . This is however not the actual value, since martensite has been suggested to have lowered the yield strength by 15 to 30 N/mm^2 . By taking this into consideration, the precipitation hardening from coherent precipitates adds up to $90\sim 105 \text{ N/mm}^2$.

6.5.1.5 As-normalised condition (N)

As in the case of the normalised and fully-aged steel, it would also be interesting to examine Crowther's results [52] in some detail, for the normalised condition. Crowther working with a modified IN-787 composition which had very little martensite present after normalising, has reported a very high LYS of 436 N/mm^2 , Table 6.11, compared to the obtained 324 N/mm^2 in the present investigation in which the steel had 11 to 12% martensite. Some of this increase in strength can be prescribed to his finer grain size, but when allowance is made for his grain size and the compositional differences, the LYS reduces to 415 N/mm^2 , i.e. it is 91 N/mm^2 higher than the observed value in the present exercise. It can therefore be concluded that the adverse effect of martensite on the LYS in the as-normalised condition, is of the region of 90 N/mm^2 and it could be said that this effect masks any dispersion strengthening.

In addition to the above comments, the observed LYS for the as normalised condition of the present work, 324 N/mm^2 , was 15 N/mm^2 less than that calculated from Equation 2.11 (and corrected for the precipitated copper content), Table 6.10. However, there has been again a large amount of coarse copper precipitation, as can

be seen from SEM and TEM photographs, Figures 6.15, 6.16, 6.17 and 6.31, and significant dispersion strengthening would be expected. That this is not observed, indicates that the martensite is reducing the yield strength and giving rise to a proof stress. Based on this assumption and in accordance with microscopic observations of a large amount of copper precipitation, it then follows that some dispersion strengthening must be apparent. It is taken that the approximate dispersion strengthening effect of copper is 74 N/mm^2 , Table 6.9. It must be also noted that the niobium will probably also contribute to the dispersion strengthening and given its fine particle size and assuming that it is all precipitated out, its effect as before can be estimated to be approximately 75 N/mm^2 , Table 6.9. The resulting value is therefore 149 N/mm^2 . That this marked dispersion strengthening is not observed, indicates that the martensite is having a marked influence in reducing the strength. Rigsbee and VanderArend [41] have also found that the approximate decrease in the LYS is $100\sim 150 \text{ N/mm}^2$ when 12% martensite (i.e. approximately the martensite content of the normalised steel in the present exercise) is present in an annealed 0.072 %C steel.

All the above observations indicate that the presence of martensite causes a yield strength reduction by a value of the order of 90 to 150 N/mm^2 .

6.5.1.6 As-quenched condition (Q)

The analysis of any oil-quenched condition other than the quenched and over-aged is very complex, because it is again difficult to assess the influence of martensite on the yield properties. Rigsbee and VanderArend [41], do not give information on the yield properties of structures where the martensite volume fractions are higher than 14% (in the present case for the quenched condition, martensite seems to occupy 20% of the structure), but it can be assumed that a further increase in the martensite percentage will result in a proportionate increase in the LYS. This suggests that the martensite adverse effect on LYS may be small.

The first attempt that was made to estimate the detrimental influence of martensite on the yield properties, was the comparison between the observed and the calculated yield strength. The calculated LYS was found to be 423 N/mm^2 , if it is assumed that 30% of the copper had precipitated out during cooling, Tables 6.9 and 6.10. This assumption is reasonable on the basis that this calculated value is lower than the observed proof stress by 52 N/mm^2 and is in reasonable agreement, with the estimated dispersion strengthening, 71 N/mm^2 , Table 6.9.

The above results suggest that martensite has no significant influence on the yield properties of the as-quenched steel. The absence of a visible evidence of niobium precipitation, makes the evaluation of any additional dispersion strengthening effect to that of copper impossible. If niobium had precipitated at the austenitising temperature - as it is likely- this would be expected to increase the strength by a further 60 N/mm². In such case, the martensite would be reducing the yield strength by a similar amount.

The above argument suggests that martensite is likely to have had some adverse effect on the yield strength, but it is impossible to accurately estimate it.

6.5.1.7 Quenched and fully-aged condition (QT500)

Ageing at peak hardness, resulted in a proof stress of 625 N/mm². This value is only slightly higher than that observed by Crowther [52] for the same condition, 614 N/mm², Table 6.11. This suggests that the effect of martensite on the yield properties may be negligible. Presumably, as has been denoted by Speich [91], most of the martensite has been tempered. Again, it is perhaps not unreasonable to assume that equilibrium conditions exist and that ~80% of the copper and all the niobium will be precipitated out of the solution. The dispersion strengthening was therefore taken to be approximately 84 and 61 N/mm² for copper and niobium respectively, Table 6.9. The $\delta\text{LYS}^{(1)}$ was found to be 226 N/mm², when it was assumed that 80% of the total amount of copper had precipitated out of the solution, thus suggesting that the coherent precipitates were contributing to the yield strength by the order of 81 N/mm². This is slightly lower than that observed for the normalised and fully-aged condition.

6.5.2 The effect of precipitation hardening on impact properties

As far as impact behaviour is concerned, it is again necessary to use the ITT Equations (2.7, 2.8 and 2.9) that were developed for ferrite/pearlite steels, in order to assess the impact properties of the steel. Again, as in chapter 5, a further deduction of 40°C from each of the ITT equations has been made, in order to allow for the higher shelf energies that were observed in this study due to lower S and C levels. The average grain boundary carbide thickness was initially taken to be the average value of the thickness of the carbides and the martensite islands that were situated at grain boundaries. However, recent work by Mintz, Adejolu and Nassar [99] has shown that both carbides and martensite films have the same detrimental influence on impact

behaviour. It is always the thicker films or carbides that determine the impact behaviour, so calculations were repeated using solely the average grain boundary martensite thickness for the non-aged and fully-aged conditions.

Although the average grain boundary martensite thickness was used, it was apparent that the sporadic presence of untempered martensitic islands in the as-normalised, normalised and fully-aged and in the as-quenched and quenched and fully-aged conditions, would still influence the ITT's to a great extent. In the normalised and fully-aged condition for example, martensitic islands as big as 10 μm were scattered around the structure, despite the fact that the average size of grain boundary martensite was not more than 0.4 μm . Previous work however, indicated that when the carbide thickness is $\geq 1 \mu\text{m}$, there is no further deterioration in impact performance [4]. Similar behaviour would be expected [99] from the martensite films (of 1 μm in thickness) that are present in the as-normalised, as-quenched and fully-aged conditions. For this reason, it was decided to repeat the calculation of the expected ITT values once more. The results are shown in Table 6.12.

In Table 6.12, the difference between the observed and the expected ITT values is estimated, this being denoted as δITT . This value will be regarded as the relative improvement of impact transition temperatures and will be referred to as the "ITT improvement" for simplicity.

6.5.2.1 Normalised and over-aged condition (NT650)

As in the assessment of the yield behaviour, the presence of martensite is expected to make comparisons difficult and for this reason it has been decided that the normalised and over-aged condition (NT650) will be examined first. This condition in which the martensite has been fully tempered, is more likely to give reliable results, than the others.

It can be seen from Table 6.12, that the calculated value for the ITT's are much higher than the observed ones. Thus the steel is behaving much better than would be expected from conventional structure/property relationships in which precipitation hardening is very detrimental to the impact performance. This can also be seen by examining a conventional 0.54% Mn, ferrite-pearlite steel of similar grain size (10 μm) and typical grain boundary particle thickness (0.17 μm), without precipitation hardening

or dispersion strengthening present (i.e. neglecting δ LYS). Such a steel would be expected to give a 54J ITT of -85°C according to Equation 2.7 and a strength of 314 N/mm^2 according to Equation 2.10. The present steel in the normalised and over-aged condition gave a similar 54 J ITT close to -100°C but has a much higher strength of 455 N/mm^2 . Thus the increase in strength of 141 N/mm^2 (Equation 2.10) due to dispersion strengthening, has had no effect in deteriorating the impact behaviour.

6.5.2.2 Quenched and over-aged condition (QT650)

It can be seen again from Table 6.12, that the steel is again behaving very much better with its impact performance, than would have been expected from the normal structure/property relationships.

In the same way as for the normalised steel, a 0.54%Mn, ferrite-pearlite steel having a grain size of $5\ \mu\text{m}$ and an average grain boundary particle thickness of $0.4\ \mu\text{m}$ as found in the oil-quenched and over-aged steel, would give an 54J ITT of -83°C (Equation 2.7), provided that there is no precipitation hardening and a strength of 375 N/mm^2 (Equation 2.10). In the case of the quenched and over-aged steel (QT650), a better 54J ITT of -117°C was observed, with again a much higher strength of 560 N/mm^2 . Thus the increase in strength due to the dispersion strengthening of 185 N/mm^2 (Equation 2.10), does not manifest itself by a deterioration in impact behaviour.

6.5.2.3 As-normalised and normalised and fully-aged conditions (N) & (NT550)

Recent work by Mintz *et al.* [99] has shown that even a very small volume fraction of martensite can be detrimental to the impact behaviour. In their work, the impact transition temperatures have been shown to rise by between 50 to 100°C . In the present work this detrimental effect was accounted for, by using the t_c value of the ITT equations to be $1\ \mu\text{m}$, even though the average grain boundary particle thickness is 0.8 and $0.4\ \mu\text{m}$ for the (N) and (NT550) conditions. As it was mentioned in section 6.5.2, the reason for doing so, is the presence of many very coarse particles ($>1\ \mu\text{m}$). These calculations estimate the expected improvement for the 54 J ITT, 24 J ITT and 50%FATT values to be 85, 76 and 37°C , for the as-normalised steel and 146, 120 and 105°C for the normalised and fully-aged steel, Table 6.12.

As in the normalised and over-aged condition, dispersion strengthening and precipitation hardening scarcely influences the impact properties. As can be seen in Table 6.12, the expected 54 J ITT is higher than the observed value by 85 to 146 °C for the respective (N) and (NT550) conditions. This improvement of the as-normalised condition is similar to that found in the normalised and over-aged stage. Thus once allowance for the presence of martensite has been made, the best improvement is now shown by the normalised and fully-aged condition; as has been shown for the simpler copper containing steels in chapter 5.

6.5.2.4 As-quenched and quenched and fully-aged conditions (Q) & (QT500)

In the case of the oil-quenched steel, the observed changes in impact properties seem to follow the same trends as those of the normalised steel, but are more pronounced, Figure 6.37 (a). The impact behaviour of the quenched steel plates was slightly better than that of the normalised steel plates, but the yield strength was also higher by 100-200 N/mm² higher. Although some of this difference could be accounted for by differences in grain size and thickness of the grain boundary particles, much of the difference required explanation from another source.

In the simpler copper containing steels, an approximate linear relationship was observed between the ITT and the yield strength on changing from the as-“normalised” to the “normalised” and fully-aged, and finally to the over-aged condition. However in the present exercise, this is not so (for both the normalised and quenched structures), Figure 6.37 (a) and the reason for this is the presence of martensite. Had this been taken into account, the resulting relationship would indeed be linear, Figure 6.37 (b).

As in the as-normalised and normalised and fully-aged steel, t_c in the ITT equations was taken to be 1 μ m for the as-quenched condition and 0.6 μ m for the quenched and fully-aged condition, and the results are given in Table 6.12. According to these, the expected 54 J ITT's were found to be 108 and 124 °C lower than the observed ones, for the as-quenched and the quenched and fully-aged conditions, respectively.

Unlike previous results, the relative improvement of ITT values did not show much variation after ageing. The oil-quenched steel (all three conditions) did however, show the best ITT improvement of all the copper containing steels that were

examined. This is an important observation because it suggests that the finer the precipitate distribution for a given volume fraction, the better will be the impact performance. The improvement of the impact behaviour of the (Q), (QT500) and (QT650) conditions can only be matched by the normalised and fully-aged, (NT550) condition, of the same steel, Table 6.13.

6.5.2.5 The influence of copper precipitate size and volume fraction on the impact transition temperatures

It is clear ~~that~~ ^{when} the results of all the steels that were tested (both commercial and simple copper-containing steels) are compared, the oil-quenched series shows the best impact behaviour. Undoubtedly, the fine grain size and the yield strength play a very important role in this case, but when these factors are eliminated, i.e. when the relative ITT improvement (δITT) is taken into consideration, it can then be observed that a large portion of the improved impact behaviour must be attributed to another factor.

Initially it was thought that one of the reasons that the quenched steel shows such a good performance, could be that the faster cooling rate has resulted in a higher volume fraction of finer copper precipitates than those obtained in the normalised structures. The idea that a dense copper precipitation is beneficial to the impact behaviour was also confirmed in chapter 5, where the 2% Cu containing steel had shown the best impact behaviour of the simple Cu containing steels. This view is strengthened by the work of Morrison [100], who studied the precipitation hardening effect of Ag on the structure and properties of a low carbon steel. In that work, it is quoted that there is a small volume fraction of Ag precipitates and that improvements in the impact behaviour were therefore only small. Also, the relative small improvements shown by the quenched-aged low carbon steels, chapter 4, is in accord, with only a low volume fraction of coherent precipitates being present.

In Morrison's paper [100], two reasons have been given for the improvement of impact behaviour. These were based on previous investigations that were carried out by other authors and are the following:

1. Cleavage resistance can be attributed to the ability of particles to reduce the tendency for microcrack initiation either by restricting the length of dislocation pile-ups, or by suppressing twin formation.

2. Particles can promote local plasticity, thus increasing the plastic work associated with crack propagation and effectively blunting microcracks.

Both these reasons would favour a greater volume fraction of particles leading to improved impact behaviour.

An important question that needs however to be answered, is that if there is a given volume fraction of copper precipitates, is it better to have the particles in a fine or in a coarse form. A possible way to investigate this, is to draw the relationship between copper precipitate size and ITT improvement. Figures 6.38 (a) and (b) show several possible relationships between the precipitate size (mean value) and the ITT improvement (the δ ITT was based on calculated values from Equations (2.7, 2.8, 2.9), Tables 5.10 and 6.12.

Although there is considerable scatter, it can be seen that essentially 3 curves can be drawn for the normalised/quenched, over-aged and fully-aged conditions, respectively. In all cases, refining the incoherent dispersion hardening Cu precipitates, leads to improved impact behaviour.

However, in the case of the normalised/quenched and over-aged conditions, above a certain incoherent precipitate size (45 nm) there seems to be little influence on the impact behaviour.

The small improvement shown by the over-aged curves compared to the normalised/quenched curves is probably related to the greater volume fraction of precipitation present in the over-aged steels. The much greater benefits shown by the fully-aged conditions are probably a result of the additional presence of the very fine coherent Cu precipitate.

The conclusion that can be derived from the above observations, is that given a constant copper content, it is better to have present a fine dispersion of the copper precipitate rather than a coarse one. This may be because the finer the precipitation, the shorter will be the dislocation pile-up.

When each group of steels is examined separately, based on steel composition and cooling rate (from the austenite region), it can be also observed, that there is not much

change in δITT when the precipitate size changes. When there is a profound change, as in the case of the normalised commercial copper steel (1P140M), then this is not linear and in almost all the cases, the best ITT improvement seems to be given by the fully-aged steels irrespective of precipitate size.

When the simple copper containing steels were examined in chapter 5, it was mentioned that the best ITT improvement came from the fully-aged condition, but it was also commented that it would be unfair to place too much weight on this observation without further work. It was then suggested that the exceptional impact behaviour of the steels should be attributed to the ability of the coarse and incoherent copper precipitate to deform. Having, now completed the exercise, it can be clearly viewed, that the observation concerning the fully-aged condition, applies to all the copper containing steels. This suggests, that the fine coherent copper precipitation is also favourable to the impact properties. As with the low carbon steels, chapter 4, the coherent precipitate may absorb dislocations, therefore preventing dislocation pile-ups and crack formation.

Another interesting feature that has to be examined, is the mode of strengthening with respect to the path of dislocations during the application of stress. Also the behaviour of the copper particles during deformation, especially the coherent ones, is required if a full understanding of the strengthening mechanism is to be found.

Knowles and Kelly [87] have developed a strengthening mechanism for the Fe-Cu system, where quantitative estimates of the strength have been obtained, by computing the interaction energy between particles and dislocations as a function of the distance of the dislocation from the centre of the particles. Their model predicts that dislocations in the deformed fully-aged and over-aged structure should thread through the copper particles, and they verified this by experiment. In the over-aged condition, they found that their results were agreeable with the Orowan strengthening mechanism.

The explanation of the above mechanism has been based on the following factors:

- Copper has a lower shear modulus than the ferrite matrix. Since the energy of a dislocation depends on the shear modulus of the surrounding medium, then if there is a particle of lower shear modulus than that of the matrix the dislocation can lower its total energy by threading its way through as many of the low-modulus particles

as possible, i.e. it will deform the particle. The exact opposite applies if the particle modulus is greater than that of the matrix, e.g. when Nb(CN) particles are present. In this case the dislocation will avoid passing through these hard particles and will either pile-up or cross-slip.

- The particle (Cu) and matrix (Fe) atoms have a similar radius (1.278 and 1.241 Å, respectively), thus there are no significant elastic strains. Niobium and other alloying element such as V, Ti and W have larger atomic radius than BCC-Fe and therefore more coherency stresses which prevent plastic deformation.

Russel and Brown [88] also studied a dispersion strengthening model for an over-aged Fe-Cu system and confirmed Knowles *et al.*'s findings, that although dispersion strengthening can be explained totally by modulus hardening, the predicted strength results are extremely close to the strength predicted by the Orowan model.

In agreement with these theories, the present examination has also noted that when the over-aged 2.02% Cu containing steel in chapter 5 was over-aged and strained, there was evidence that the copper precipitate was deformable (size change), Table 5.7 (b) and that dislocations appeared to thread through particles, Figure 5.34. The elastic modulus strengthening model therefore gives the most likely explanation for the precipitation strengthening of copper in this exercise and would account for the difference between the impact behaviour copper containing steels and other steel alloys such as niobium containing steels.

In the light of the above strengthening mechanism, it is reasonable to suggest that the improved impact behaviour of the copper containing steels lies in the ability of the copper precipitates to deform and lower the energy of moving dislocations rather than allow them to pile-up, thus retarding crack formation and propagation.

Previous suggestions that copper particles promote cross-slip or that the improved impact behaviour of copper steels only be attributed solely to the austenite grain refinement would seem unlikely. Cross slip is always very easy in BCC ferrite and there seems little reason to support that cross slip will be easier as to whether the hardening particles are coherent or incoherent, i.e. whether precipitation is incoherent Nb(CN) or coherent Cu or iron carbide precipitation.

6.5.2.6 The impact behaviour of the normalised, commercial 1.26% Cu and the simpler 2.02% Cu containing steels

The comparison between all the copper-containing steels regarding their relative ITT improvement has verified the importance of a fine dispersion of copper precipitation. It has also shown that by increasing the precipitated copper amount through ageing, there is an additional ITT improvement which is enhanced by the presence of coherent precipitation.

It would, however, be equally interesting to examine the impact behaviour of two steels on the basis of their copper content and alloying additions. To do this, it would be important that the microstructure of the two steels does not have many differences. After careful consideration of these factors, the steels chosen to be compared are: 1) the 1.26% Cu-containing steel, of a commercial alloy composition, in the normalised and over-aged condition ($LYS=415 \text{ N/mm}^2$) and 2) the 2.02% copper containing steel, of a relatively simple alloy composition, in the normalised and over-aged condition ($LYS=455 \text{ N/mm}^2$). These two steels have the following characteristics:

In common

- 1) Grain size
- 2) Copper precipitate size
- 3) $50\text{-}55 \text{ N/mm}^2$ dispersion strengthening due to the presence of coarse copper precipitation
- 4) Polygonal ferrite-pearlite/tempered martensite microstructure
- 5) Tempering parameters

Different

- 1) Grain boundary carbide thickness
- 2) Copper content
- 3) Alloying additions
- 4) The commercial steel has an additional dispersion strengthening effect from the presence of niobium ($\sim 56 \text{ N/mm}^2$)
- 5) Volume fraction of the second phase
- 6) Cooling rate from the austenite region

The differences between the grain boundary carbide thickness imply that the 54J ITT of the commercial copper containing steel benefits from a 35°C decrease. However,

the additional dispersion strengthening effect, would be expected to deteriorate the 54J ITT by 30-35°C, i.e. the two effects are counterbalanced.

Yet again the 54 and 27 J ITT values of the commercial alloy were lower than the equivalent values of the other steel by 20~25 °C. This suggests that the additional ITT improvement may be a result of the differences in alloying composition and the cooling rate from the austenite region. It has been reported [60,89] that the presence of Nb and Mo retard the premature precipitation of copper, therefore promoting a more uniform dispersion of the copper precipitate, which in turn favours the impact properties.

Finally, it could be concluded that a well balanced alloy composition is equally important to a high copper content.

Alloying element	IN787	Modified IN787 [52]	ASTM A710		1P140M
			Grade A	Grade B	
C	0.06	0.063	<0.07	<0.060	0.046
Si	0.20-0.35	0.30	<0.40	0.15-0.4	0.38
Mn	0.40-0.65	1.51	0.4-0.7	0.4-0.65	0.54
P	0.010	0.022	<0.025	<0.025	0.013
S	0.009	0.003	<0.025	<0.025	0.003
Cr	0.730	<0.02	0.6-0.9	--	0.60
Mo	0.180	<0.01	0.15-0.25	--	0.210
Ni	0.70-1.00	0.72	0.7-1.0	1.20-1.50	0.710
Al	0.05	0.03	--	--	0.041
Cu	1.00-1.30	1.16	1.00-1.30	1.00-1.30	1.26
N	0.0094	0.0055	--	--	0.0040
Nb	0.02, min	0.03	0.02	0.002	0.042

Table 6.1 Chemical compositions of copper containing steels (% by weight).

Condition	TENSILE		IMPACT	
	LYS (N/mm ²)	UTS (N/mm ²)	Energy (J)	Temperature (°C)
N & T	450	495	69	-45
Q & T	515	585	69	-62

Table 6.2 Designated tensile and impact properties of ASTM A710.

Condition	Heat treatment		Soaking time (h)	Cooling medium	Cooling rate (°C/min)
	Type	Temp(°C)			
N	austenitising	920	1/2	air	27
NT550	austenitising	920	1/2	air	37
	tempering	550	1	air	--
NT650	austenitising	920	1/2	air	36
	tempering	650	1	air	--
Q	austenitising	920	1/2	oil	1105
QT500	austenitising	920	1/2	oil	1048
	tempering	500	1	air	--
QT650	austenitising	920	1/2	oil	1142
	tempering	650	1	air	--

Table 6.3 Heat treatments of steel 1P140M.

Condition	Hr (HV10)	LYP (N/mm ²)	UTS (N/mm ²)	ε (%)	RA (%)
N	175	324*	548	35	85
NT550	227	509*	664	31	80
NT650	187	455	533	33	83
Q	242	475*	638	20	78
QT500	282	625*	734	22	72
QT650	231	560	636	21	78

* Values were taken at 0.2% proof stress

Table 6.4 Tensile properties of steel 1P140M.

Condition	Impact Transition Temperature (°C)				Energy absorbed (J)		
	at 54 J	at 27 J	at 69 J	50%FATT	at 0 °C	at RT	Shelf
N	-50	-63	-47	-20	254	261	261
NT550	-20	-40	-16	-7	202	267	290
NT650	-98	-104	-96	-76	298	300	298
Q	-71	-87	-67	-56	250	298	298
QT500	-55	-69	-55	-46	200	275	275
QT650	-117	-121	-115	-110	298	298	298

Table 6.5 Impact properties of steel 1P140M.

Condition	Ferrite grain size		Phase volume fraction (%)		
			Ferrite	Second phase	
	(μm)	($\text{mm}^{-1/2}$)		Martensite	Upper bainite
N	10.3	9.9	88	11	1
NT550	10.1	10	87	13	
NT650	10.1	10	89	11	

Table 6.6 Optical microscopy of steel 1P140M.

Condition	Grain boundary carbide thickness (μm)			Volume fraction of grain boundary particles (%)		Linear density of grain boundary particles (part./mm)		
	t_c	t_m	t_{cm}	carbide	martensite	ρ_c	ρ_m	ρ_{cm}
N	0.29	0.8	0.53	52	48	16	14	30
NT550	0.13	0.4	0.18	83	17	17	--	--
NT650	0.16	0.4	0.17	97	3	34	--	--
Q	0.24	0.91	0.62	44	56	--	--	--
QT500	--	0.6	--					
QT650	--	0.4	--					

c: grain boundary carbide

m: MA particles situated at grain boundaries

cm: grain boundary particle (carbide and/or martensite)

Table 6.7 Scanning electron microscopy of steel 1P140M.

Condition	Copper precipitate size (nm)					
	Elliptical particles				Spherical particles	
	thickness (t_p)		length (l_p)		diameter (d_p)	
	coarse	fine	coarse	fine	coarse	fine
N	33 ₍₁₉₎	none	41 ₍₁₉₎	none	41 ₍₅₎	4~8 ₍₇₀₎
NT550	47 ₍₉₎	none	76 ₍₉₎	none	51 ₍₉₎	11~22 ₍₁₅₎
NT650	50 ₍₄₇₎	14 ₍₁₂₎	102 ₍₄₇₎	26 ₍₁₂₎	70 ₍₇₎	10 ₍₃₀₎
Q	30 ₍₂₀₎	none	52 ₍₂₀₎	none	30 ₍₃₅₎	none
QT500	30 ₍₇₎	none	65 ₍₇₎	none	45 ₍₄₎	9 ₍₁₉₎
QT650	26 ₍₁₇₎	10 ₍₁₉₎	49 ₍₁₇₎	17 ₍₁₉₎	34 ₍₉₎	10 ₍₃₈₎

Numbers in brackets indicate the precipitate number, from which the above average figures were calculated.

Table 6.8 TEM (replica) copper precipitate size measurements on steel 1P140M.

Condition	Cu and Nb available for precipitation		Precipitate volume fraction (f)		Dispersion strengthening effect $\sigma = 2\tau$, (N/mm ²)		
	%Cu	%Nb	'f' _{Cu} × 10 ⁻³	'f' _{Nb} × 10 ⁻⁴	σ_{Cu}	σ_{Nb}	σ_{total}
N	0.63	0.042	5.598	4.904	74	75	149
NT550	0.97	0.042	8.600	4.904	62	46	108
NT650*	0.97	0.042	8.600	4.904	58	56	114
Q	0.38	--	3.359	--	71	--	71
QT500	0.97	0.042	8.600	4.904	84	61	145
QT650*	0.97	0.042	8.600	4.904	96	56	152

* Equilibrium condition

Table 6.9 Estimated dispersion strengthening effect (Ashby model), based on copper and niobium precipitate size as measured from TEM photographs.

Condition	LYS (N/mm ²)						
	obs	calc ⁽¹⁾	δ LYS ⁽¹⁾	calc ^{(1)*}	δ LYS ^{(1)*}	calc ⁽²⁾	δ LYS ⁽²⁾
N	324	363	-39	339	-15	312	+12
NT550	509	365	+144	326	+183	314	+195
NT650	455	365	+90	326	+129	314	+141
Q	475	438	+37	423	+52	375	+100
QT500	625	438	+187	399	+226	375	+250
QT650	560	438	+122	399	+161	375	+185

(1) LYS is calculated by using equation 2.11, i.e. taking alloying additions into account.

(2) LYS is calculated by using equation 2.10, i.e. for plain ferrite-pearlite C-Mn steels.

* corrected values for LYS⁽¹⁾ and δ LYS after taking into account the amount of copper that has precipitated out of the solution.

Table 6.10 Comparison between observed and calculated lower yield strength values, of steel 1P140M.

Condition	Yield strength (N/mm ²)	Transition Temperature (°C)		
		27 J	54 J	50%FATT
Normalised	436	-105	-80	-45
Normalised + T 500 °C	527	-103	-92	-35
Normalised + T 550 °C	544	-105	-95	-25
Normalised + T 600 °C	522	-110	-90	-50
Quenched + T 500 °C	614	-95	-70	-10
Quenched + T 550 °C	588	-100	-90	-20
Quenched + T 600 °C	530	-110	-108	-65

Table 6.11 Crowther's results for a modified IN787 steel [52].

Condition	t_c (μm)	Impact Transition Temperatures ($^{\circ}\text{C}$)								
		at 54 (J)			at 27 (J)			50% FATT		
		obs	calc	δITT	obs	calc	δITT	obs	calc	δFATT
N	1	-50	+35	-85	-63	+13	-76	-20	+17	-37
NT550	1	-20	+126	-146	-40	-80	-120	-7	+98	-105
NT650	0.17	-98	-14	-84	-104	-41	-63	-76	-3	-73
Q	1	-71	+37	-108	-87	+12	-99	-56	+4	-60
QT500	0.6	-55	+69	-124	-69	+28	-97	-46	+42	-88
QT650	0.4	-117	+9	-126	-121	-20	-101	-110	-6	-104

The ITT values were calculated using $\delta\text{LYS}^{(2)}$ values, (table 6.10), i.e. not taking alloying elements into account

t_c : the value of grain boundary carbide thickness used in Equations 2.7, 2.8 and 2.9

Table 6.12 Comparison between observed and calculated impact transition temperatures, of steel 1P140M.

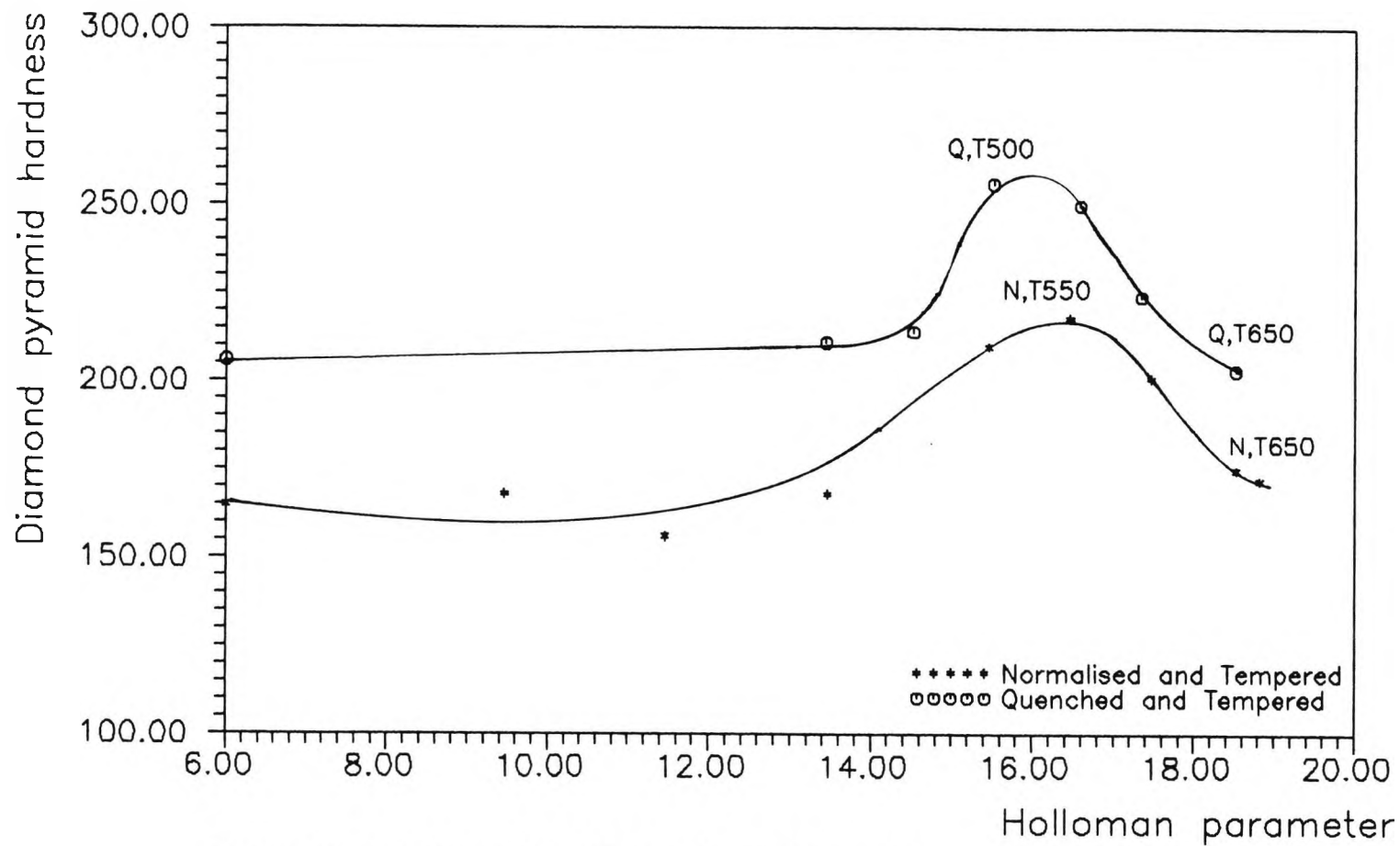


Figure 6.1 Age-hardening effect of tempering on normalised and oil-quenched 1P140M steel plate.

ITT curves

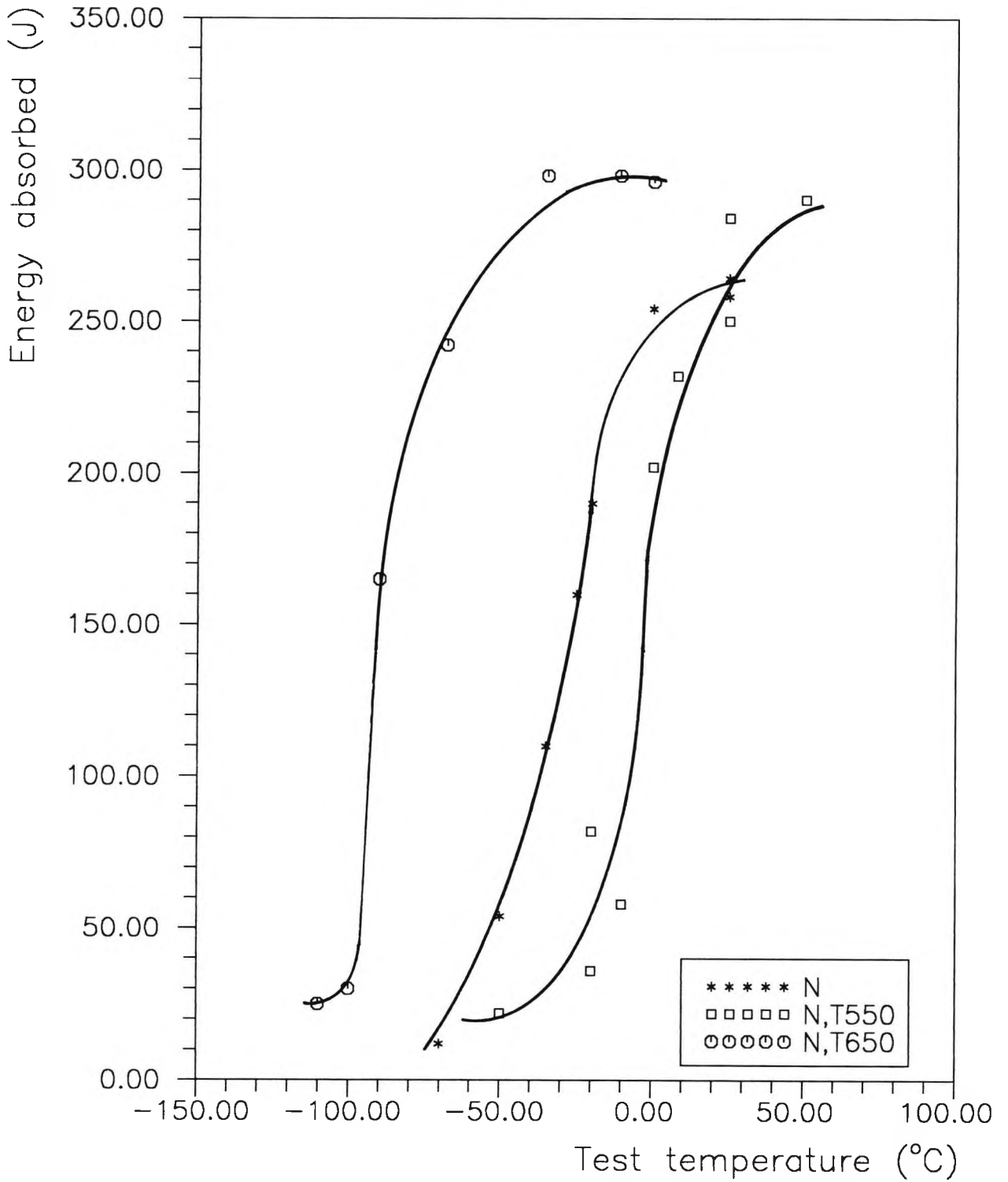


Figure 6.2 Impact transition temperature curves for normalised and aged 1P140M steel.

ITT curves

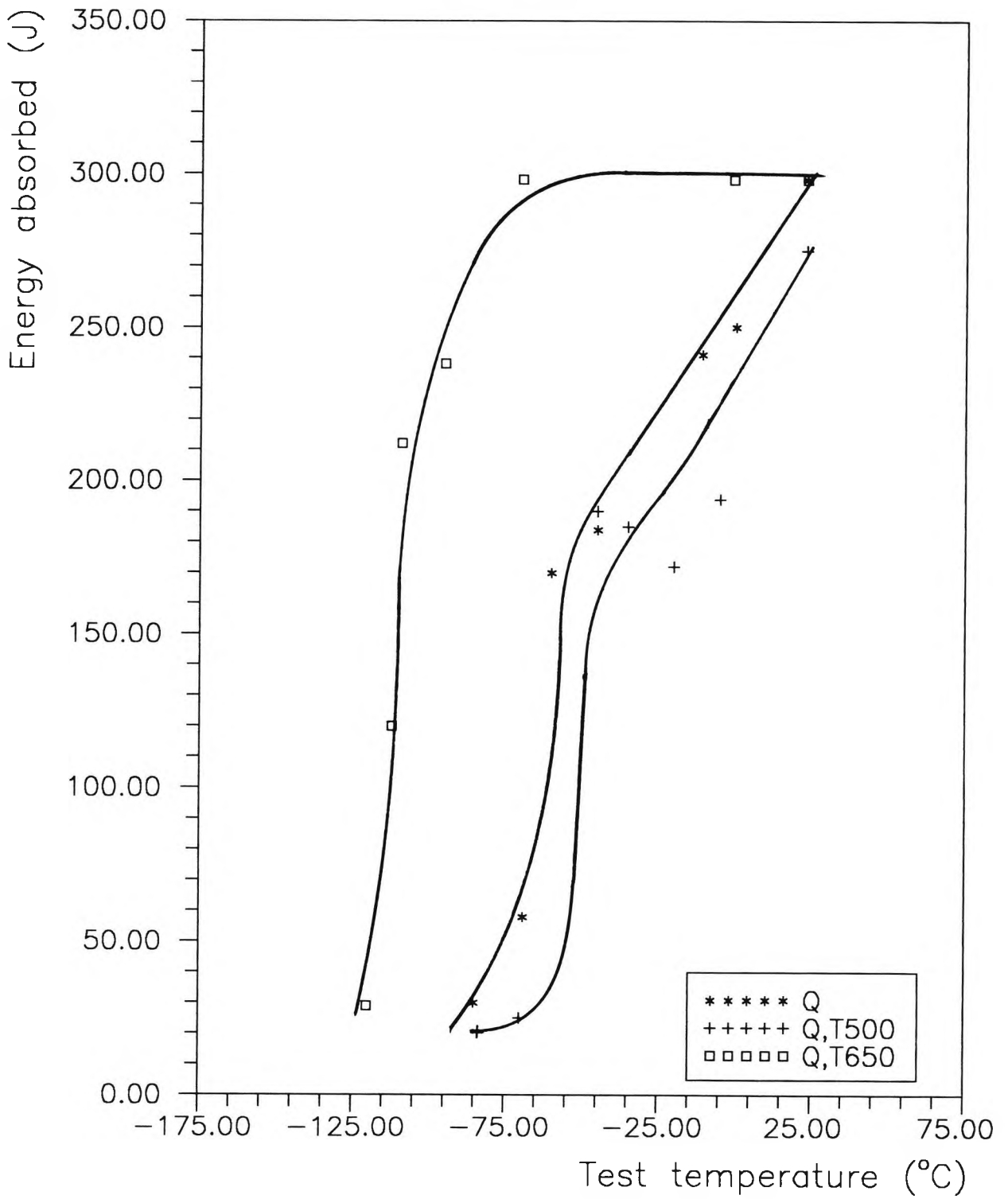


Figure 6.3 Impact transition temperature curves for quenched and aged 1P140M steel.

50% FATT curves

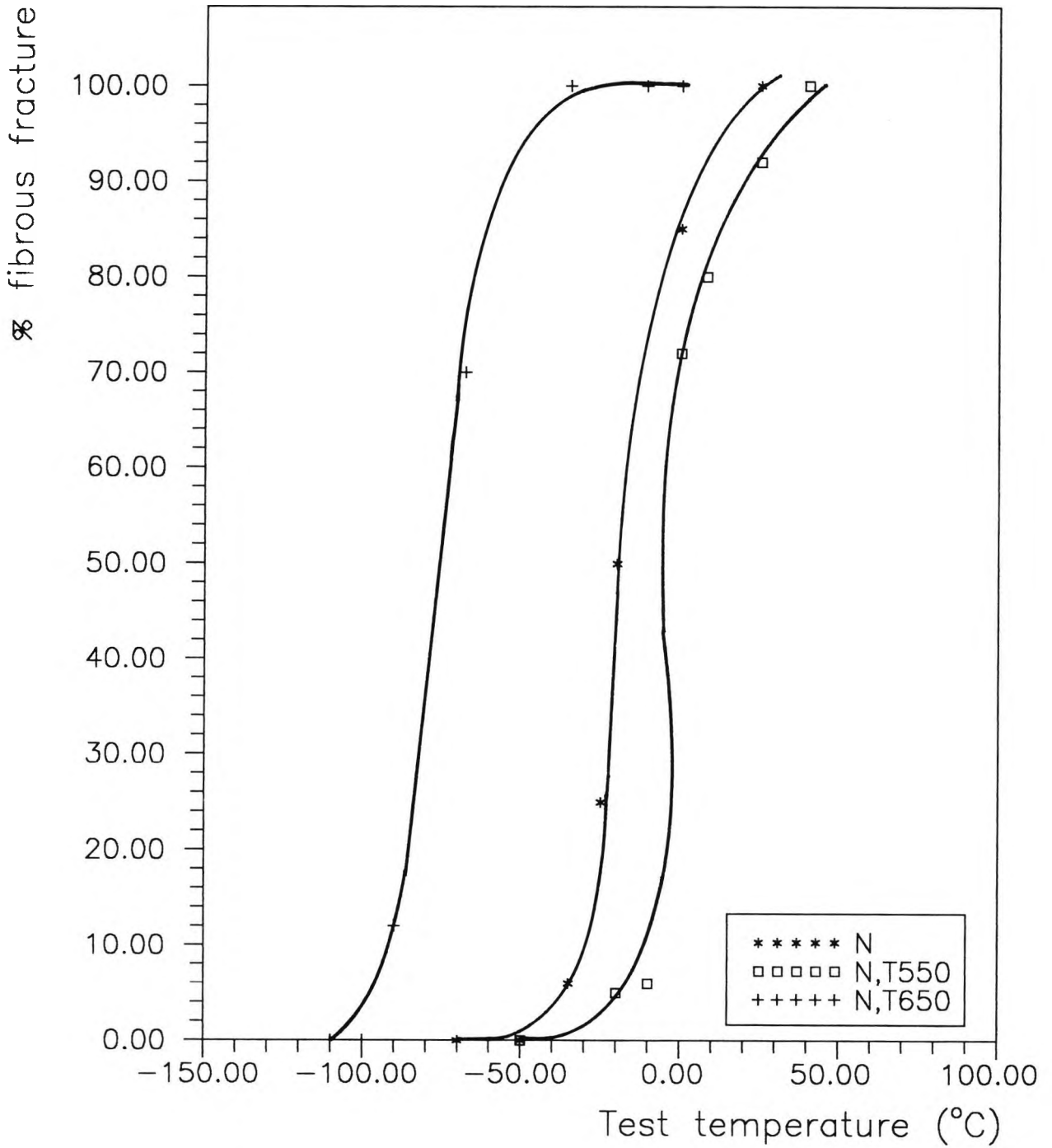
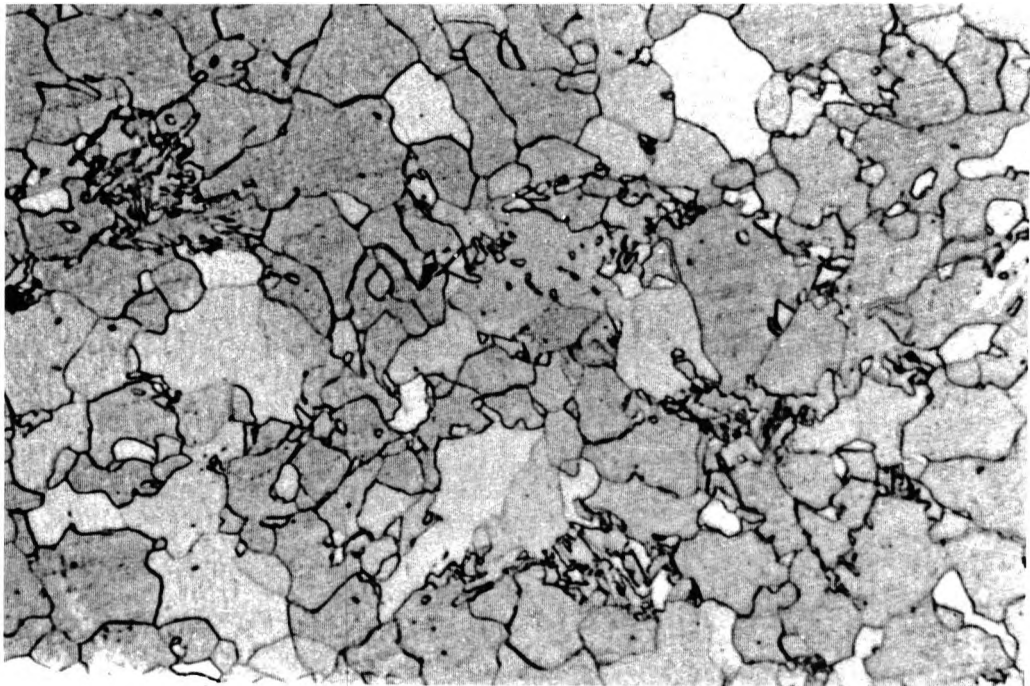
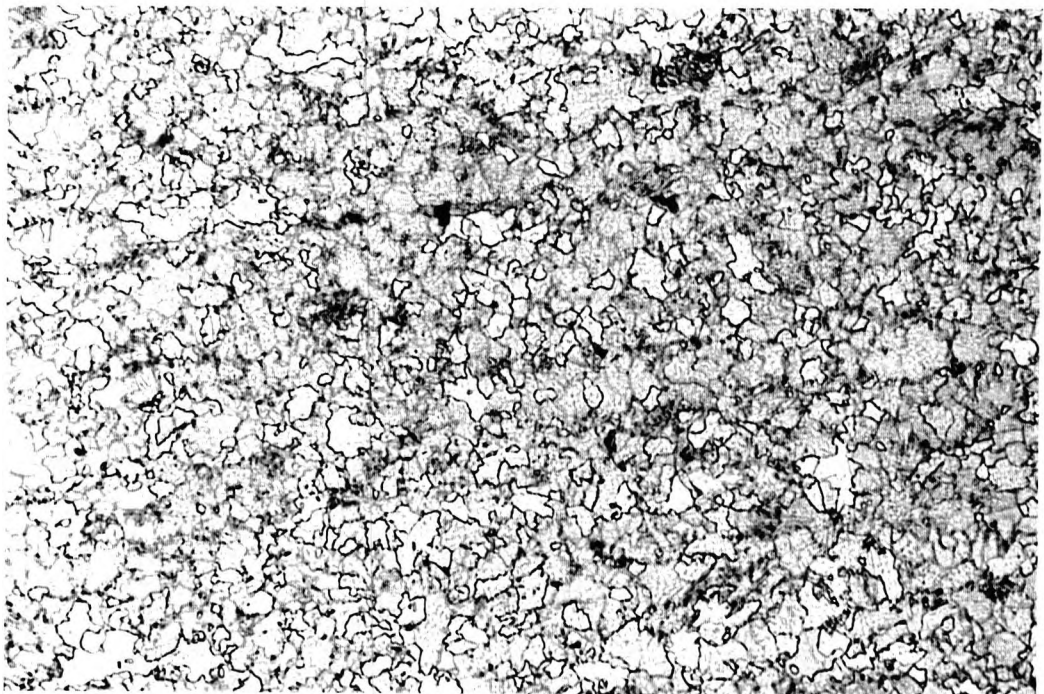


Figure 6.4 50% Fibrous appearance transition temperature curves for normalised and aged 1P140M steel



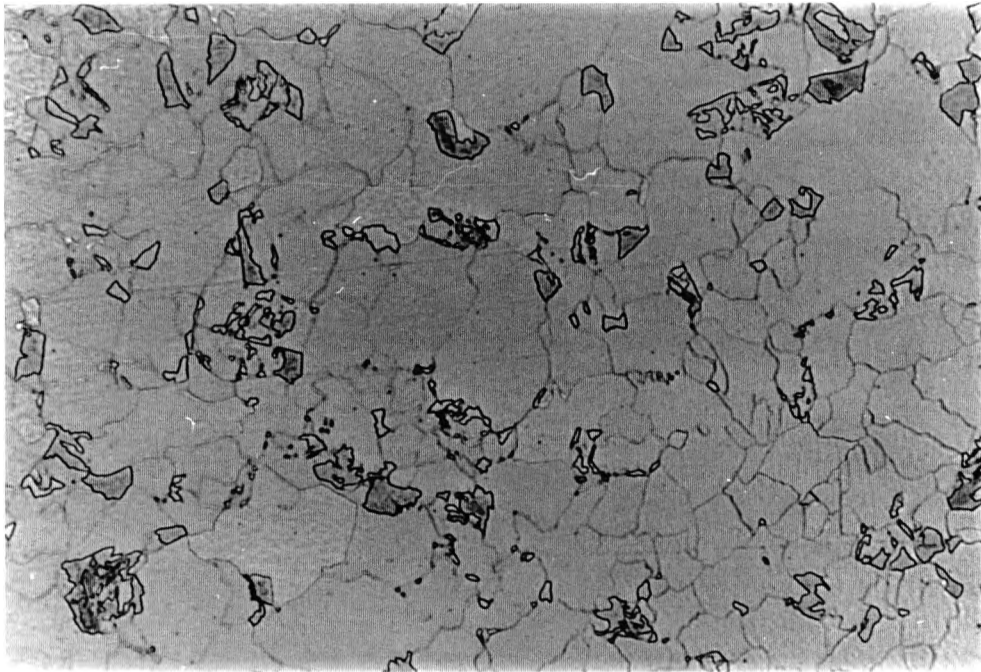
x800

Figure 6.5 Optical micrograph of the as-normalised 1.26% Cu-steel.



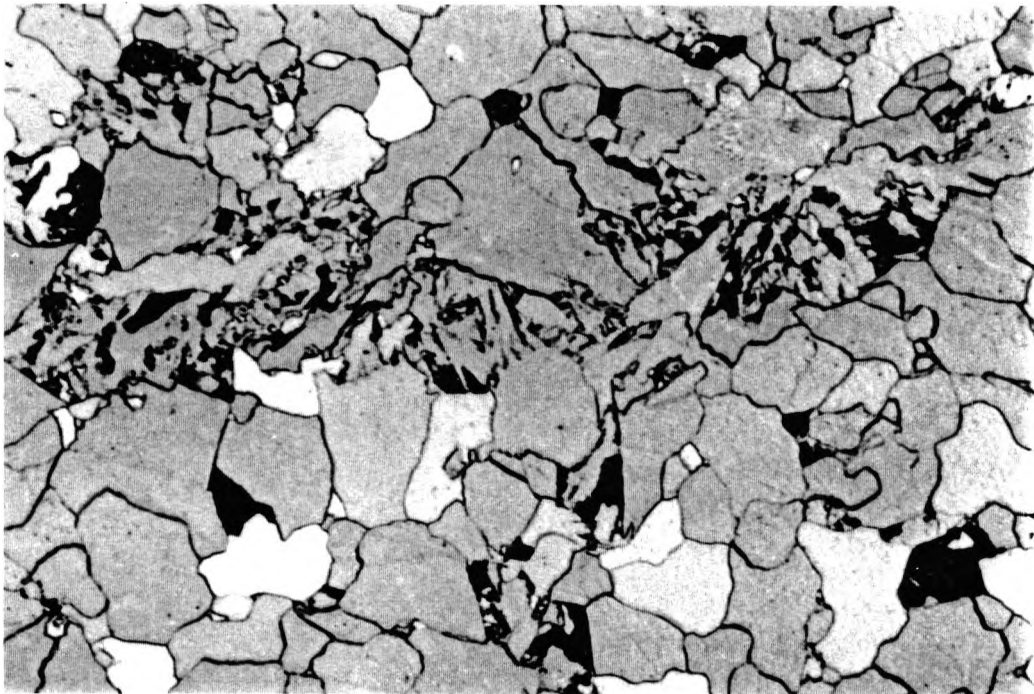
x200

Figure 6.6 Optical micrograph of the as-normalised 1.26% Cu-steel.



x800

Figure 6.7 The distinction between the ferrite and the second phase in the normalised and aged (200°C for 1h) 1.26% Cu steel (light etching, optical micrograph).



x800

Figure 6.8 The darkening of the second phase after tempering the normalised 1.26% Cu-steel at 550°C for 1h. (Optical micrograph)

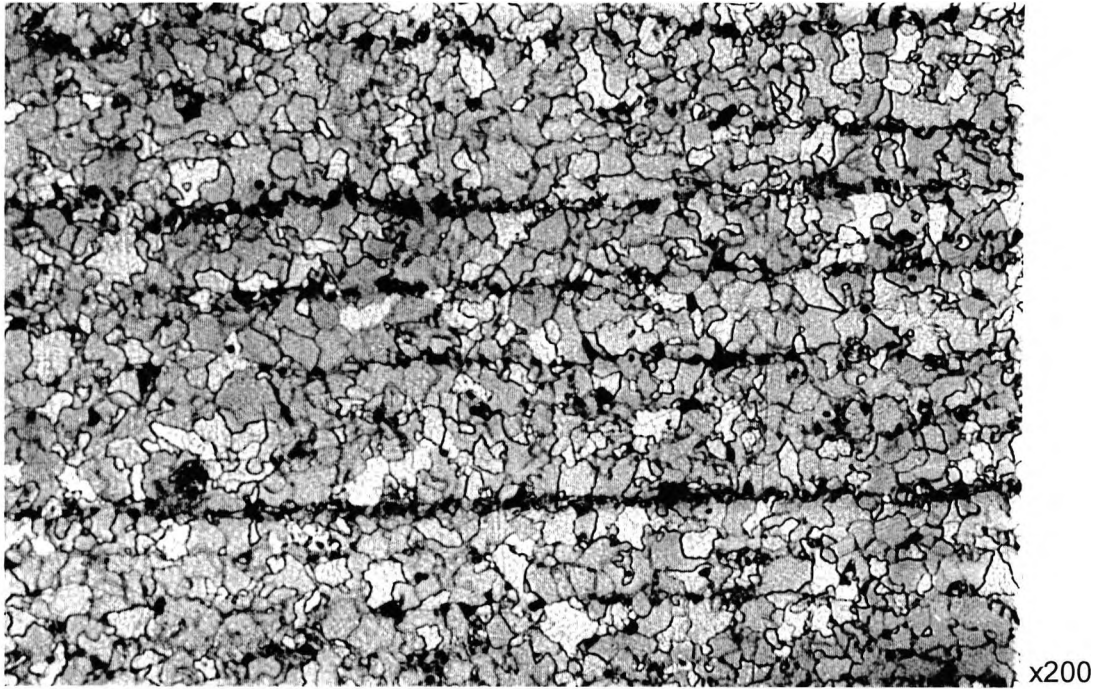


Figure 6.9 Optical micrograph of sample (NT550), 1.26% Cu-steel.

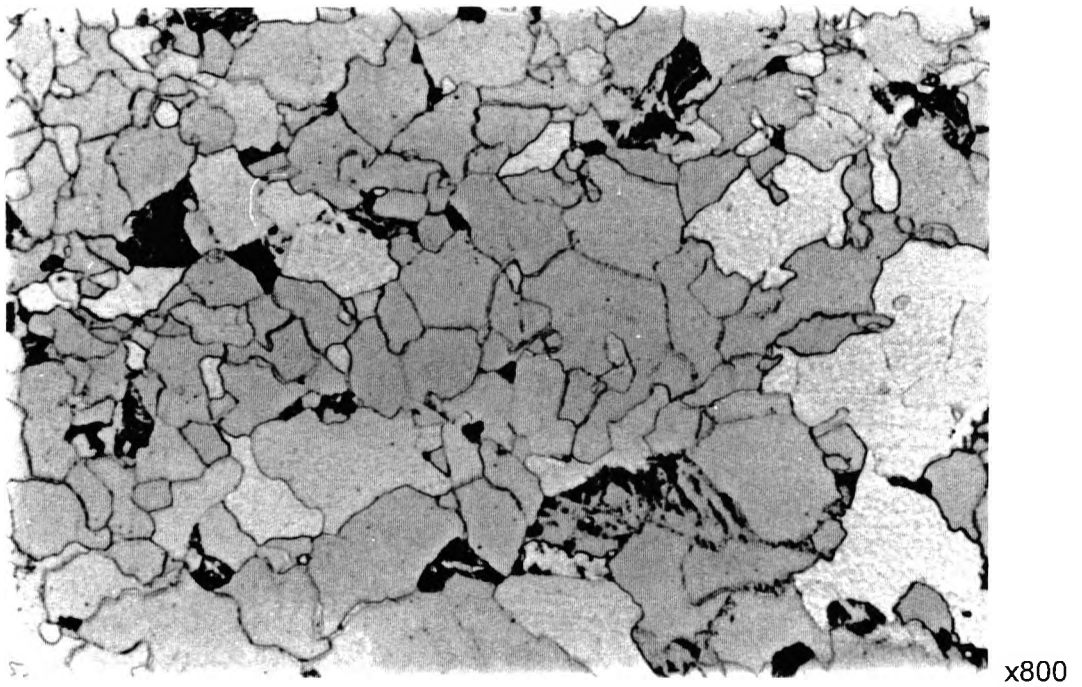


Figure 6.10 Optical micrograph of the normalised and over-aged 1.26%-Cu steel plate, (NT650).

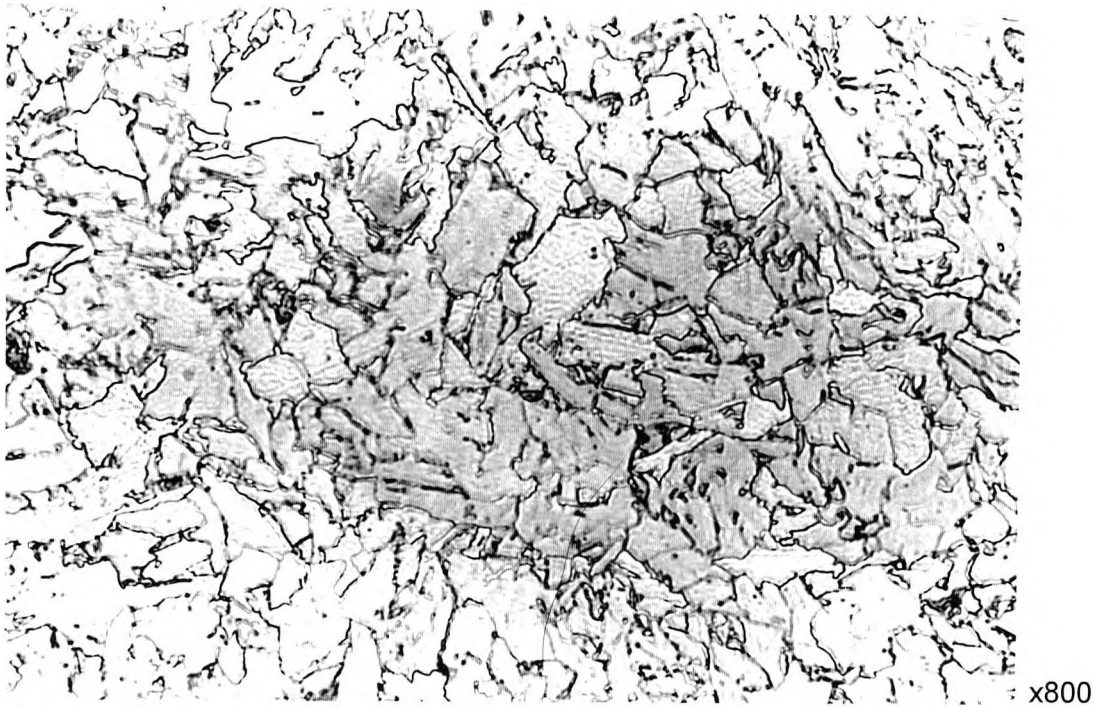


Figure 6.11 Optical micrograph of the oil-quenched 1.26% Cu-steel, (Q).

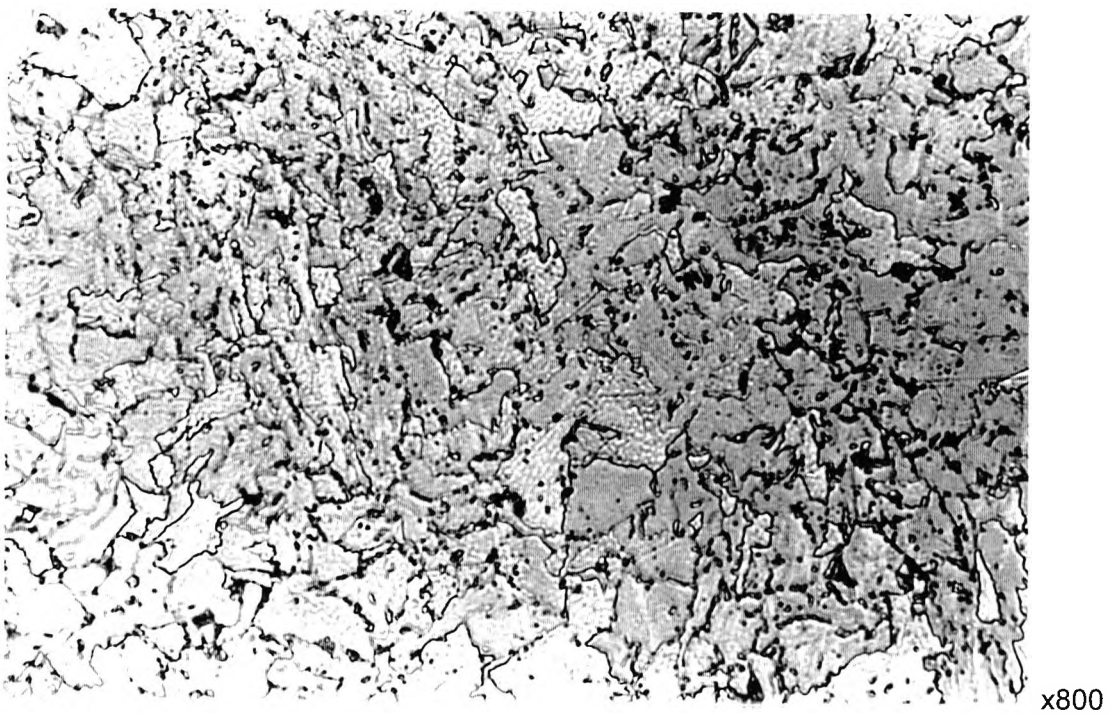


Figure 6.12 Quenched and fully-aged (QT500) microstructure of 1.26% Cu-steel.

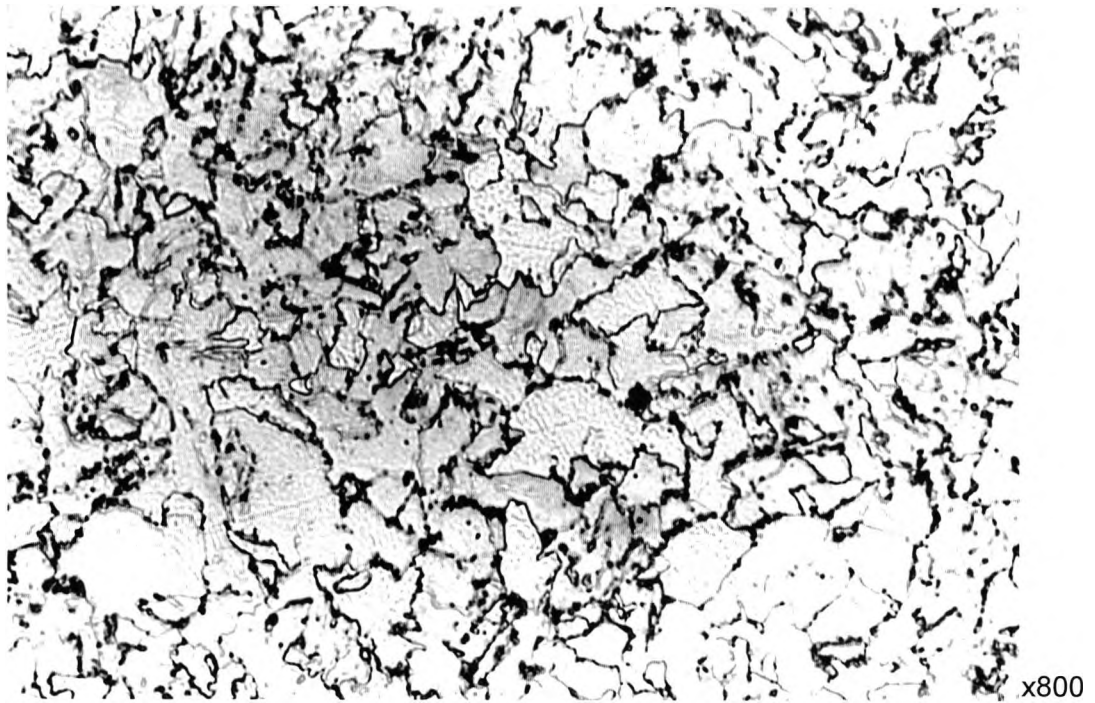


Figure 6.13 Optical micrograph showing the darkening of the martensite after tempering the quenched 1.26% Cu-steel at 650°C for 1 h, (QT650).

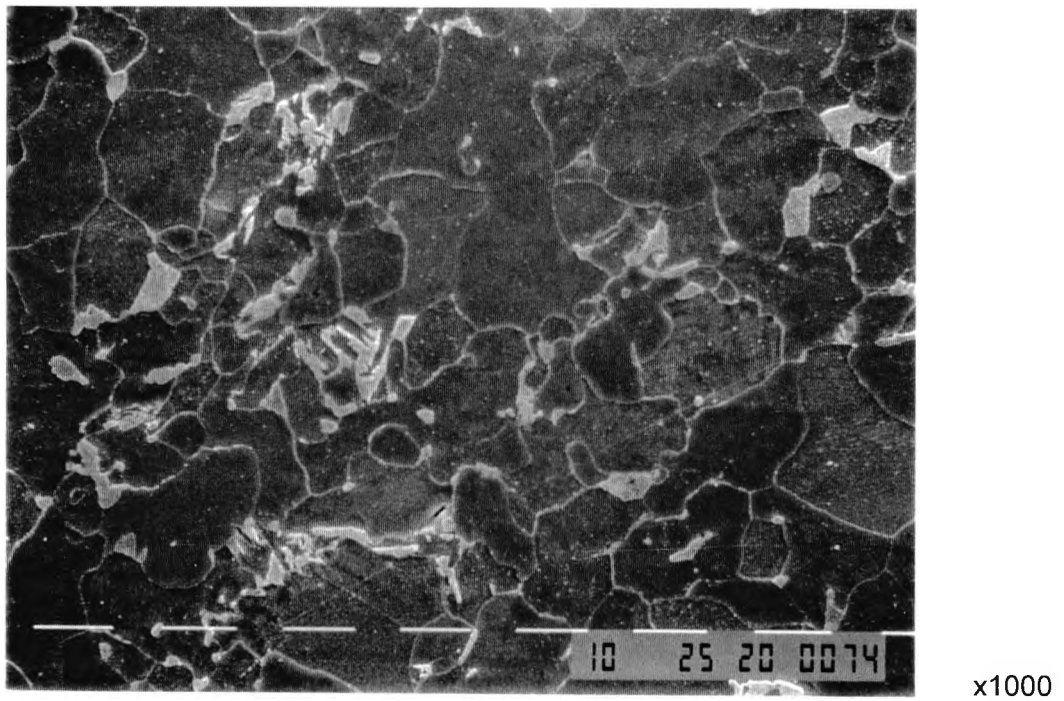
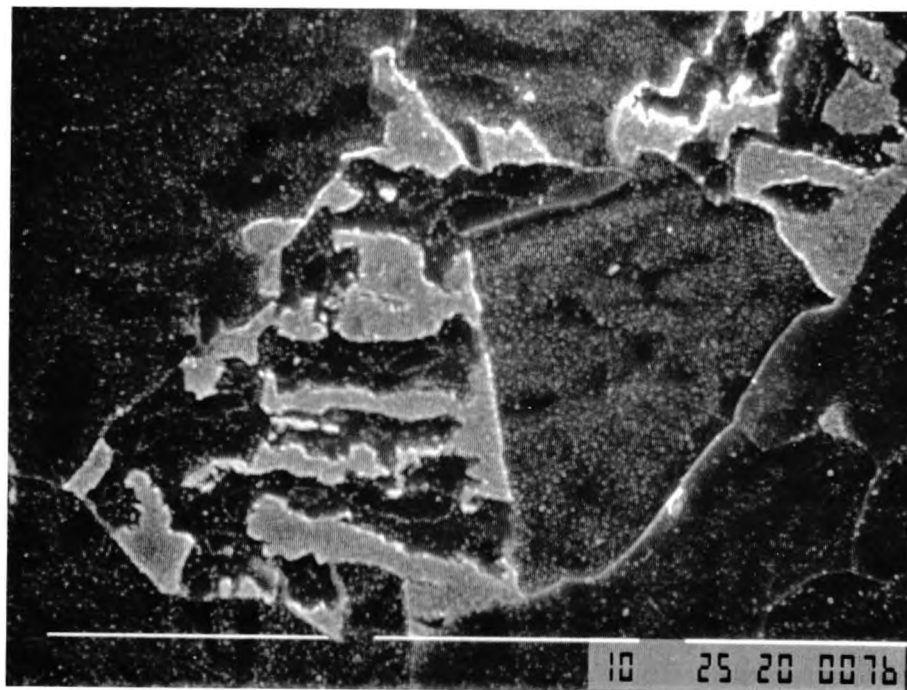
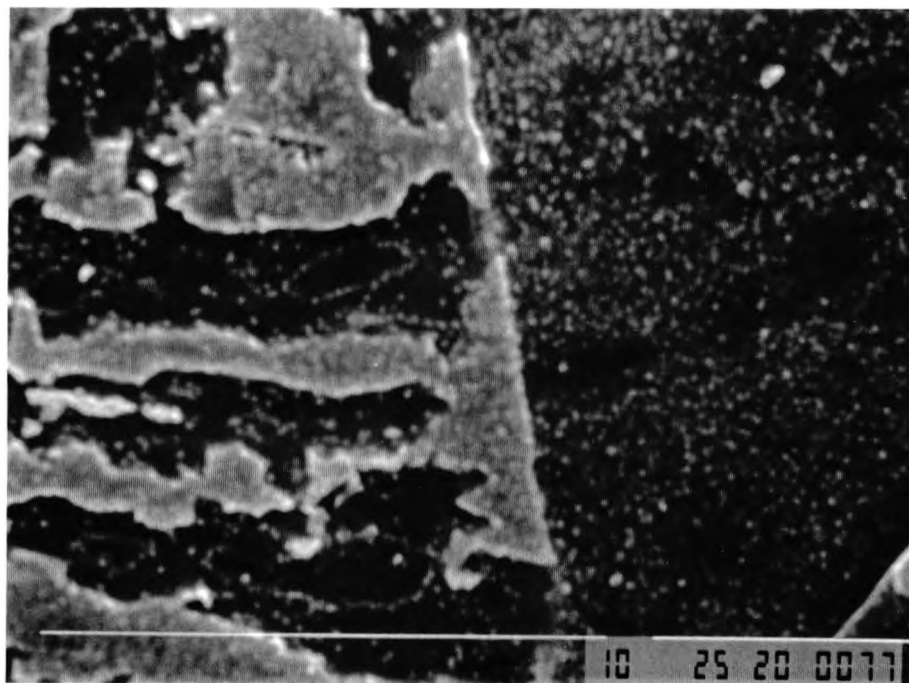


Figure 6.14 Scanning electron micrograph showing the microstructure of the as-normalised 1.26% Cu-steel.



(a)



(b)

Figure 6.15 Scanning electron micrograph of the as-normalized, (N), 1.26% Cu steel, showing: (a) a group of martensite-austenite islands (b) coarse precipitation -possibly copper- in the ferrite matrix and in the (MA) constituent.

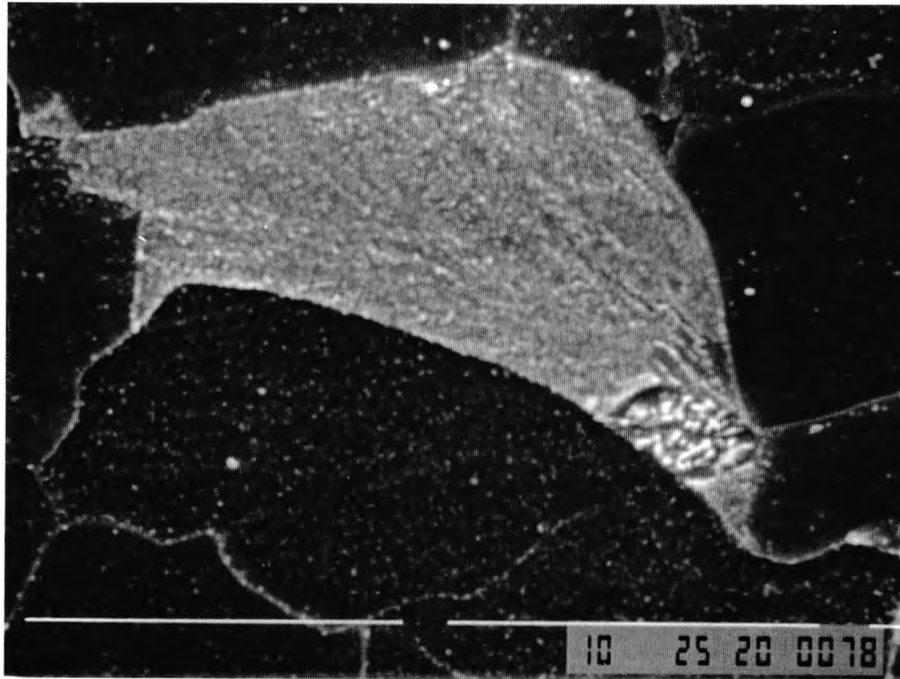


Figure 6.16 Scanning electron micrograph of the as-normalised 1.26% steel, showing a coarse martensite colony.

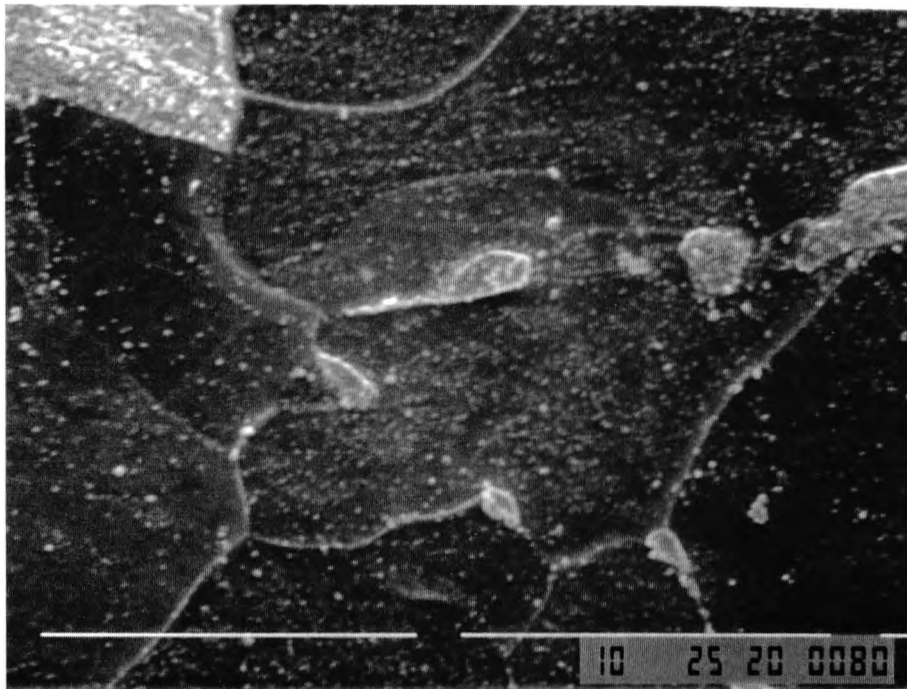


Figure 6.17 Scanning electron micrograph, showing coarse grain boundary particles, in the as-normalised 1.26% Cu-steel.

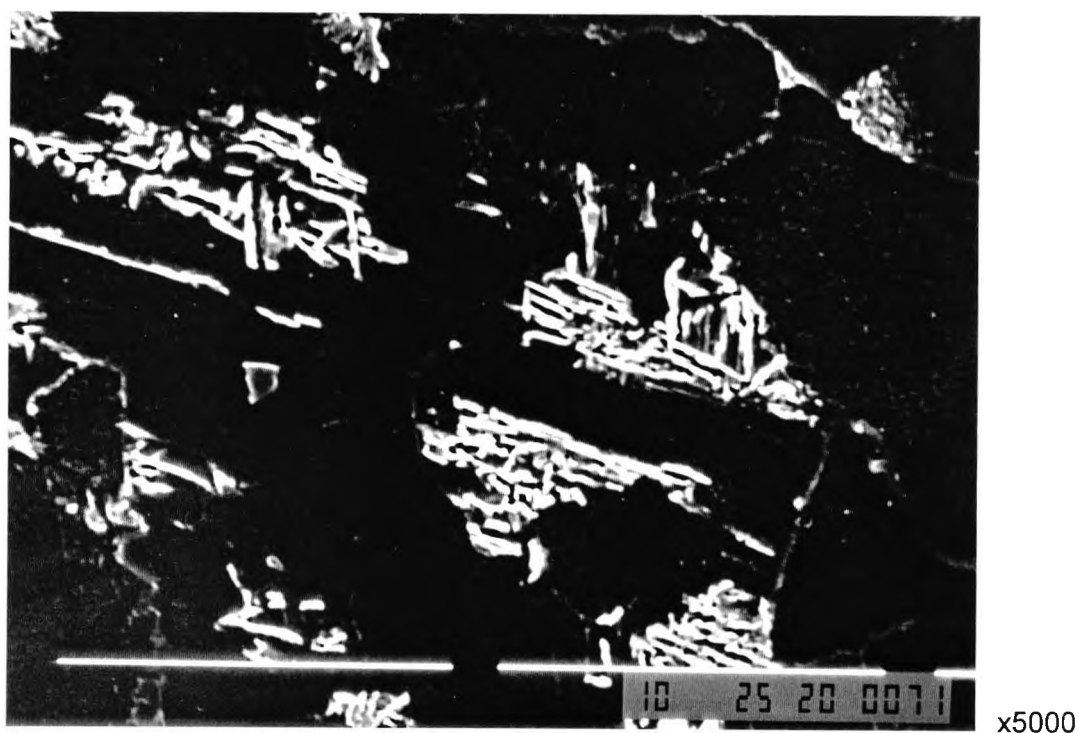
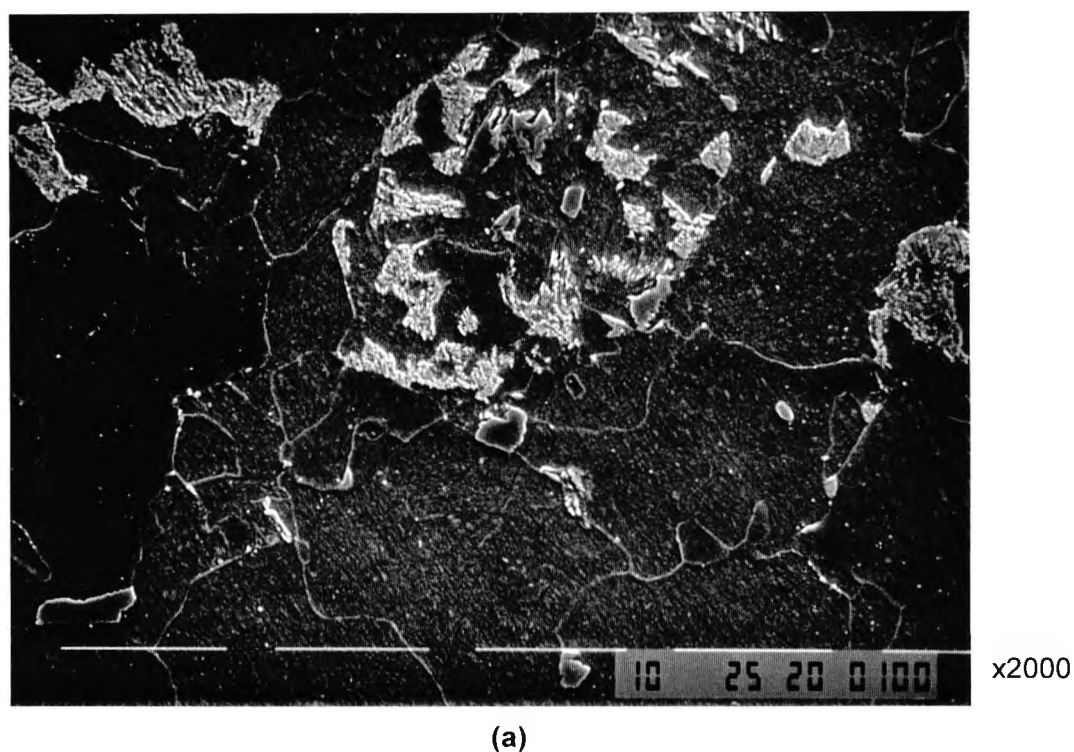
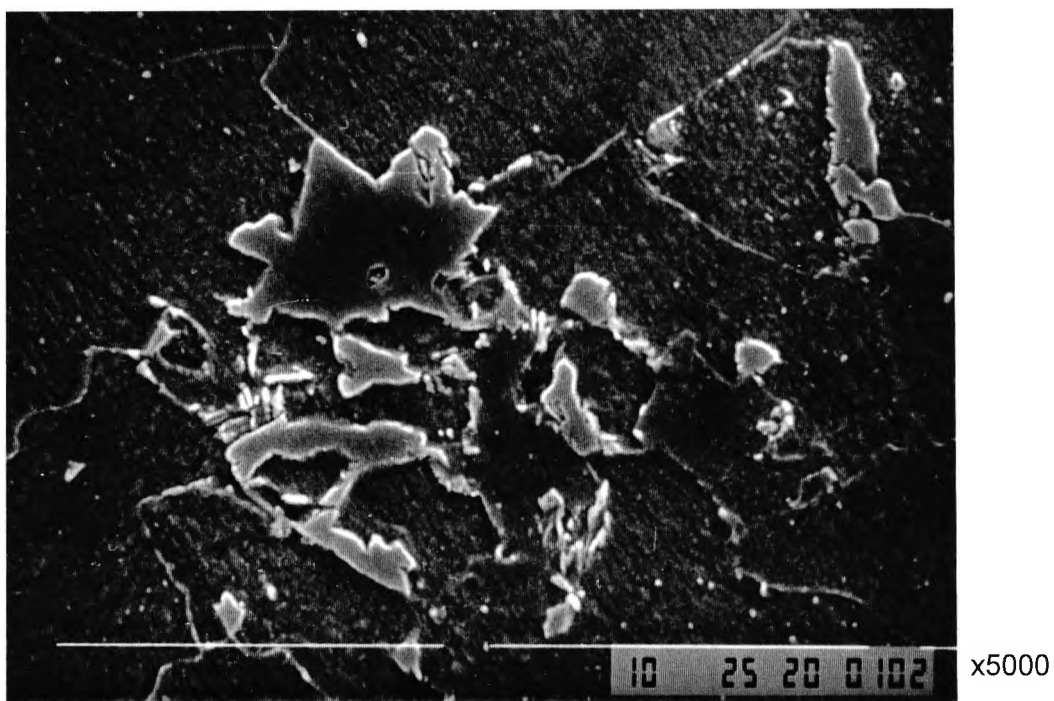


Figure 6.18 Scanning electron micrograph of the normalised and fully-aged 1.26% Cu-steel (NT550), showing tempered (MA) particles.



(a)

Figure 6.19 Scanning electron micrographs of (NT550) 1.26% Cu-steel, showing groups of (MA) islands: (a) fully tempered (b) unaffected by the tempering treatment.



(b)

Figure 6.19 Scanning electron micrographs of (NT550) 1.26% Cu-steel, showing groups of (MA) islands: (a) fully tempered (b) unaffected by the tempering treatment.

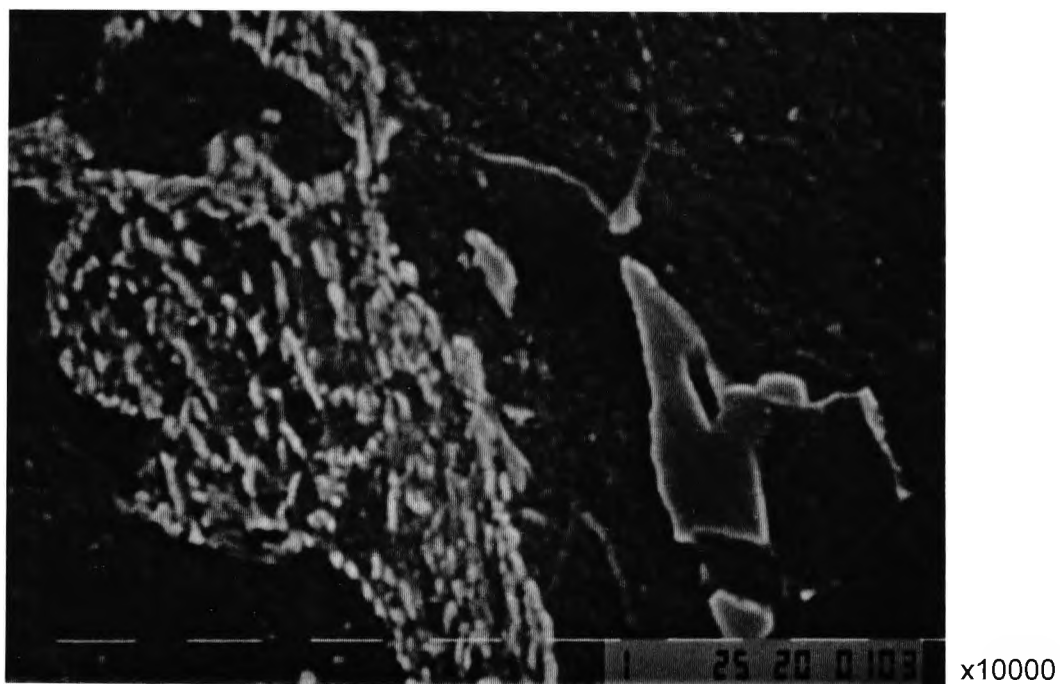


Figure 6.20 Scanning electron micrograph of the (NT550) 1.26% Cu-steel, showing two (MA) particles, one showing carbide precipitation, the other being unaffected by tempering.

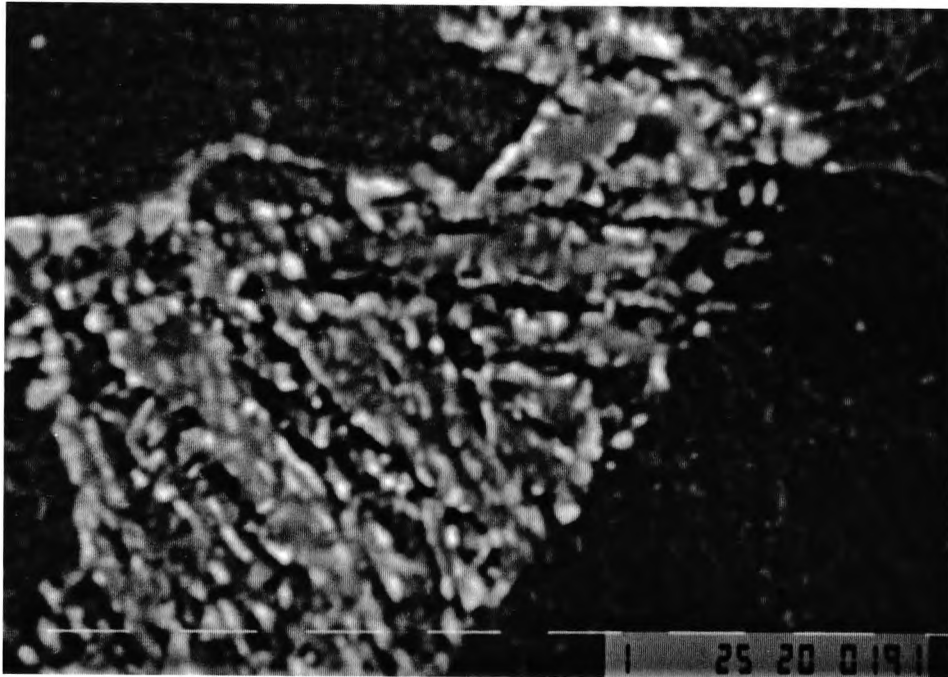


Figure 6.21 Scanning electron micrograph of normalised and over-aged 1.26% Cu-steel (NT650), showing carbide precipitation from a tempered martensitic particle.

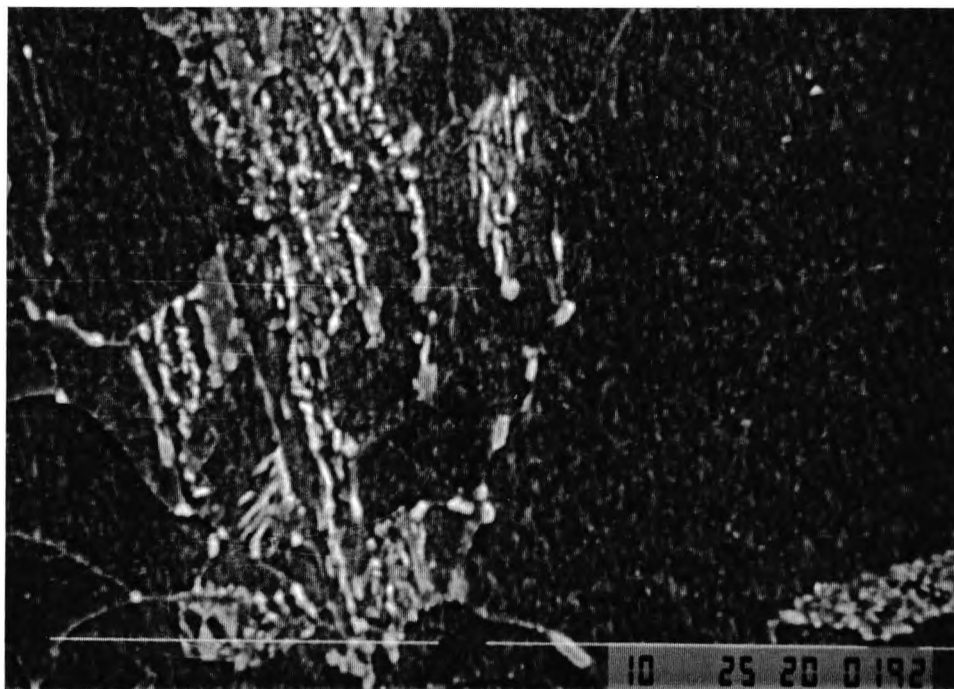


Figure 6.22 Scanning electron micrograph of 1.26% Cu-steel, in the normalised and over-aged condition (NT650).

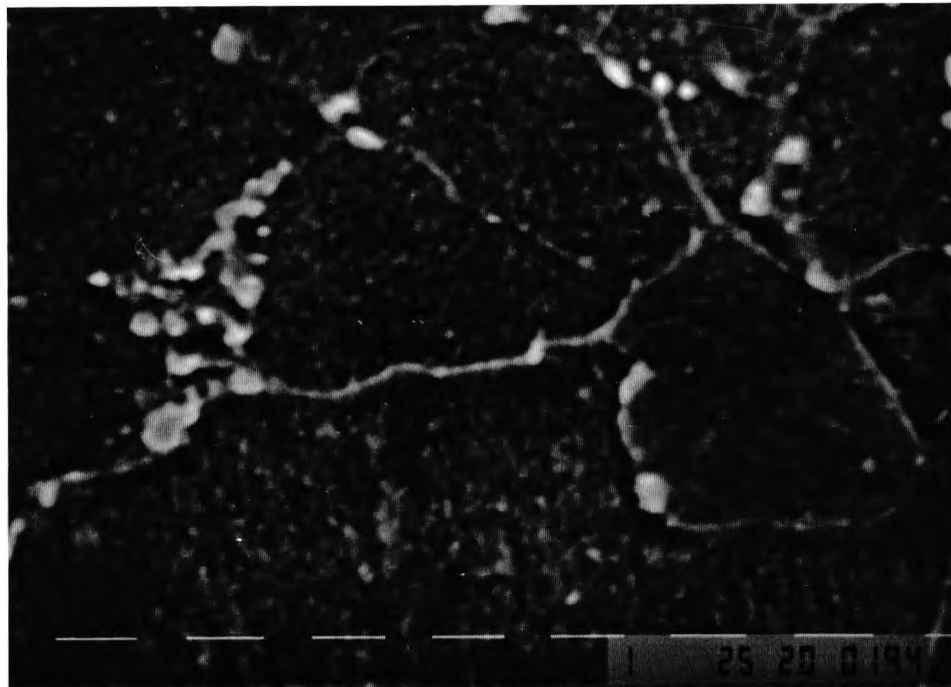


Figure 6.23 Scanning electron micrograph of sample (NT650), 1.26% Cu-steel, showing the increased number of grain boundary carbides.

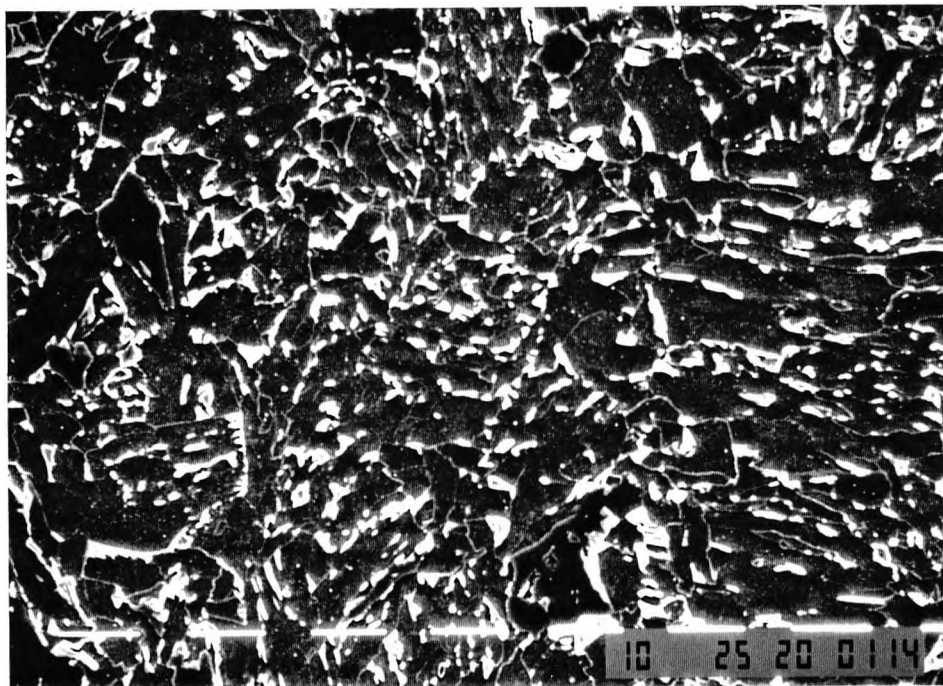
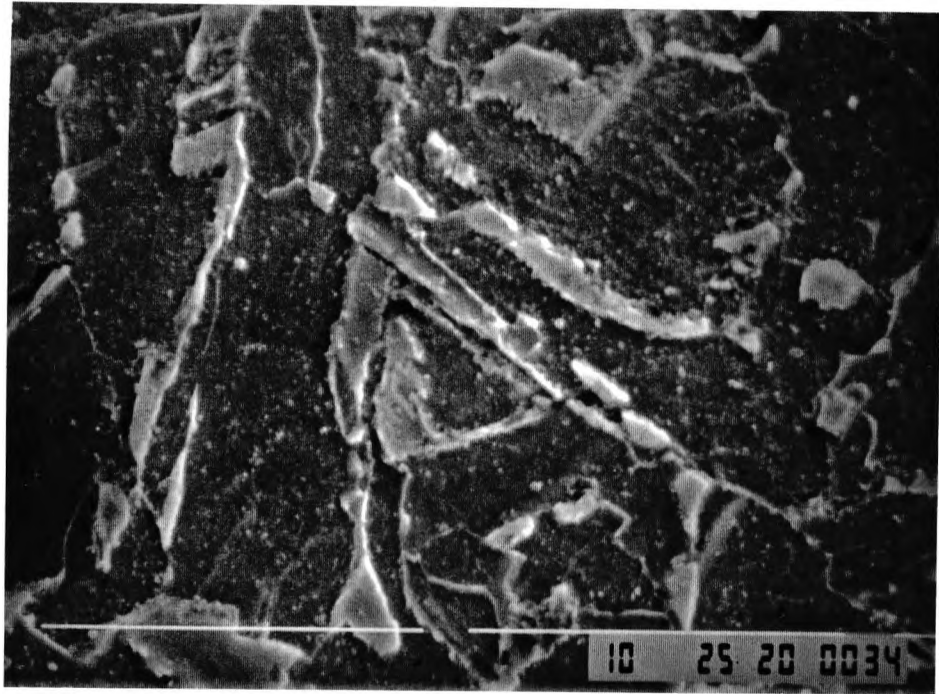
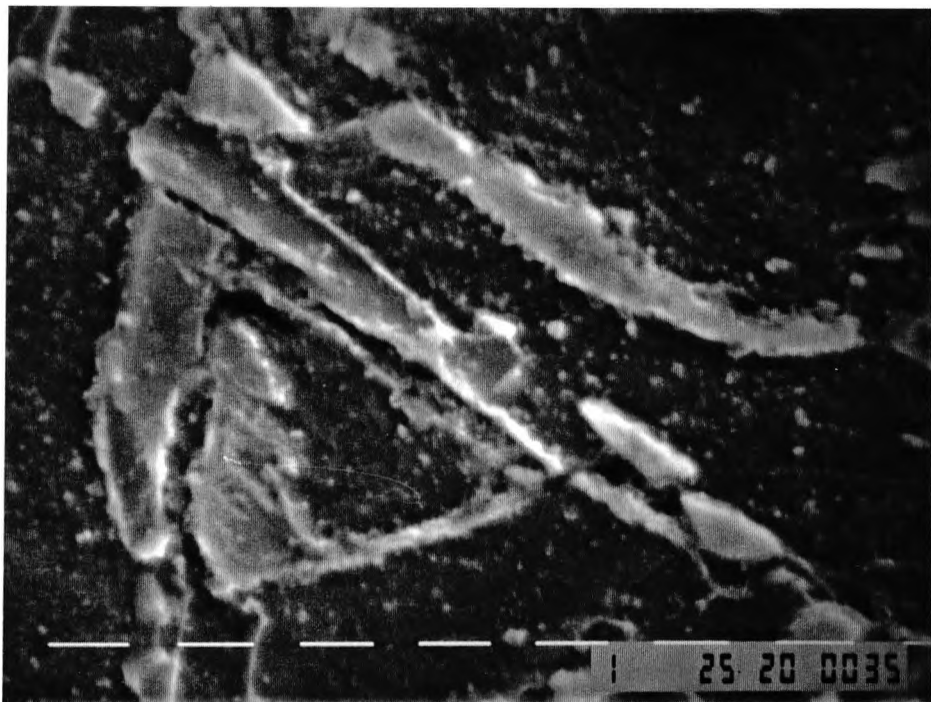


Figure 6.24 Scanning electron micrograph, of the as-quenched (Q), 1.26% Cu-steel.



(a)



(b)

Figure 6.25 Scanning electron micrographs, showing (MA) particles, in the as-quenched 1.26% Cu-steel.

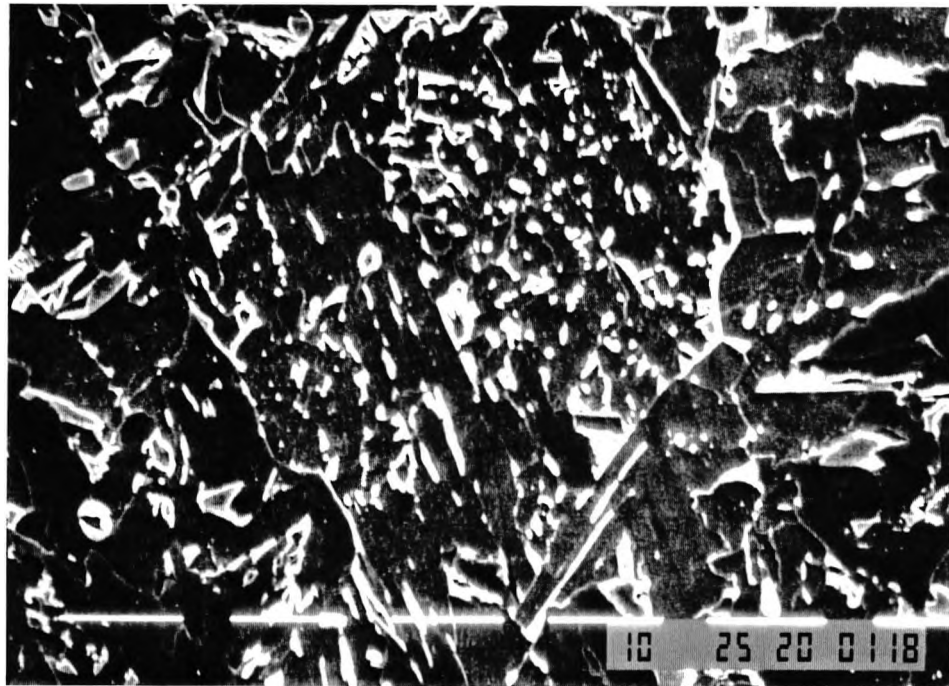


Figure 6.26 Scanning electron micrograph of the as-quenched (Q) 1.26% Cu-steel, showing the arrangement of ferrite laths and (MA) particles.

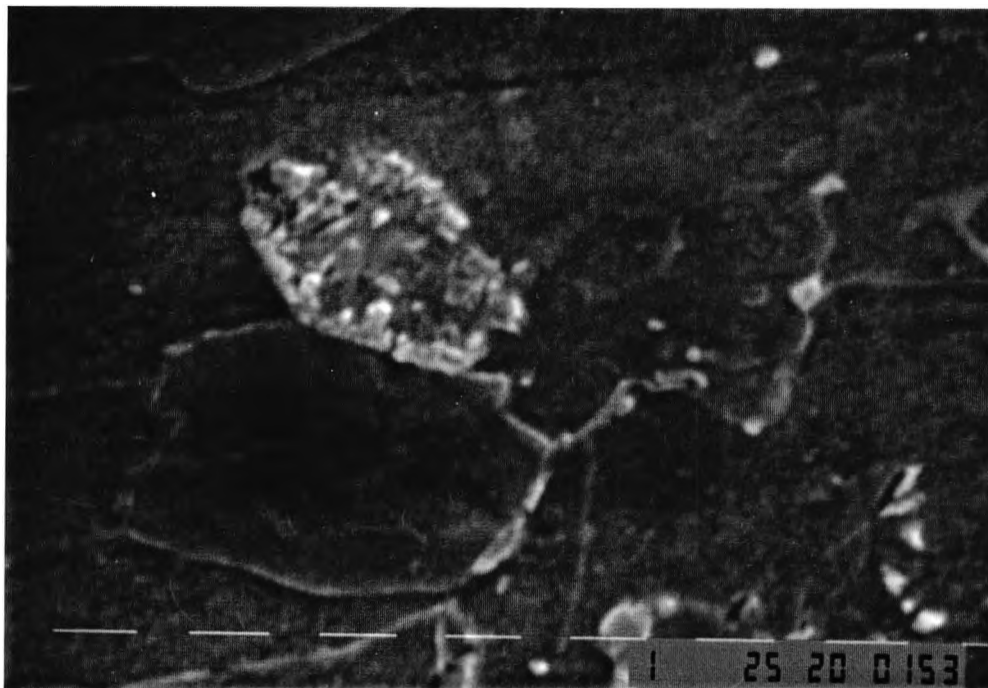


Figure 6.27 Scanning electron micrograph of the quenched and fully-aged (tempered at 500°C for 1 h) 1.26% Cu-steel, showing carbide precipitation from a martensitic particle..

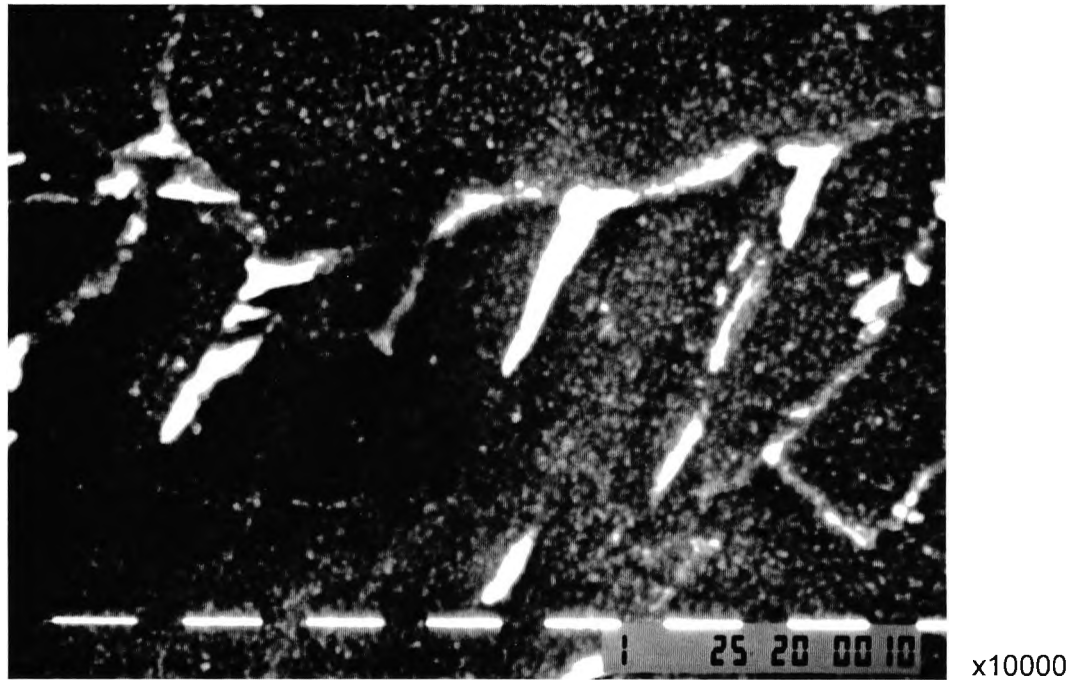


Figure 6.28 Scanning electron micrograph of the quenched and fully-aged 1.26% Cu-steel (QT500), showing evidence of copper precipitation.

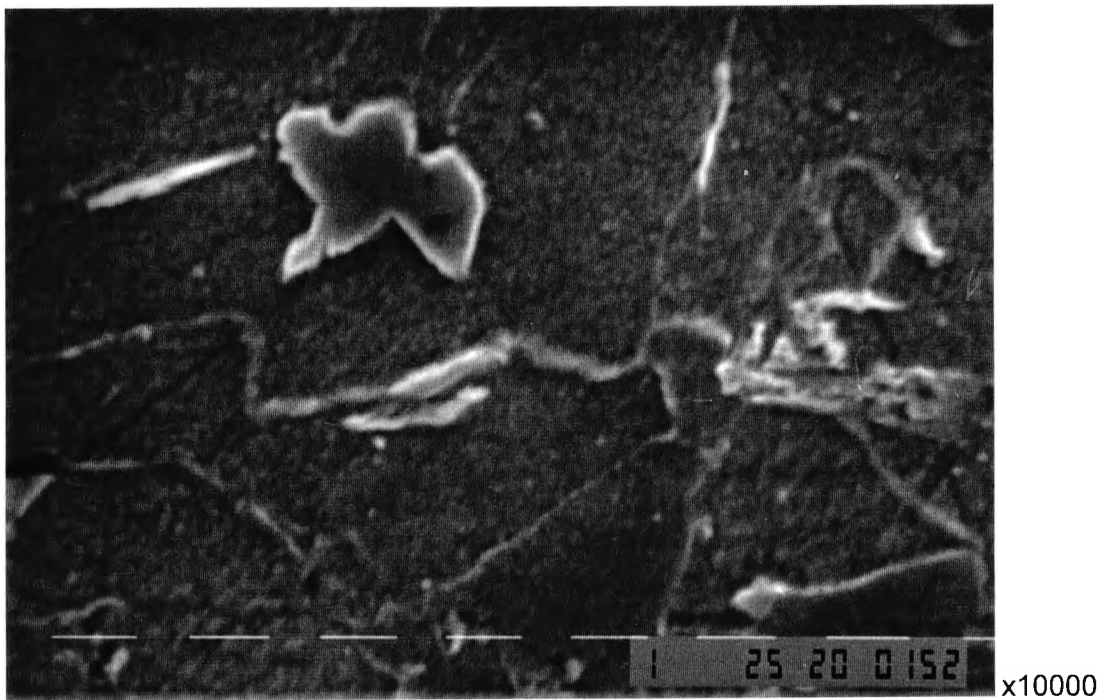
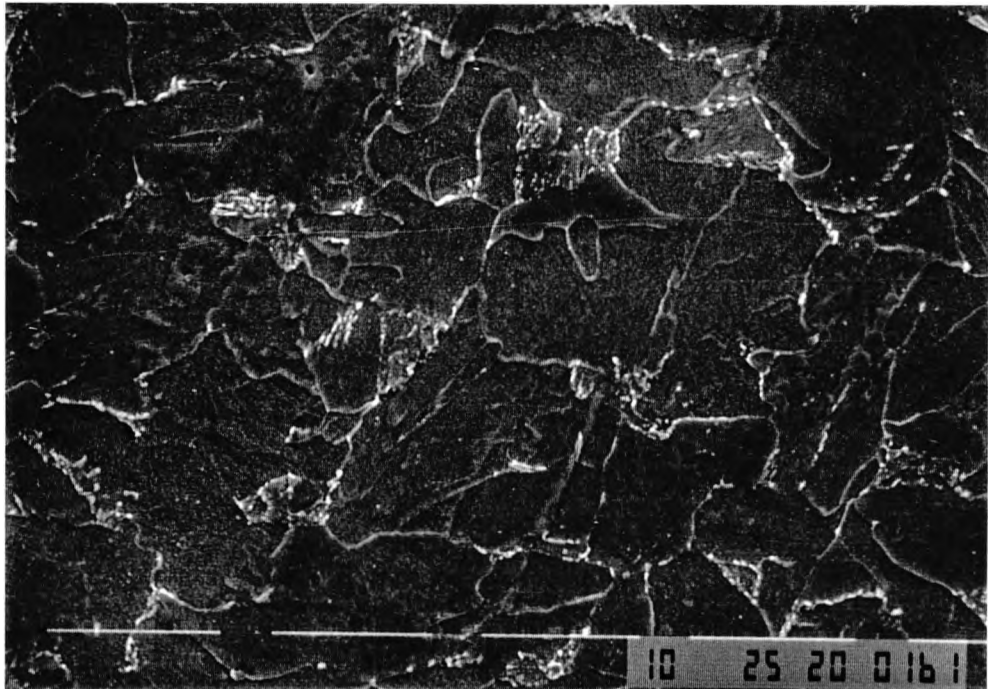
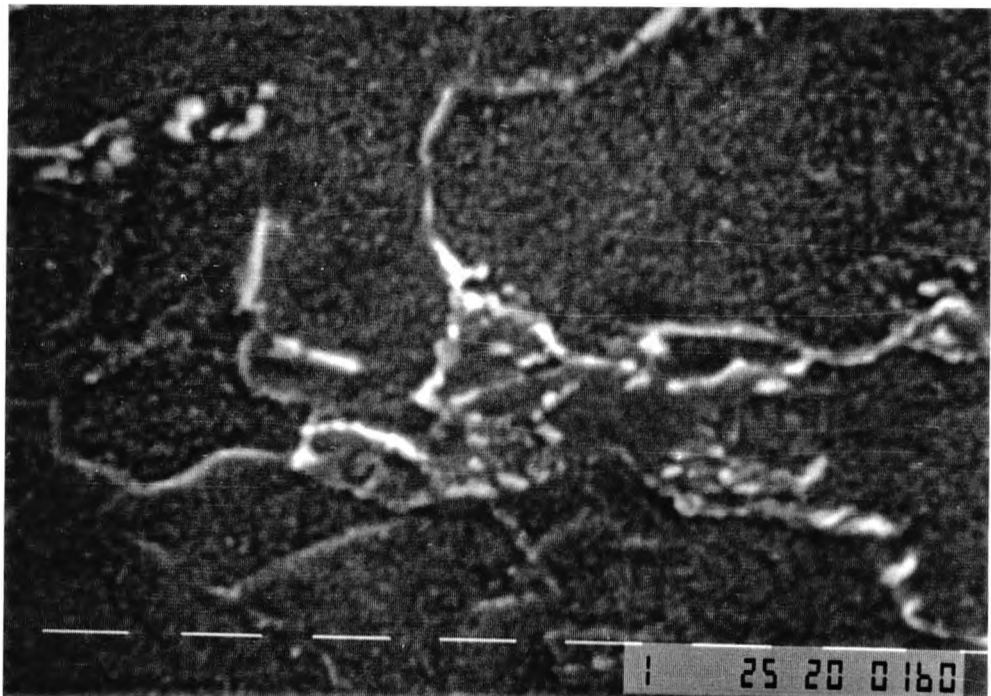


Figure 6.29 Scanning electron micrograph of the (QT500) condition, 1.26% Cu-steel, showing a martensitic particle unaffected by tempering.

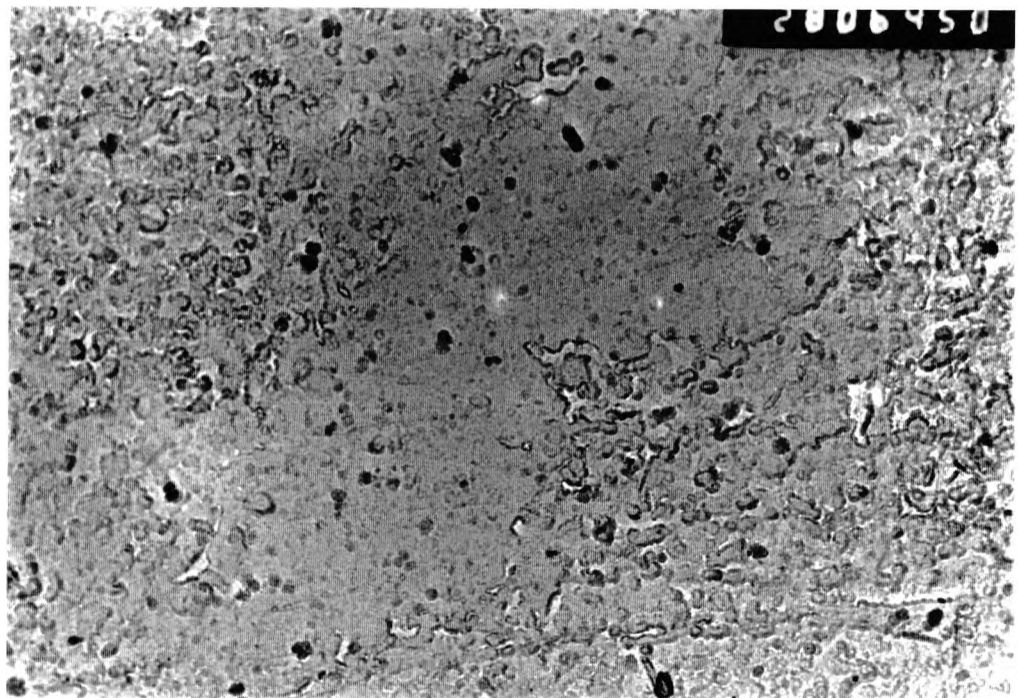


(a)

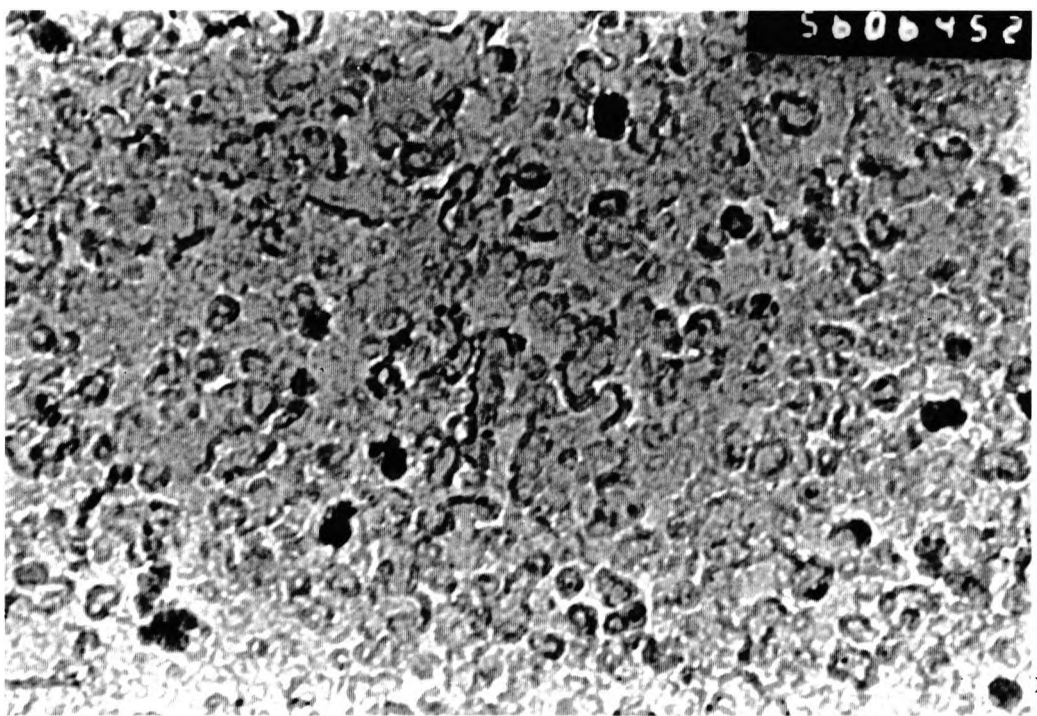


(b)

Figure 6.30 Scanning electron micrographs of the 1.26% Cu-steel plate, showing complete carbide precipitation of the (MA) particles after tempering the quenched plate at 650°C for 1h.



(a)



(b)

Figure 6.31 Transmission electron micrographs (replica) of the as-normalised 1.26% Cu-steel. The coarse precipitates are Cu, the fine are Nb(CN).

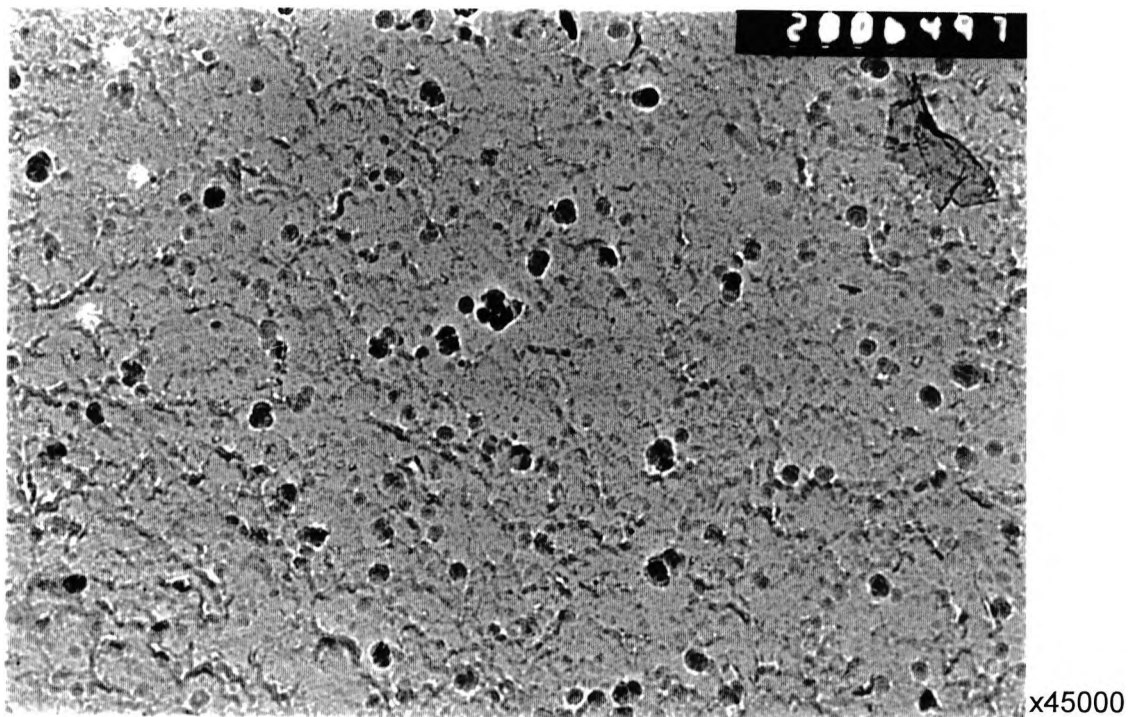


Figure 6.32 Transmission electron micrograph (replica), showing copper precipitation in the normalised and fully-aged (NT550) 1.26% Cu-steel.

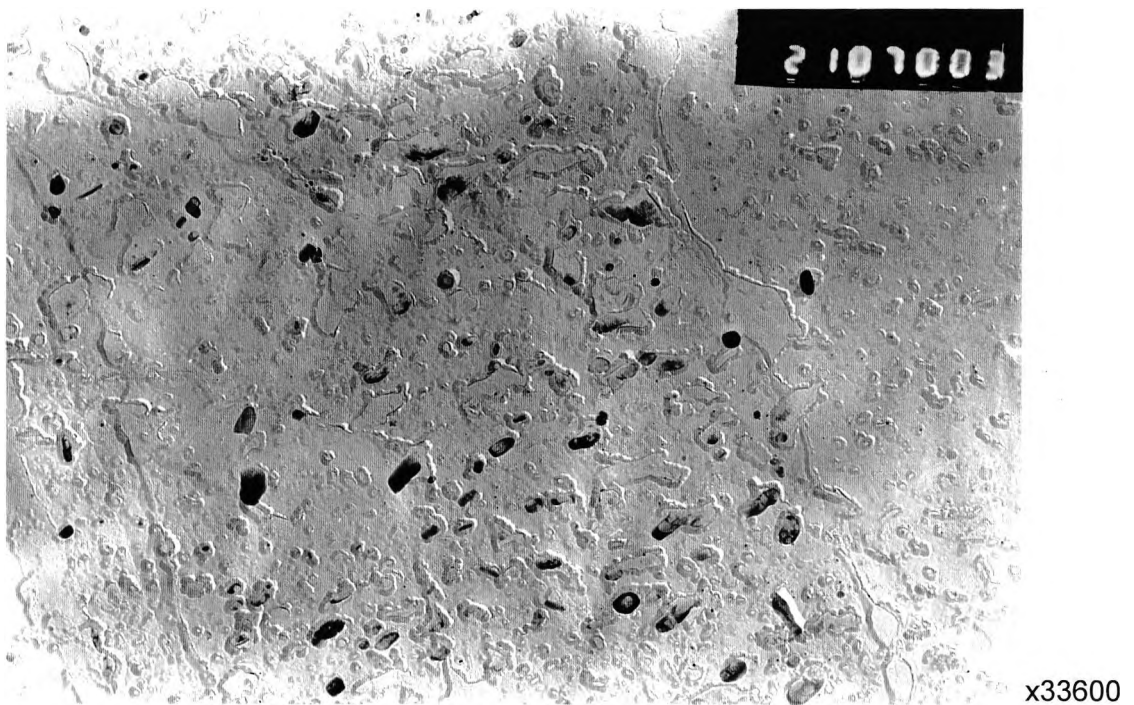


Figure 6.33 (a) Cu and Nb(CN) precipitation in the normalised and over-aged (NT650) 1.26% Cu-steel, (TEM replica).

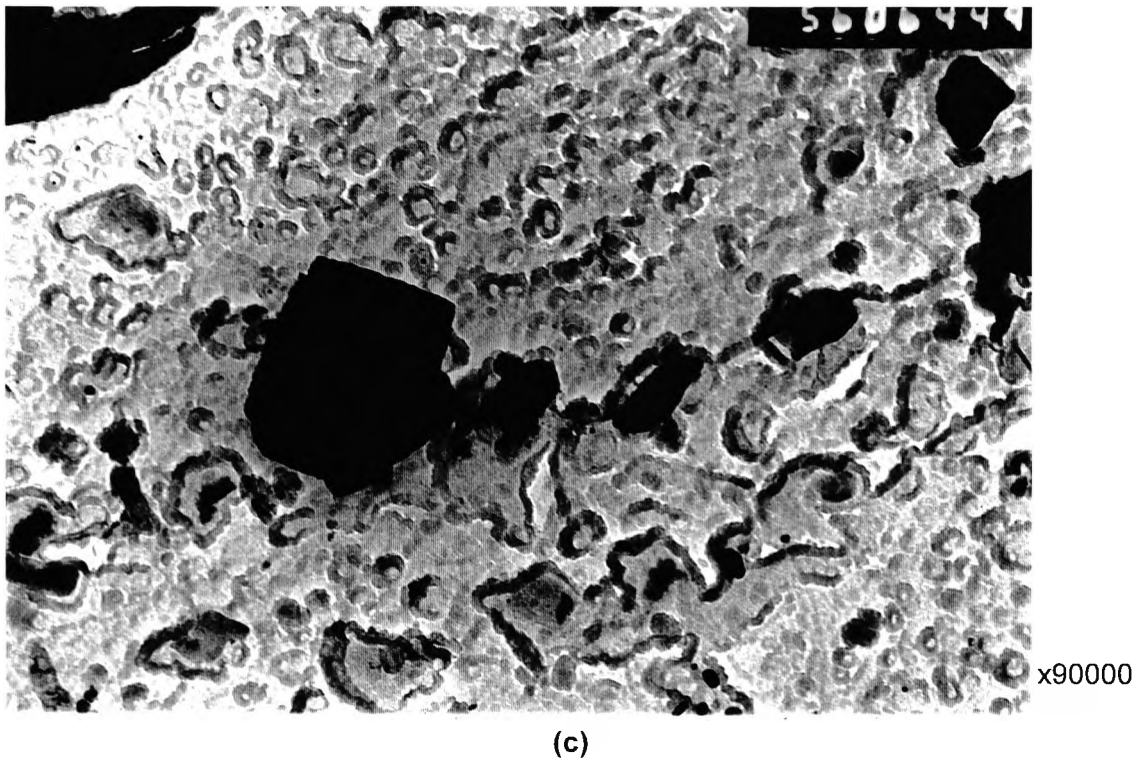
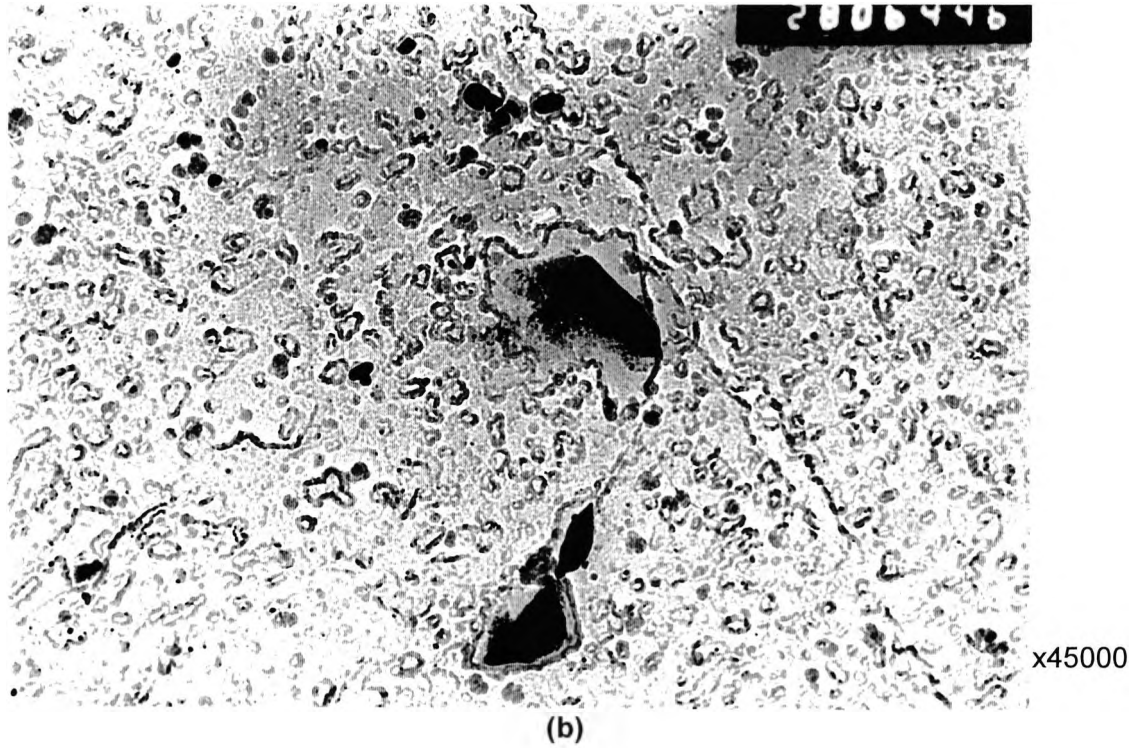
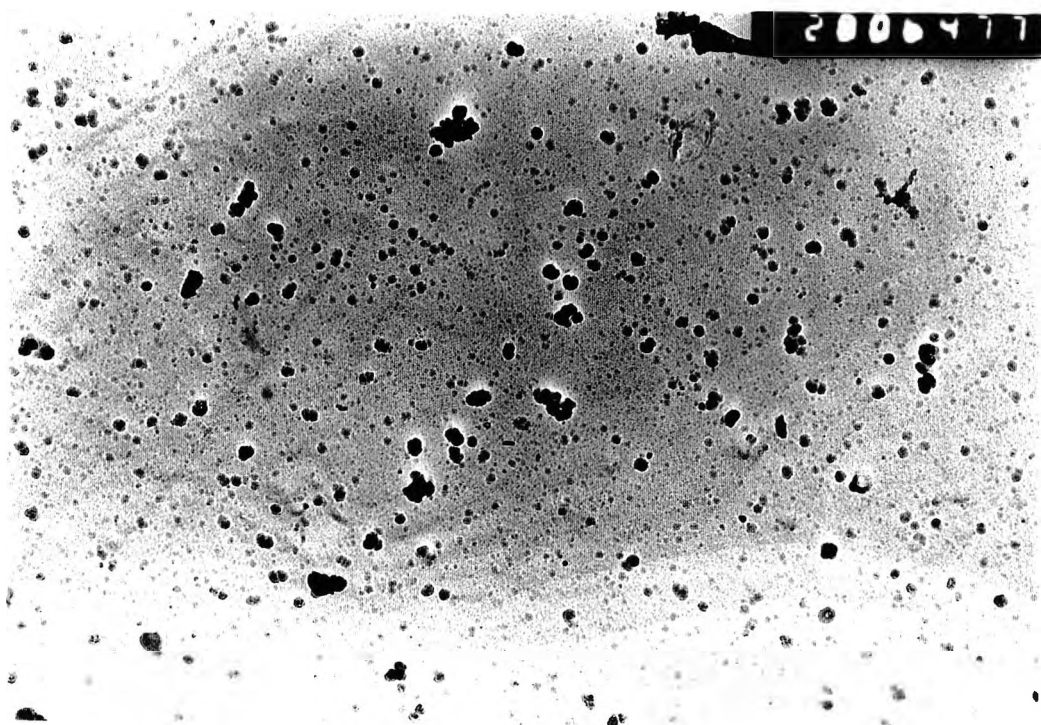
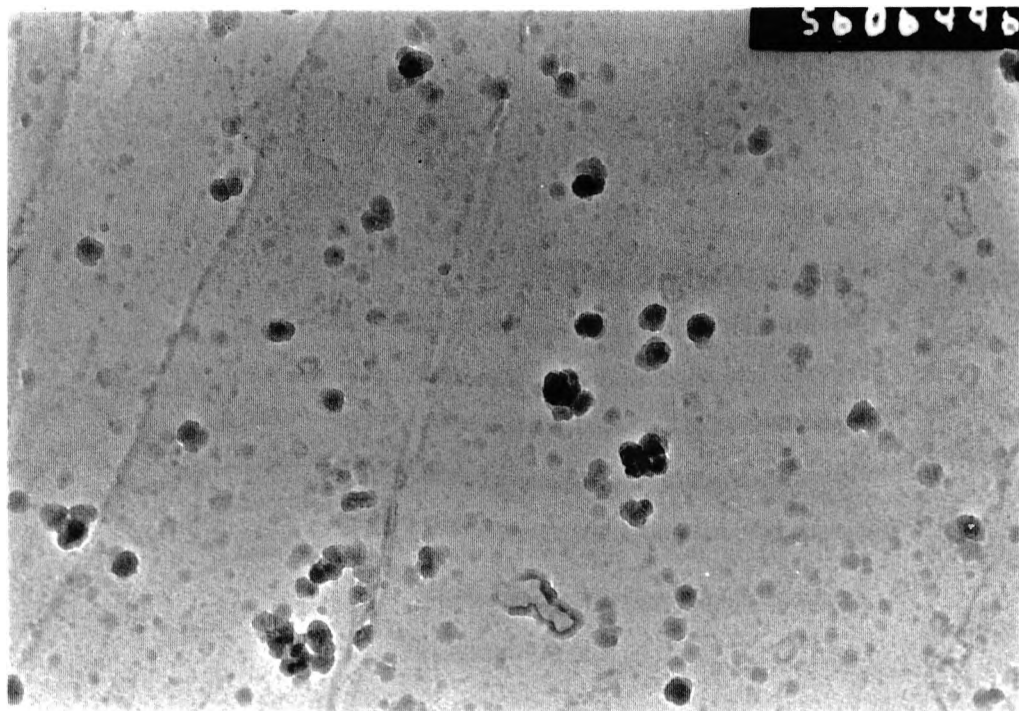


Figure 6.33 Transmission electron micrographs (replica) of the normalised and over-aged (NT650) 1.26% Cu-steel, showing : (b) Cu and Nb(CN) precipitation and grain boundary carbides, (c) grain boundary particles and Nb(CN) precipitates.



x45000

(a)



x90000

(b)

Figure 6.34 Transmission electron micrographs (replica) showing copper precipitation in the as-quenched (Q) condition of 1.26% Cu-steel.

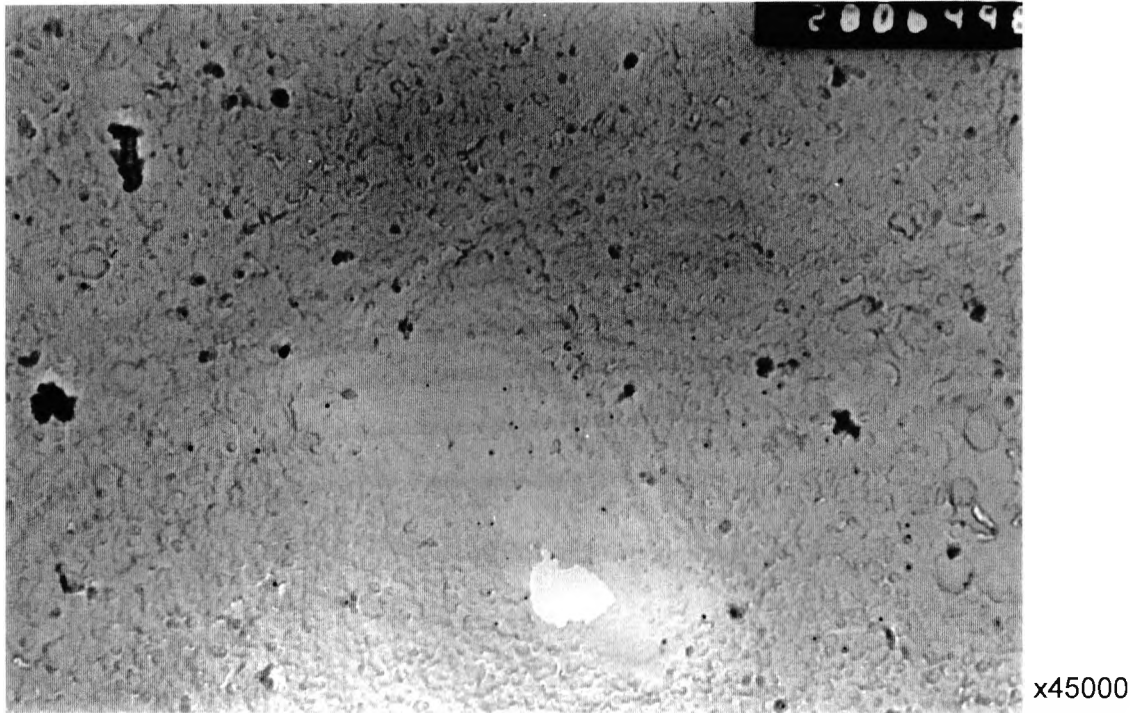


Figure 6.35 Transmission electron micrograph (replica), showing coarse Cu and fine Nb(CN) precipitates in the quenched and fully-aged condition, (QT500), of 1.26% Cu-steel plate.

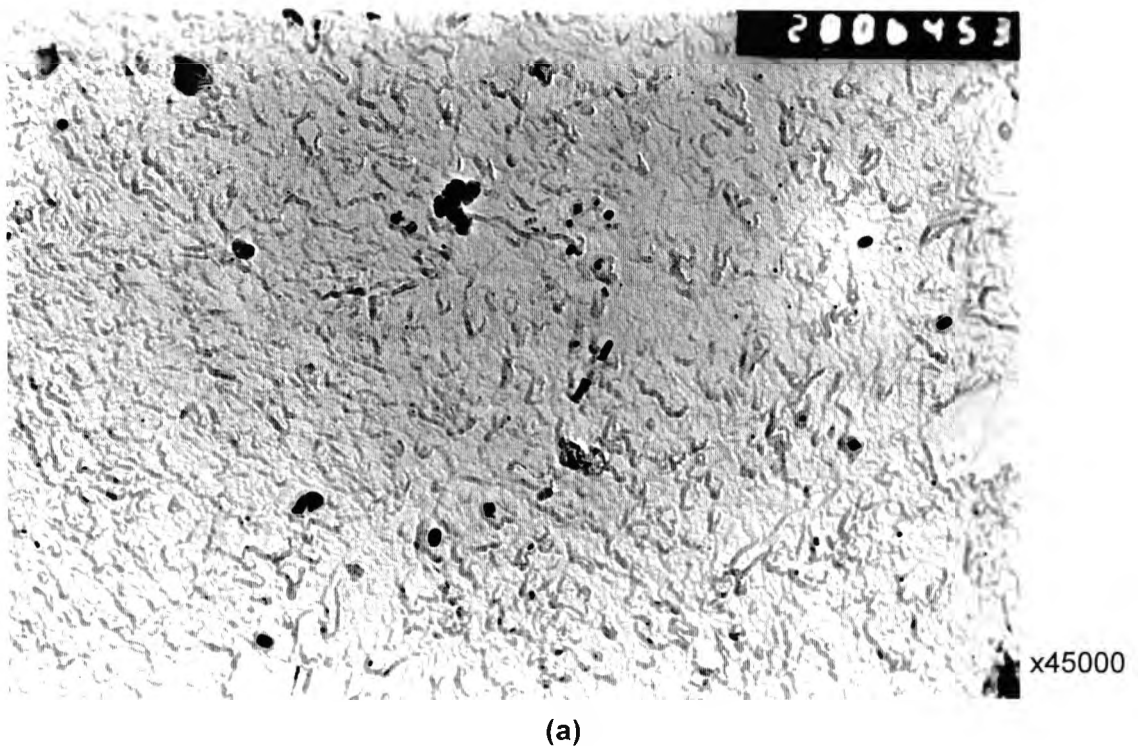


Figure 6.36 Transmission electron micrographs (replica) of the quenched and over-aged (QT650) 1.26% Cu-steel plate showing Cu and Nb(CN) precipitation.

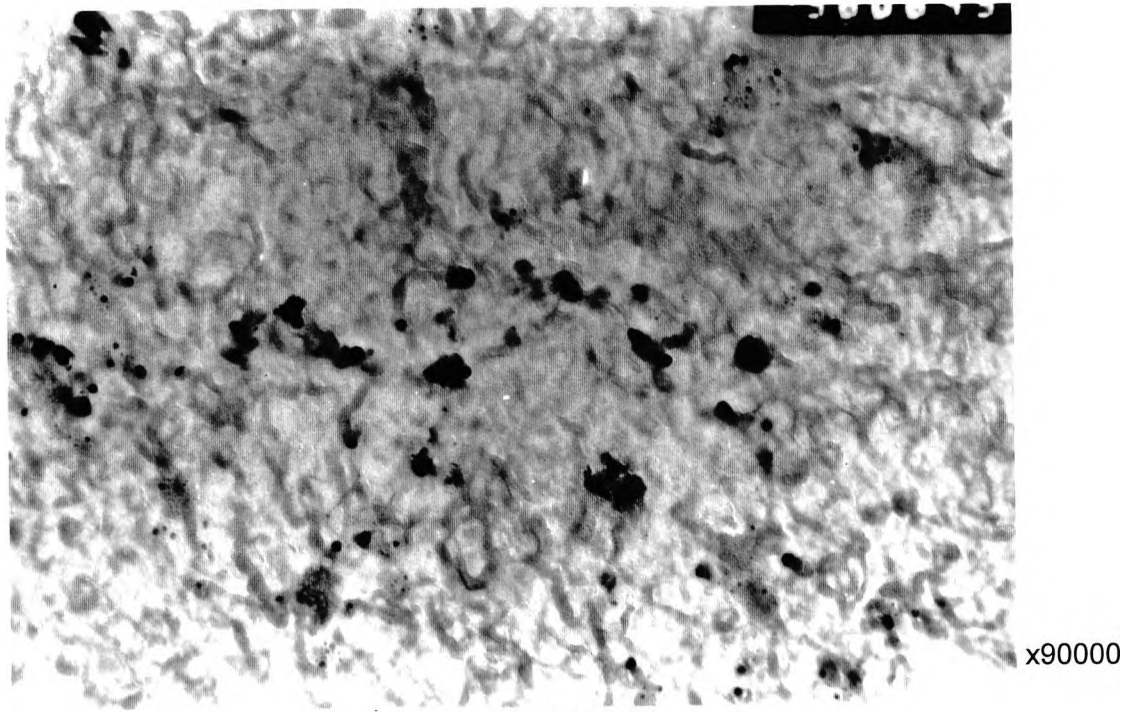
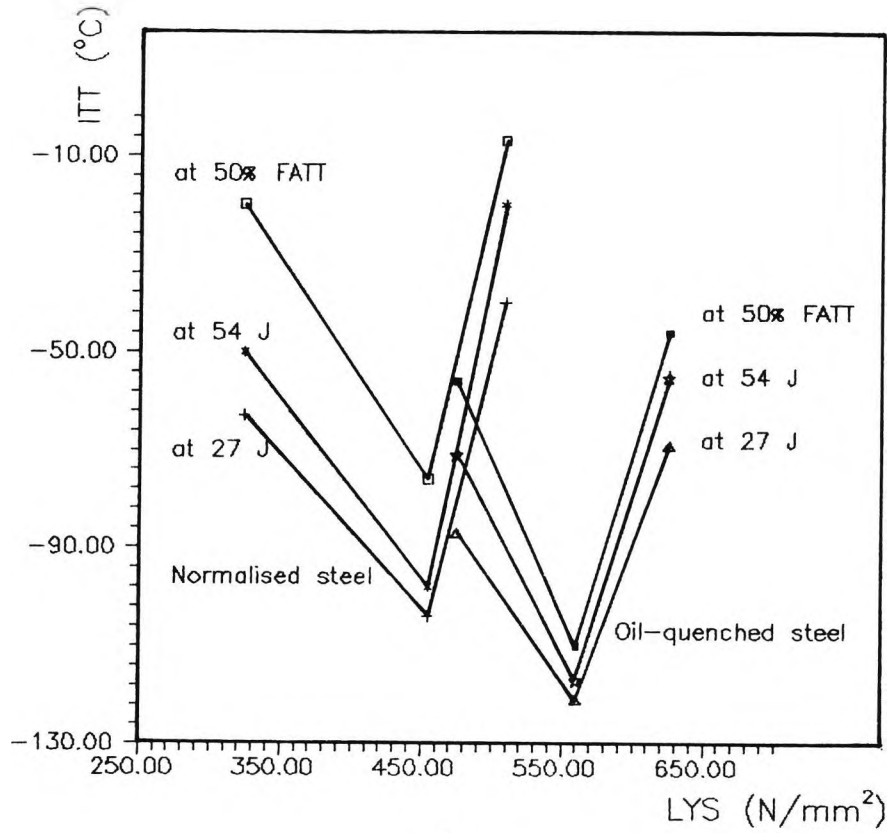
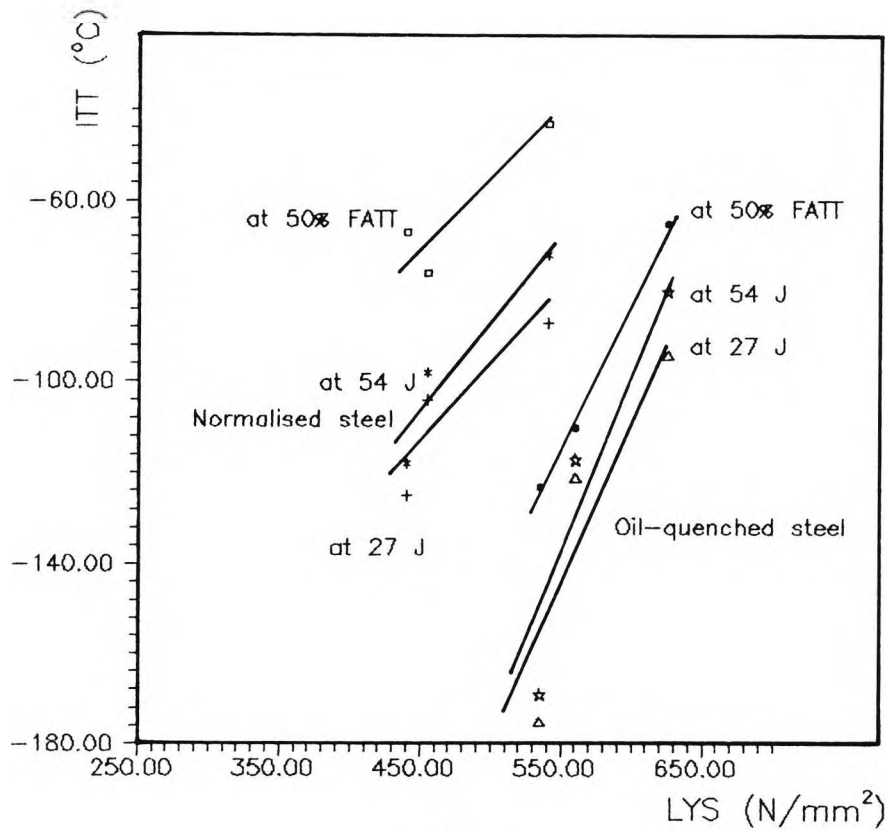


Figure 6.36 Transmission electron micrographs (replica) of the quenched and overaged (QT650) 1.26% Cu-steel plate showing Cu and Nb(CN) precipitation.

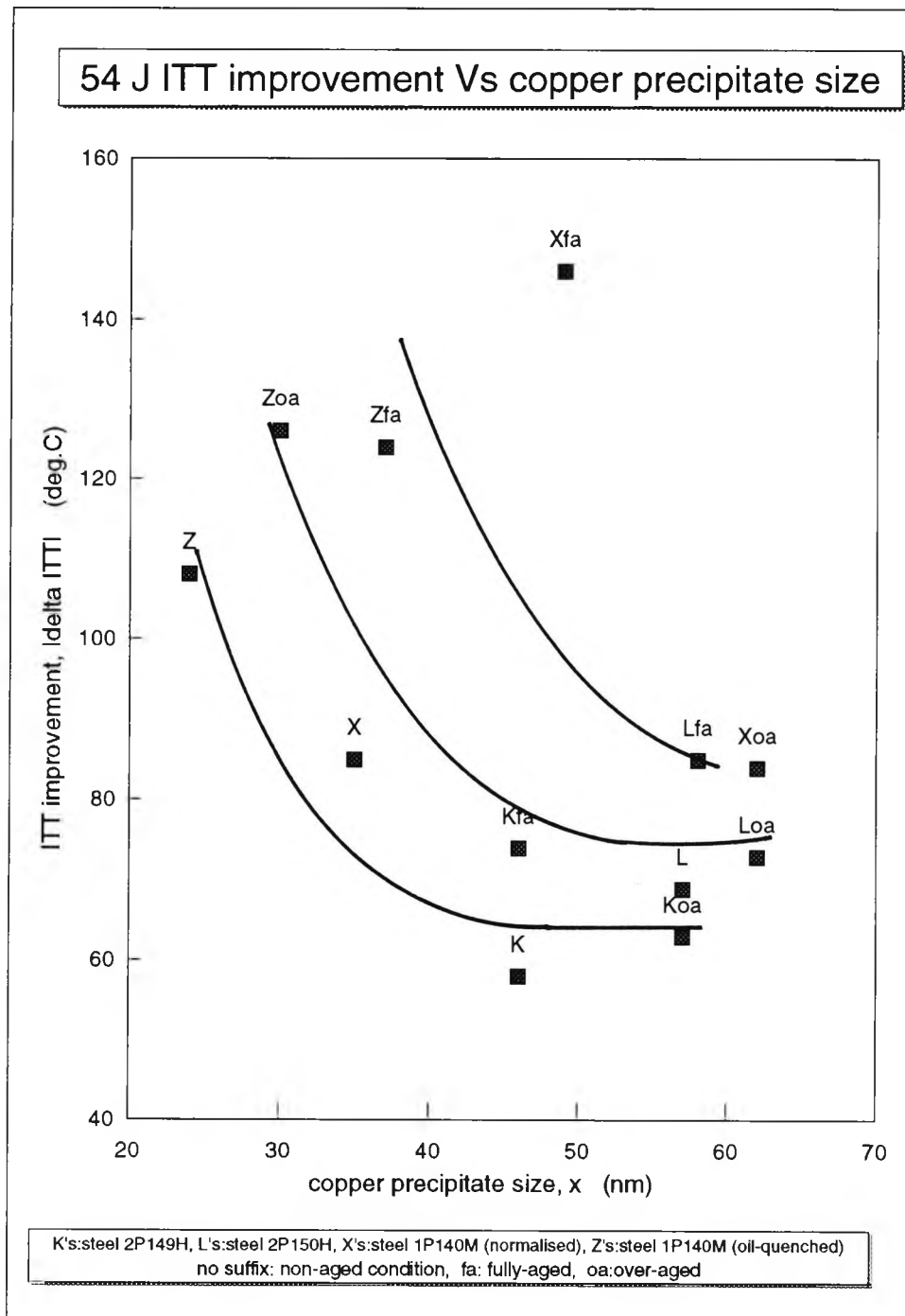


(a)



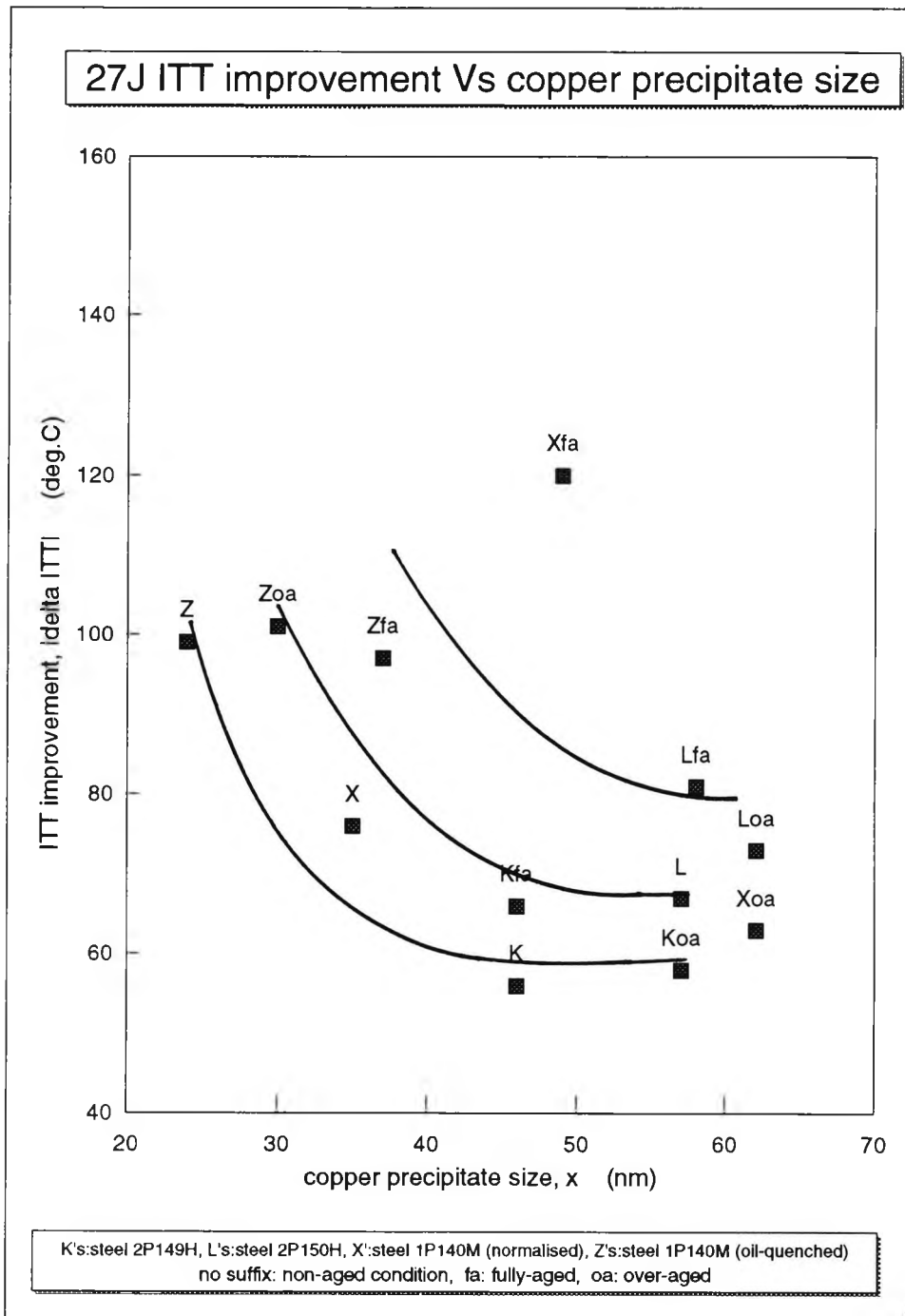
(b)

Figure 6.37 The variation of the observed impact transition temperatures as a function of the observed lower yield strength, of steel 1P140M. (a) Recorded values. (b) Corrected values of LYS and ITT to account for the presence of martensite in the non-aged and fully-tempered conditions.



(a)

Figure 6.38 The relationship between impact transition temperature improvement and copper precipitate size (a) 54J ITT criterion (b) 27J ITT criterion.



(b)

Figure 6.38 The relationship between impact transition temperature improvement and copper precipitate size (a) 54J ITT criterion (b) 27J ITT criterion.

7

CONCLUSIONS

7.1 Plain low carbon steels

- Heating three steels in the ferrite (α -Fe) phase (700-720 °C) resulted in bringing a large proportion of the carbon and nitrogen into solution. Rapid cooling did not allow the carbon to diffuse; the result was a supersaturated solid solution of carbon and nitrogen.
- The microstructure was coarse (25-80 μm) and consisted of polygonal ferrite. There were not any carbides present after quenching except in one of the three steels.
- Subsequent ageing at 60°C for 10-16 hours, resulted in peak hardness and strength. The strength increment ranged from 22 to 100 N/mm².
- The increase in strength and hardness was in accord with the presence of a coherent carbide precipitation.

- Ageing at peak hardness did not significantly influence the impact behaviour. The impact transition temperatures showed a very small variation in the region $\pm 15^{\circ}\text{C}$.
- The analysis of the impact test results suggested that fully-ageing might have improved the impact transition temperatures by 10 to 30 $^{\circ}\text{C}$.
- The improved impact behaviour was attributed to the presence of the coherent iron-carbide precipitate which does not crack and could somehow be able to provide some stress relief (by lowering the energy of the moving dislocations) and therefore delay fracture.
- Ageing the steels at 100°C for more than 3 hours resulted in over-ageing. The precipitate lost its coherency and the yield strength and hardness were observed to drop down to the initial values.
- Over-ageing for longer periods of time ($>3\text{h}$) caused the hardness to drop below the initial value.

7.2 Low-carbon Copper-containing steels

- Heating the steels into the austenite ($\gamma\text{-Fe}$) phase ($910\text{-}920^{\circ}\text{C}$) for 1/2 hour increases the solubility of copper which forms a supersaturated solution after subsequent rapid cooling. The degree of supersaturation depends on the rate of cooling. Slow cooling rates lower the degree of supersaturation by favouring a coarse copper precipitation during cooling. The simple 1.22 and 2.02% copper containing steels were slowly cooled ($5^{\circ}\text{C}/\text{min}$) whereas the commercial copper containing steel was cooled more quickly ($36^{\circ}\text{C}/\text{min}$ in air and $1110^{\circ}\text{C}/\text{min}$ in oil).
- The addition of alloying elements is also very important. Nickel, chromium and molybdenum increase the solubility of copper by decreasing the transformation temperatures. However the presence of such alloying elements in the commercial alloy composition promoted the formation of martensite. In contrast, the microstructures of the simple copper containing steels consisted of polygonal ferrite and pearlite ($\sim 5\%$).

- Subsequent tempering at temperatures between 400 and 650 °C for one hour, caused the solute copper atoms to diffuse and precipitate. Peak hardness and yield strength were found to occur between 500 and 550 °C. All the steels exhibited a yield strength increase of at least 80 MPa. The highest increase was achieved by the commercial steel (150-185 MPa) (although part of that increase was attributed to some extent to the tempering of martensite which would raise the yield strength).
- Tempering the steels at 650°C for one hour, resulted in over-ageing and the initial hardness value was restored. The yield strength was sometimes observed to be slightly higher than the initial value.
- There was clear evidence for the presence of an incoherent and relatively coarse copper precipitation in all the steel conditions. The coarsest form of precipitation was observed in the microstructure of the 2.02% simple copper containing steel, whereas the finest form of precipitation was observed in the microstructure of the oil-quenched, commercial steel. The presence of this precipitate was attributed to: 1) inadequate austenitising time to dissolve all the copper, and/or 2) precipitation during cooling from the austenite region.
- The presence of dispersed incoherent copper precipitates in all the steel conditions increased the strength of the matrix. The magnitude of this strengthening component was successfully estimated by the application of the Ashby-Orowan model for dispersion strengthening and found to be between 60 and 85 MPa for all the steels and their conditions.
- The approximate contribution from the coherent copper precipitates to the yield strength of the fully-aged steels, was found to be 70 MPa for the simple 2.02% copper containing steel and 80-100 MPa for the 1.2% copper containing steels.
- The lowest contribution to the yield strength was observed for the 2.02% copper containing steel. The short austenitising time and the slow cooling rate from the austenite phase, resulted in only a very small amount of copper remaining in solution for further precipitation.

- The yield strength of the commercial steel was found to benefit from the presence of niobium by 45-75 MPa. The proposed strengthening mechanism is dispersion strengthening (Ashby-Orowan model).
- The presence of martensite in the as-normalised/quenched structures of the commercial steel, was found to lower the yield strength by 60-150 MPa and raise the impact transition temperatures. Ageing at peak hardness restored most of the strength properties but not the impact properties.
- Ageing at peak hardness caused a deterioration in the impact behaviour of all the steels. In all the steels the 27 and 54 J ITT's increased by 20-30 °C. This increase was however, much lower than the expected value. The impact properties were restored after over-ageing.
- The analysis of the impact test results indicated that the presence of the coarse incoherent copper precipitates favours the lowering of the impact transition temperatures. The estimated ITT decrease was found to be approximately 60°C for the simple 1.22% Cu containing steel, 70°C for the simple 2.02% Cu containing steel, 85°C for the normalised commercial steel and 110°C for the oil-quenched commercial steel.
- The estimated ITT decrease (improvement) was found to be inversely proportional to the coarseness of the copper precipitation, i.e. it is preferable to have a fine dispersion of the incoherent precipitate rather than a coarse one.
- In all the steels, the presence of coherent precipitates caused a further improvement of the impact transition temperatures by 15°C, with the exception of the commercial steel. The coherent precipitates of the normalised and fully-aged condition of that steel, caused an apparent 50°C ITT improvement.
- It is suggested that the improved impact behaviour of the copper containing steels lies in the ability of the copper precipitates to deform and therefore lower the energy of the moving dislocations. Thus, the dislocation pile-up is minimised and the crack formation and propagation retarded.

- There was a very small number of dislocations in a plastically deformed 2.02% copper containing sample, the dislocations were situated across the coarse copper particles and there was evidence of particle thickness reduction. It is suggested that the increase in strength is due to elastic modulus hardening. This strengthening mechanism is in very good agreement with the Orowan strengthening model and requires that: 1) the precipitate has a lower shear modulus than the matrix and 2) the solute atoms have a similar radius to the solvent atom radius.
- The commercial steel meets the ASTM A710 Grade A specification for classes 2 and 3. The A710 class 2 specification is also met by the simple 2.02% copper containing steel.
- The yield strength results obtained from the simpler copper containing steels and from the over-aged commercial steel plate, were successfully predicted by Morrison *et al.*'s equations [31]. The estimation of the ITT improvements is also considered to be relatively accurately estimated by using the ITT equations that had been developed by Mintz *et al.* [4] for polygonal ferrite-pearlite microstructures.



FUTURE WORK

The main purpose of the present work has been the examination of coherent and non-coherent precipitation on the strength and impact behaviour of steels. The results have shown that the deformable incoherent Cu precipitation can strengthen the material without affecting the impact transition temperatures. Similarly coherent precipitation by copper in Cu-containing steels and coherent precipitation by iron carbide in quenched low carbon steels can increase the strength without materially influencing impact behaviour. However, in order to obtain a deeper understanding of how these particles are able to enhance properties, the following work is required:

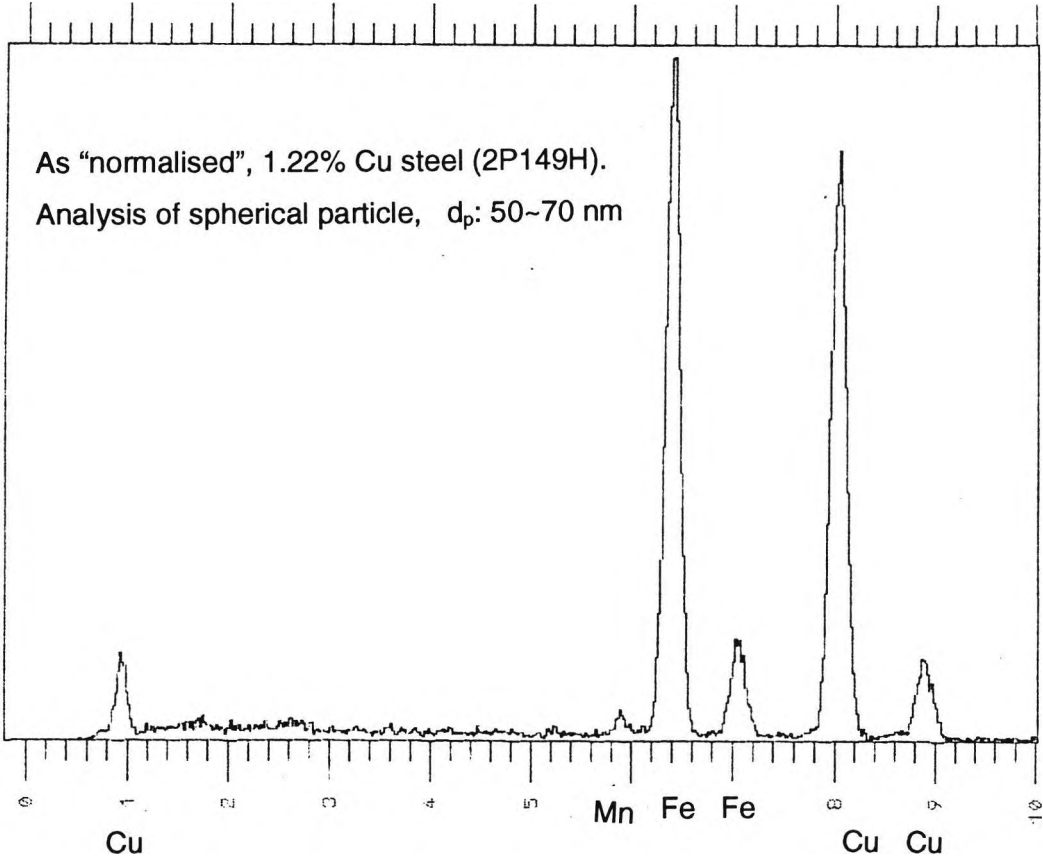
- More detailed TEM work is required to establish the particle sizes more accurately. Furthermore the interaction between dislocations and the particles needs to be obtained by straining the steels in the region of 10%. It is important to confirm that the Cu precipitates and the coherent iron-carbide precipitates can be deformed and absorb dislocations.
- The present work has also suggested that a fine dispersion of incoherent precipitation is more favourable to the impact properties rather than a coarse one. It

would therefore be interesting to establish a quantitative relationship between the impact transition temperature changes and the precipitate size by the application of a series of heat treatments in a simple system, e.g. the simple copper containing steels.

- In the copper containing steel it is necessary to establish the origin of the incoherent copper precipitates. It has been suggested that there are two possibilities: 1) the formation of the incoherent particles takes place during cooling from the austenitising temperature or 2) the incoherent particles are present during the austenitising treatment and need longer austenitising times, in order to go fully into solution. The investigation could include the TEM examination of the structure of the as-received plate, in comparison to a water-quenched (after longer austenitising time) structure of the same steel plate.
- An interesting method of determining the dislocation pattern during plastic deformation, is by measuring the acoustic emission from dislocation motion [101]. This method has been developed for precipitation strengthened alloys and can define whether there is cross-slip in an alloy system and how moderate this is. Acoustic emission measurements as a function of heat treatment have been reported from a variety of age-hardening systems with various stacking fault energies and elastic moduli [101]. Such a method could be used in accordance with further TEM examination of the interaction between dislocations and copper precipitates.

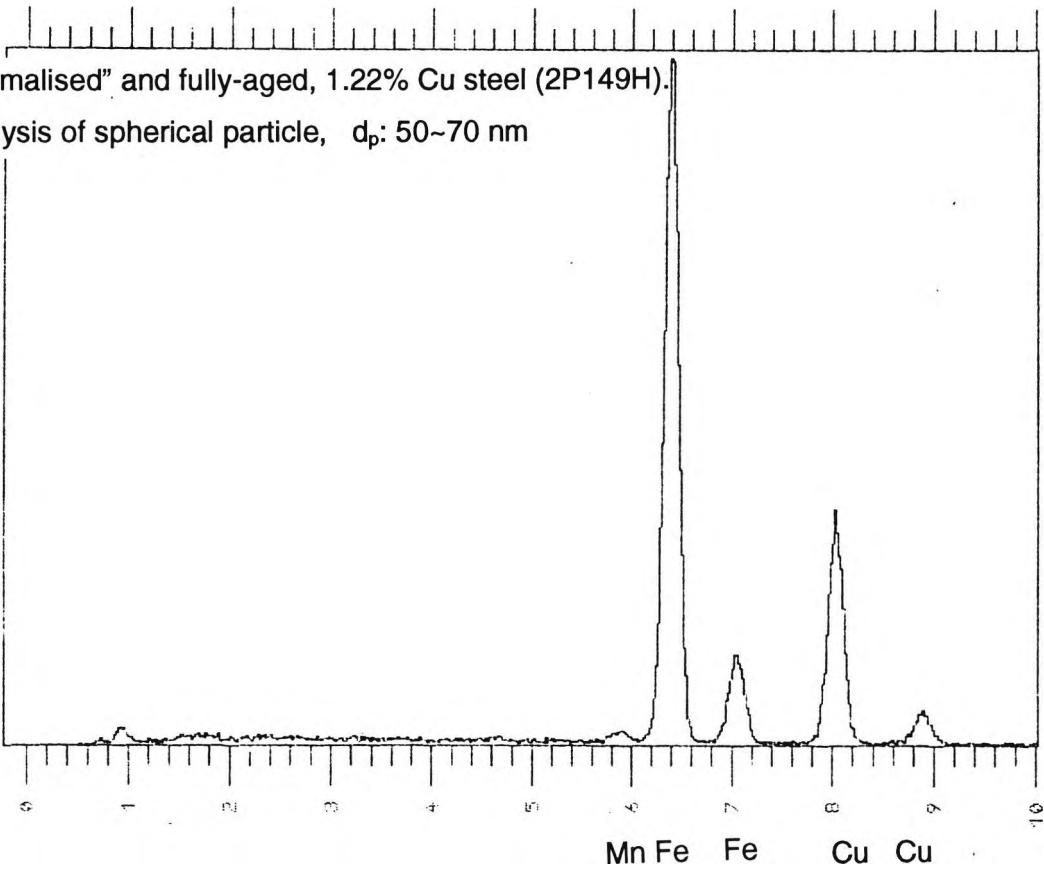
APPENDIX

K 1
20 EV/CHAN, LIVE TIME = 35 SECS
SPECTRUM LENGTH = 1024 CHAN



K 5.25 1
20 EV/CHAN, LIVE TIME = 19 SECS
SPECTRUM LENGTH = 1024 CHAN

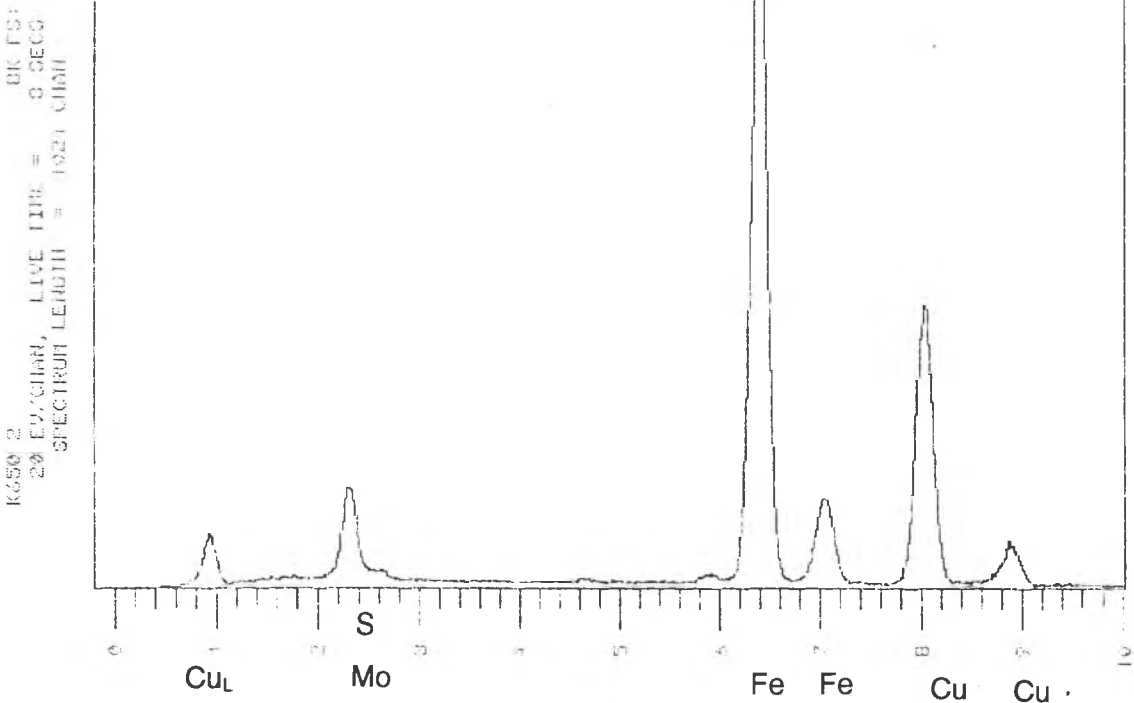
"Normalised" and fully-aged, 1.22% Cu steel (2P149H).
Analysis of spherical particle, d_p : 50~70 nm



"Normalised" and over-aged, 1.22% Cu steel (2P149H).

Analysis of spherical particle, d_p : 50~70 nm

K650 2
20 EV/CHAR, LIVE TIME = 9 SECS
SPECTRUM LENGTH = 1024 CHAR

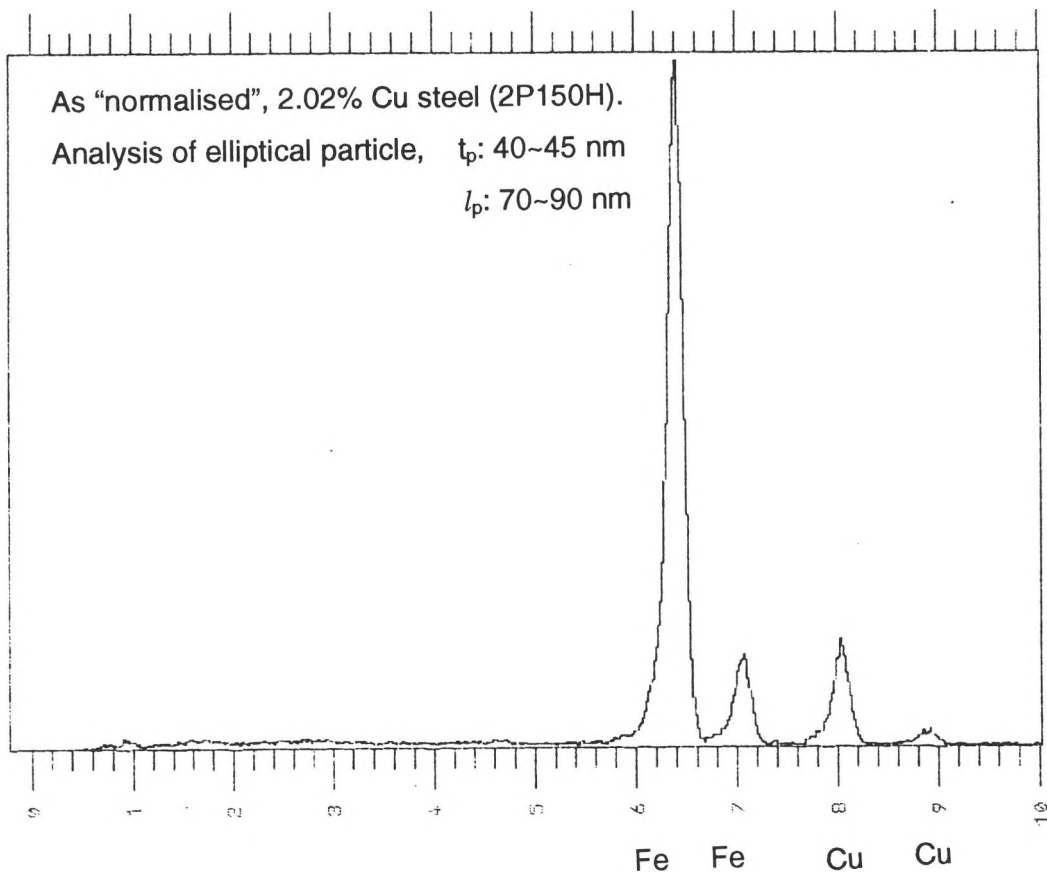


As "normalised", 2.02% Cu steel (2P150H).

Analysis of elliptical particle, t_p : 40~45 nm

l_p : 70~90 nm

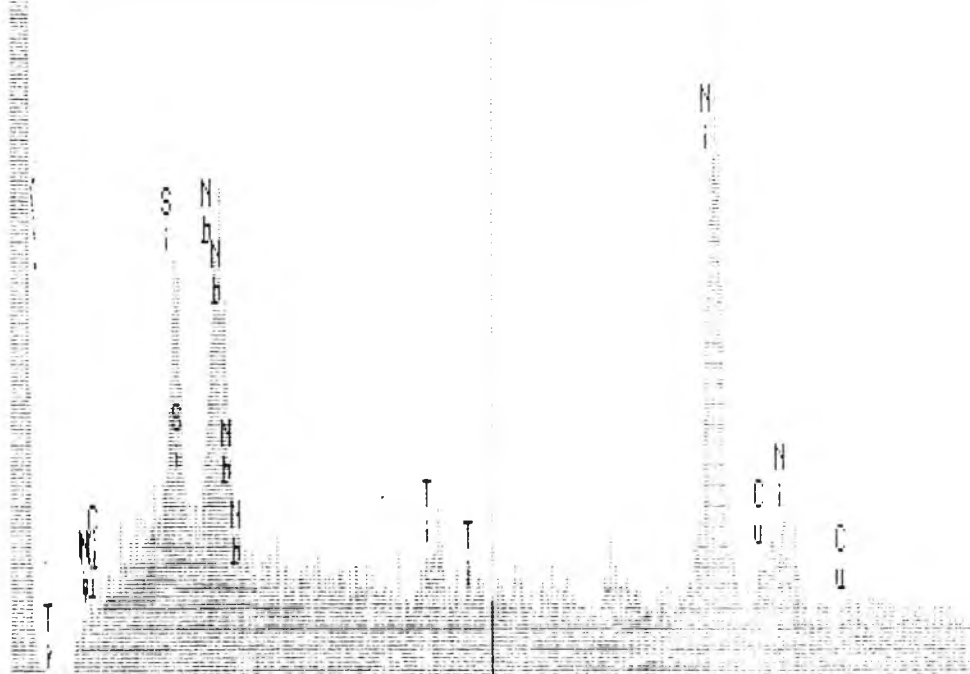
L
20 EV/CHAR, LIVE TIME = 11 SECS
SPECTRUM LENGTH = 1024 CHAR



X-RAY

Live: 300s Preset: 300s Remaining: 0s
Real: 326s 8% Dead

1.26% Cu steel with a commercial composition (1P140M).
Analysis of spherical particle, d_p : 10-30 nm



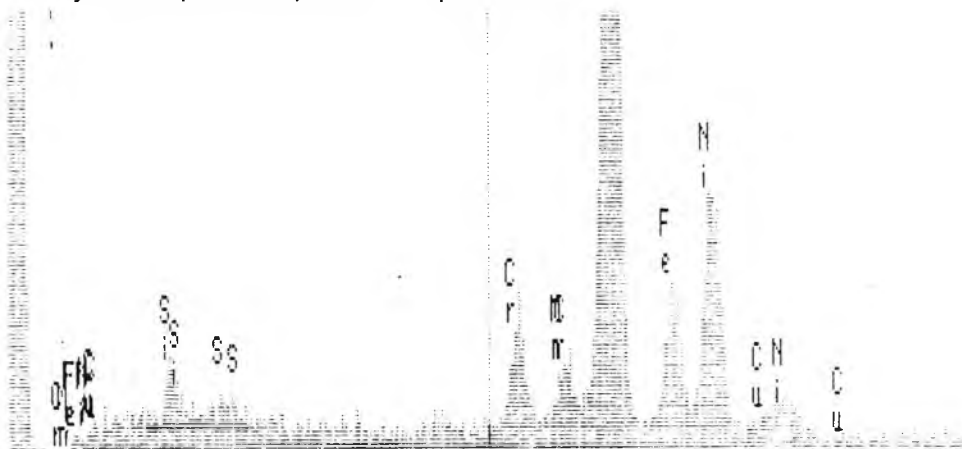
< .000 5.120 keV 10.240 >
FS=255 CH 266= 24 CTS
MEM1:ELG3

X-RAY

Live: 300s Preset: 300s Remaining: 0s
Real: 322s 7% Dead



1.26% Cu steel with a commercial composition (1P140M).
Analysis of spherical particle, d_p : 10-30 nm



< .000 5.120 keV 10.240 >
FS=511 CH 266= 21 CTS
MEM2:ELG5 263

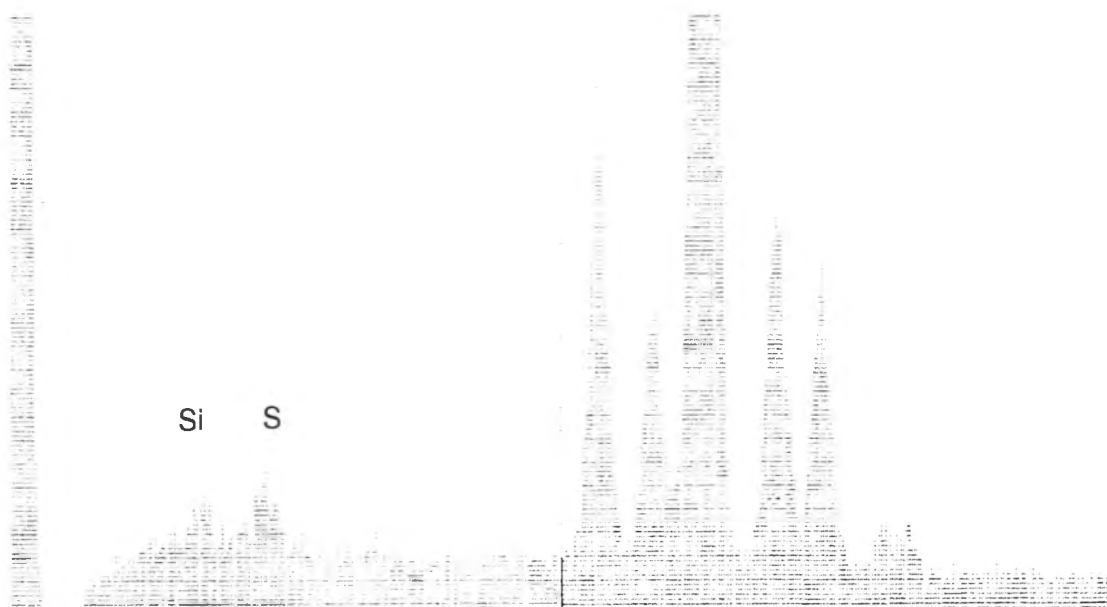
1.26% Cu steel with a commercial composition (1P140M).

Analysis of spherical particle, d_p : 10~30 nm

X-RAY

Live: 300s Preset: 300s Remaining: 0s

Real: 337s 11% Dead



< -.040 5.080 keV Fe Ni Cu Ni 10.200 >
FS=511 CH 264= 46 CTS
MEM1:

REFERENCES AND BIBLIOGRAPHY

- [1] Krishnadev, M.R., Gosh, R., Cutler, L.R., Prince J.R., Gauvin, P., (1980), "An evaluation of the effect of low temperatures on mechanical properties of a commercial steel to be used in the arctic," *J. of Testing and Evaluation*, **8**, pp. 42-47.
- [2] Miglin, M.T, Hirth J.B., Rosenfield, A.R., (1983), "Effects on microstructure on fracture toughness of a high-strength low-alloy steel," *Met. Trans. A, AIME*, **14A**, pp. 2055-2061.
- [3] Jesseman, R.J., Murphy, G.I., (1983), "Mechanical properties and precipitation hardening response in ARMCO NI-COP (ASTM A710 grade A and A736) alloy steel," *Proc. Conf. 'Copper in Steel'*, Luxembourg.
- [4] Mintz, B., Morrison, W.B., Jones, A., (1979), "Influence of carbide thickness on impact transition temperature of ferritic steels," *Met. Technol.*, **551**, pp. 252-260.
- [5] Irani, J.J., Dulieu, D., Tither, G, (1969), "Role of copper in low-alloy steels," Conf. Proc. on: "*Low-alloy steels*", Scarborough (April 1968), ISI Publ, pp. 75-89.
- [6] Hicho, G.E., Fields, R.J., (1988), "Effects of varying austenitising temperature and cooling rate on the ability of HSLA-80 steel to achieve a yield strength comparable to HSLA-100," *J. Heat Treating*, **6**, pp. 77.
- [7] Habraken, L., Greday, T., (1966), "Copper in carbon and low-alloy steels," *metalen en andere constructie-materialen*, **40**, p. 262.
- [8] Cottrell, A.H., (1965), *Theoretical structural metallurgy*, Arnold, London, pp. 223-243.
- [9] Nabarro, F.R.N., (1948), *Symposium on internal stresses in metals and alloys*, *The Inst. of Met.*, pp. 61-72, 237-250.
- [10] Friedel, J., (1964), *Dislocations*, Pergamon, Oxford.
- [11] Askeland, D.R. (1990), *The science and engineering of materials*, Chapman & Hall, London.
- [12] LeMay, I. Krishnadev, M.R., "Fundamental metallurgical considerations," *Copper in iron and steel*, I.LeMay and L.McDonald Shetky (Ed.), Wiley-Interscience publ., pp. 5-43.
- [13] Polmear, I.J. (1989), *Light Alloys*, Arnold, London.
- [14] Chandra-Holm, H. (1983), "The development of substructure in aluminium and aluminium alloys," *Yield, flow and fracture of polycrystals*, T.N.Baker (Ed.), Applied Science Publishers, London, pp. 275-310.

- [15] Smallman, R.E., (1970), *Modern Physical Metallurgy*, Butterworths, London.
- [16] Orowan, F.R.S., (1948), "Classification and Nomenclature of internal stresses," *Symposium in internal stresses in metals and alloys, Inst. of Met.*, London.
- [17] Brown, L.M., Ham, R.K., (1971), *Strengthening methods in crystals*, Elsevier, London.
- [18] Honeycombe, R.W.K., (1992), *Steels*, Arnold, London.
- [19] Thompson, A.W., Knott, J.F., (1993), "Micromechanisms of brittle fracture," *Met.Trans. A, AIME*, **24A**, p. 523.
- [20] McMahon, C.J., Cohen, M., (1965), "Initiation of cleavage in polycrystalline iron," *Acta Metallurgica*, **13**, p.591.
- [21] Hahn, G.T., (1984), "The influence of microstructure on brittle fracture toughness," *Met.Trans. A, AIME*, **15A**, p.947.
- [22] Almond, E.A., Timbres, D.H., Embury, J.D., "The influence of second phase particles on brittle fracture," *paper 21*, pp. 253-265.
- [23] Leslie, W.C., Williams, G.B., (1961), "The tensile properties of high-purity low-carbon iron and iron-manganese alloys," *J.I.S.I.*, **1920**, pp. 21-29.
- [24] Allen, N.P., Rees, W.P., Hopkins, B.E., Tipler, H.R., (1953), "Tensile and impact properties of high-purity iron-carbon and iron-carbon-manganese alloys of low carbon content," *JISI*, **761**, pp. 108-120.
- [25] Petch, N.J., (1987), "The influence of some substitutional alloys on the cleavage of ferritic steels," *Acta Metall.*, **35** No8, pp. 2027-2034.
- [26] Petch, N.J., "The influence of grain boundary carbide and grain size on the cleavage strength and impact transition temperature of steel," University of Strathclyde, Glasgow, private communication.
- [27] Knott, J.F, (1983), "Cleavage fracture and toughness of structural steel," *Yield, flow and fracture of polycrystals*, T.N.Baker (Ed.), pp. 81-100.
- [28] Pickering, F.B.,(1992), "structure-property relationships in steels," *Mat. Sci. & Technology.*, **7**, F.B. Pickering (Ed.), pp. 41-94.
- [29] Mintz, B., (1974), "Influence of manganese on the impact transition temperature of as-rolled plain carbon-manganese steels," *Met. Tech.*, **6**, pp. 226-232.
- [30] Mintz, B., Peterson, G., Nassar, A., (1994), "Structure/property relationships in ferrite/pearlite steels," City University, private communication.
- [31] Morrison, W.B., Mintz, B., Cohrane, R.C., (1976), *Conference on controlled processing of HSLA steels*, York University, paper 1.
- [32] Mintz, B., "Low carbon steels for pipe line applications," *Low carbon steels for the eighties*, British Steel Co., priv.comm.

- [33] Morrison, W.B., Cohrane, R.C., Mintz, B., (1976), "Structure property relationships in controlled processed steels," *British Steel Corporation report*.
- [34] Thompson, S.W., Colvin, D.J., Krauss, G., (1990), "Continuous cooling transformations and microstructures in a low-carbon, high strength low-alloy plate steel, *Met. Trans. A, AIME*, **21A**, pp. 1493-1507.
- [35] Habraken, L.J., Economopoulos, M., (1967), *Transformation and hardenability in steels*, Climax Molybdenum Company, Ann Arbor, MI, pp. 69-108.
- [36] Fox, A.G., Mikalac, S., Vassilaros, M.G., (1992), "The microstructure and mechanical properties of two Navy HSLA-100 steels in plate form," *Speich Symposium Proceedings*, pp. 155-161.
- [37] Gladman, T., Dulieu, D., Mclvor, I.D., (1977), *Microalloying '75*, Korchynsky, M., (Ed.), New York, Union Carbide Corporation, 32.
- [38] Onel, K., Nutting, J., (1979), *Met. Sci.*, **13**(10), 573.
- [39] Lis, A.K., Mujahid, M., Garcia, C.I., DeArdo A.J., (1992), "The role of copper in the ageing behaviour of HSLA-plate steel," *Speich Symposium Proceedings*, pp. 129-138.
- [40] Lanzilotto, C.A.N., Pickering, F.B., (1982), *Met. Sci.*, **16**, 371.
- [41] Rigsbee, J.M., VanderArend P.J., "Laboratory studies of microstructures and structure-property relationships in dual-phase HSLA steels," *Republic Steel Corporation*, Ohio, pp. 56-86.
- [42] *Metals Handbook*, (1973), 8th Ed., **8**, ASME, Metals Park, Ohio, p.236.
- [43] Leslie, W.C., (1961), "The quench-ageing of low-carbon iron and iron-manganese alloys," *Acta Met.*, **9**, pp. 1004-1021.
- [44] Leslie, W.C., Rauch, G.C., (1978), "Precipitation of carbides in low-carbon Fe-Al-C Alloys," *Met. Trans. A, AIME*, **9A**, pp. 343-349.
- [45] Gladman, T., Holmes, B., Mclvor, I.D., (1971), "The effects of second phase particles on strength, toughness, and ductility," *Iron and Steel Inst.*, London, p.68.
- [46] Pickering, F.B., (1992), "High strength low alloy steels," *Mat. Sci. & Technology*, **7**, pp. 335-400.
- [47] Morrison, W.B., (1963), "The influence of small niobium additions on the properties of carbon-manganese steels," *JISI*, pp. 317-325.
- [48] Repas, E., (1988), "Metallurgical fundamentals for HSLA steels," *Proc. Conf. Microalloying '88*, Chicago.
- [49] Andrews, K.W., (1965), "Empirical formulae for the calculation of some transformation temperatures," *JISI*, **2570**, pp. 721-727.

- [50] Norton, J.T., (1934), "Solubility of copper in iron and lattice changes during ageing," *AIME*, Tech. Publ. No. **586**.
- [51] Hornbogen, E., Glenn, R.C., (1960), "A metallographic study of precipitation of copper from alpha iron," *Trans. of Met. Soc. of AIME*, **218**, pp. 1064-1070.
- [52] Crowther, D.N., (1987), "Evaluation of the mechanical properties in a Cu containing age hardening steel," *British Steel Corporation report*.
- [53] Speich, G.R., Oriani, R.A., (1965), "The rate of coarsening of copper precipitate in an alpha-iron matrix," *Trans. of Met. Soc. of AIME*, **223**, pp. 623-631.
- [54] Cox, A.R., (1967), "Metallography and strengthening mechanisms of 0.3%C and 0.3%C-1.5%Cu steels," *JISI*, **2843**, pp. 51-57.
- [55] Mclvor, I.D., (1969), "Precipitation effects in mild steel containing 1.5% copper," *JISI*, p.106.
- [56] Krishnadev, M.R., LeMay, I., (1970), "Microstructure and mechanical properties of a commercial low-carbon copper-bearing steel," *JISI*, **3522**, pp. 458-462.
- [57] Mclvor, I.D., Gladman, T., Pickering, F.B., (1972), "Dispersion strengthening of ferrite by overaged copper precipitates," *British Steel Corporation, tech. report*.
- [58] Tsukada, K., Koshaka, Y., Hatakeyama, K., Shimoda, T., Iwasaki, N., Kaneko, Y., (1981), "1.2% Cu bearing steel for fitting pipe with high strength and high toughness," *Nippon Kokan tech. report*, **32**.
- [59] Hornbogen, E., Staniek, G., (1974), "Grain-size dependence of the mechanical properties of an age-hardening Fe-1%Cu-alloy," *J. of Mat. Sci.*, **9**, pp. 879-886.
- [60] Krishnadev, M.R., Galibois, A., (1974), "Development of a high-strength low-alloy steel strengthened by transformation substructure and precipitation of copper and niobium," *Met. Tech.*, **69**, pp. 800-802.
- [61] Ricks, R.A, Howell, P.R., Honeycombe, R.W.K., (1980), "Formation of supersaturated ferrite during decomposition of austenite in iron-copper and iron-copper-nickel alloys," *Met. Sci.*, pp. 562-568.
- [62] Krishnadev, M.R., (1980), "Development of strong, tough structural steels based on copper-high-silicon additions," *Met. Tech.*, p.305.
- [63] Hicho, G.E., Singhal, S., Smith, L.C., Fields, R.J., (1983), "Effect of thermal processing variations on the mechanical properties and microstructure of a precipitation hardening HSLA steel," *HSLA steels technology and application*, **8306-051**, pp. 705-712.

- [64] Jesseman, R.J., Murphy, G.J., (1983), "Mechanical properties and precipitation hardening response in ASTM A710 Grade A and A736 alloy steel plates," *HSLA steels technology and application*, **8306-029**, pp. 655-665.
- [65] Krishnadev, M.R., (1983), "Development and characterisation of a new family of copper-containing steels," *HSLA steels technology and application*, **8306-079**, pp. 129-147.
- [66] Wada, H., Houbaert, Y., Penning, J., Dilewijns, J., (1983), "Strengthening effects of copper in steel," *Conf. on Copper in Steel*, Luxembourg, pp. 3.1-3.30.
- [67] Krishnadev, M.R., Bouchard, R., Romhanyi, K., Voyzelle, B., "Fracture-microstructure-mechanical property relations in an advanced HSLA steel," *Microstructural Science*, **14**, Louthan, M.R., LeMay, I., VanderVoort, G.F., (Ed.), pp. 189-203.
- [68] Miglin, M.T., Hirth, J.P., Rosenfield, A.R., Clark, W.A.T., (1986), "Microstructure of a quenched and tempered Cu-bearing high-strength low-alloy steel," *Met. Trans. A, AIME*, **17A**, pp. 791-798.
- [69] Abe, T., Kurihara, M., Tagawa, H., Tsukada, K., (1987), "Effect of thermo-mechanical processing on mechanical properties of copper bearing age hardenable steel plates," *Trans. ISIJ*, **27**, pp. 478-484.
- [70] Hicho, G.E., Brady, C.H., Smith, L.C., Fields, R.J., (1987), "Effects of heat treatments on the mechanical properties and microstructures of four different heats of a precipitation hardening HSLA steel," *J. Heat treat.*, **5**, No. 1, pp. 7-19.
- [71] Hydrean, P.P., Kitchin, A.L., Schaller, F.W., (1971), "Hot rolling and heat treatment of Ni-Cu-Cb-(Nb) steel," *Met. Trans.*, **2**, pp. 2541-2548.
- [72] Aroztegui, J.J., Urcola, J.J., Fuentes, M., (1989), "The influence of copper precipitation and plastic deformation hardening on the impact transition temperature of rolled structural steels," *Met. Trans. A, AIME*, **20A**, pp. 1657-1668.
- [73] Foley, R.P., Fine, M.E., (1991), "Microstructure and property investigations of quenched and tempered HSLA-100 steel," *Proc. Int. Conf. 'Processing, microstructure and properties of microalloyed HSLA steels'*, Pittsburgh, pp. 315-330.
- [74] Goodman, S.R., Brenner, S.S., Low, J.R., (1973), "An FIM-Atom probe study of the precipitation of copper from iron-1.4 at.% copper, Part I: Field-ion microscopy," *Met. Trans.*, **4**, pp. 2363-2369.

- [75] Goodman, S.R., Brenner, S.S., Low, J.R., (1973), "An FIM-Atom probe study of the precipitation of copper from iron-1.4 at.% copper, Part II: Atom probe analyses," *Met. Trans.*, **4**, pp. 2371-2378.
- [76] DePaul, R.A., Kitchin A.L., (1970), "The role of nickel, copper and niobium in strengthening a low-carbon ferritic steel," *Met. Trans.*, **1**, pp. 389-393.
- [77] Cassidy, D.P., Shelton, C.H., "Nickel-copper-columbium steel - a new concept in high strength constructional materials," *Soc. of Automotive Eng., Inc.*, **680246**, pp. 810-818.
- [78] Kvidahl, L.G., (1983), "Shipyard experience in welding ASTM A710," *Conf. Proc. on Copper in Steel*, Luxembourg, pp. 4.2-4.30.
- [79] Losz, J.M., Challenger, K.D., (1989), "Microstructure and properties of a copper-precipitation strengthened HSLA steel weldment," *Conf. Proc. on Trends in Welding Science and Technology*, Tennessee, pp. 229-235.
- [80] Khalid, F.A., Farooque, M., Edmonds, D.V., (1990), "Precipitation of copper in proeutectoid cementite in steel," *Proc. of the Int. Congress for Electron Microscopy*, San Francisco, pp. 916-917.
- [81] Dilewijns, J.A., (1983), "High yield strength copper-bearing steels for crane rails," *Conf. Proc. on Copper in Steels*, Luxembourg, pp. 1.1-1.18
- [82] Creswick, W.E., (1967), "Commercial development of a rimmed low-alloy precipitation-hardening high-strength steel," *Conf. Proc.*, pp. 86-92.
- [83] Grange, R.A., Lambert, V.F., Harrington, J.J., (1959), *Trans. ASM*, **51**, p. 377.
- [84] Goodenow, R.H., Heheman, R.F., (1965), *Met. Trans. AIME*, **233**, p.1777.
- [85] Hornbogen, E., (1962), "The role of strain energy during precipitation of copper and gold from alpha iron," *Acta Met.*, **10**, pp. 525-533.
- [86] Ricks, R.A., Howell, P.R., Honeycombe, R.W.K., (1979), "The effect of Ni on the decomposition of austenite in Fe-Cu alloys," *Met. Trans. A AIME*, **10A**, pp. 1049-1058.
- [87] Knowles, G., Kelly, P.M., "Elastic modulus hardening," *Conf. Proc.**, pp. 9-15, (1971)
- [88] Russel, K.C., Brown, L.M., (1972), "A dispersion strengthening model based on deferring elastic moduli applied to the iron-copper system," *Acta Met.*, **20**, pp. 969-974.
- [89] Krishnadev, M.R., Galibois, A. (1975), "Some aspects of precipitation of copper and columbium (Nb), carbide in an experimental high strength steel," *Met. Trans. A AIME*, **6A**, pp. 222-224.

* On the "Effect of second-phase particles on the mechanical properties of steel", Scarborough.

- [90] Thompson, S.W., Colvin, D.J., Krauss, G. (1988), "On the bainitic structure in a modified A710 steel," *Scripta Met.*, **22**, pp. 1069-1074.
- [91] Speich, G.R., (1969), "Tempering of low-carbon martensite," *Trans. of the Met. Soc. of AIME*, **245**, pp. 2553-2564.
- [92] Irving, Pickering, F.B., (1960), *JISI*, **194**, p.137.
- [93] Standard specification for "low-carbon, age-hardening, Ni-Cu-Cr-Mo-Nb- and Ni-Cu-Nb alloy steels, *ANSI/ASTM*, pp. 750-754.
- [94] Danko, J.C., Stout, R.D., (1957), "The effect of subboundaries and carbide distribution on the notch toughness of an ingot iron," *Trans. of the ASM*, **49**, pp. 189-203.
- [95] Hahn, G.T., Rosenfield, A.R., (1967), "The influence of a fine dispersion on the cleavage strength of iron," *Trans. of the Met. Soc. of AIME*, **239**, pp. 668-674.
- [96] Mintz, B., Thulaseetharan, Crowther, D.N., (1996), "Age hardening behaviour of low carbon steels," *British Steel Corporation tech. report*.
- [97] Gray, J.M., (1972), "Strength-toughness relations for precipitation-strengthened low-alloy steels containing columbium," *Met. Trans.*, **3**, pp. 1495-1500.
- [98] Mintz, B., Kolahi-Aval, J., (1988), "Intercritical annealing as a means of improving impact properties of plate steel," *Met. Trans. A, AIME*, **19A**, pp. 1481-1489.
- [99] Mintz, B., Adejolu, K., Nassar, A., (1995), "The influence of martensite on the strength and impact behaviour of steels," *to be published in Mat. Sci. & Technology*.
- [100] Morrison, W.B., (1985), "Influence of silver on structure and properties of low-carbon steel," *Mat. Sci. & Technology*, **1**, pp. 954-960.
- [101] Heiple, C.R., Carpenter, S.H., Carr, M.J., (1981), "Acoustic emission from dislocation motion in precipitation-strengthened alloys, *Met. Sci.*, **15**, pp. 587-598.
- [102] Mintz, B., Kolahi-Aval, J., (1989), "Influence of tempering on impact behaviour of normalised steels," *Mat. Sci. & Technology*, **5**, pp. 457-464.
- [103] Mehrabi, H., Mintz, B., (1996), "Influence of tempering on the impact behaviour of quenched and tempered steels with low hardenability," *report, City University, London*.
- [104] Armstrong, R.W., Robertson Link, L., Speich, G.R., (1988), "Analysis of ductile-brittle transition temperatures for controlled-rolled, microalloyed, C-Mn based steels," *Processing, Microstructure and Properties of HSLA Steels*, DeArdo, A.J. (Ed.).
- [105] Petch, N.J., "Theory of yield point and strain-ageing theory," *Advances in Physical Metallurgy*, pp.11-25.

- [106] Mintz, B., Tajik, S., Kavishe, F., Baker, T.J., (1991), "Influence of grain boundary carbide thickness and grain size on cleavage fracture strength and Charpy impact behaviour of steels," *Mat. Sci. & Technology*, **7**, pp. 1005-1010.
- [107] Petch, N.J., (1958), "The ductile-brittle transition in the fracture of α -iron," p.1089.
- [108] Kühlmeyer, M., "Relation between statistical grain size distribution and yield strength," *Conf. Proc.*, pp. 855-860.
- [109] Atkinson, M., "Effects of grain size and of carbon content in the strain hardening of polycrystalline iron and low-carbon steels," *Conf. Proc.*, pp. 789-794.
- [110] Lapointe, A.J., Baker, T.N., "The influence of cooling rate on the strength and microstructure of low-carbon niobium steels," *Conf. Proc.*, pp. 1443-1448.
- [111] Greday, T., Lamberigts, M., "Effects of aluminium and nitrogen on the microprecipitation in HSLA steels," *Conf. Proc.*, pp. 731-736.
- [112] Armstrong, R.W., "Effects of micro-cracking and intrinsic obstacle strength of the Hall-Petch relation for ultrafine grain size polycrystals," pp. 795-800.
- [113] Clay, D.B., McCutcheon, D.B., "Development of line pipe steels," **282A**, pp. 305-318.
- [114] Kozasu, I., (1983), "Recent development of microalloyed steel plate (Metallurgical design of 500 MPa arctic grade plate)," *Conf. Proc. on HSLA steels technology and applications*, **8306-056**, pp. 593-607.
- [115] Hansen, S.S., (1988), "Justification for the use of HSLA steels in various applications," *Conf. Proc. on Microalloying '88*, Chicago, pp. 31-42.
- [116] Khalid, F.A., Edmonds, D.V., (1993), "A transmission electron microscopy study of copper precipitation in the cementite phase of hypereutectoid alloy steels," *Met. Trans. A, AIME*, **24A**, pp. 781-793.
- [117] Wagner, J.A., Shenoy, R.N., (1991), "The effect of copper, chromium, and zirconium on the microstructures and mechanical properties of Al-Zn-Mg-Cu alloys," *Met. Trans. A, AIME*, **22A**, pp. 2809-2818.
- [118] Galibois, A., Krishnadev, M.R., Dubé, A., (1979), "Control of grain size and substructure in plain carbon and high strength low alloy (HSLA) steels-the problem and the prospect," *Met. Trans. A, AIME*, **10A**, pp. 985-995.
- [119] Krishnadev, M.R., Ghosh, R., (1979), "Low-temperature mechanical behaviour of an "acicular" ferrite HSLA line pipe steel," *communications in Met. Trans. A, AIME*, **10A**, pp. 1941-1944.

- [120] Hornbogen, E., (1978), "Discussion of "Application of heterogeneous nucleation theory to precipitate nucleation at GP zones," *Met. Trans. A, AIME*, **9A**, pp. 134-138.
- [121] Harvig, H., Kirchner G., Hillert M., (1972), "On the ferrite-austenite equilibrium in the Fe-Cu system," *Met. Trans. AIME*, **3**, pp. 329-332.
- [122] Hook, R.E., (1970), "The effect of quench-ageing on inhomogeneous yielding of steels with very low interstitial solute content," *Met. Trans., AIME*, **1**, pp. 85-92.
- [123] Mintz, B., Ke, H., Smith, G.D.W., (1992), "Grain size strengthening in steel and its relationship to grain boundary segregation of carbon," *Mat. Sci. & Technology*, **8**, pp. 537-540.
- [124] Emenike, C.O.I., Billington, J.C., (1989), "Formation of precipitates in multiple microalloyed pipeline steels," *Mat. Sci. & Technology*, **5**, pp. 566-574.
- [125] Honeycombe, R.W.K., (1980), "Ferrite," *Metal Science*, pp. 201-214.
- [126] Irani, J.J., Tither, G., (1667), "Quenched and tempered low-carbon steels," *Conf. Proc.*, pp. 135-149.
- [127] Wilson, A.D., (1987), "High strength, weldable precipitation aged steels," *Journal of metals*, pp. 36-38.